The effect of rudder concepts on ship manoeuvrability and energy savings

by

Piotr Pietrzak

performed at

Wärtsilä Netherlands B.V.

to obtain the degree of Master of Science in Marine Technology
in the specializations of Ship Design and Ship Hydrodynamics,
at the Faculty of Mechanical Engineering of Delft University of Technology,
to be defended publicly on Monday, November 4th, 2024 at 2:00 PM.

Student number:	5717086	
Project duration:	January 2024 – October 2024	
Thesis number:	MT.24/45.003.M	
Thesis committee:		
	Prof. dr. ir. T.J.C. van Terwisga,	TU Delft, supervisor
	I. Hubbard, MSc,	Wärtsilä Netherlands B.V., supervisor
	Dr. D. Fiscaletti,	TU Delft, committee member
	Dr. G. Jacobi,	TU Delft, committee member

An electronic version of this thesis is available at http://repository.tudelft.nl/.

TU Delft

WÄRTSILÄ

Abstract

The increased focus on the reduction of emissions in the maritime sector has been the driving force behind many technological advancements related to marine engineering. Among those is the invention of the gate rudder system, which, while still at an early stage of development, promises improvements in propulsion efficiency and ship manoeuvrability. This thesis investigates the concept from the perspective of time domain simulation in order to pave the way towards identification of the working principle of the gate rudder power savings.

First, an extensive literature review is presented. A number of subjects related to the project was studied, starting from the principles of ship manoeuvrability, which comprises of ship hull hydrodynamics, hydrodynamics of control surfaces and regulations on manoeuvrability of ships. Afterwards, the current state of research into the gate rudder concept is investigated. Then, techniques of modelling of ship motion are laid out, with a focus on mathematical modelling of ship motion and rudders. Machine learning is identified as a potentially useful tool in the research, therefore a dedicated section consists of a brief introduction of the concept, some example regression algorithms and practical techniques utilized in conjunction with their use. Finally, the concept of time domain simulation in the context of maritime engineering is investigated and the options of simulator software available for the project are reviewed.

Initial decisions made for the execution phase of the project are described, including the choice of Manwav as the preferred time domain simulation software and S175 container ship as the benchmark vessel to carry out model tests on. An effort to tune the ship's model in Manwav to better match its performance found in literature is also described at the end of the chapter.

A physics-based gate rudder model is adapted into Manwav from a scientific paper. It is based on a mathematical model of a rudder derived from the MMG methodology, and the goal of its implementation was to pave the way in terms of code structure in Manwav and to serve as a reference point to the focus of the project, which is the data-driven model.

The data-driven gate rudder model uses a machine learning regression algorithm to build a set of rudder force coefficient predictors using a CFD dataset containing the values of force coefficients within a range of rudder and drift angles of a vessel equipped with a gate rudder system. A well-behaving model is successfully built using support vector regression and deployed in Manwav.

Both gate rudder models are put to test in the case study, where three ships with different rudder models are seen performing a set of benchmark manoeuvres, comprising of turning circles and zig-zag manoeuvres at different vessel speeds and rudder deflection settings. While the physics based model was found to be generating abnormal vessel behaviour, the data-driven model performed as expected, providing some insight into a potential impact a gate rudder system might have on a real ship's manoeuvrability and power consumption.

The thesis is concluded with a discussion on the data driven model's applications, along with limitations that prevent it from reaching its true potential. What follows is an extensive list of recommendations that go into detail on how the project could be improved in the future. The overall conclusion from the project is that a relatively limited amount of CFD data was successfully used to produce a rudder model that provides simulation possibilities otherwise beyond the reach of high fidelity methods due to scenario complexity and computational cost associated with them. With not a lot of additional effort, the model will make it possible to test whether or not gate rudder power savings reported in literature come from sailing in realistic weather conditions.

Acknowledgements

This thesis is a culmination of not only my Master's degree studies at TU Delft, but also of my academic adventure (so far?), which yielded a total of a Bachelor's degree and two Master's degrees. I've been looking forward to this moment for a long time, and I am convinced that my education has made me as ready as ever for any engineering challenges that might be waiting for me in the future.

I'd like to extend my gratitude to Wärtsilä Netherlands for welcoming me as a part of their Hydrodynamics R&D team and for making this project possible. It was an ambitious undertaking and I feel very satisfied that I could bring it to a completion. I'd like to thank Teus van Beek for giving me this opportunity to improve as an engineer in a professional environment.

I am grateful to my colleagues from my team, Marc, Wout, Maarten, Themis, Iulia, Stijn and Marcel, but also Anna, Zoi, Igor, Robert, Menno and other members of various other teams at Wärtsilä for the discussions we had and for making me feel like a part of our small community.

I'd like to express my sincerest thanks to Ian Hubbard, my daily supervisor from Wärtsilä, for hours upon hours of meetings, discussions, ramblings, whiteboard drawings and laughs, sometimes at questionable times of day and night. Your bombardment with questions and picking at my reasoning to find weak spots made my confidence in the logic behind my work truly rock solid.

I wish to express my gratitude to Tom van Terwisga, my supervisor from TU Delft, for his unwavering kindness, ensuring the academic qualities of my work are held to a high standard and for providing me the freedom to shape my research in this project.

I also want to extend my warm thanks to Jaap Geling, my lecturer from TU Delft, for his trust in getting me in contact with Teus van Beek in the first place, as well as for his fantastic attitude towards students and his role as a teacher.

Additionally, I'd like thank my friends from TU Delft, who shared the struggles with me, and my friends back in Poland and other parts of the world. Time spent with you, both in person and online, made my unique experience here an unforgettable one.

To my climbing dream team, Zachos, Kuba, Carlos and Martin, thank you for the shockingly consistent effort in keeping my sanity in check and making sure that in addition to the gains in our *galaxy brains*, we also spared some time to get slightly better at going up.

Lastly, I'd like to thank my dear Mama and Tata, for making this whole adventure possible, their trust and for always being there for me.

Piotr Pietrzak
Delft, October 2024

Contents

Nomenclature

Abbreviations

Abbreviation	Definition
IMO	International Maritime Organization
EU	European Union
MARPOL	International Convention for the Prevention of Pollution from Ships
EEDI	Energy Efficiency Design Index
SEEMP	Ship Energy Efficiency Management Plan
EEXI	Energy Efficiency Existing ship Index
CII	Carbon Intensity Indicator
SOLAS	Internatoinal Convention for the Safety of Life at Sea
ABS	American Bureau of Shipping
DNV	Det Norske Veritas
BV	Bureau Veritas
LR	Lloyd's Register
CRS	Cooperative Research Ships
GRS	Gate Rudder System
ESD	Energy Saving Device
CFD	Computational fluid dynamics
NMRI	National Maritime Research Institute
HSVA	Hamburgische Schiffbau-Versuchsansalt (Hamburg Ship Model Basin)
RANS	Reynolds-averaged Navier-Stokes
COG	Center of gravity
MMG	Manoeuvring Modelling Group
MPP	Manoeuvrability Prediction Programme
VSY	Virtual Ship Yard
DDM	Data-driven models
ML	Machine learning
KRISO	Korea Research Institute of Ships and Ocean engineering
DTMB	David Taylor Model Basin
VLCC	Very large crude carrier
SVM	Support vector machine
RBF	Radial basis function
RMSE	Root mean square error
QTF	Quadratic transfer function

Symbols

Symbol	Definition	Unit
V	Velocity	m/s
ρ	Density	kg/m^3
β	Drift angle	$^\circ$ or rad
LPP or L_{PP}	Length between perpendiculars	m
B	Breadth	m
T	Draught	m
u	Longitudinal velocity	m/s
v	Transverse velocity	m/s
U	Velocity magnitude	m/s
r	Yaw rate	$^\circ$/s or rad/s
t	Time	s
δ	Rudder angle	$^\circ$ or rad
x	Longitudinal coordinate	m
y	Transverse coordinate	m
z	Vertical coordinate	m
m	Mass	kg
F	Force	N
X	Longitudinal force	N
Y	Transverse force	N
N	Torque/moment of force	Nm
I	Moment of inertia	kg*m^2
L	Lift	N
D	Drag	N
C_L	Coefficient of lift	-
C_D	Coefficient of drag	-
A	Surface area	m^2
J	Added moment of inertia	kg*m^2
t_R	Steering resistance deduction factor	-
a_H	Rudder force increase factor	-
D$_P$	Propeller diameter	m
ψ	Heading	$^\circ$
μ	Covered area ratio	-
η	Ratio of propeller diameter to rudder span	-
f_α	Lift gradient coefficient	-
α	Angle of attack	$^\circ$
AR	Aspect ratio	-
KT or K_T	Coefficient of thrust	-
ω	Wake fraction	-
ε	Ratio of wake fraction at rudder and propeller positions	-
J	Advance ratio	-

1. Introduction

1.1. Environmental sustainability of the shipping sector

The shipping sector is one of the most significant driving forces in global trade. Accounting for over 80% of total worldwide goods transport [48], maritime shipping is directly bound to global economy. Even though maritime shipping far outshines most other modes of transport when compared in terms of emissions per tonne-kilometre, the sheer scale of the world merchant fleet causes its total CO2 emissions to be nonetheless significant [10], with lots of room for improvement.

For over two decades, there has been ongoing a global effort to reduce the environmental impact of the maritime sector. This effort is mostly lead by the International Maritime Organization (IMO), through the introduction of several measures with a goal of making it mandatory for shipowners to strive for more efficient and environmentally friendly solutions in new and existing vessels. The most notable of these measures are part of amendments to Annex VI of the International Convention for the Prevention of Pollution from Ships (MARPOL) and consist of the following:

- Long-term measures:
  - Energy Efficiency Design Index (EEDI)
  - Ship Energy Efficiency Management Plan (SEEMP)
- Short-term measures:
  - Energy Efficiency Existing ship Index (EEXI)
  - Carbon Intensity Indicator (CII)

EEDI is a measure of a ship's overall efficiency, expressed as a single figure in grams of emitted carbon dioxide per an individual vessel's capacity-mile, where the smaller the number, the more efficient the ship design is. Based on a baseline calculated for ships built between 2000 and 2010, the index mandates that newly built ships be more efficient than that baseline by a set percentage. It is applied to new vessels and every 5 years, the requirements are tightened in order to stimulate innovation that drives the continuous improvement of the sector's sustainability. Shipowners are free to decide through which technological solutions an acceptable EEDI level will be achieved. The scope of this measure consists of most cargo and passenger vessels, such as tankers, bulk, LNG and container carriers, ro-ro car carriers, cruise ships and more. Combined, the vessel types within the scope of EEDI account for around 85% emissions of the maritime sector.

SEEMP is an operational mechanism that incentivises shipowners and operators to consider optimisations in the operational performance of a ship over set stages of her lifespan. Additionally, it provides guidance for shipping companies to properly manage ship and fleet efficiency strategies using recognized monitoring tools. Along with Data Collection System (DCS), which is a set of requirements for the collection of ship's performance data, it forms the basis for CII, which employs the continuous evaluation of a ship's efficiency over its lifespan (described in more detail below).

EEXI is a framework that requires all ships above 400 GT to calculate Attained EEXI, a measure representing their technical efficiency. When compared to Required EEXI, it determines whether the vessel meets the emissions standards. It corresponds to the requirements of EEDI and is meant to extend the EEDI's functionality to include existing ships.

CII is the mechanism that ensures continuous improvement of efficiency ratings of an individual ship. Applicable to all vessels of 5000 GT or above, it assigns a rating to a ship annually based on its performance data collected on board. When compared to that year's required annual CII baseline, each ship is given a CII grade from A to E. If a rating of D for three consecutive years or E is assigned, corrective actions need to be undertaken for the specified vessel in order to boost the ship's subpar performance [53]. Administrations, port authorities and other relevant parties are encouraged to provide favourable treatment to ships rated A and B [46].

In the context of improvement of ship efficiency through the introduction of innovative solutions in propulsion systems, EEDI is the most important when it comes to introduction of superior technology on newly designed ships, while EEXI is the most relevant for existing ships that might be subject to efficiency improving retrofits of parts of their propulsion systems. These measures are one of the reasons why shipowners should seek to apply the latest developments in ship propulsion systems. One of the areas currently under investigation where overall propulsive efficiency could be enhanced both in new and existing vessels is the concept of alternative steering systems. The conventional rudder placed behind a propeller in cargo ships has a lot of inherent advantages compared to a lot of other configurations, but certain drawbacks were identified thanks to advancements in Computational Fluid Dynamics (CFD) and knowledge of the flow field in the stern part of the ship, leading to proposed improvements in the placement and shape of the ruder blade, among others [8].

1.2. Gate rudder concept

An unconventional approach to the idea of ship's yaw control surface was proposed by Japanese researchers in 2013 [15]. The so called "Gate Rudder" consists of twin rudders forming an open-type duct around the ship's propeller. The rudders' pivots are located in the propeller plane, outside of the rudder blade profiles, offset towards the vessel's center line. The layout of the Gate Rudder system can be seen in figure 1.1. While the proposed rudder type was initially classified as an Energy Saving Device (ESD), the complexity of the system, as well as the significance of the advantages unrelated to thrust-augmenting effects soon caused it to be called an "Energy-Saving propulsion and Manoeuvring Device" (ESMD), highlighting the hybrid nature of the concept.

Figure 1.1: Example of a gate rudder system (GRS) installed on a Japanese domestic container vessel, Shigenobu. Credit: Yamanaka Shipbuilding.

The gate rudder comes with a set of several potential advantages over a conventional rudder. The most straight-forward of them is the possibility to operate in different steering modes: under normal operating conditions, the rudder blades typically do not deflect significantly from the default position. However, when performing low-speed manoeuvres, such as docking in a port, a "crabbing" steering mode may be employed by the helmsman, where the rudder blades are asymmetrically "closed" behind the propeller, allowing for a certain degree of thrust vectoring, wit ha possibility to achieve thrust angle almost perpendicular to the vessel's center line. In emergency situations, rudder blades could be deflected further than normal into the propeller slipstream, in order to increase the steering forces at the cost of higher steering resistance. Additionally, an emergency stop manoeuvre could be assisted by the rudder blades both deflecting towards the ship's bow, acting similarly to a speed brake on an aircraft. The different steering modes were visualized in figure 1.2.

Another significant advantage of the gate rudder is the increased energy efficiency resulting from the shape of the rudder blades and the hull's wake field. This enables the rudder to create additional thrust. In addition to this, during normal operation, the rudder does not interfere with the propeller's slipstream, resulting in a decreased thrust deduction factor t, which translates to more efficient propeller operation. A theory proposed by researchers also suggests that the position of the rudder blades also allows for a more effective redirection of lower momentum, hull-adjacent streamlines into the propeller, which recovers viscous losses, increasing the propulsive efficiency [26].

Additionally, this innovative rudder concept provides other advantages. The gate rudder's placement in the vicinity of the propeller plane eliminates the need for the hull extending aft beyond what is necessary to accommodate the propeller, allowing for a shorter hull with the same cargo capacity or enlarged cargo capacity at the same hull length. The rudder blades being positioned outside of the propeller slipstream during normal operation significantly reduce underwater radiated noise (URN) and aft end vibrations [28]. The gate rudder system also features higher redundancy, since the two rudder blades are operated by two independent hydraulic systems - in case one of them fails, the vessel does not completely lose the ability to manoeuvre. Lastly, because no significant modifications in the hull form are required to install a Gate Rudder System on an existing ship, as well as majority of the modifications being possible to perform while at sea, the ease of retrofitting is another advantage.

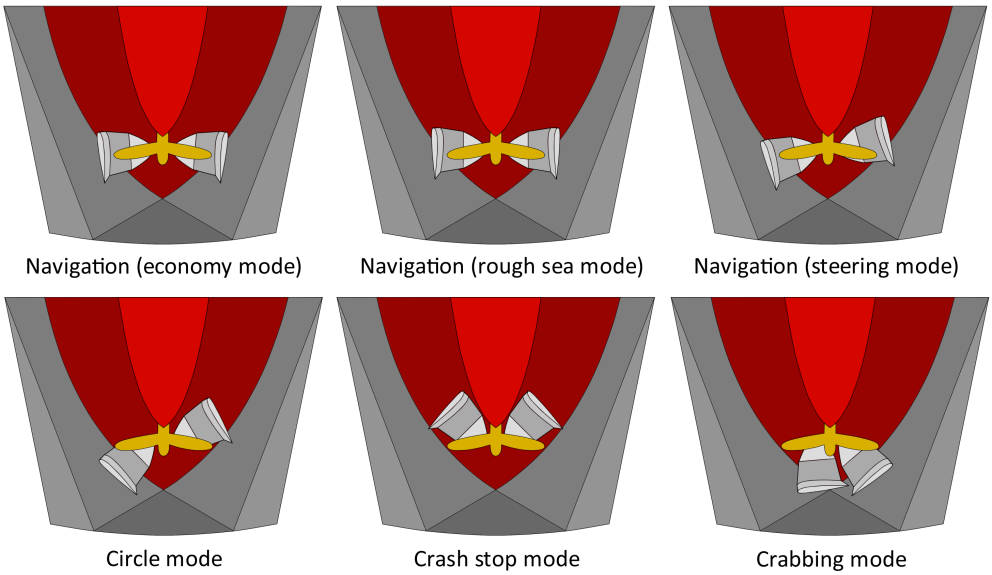

Figure 1.2: Schematic of gate rudder steering modes. In this bottom view of a ship's aft end, different configurations of the rudder blades in relation to the propeller are presented. Author's recreation of the diagram seen in literature [20].

Since the introduction of the concept, it has been subject to extensive CFD studies, model experiments, and even sea trials on ships equipped with the new rudder type. Initial theoretical studies showed optimistic prospects for possible power savings, which prompted the construction of the first vessel fitted with a Gate Rudder, MV Shigenobu. It was launched in 2017 and the first full-scale performance reports of the sister ships (GRS-equipped Shigenobu and her sister, Sakura, equipped with a conventional flap rudder) showed that in service conditions, the Gate Rudder can offer very significant power savings, far higher than predicted before. Decreased vibrations and URN were also confirmed through these experiments. Reports from the crew of one of the vessels equipped with the GRS also indicate that the system increases the ship's seakeeping and responsiveness to steering inputs, resulting in even higher performance gain over the conventional rudder in rough weather.

However, despite the multitude of optimistic results of the sea trials of a number of ships, there still exists a discrepancy between real-life performance of the Gate Rudder and theoretical studies. Many authors suggest that this new rudder is subject to a significant scale effect, which causes the disconnection between experiments and practical applications of the technology. Additionally, not many studies investigating the details of an optimal gate rudder design have been performed, which further increases the uncertainty of actual potential efficiency gains achievable with the Gate Rudder.

In addition to the potential benefits of the gate rudder system, the concept might suffer from some drawbacks. The most straight-forward one is the increased parasitic drag due to the fact that the gate rudder typically features a larger surface area to compensate for the lower steering forces resulting form the rudder blades not operating fully in the propeller slipstream. Even if the steering forces at large deflection angles are matched with an equivalent conventional rudder, a vessel with a gate rudder system might suffer from decreased responsiveness to steering inputs in tighter waterways, because the steering forces at lower deflection angles will be typically smaller. Additionally, two separate steering gear systems increase the price of the installation of such a rudder system.

Due to the limited ability to simulate actual performance of the concept, it is not yet clear which ship types would benefit most from the application of the gate rudder. Prospective applications on medium-sized sea going cargo vessels with optimistic sea trial results present one of the possible areas of applicability, but no data is currently available on the performance of other cargo ships of the Imoto Line which were built with a gate rudder system. The level of uncertainty is very high due to shortage of full-scale performance data and inaccuracies in numerical and scale tests.

1.3. The investigation of gate rudder power savings

Wärtsilä has acquired the license for development and deployment of the Gate Rudder through an agreement with the Japanese patent holders in 2020 [38]. The company's goal is to further develop the scientific understanding behind the hydrodynamics of the concept, determine the range of practical applications of the GRS as a product, and provide potential customers of the product tangible numerical claims to support the theoretical advantages in product comparisons. Aside from extensive CFD investigations into the Gate Rudder currently being conducted, another prospective area of research was put forward - use of ship motion simulation as means for macro-scale evaluation of the performance of vessels equipped with the GRS in more complicated scenarios.

A review of literature research, described in chapter 2 has indicated that a fact worth investigating further is the power savings achieved by Shigenobu a vessel equipped with a gate rudder system in comparison to her sister vessel, Sakura, equipped with a conventional rudder during their sea trials in operational conditions. These power savings were not reproduced through CFD analyses aimed at determining the power consumption of a vessel under static flow conditions. A hypothesis was therefore put forward that these power savings identified in the sea trials are caused by the flow conditions present during realistic wave and wind conditions, in which the unique construction of the gate rudder system allows for a higher overall efficiency. Because a vessel's voyage through such realistic weather conditions would not be practical to simulate using high fidelity methods such as CFD, other tools to reproduce them would be necessary. One such tool is time domain simulation, where a vessel's motion can be simulated using a mathematical model of its behaviour and reactions to forces that act upon it from hull resistance, its propulsion system, its rudder system or wave loads. This tool trades off the fidelity of the calculations for a lower computational cost and increased complexity of realizable scenarios.

If a sufficiently robust gate rudder hydrodynamics model implementation in a time domain ship motion simulator was to be developed, the current state of collective knowledge on the strengths and weaknesses of the concept, as well as its range of applications could be expanded. Most importantly, it would allow for the hypothesis introduced above to be investigated. If it was found to be true, it would constitute a significant breakthrough in the state of scientific research on the concept as well as in commercial viability of GRS as a product.The project that will build on the findings described in this report will be aimed at the development of such a hydrodynamic model of a gate rudder and its application in an adequate scenario.

1.4. Research questions

Typically, research projects such as the one described in the report are accompanied by a number of research questions that allow for a more structured approach towards the completion of the project's objective. The main research question was formulated as follows:

How to model a gate rudder system performance using a limited amount of data in order to investigate its impact on a ship's manoeuvrability and power consumption?

To make the problem easier to understand and to dissect it into smaller parts, supporting research questions were introduced. They comprise of three questions, each meant to relate to one of the main challenges standing in the way of reaching the goal:

1. What are the principles of ship manoeuvrability?
2. What method can be used to model the forces on a gate rudder in a time domain simulation software?
3. How can the impact of a rudder model on a ship's manoeuvrability be evaluated?

To find an answer to these questions and to achieve the main objective of the project, first, a thorough understanding of related physical concepts and tools needed to be acquired. This was achieved through an extensive literature study presented in the next chapter.

1.5. Thesis outline

The thesis is divided into several chapters, each focusing on a specific task in the project:

- Chapter 2 is a description of the findings of the literature review performed prior to the execution phase of the project.
- Chapter 3 covers key decisions made before the development of the rudder models was carried out.
- Chapter 4 presents the development process of the two distinct models of a gate rudder system for a time domain simulator.
- Chapter 5 is a presentation and discussion of results of a case study which saw a practical use case for the previously developed rudder models.
- Chapter 6 provides a summary of the work carried out in the project, its practical applications, its limitations and future recommendations.

2. Literature review

This chapter describes in detail the findings from the review of available literature on subjects related to the project. The main areas of focus were ship hull hydrodynamics, physics of ship control surfaces, hydrodynamics of ship manoeuvres and the research on the Gate Rudder concept. The first step towards the completion of the project is the presentation of the current state-of-the-art understanding of those engineering concepts and the designation of the viable modelling methods, available ship motion simulators and scenarios in which the rudder model could be tested.

2.1. Ship motion and manoeuvring

2.1.1. Ship hull hydrodynamics

The most fundamental physics knowledge relevant to the project is related to the understanding of flows around ship hulls and their effect on ship motion. This area of research is very broad and has been under investigation for a very long time. In principle, the concept of prediction of ship hydrodynamic performance can be divided into separate general areas: resistance and propulsion, seakeeping, ship vibrations, and manoeuvring. All of these areas are to some extent relevant to the concept of Gate Rudder through its numerous advantages, but in the context of its effect on ship manoeuvrability and power savings, vibrations are considered not important.

Resistance is the external force exerted on a ship's hull during its movement in the water. To counteract it, ships require propulsion systems that generate thrust. In theory, a ship's resistance can be divided into individual mechanisms which sum up to the total resistance force. These decompositions can be performed in different ways, but the following interpretation of resistance components is considered by the author to be the most comprehensive one:

- Viscous resistance - loss of energy through momentum transfer into water particles adjacent to the hull (generation of boundary layer) and through formation of turbulent vortices.
- Wavemaking resistance - loss of energy through the generation of a wave system, due to the distribution of pressure around the hull.
- Wavebreaking resistance - the hull generated waves break in bow and aft sections, further contributing to overall wave resistance. Can be reduced by a bulbous bow.

Naturally, the wave drift forces from ocean waves can also contribute to overall resistance of a vessel in real life conditions, but this effect is usually assessed in conjunction with other aspects of a ship's seaworthiness.

Wake is the disturbance in the flow formed behind a ship as it moves through the water. It is where the energy losses from hull movement are directed in the form of waves and turbulent eddies. The aft part of the ship is the section of the hull where the flow converges back after being pushed aside by the vessel. It is also the location of a ship's propeller and rudder in most cases. Because of the wake, the inflow to the propeller cannot be treated as uniform, as if the propeller was suspended in open water. This is why when describing the propeller's action with mathematical formulas, a propeller's open water performance is usually corrected by several factors to account for the environment around the propeller. The wake is represented by a wake factor w, which is typically a fraction that describes the average decrease in inflow velocity to the propeller. Similarly, the zone behind the propeller may also influence its performance - for instance, in most ships, the rudder is located in the propeller's slipstream. This is why a thrust deduction factor, t, is used to account for the effects that decrease open water thrust in operational conditions. Both of these factors are a simplification, a single number representing the average of a phenomenon that influences the flow field on a three-dimensional level.

The flow velocity field in the aft section of a vessel is usually symmetrical with respect to the ship's center plane. In this zone, the streamlines from the hull's sides are directed inward, towards the centerline. While this does not influence propellers and rudder blades positioned in the center plane of the ship, it obviously significantly changes the flow pattern on off-center rudders.

Seakeeping, or seaworthiness, is a broad term encompassing many different aspects of a ship's general ability to withstand the environmental conditions it is designed for. It is comprised of the following:

- Speed reduction as result of added resistance of the sea state, or how much the speed needs to be reduced in order to avoid excessive motions or loads
- Structural integrity of the hull subject to wave impacts and related loading
- Habitability - comfort and safety of occupants in rough conditions
- Safety - resistance to capsizing, how well the ship handles large roll motions and accelerations, slamming and other wave impacts, green water impacts, cargo safety

- Operational limits for ships - how harsh conditions will cause the ship to be unable to safely or effectively carry out its tasks

Ship manoeuvring involves the ability of a vessel to stay on course (or on track when in restricted waters) while underway, change its course when needed, change its speed and precisely position while performing low-speed manoeuvres, such as when docking in a port. The IMO and classification societies specify minimum requirements through standards for ship manoeuvrability, described in more detail in 2.1.3. Elements that influence the ship's ability to fulfill or exceed these requirements are its hullform, its propulsion system, its steering system (such as a rudder) and its mass.

The primary manoeuvring device on a vessel, in most cases, is its rudder. To make the ship turn, the rudder needs to produce a sideways force that places and holds the hull at an angle of attack to the flow of water, or drift angle β. The hull then begins to act like a hydrofoil, with the resulting lift making up the majority of the centripetal force that keeps the ship on a circular path.

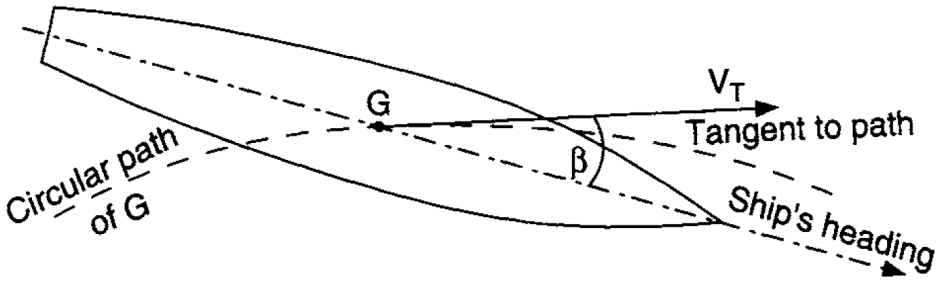

Figure 2.1: Graphical description of the drift angle [8]

A ship's directional stability (or course/yaw/straight-line stability) is a quality of the hull that describes the tendency of the ship to settle on a course without any steering corrections, after a deviation caused by external forces. A directionally unstable ship will begin and may continue its deviation from course even in the absence of external forces. This effect influences the ship's response to rudder inputs significantly. A directionally stable ship will be easier to keep on course, but will also resist attempts at inducing yaw rates, making it harder to change its heading. On the contrary, directionally unstable ships will require more rudder inputs to stay on course, but will be much easier to turn to a different heading when desired and to manoeuvre [21]. Typically, cargo ships are more directionally stable when in ballast condition, and this stability is gradually reduced the more loaded they are. This is due to the vessel's draft increasing, which increases the transverse resistance forces and changes the distribution of pressure along the hull's side.

In low-speed manoeuvres, the flow around the rudder from ship movement alone is too slow to generate sufficient steering forces. That's why in such conditions, most ships rely on propeller slipstream on the rudder to steer. Some vessels are also equipped with thrusters mounted on the bow and sometimes also on the stern to produce sideways forces without longitudinal components. They are not effective outside of low speed conditions, though [23].

Additionally, an aspect that affects a ship's manoeuvring performance is the depth of the sea bed. In shallow waters, sea waves become steeper and other hydrodynamic phenomena become apparent, such as the squat effect, which increases the ship's draft when underway in shallow water. The vessel's turning time and yaw rate are also affected, depending on the yaw stability of the hull. In tight waterways, the bank effect may also occur. It is described as a suction force acting on underwater zones of the ship's hull that are in close proximity to a waterway's banks or walls [13]. It is a phenomenon not unlike the ground effect in racing cars, which utilize it to achieve higher downforce.

2.1.2. Hydrodynamics of rudders

Rudders serve in most ships as the principal course-keeping and manoeuvring device. Dating back to the very inception of maritime travel, they provide an effective way to use the ship's speed in water and/or slipstream from the propeller to generate sideways forces. Historically taking the form of simple plates, with the advent of airfoil theory and advancements in fluid dynamics, more sophisticated shapes and arrangements were proposed, such as stall-postponing Schilling and flap rudders, or energy recovering twisted rudders.

In principle, a rudder's objective is to produce a force used for the control of the yaw motion of a vessel. Most rudder types achieve this using principles of lifting surfaces in fluid flows though the controlled disturbance of flow. The resulting lift and drag forces allow the vessel to control its heading and manoeuvre.

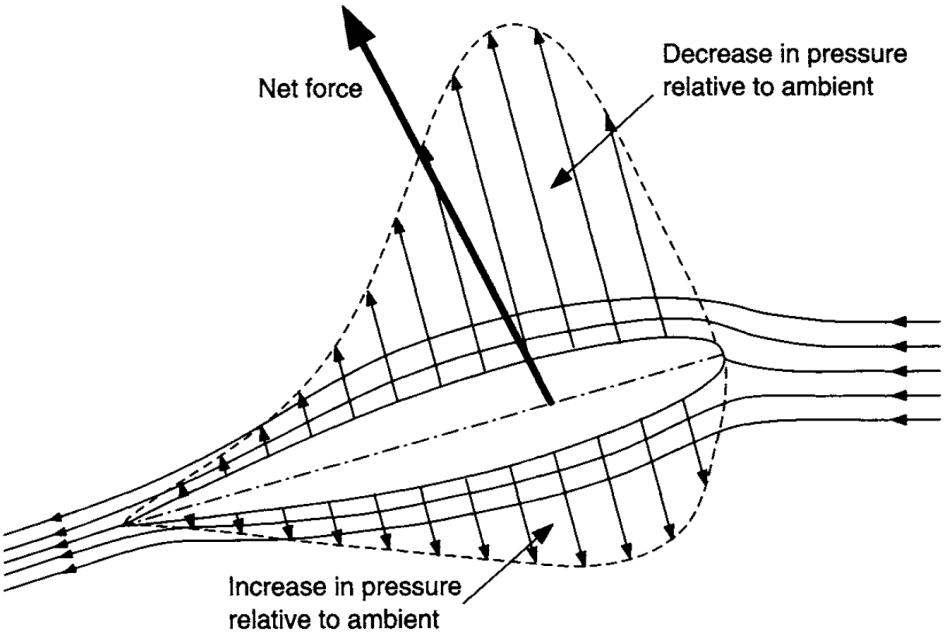

Figure 2.2: Distribution of pressure around a lifting foil [8]. The high pressure side of the foil is called the pressure side, while the low pressure side is referred to as the suction side.

The lift and drag on an airfoil depend on the flow velocity, the angle of attack and the airfoil's shape. In normal operating conditions and sufficiently small angle of attack, the flow around the foil is laminar and attached to both sides. As this angle increases through the rotation of the steering gear due to helm commands, the lift and drag forces increase. When the angle of attack exceeds a certain threshold, the flow on the suction side of the foil will separate, creating a turbulent zone in its wake. This effect is referred to as stall and results in a drop of lift and a further increase of drag.

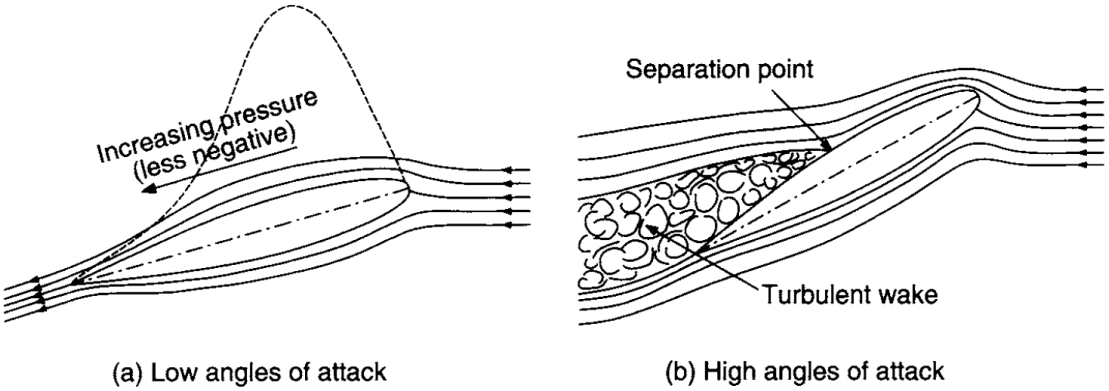

Figure 2.3: Typical flow regimes around an airfoil in a) normal operation and b) stall [8]

Typically, rudders are located in the stern section of the vessel, behind the propeller. This allows for a more efficient moment arm to steer the ship when compared to bow-mounted rudders, as well as puts the rudder foil within the slipstream of the propeller. This allows for an increased flow velocity past the rudder, which increases the steering force. However, this advantage comes at a cost. The rudder acts as an obstacle, which blocks and redirects the flow upstream of the propeller, even when the rudder is at the zero position. This influences the blade loading and consequently, the thrust and torque. Additionally, increased flow velocity past the rudder blade due to propeller slipstream also increases the drag. While this is partially alleviated by the flow straightening effect due to the rotational energy of the flow induced by the rotating propeller being recovered by the surface of the rudder acting like a stator, it nonetheless results in an overall decrease of efficiency, reflected by the previously mentioned thrust deduction factor t [8].

Wings in aircraft often are equipped with flaps, which change the effective profile of the airfoil, changing the pressure distribution around it and consequently, its maximum lift coefficient, in order to better fit the lower airspeeds necessary for takeoff and landing. When deflected, the flap causes a shift of pressure in its general vicinity when compared to an airfoil with a retracted flap at the same flow velocity [1]. In a similar manner, when a ship's rudder is rotated, it begins

to act like a flap with respect to the hull, which also generates additional pressure differential within the aft section. This effect is known as the flap effect and generally increases the steering force, depending on the distance from the rudder to the hull [8].

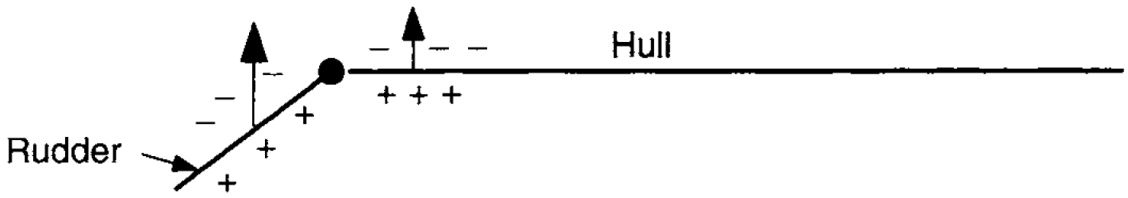

Figure 2.4: A simplified diagram depicting the distribution of pressure in the vicinity of a deflected rudder [8]

2.1.3. Ship manoeuvrability regulations

The minimum acceptable manoeuvrability of ships is regulated by the IMO. The Resolution MSC.137(76), enacted in 2002, dictates the standards for manoeuvrability of sea going vessels and serves as the baseline for the norms set by most classification societies. Ship's capability to perform a set of dynamic manoeuvres within specified parameters, usually expressed in ship lengths, needs to be demonstrated either through full-scale sea trials, or through scale or computer model prediction methods, with sufficient validation ensured by sea trials. These rules apply to all new ships of 100 m in length and above, as well as chemical tankers and gas carriers regardless of their size. A ship that underwent significant modifications may also be subject to a reevaluation of compliance with these standards. The standards define a set of standard manoeuvres meant for evaluation of ship's overall manoeuvrability, listed below.

1. Turning circle
2. Zig-zag test
3. Full astern stopping test

Each of the tests has set criteria which determine the ship's compliance with the standards. The ship length parameter L used in these criteria is the length between perpendiculars (Lpp). To better describe the criteria, some definitions are also provided in the document. Advance is distance travelled in the direction of the original course by the midship point of the vessel from the position at which the rudder order is given to the position at which the heading of the vessel has changed 90° from the original course. The tactical diameter is defined as the distance travelled by the midship point of the vessel from the position at which the rudder order is given to the position at which the heading has changed 180° from the original course. It is measured in a direction perpendicular to the original heading of the ship. In zig-zag tests, overshoot angle is the additional heading deviation experienced in the test following a change of rudder angle. Lastly, track reach is the distance along the path described by the midship point of a ship measured from the position at which an order for full astern is given to the position at which the ship stops in the water. The tests are performed at a steady approach at the test speed V, defined as a ship velocity of at least 90% of the ship's velocity corresponding to 85% of the maximum engine output. Additionally, the document mandates that the tests need to be conditions are described as deep, unrestricted water, calm environment and the ship loaded to full at the summer load line draught.

The turning circle is defined as a manoeuvre where, after a steady approach with zero yaw rate, the rudder is put at 35° (or maximum rudder angle permissible at test speed). The vessel's advance shall not exceed 4.5 L during this manoeuvre, while the tactical diameter has to be lower than 5 L. The turning circle evaluation involves the manoeuvre being performed in both port side and starboard side directions.

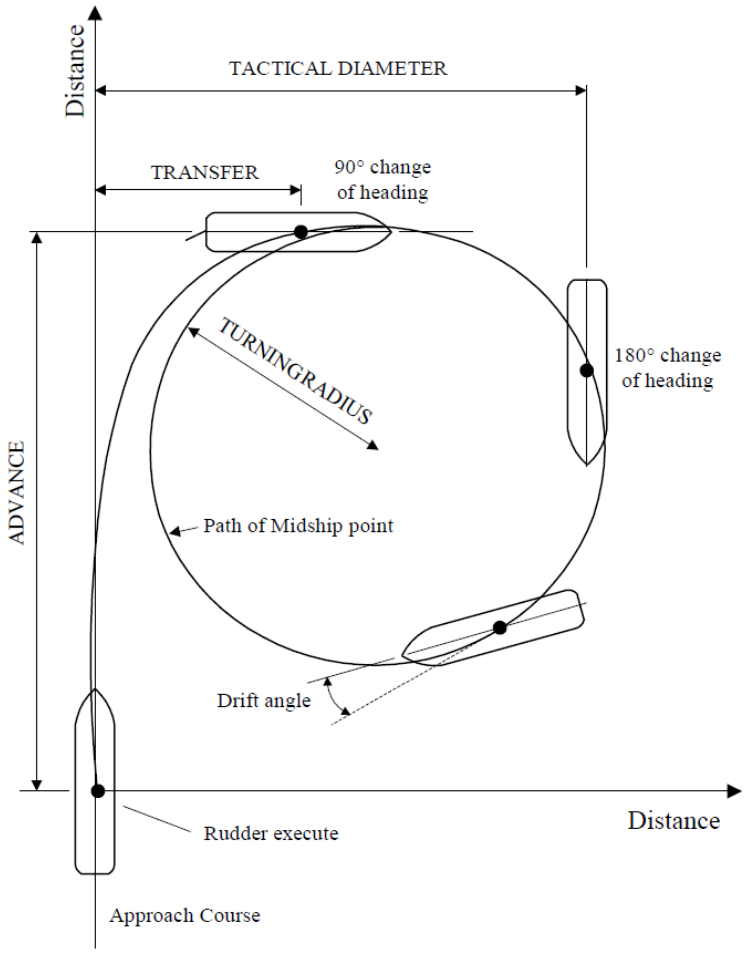

Figure 2.5: A typical ship's midship point trajectory during a starboard turning circle test, with key parameters marked [21].

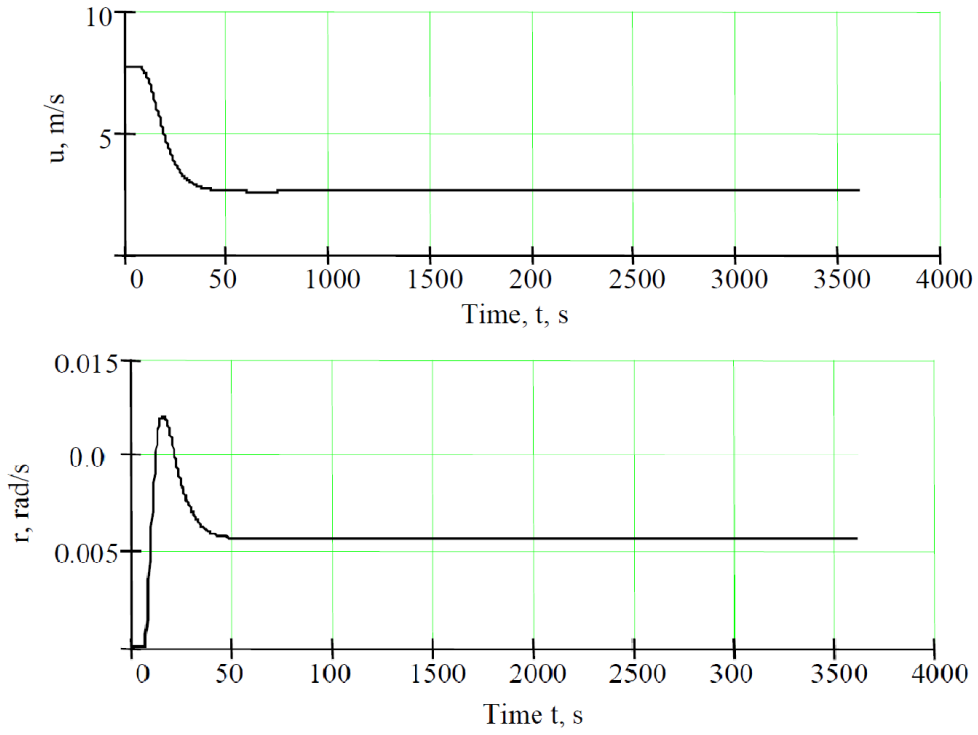

Figure 2.6: A typical ship's longitudinal velocity and yaw rate graphs during a turning circle manoeuvre [21].

The zig-zag test is a manoeuvre in which a set amount of helm is applied alternately to either side when a known heading deviation from the original heading is reached. Standard practice involves a 10°/10° and a 20°/20° zig-zag tests, where the first number is the designation of the rudder angle, while the second number defines the heading deviation angle objective. The zig-zag test procedure is the following: after an initial steady approach, thee rudder commands are ordered (known as executes): first, the rudder is put to the set angle (typically 10° or 20°) to starboard or port side. When the ship's heading has deviated from the original course by the specified angle (again, typically 10° or 20°), the second execute is performed by ordering the rudder angle to reverse to the same angle on port or starboard side. Finally, when the heading deviation from the original course is reversed to the set angle on the other side, the rudder is again reversed to the set helm angle on starboard or port side (third execute). In this type of test, several dynamic parameters are examined. In the 10°/10° test, the ship should not have travelled more than 2.5 ship lengths by the time the heading has changed by 10° from the original heading. In the same test, the first overshoot angle requirement (measured after the second execute) is scaled with the L/V ratio, which is expressed in seconds. It ranges from 10° to 20° for respective L/V ratios of 10 s or less and 30 s or more, with linear L/V scaling for the L/V ratios between 10 s and 30 s. Similarly, the second overshoot angle (measured after the third execute) shall not exceed 25° to 40° for L/V ratio values of 10 s or less and 30 s or more, respectively, with similar linear scaling for in-between L/V values. In case of the 20°/20° test, the first overshoot angle shall must be lower than 25°.

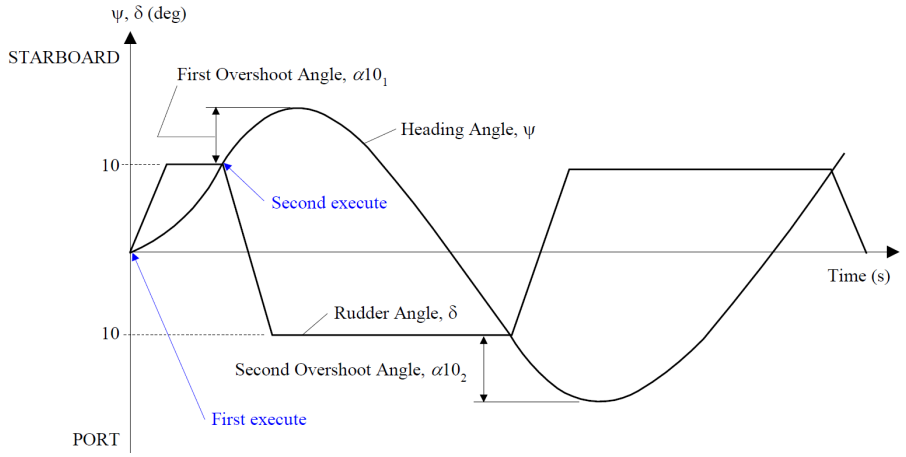

Figure 2.7: A typical ship's combined heading and rudder angle graph during a 10°/10° zig-zag test, with key parameters marked [21].

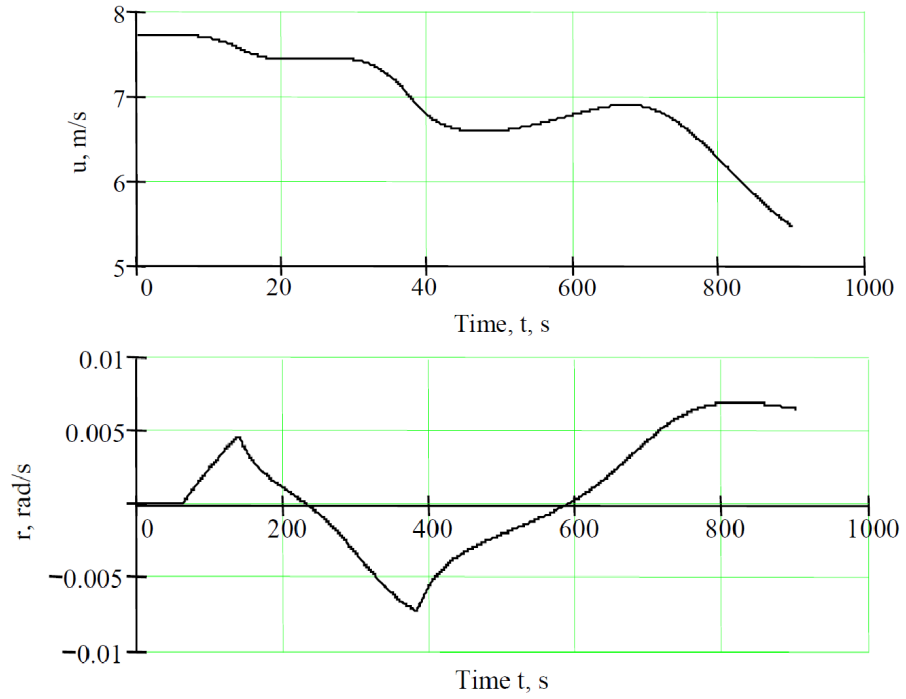

Figure 2.8: A typical ship's longitudinal velocity and yaw rate graphs during a 10°/10° zig-zag test [21].

The full astern stopping test is defined as a manoeuvre in which, after the initial steady approach at test speed, a full astern order is given. Nominally, the track reach cannot exceed 15 ship lengths in this test. However, for ship's with large displacement an exception can be made, increasing the allowable track reach to no more than 20 ship lengths [6].

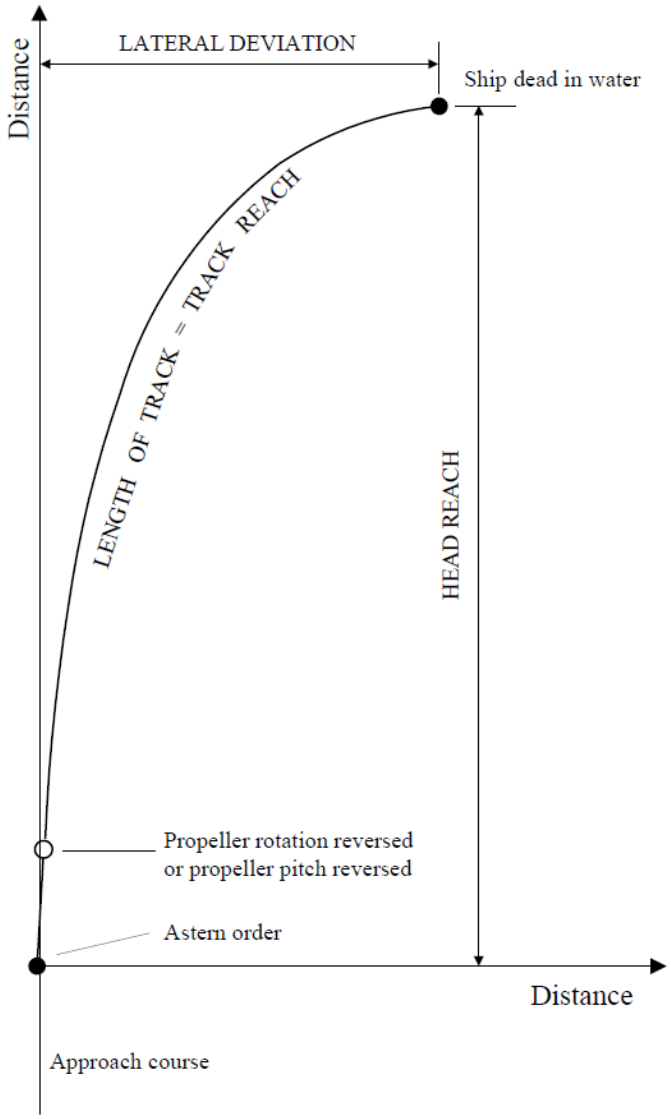

Figure 2.9: A typical ship's trajectory during a full astern test with key parameters marked [21].

There also exist standard manoeuvres that are meant to test a ship's directional stability. The most popular type of manoeuvre, typically performed right after a turning circle test, is the pull-out test. After a stable turning circle is achieved, the rudder is returned to neutral and is kept there until a stable yaw rate is achieved. In directionally stable ships, the yaw rate will decay to zero, while course unstable ships will stabilise on a residual rate of change of heading, usually of a different magnitude for portside and starboard side manoeuvres. Another method of testing a ship's yaw stability is a spiral manoeuvre. The typically performed variant of this test is the Bech (or reverse) spiral. In this manoeuvre, the ship is steered to obtain different steady turning rates, which creates the plot of the relation between steady yaw rates and rudder angle. Course unstable vessels will have a portion of the plot reversed - this part is called the unstable loop [21].

Classification societies implement these standards for manoeuvrability in their own requirements for verification of ship designs. Four societies were chosen as the most representative: Det Norske Veritas (DNV), Lloyd's Register (LR), American Bureau of Shipping (ABS) and Bureau Veritas (BV). DNV's Rules for Classification of Ships includes a chapter about ship manoeuvring characteristics, which copies most of the IMO's standards with a few changes. These consist of specifying requirements for conditions in which sea trials have to be made, extended turning circle procedure for current corrections and omission of direct requirements for results of the turning circle and full astern stopping manoeuvres. Additionally, a note is added, specifying that for non-conventional steering and propulsion systems, the use of comparative steering angles during sea trials may be permitted, where applicable [30]. Naturally, they still need to be fulfilled in accordance to IMO regulations. LR's Rules and Regulations for the Classification of Ships similarly includes a chapter

on steering machinery and ship manoeuvrability, where the IMO Standards are cited directly as a set of requirements. Additionally, it provides an additional redundancy requirement for manoeuvrability in the event of reduced prime mover power and loss of propulsion systems [55]. ABS provides a separate Guide for Vessel Maneuverability, where the IMO Standards are set as a baseline, with possibility to obtain higher manoeuvrability grading based on the ship's exceedance of those rules. Additional criteria are provided for course unstable ships, which have to limit their instability measured by the width of their unstable loop [21]. Finally, BV's Rules for the Classification of Steel Ships contains a chapter dedicated to ship manoeuvrability. The IMO Standards are copied, with a possibility for additional class notations granted to ships that demonstrate course keeping abilities in adverse conditions [56].

In addition to regulations on ship manoeuvrability, the steering gear characteristics are also regulated. The standards for certain parameters of the rudder machinery and its mechanical components can be found in SOLAS - the International Convention for the Safety of Life at Sea, enacted by the IMO in 1974. In the context of ship rudders, the document provides requirements for the rudder stock and machinery overall strength, rudder position indication, steering gear speed and redundancy of the steering gear power systems [2].

2.2. Gate Rudder research

The Gate Rudder, briefly described in the introduction, is a rudder concept that promises a range of significant advantages over a conventional rudder behind a propeller system. Those advantages, of which power savings are only one, caused it to be quickly reevaluated as much more than a simple energy-saving device it was initially considered [16], [36]. Fundamentally, the Gate Rudder System relies on removing the rudder blades from the propeller slipstream in free sailing conditions in order to increase propulsive efficiency and take advantage of the angled flow in the hull's stern in off-center zones in an attempt at recovering a portion of the energy losses caused by the hull moving through the water. At the same time, the ability to move the rudder blades into the prop slipstream when larger steering forces are required, for instance in tight turns or when manoeuvring, is maintained through the offset pivot points. As an additional benefit, the two rudder blades can be positioned independently, allowing for the manoeuvring modes mentioned in the introduction - the most significant one being the crabbing mode, which showcases the thrust-vectoring ability of the gate rudder through asymmetrical, drag-dominated obstruction of the propeller slipstream.

The advantages of the Gate Rudder System were described in the introduction. One of its features most attractive to shipowners is the reduction in power requirement of the ship and the resulting reduction in fuel consumption. Most research on the GRS is centered on this capability. The hydrodynamic mechanisms behind these power savings are not yet fully understood. Many studies investigating the power savings potential of GRS have been published to date, comprising of CFD analyses, model scale towing tank and manoeuvring basin experiments as well as full scale sea trials. Most of the publicly available research is conducted by the GATERS, an EU research project launched in 2021 as part of the Horizon 2020 programme. The results of the experiments conducted by GATERS show very promising performance of the Gate Rudder System.

2.2.1. Gate Rudder experiments

Initial CFD tests were conducted with the assumption that the Gate Rudder functions as a duct, producing thrust due to the acceleration of the flow between the rudder blades. The power saving capability was successfully demonstrated in these studies, which predicted that the difference between absorbed power could be approximately 7% lower when compared to a conventional rudder system. This finding was supported by towing tank tests conducted at the National Maritime Research Institute (NMRI) in Japan [16]. Similar results were found by a separate numerical study performed in the same year, which provided more insight into the setup as well as a broader analysis of the results [17]. Several other CFD analyses were conducted in the following years, investigating mostly different aspects of the Gate Rudder's hydrodynamics during freesailing. Usually, the conclusion were optimistic, but with the introduction of results from full-scale sea trials of Shigenobu and Sakura, two sister ships equipped with GRS and a conventional rudder system, respectively, it was revealed that the prior CFD and model studies did not match the real-life performance of the system - Shigenobu achieved power savings of up to 14% during sea trials when compared to Sakura. In addition to the power savings, it was reported that the responsiveness of the vessel to steering inputs was increased, and crucially, the resistance when steering in cruise speed was lower, meaning that the speed drop due to helm inputs was decreased [25]. The amount of data points recorded during sea trials and used in the paper to calculate the power savings was not very large, but similar results were later reported during other sea trials of the same ships as well as trials of another ship equipped with the GRS [41], [50]. Later reports from the ships' logbooks indicated that in service conditions, these savings are even higher, as high as 33%. No information was given whether the influence of instantaneous weather conditions were accounted for through corrections, nor was an uncertainty analysis performed. As seen in figure 2.10, the trendline for the Gate Rudder in service condition (in red) seems to only follow the on-board measurements taken by one of the authors of the paper while ignoring the rest of the data from the ship's log book, but the overall tendency of GRS to achieve higher speed at similar engine power is clear, at least if judged only by the data available in the plot.

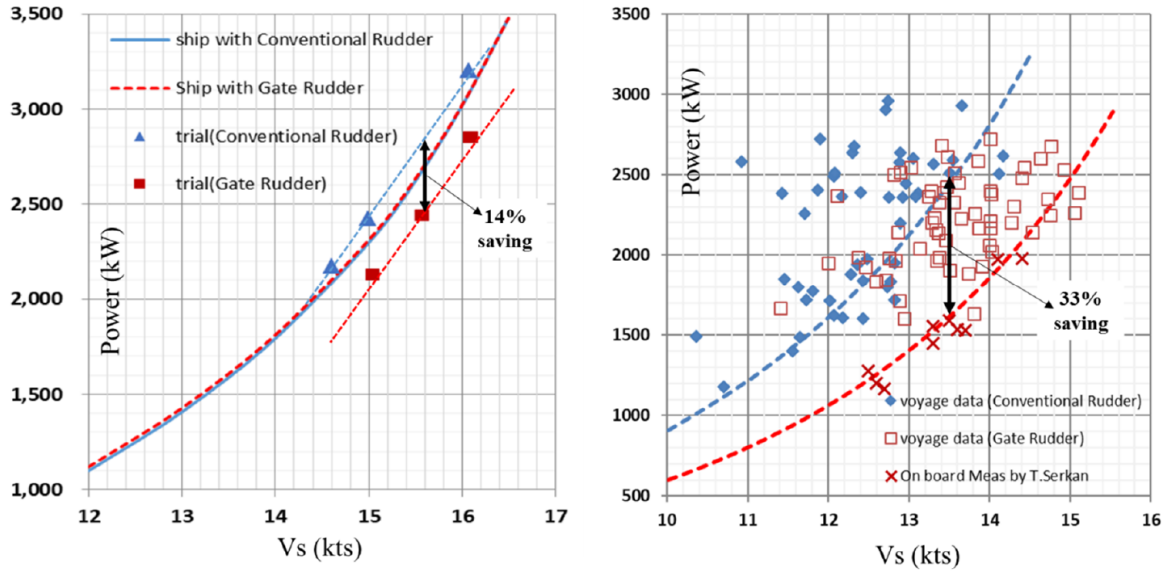

Figure 2.10: Comparison of full-scale measurements of the Gate Rudder and the flap rudder vessel performance during sea trials and service [36].

A theory was put forward that this discrepancy between full-scale performance of GRS and model experiments was caused by the scale effect of the gate rudder, where the Reynolds number in critical zones around the hull, indicative of the turbulence in the flow, was not represented correctly in scale tests. This resulted in inaccurate predictions of flow separation and boundary flow by the scale models, leading to inaccurate results. More importantly, this scale effect is noticeably more significant in case of the Gate Rudder in comparison to a conventional rudder [32]. Model tests and CFD analyses conducted to investigate this phenomenon showed inconsistent results, with a smaller scale model (Lpp = 2 m) overestimating the power requirement and a larger scale model (Lpp = 5 m) underestimating those values when compared to sea trials [37]. Very extensive CFD experiments carried out in 2021 for a 3 m model, a 6 m model and full scale vessel showed power savings in all investigated cases for speeds between 12 and 14 knots, with the magnitude of those predicted savings being the highest for the full scale study [45]. Interesting scale model tests performed in towing tanks by University of Strathclyde and Istanbul Technical University (ITU) for models of Shigenobu, Sakura and Erge ranging from 3.9 m (UoS) to 5.1 m (ITU) in length were published in 2022, both concluding that even in calm seas, power savings ranging from 2 (UoS) to 20% (ITU) are achievable with the use of the Gate Rudder for corresponding full-scale ship speeds of 11 to 13 knots, depending on the applied scale correction factors as well as load conditions [42], [47]. The model scale tests, however, will not be too relevant to the project, because its goal is to test manoeuvrability performance of the Gate Rudder in full scale.

In contrast to the optimistic results of CFD studies, some model experiments and full scale tests published by GATERS and associated institutions, the reported flawless performance of the Gate Rudder does not always seem to be reflected in the results of theoretical investigations conducted by outside organisations. According to various internal sources available within Wärtsilä, it is often the case that advanced CFD studies for specific ships as potential targets for retrofitting of GRS show no improvement in or even worse propulsive performance when compared to traditional rudder systems. The studies that showcased the negative impact of the Gate Rudder on ship's power requirements were mostly self-propulsion analyses for design speeds higher than those of the vessels that GATERS project published their results on. Unfortunately, these sources are confidential and cannot be published within this report.

In general, at the time of writing of this report, there is a lot of uncertainty with regard to the Gate Rudder's actual power saving performance and consequently, its viability as a product. It is not confirmed whether the differences between theoretical studies and real-life measurements are a result of improper methodologies or problems with data gathering. Similarly, it is yet unknown which parameters determine the applicability of the GRS. Test results seem to suggest that a ship's design velocity plays a large role.

Based on the available research, it is the author's conclusion that, despite not relying on the same hydrodynamic principles to decrease power requirements as a duct, the Gate Rudder suffers from decreased efficiency at higher speeds for the same reason as a duct - the increased frictional resistance on the larger surface area of the rudder blades, just like a duct, causes the overall efficiency of the system to decrease in higher velocities [23].

Another CFD study, published in 2022, focused on the optimisation of the design of GRS found that the rudder blades optimised for maximum thrust generation present inferior overall power saving performance compared to the blades optimised for highest power savings [44], which by themselves only negate drag due to the direction of the hydrodynamic

forces generated at zero position. They do, however, generate thrust when the hull is at a non-zero drift angle. This is likely the cause of the reduced steering resistance on the Gate Rudder experienced in sea trials.

2.2.2. Manoeuvring performance

The manoeuvring performance of the GRS was first studied in 2016, where CFD and model tests were used to create and validate a hydrodynamic model of the rudder based on the Manoeuvring Modelling Group (MMG) approach. In that paper, results of several standard manoeuvres, such as a turning circle or a zig-zag test, were presented, with good accordance between the simulation and model experiments. No comparison was made with a conventional rudder system, though [19]. These results were later expanded in another paper published in 2020, which presents a more in-depth development of the rudder's model, taking into account other studies published in the meantime. The model was based on an existing ship equipped with a Gate Rudder, Shigenobu - a Japanese domestic container vessel. Her sister, Sakura, equipped with a conventional rudder for comparison, was also modelled in the study. The results of the simulation with the model of both rudder types could therefore be compared to full-scale manoeuvring trials of the real-life counterparts and it was concluded that in most cases, the model represents the actual performance reasonably well. Additionally, interesting results from full-scale manoeuvring trials were presented. It was shown that in cruise speed manoeuvres (turning circle and zig-zag tests), the Gate Rudder produces lower steering forces than the conventional flap rudder. An example of such behaviour can be seen in figure 2.11, where the vessel equipped with a flap rudder performed a considerably tighter turning circle manoeuvre.

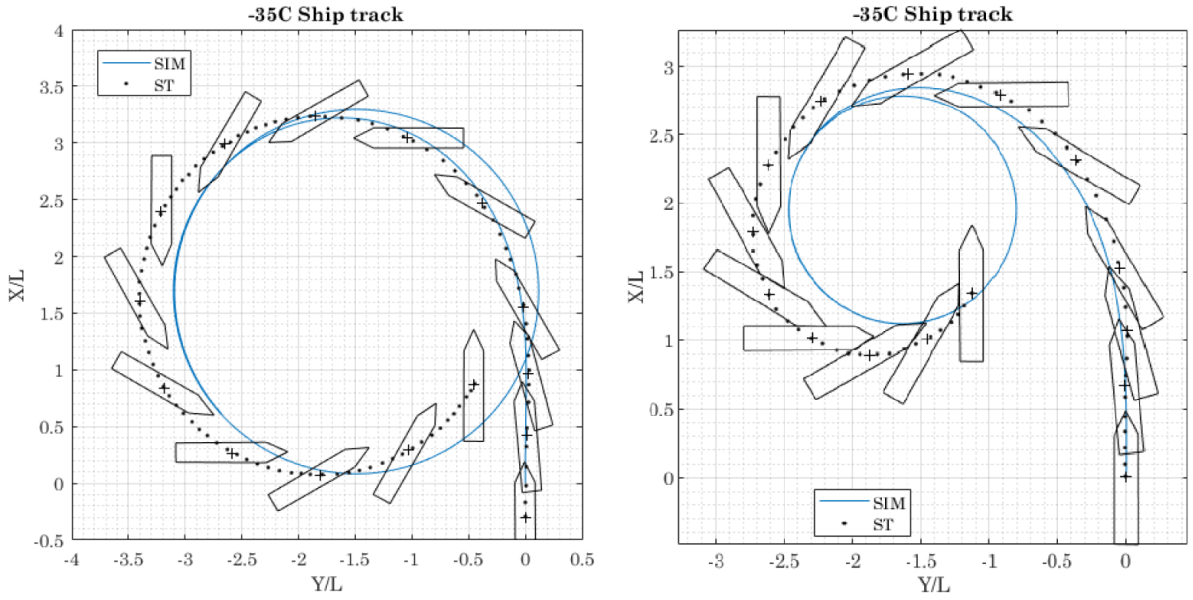

Figure 2.11: Comparison of full-scale measurements and simulation results of the Gate Rudder (left) and the flap rudder (right) vessels conducting the -35° turning circle test at 9 kn

On the other hand, the manoeuvring performance of GRS in low speeds was far superior to the conventional rudder. In the plot from the paper shown below, a comparison is made between the Gate Rudder's crabbing steering mode (110° PS and 60° SB) and the maximum feasible flap rudder angle of -70° [35]. The results showcase the advantage of the asymmetrical deflection of the blades enabling the superior manoeuvrability achievable through steering modes. As seen in figure 2.12, the vessel equipped with a gate rudder system performed a tighter manoeuvre than the vessel with the conventional rudder. Another observation from the plot is the fact that while the conventional rudder vessel surged forward at the start of the manoeuvre with only slight sway movement likely caused by propeller walk at low ship speed, the gate rudder vessel experienced stable sway movement immediately. This shows that a larger portion of the forces generated by the rudder system was directed to the side, indicating superior thrust vectoring capabilities.

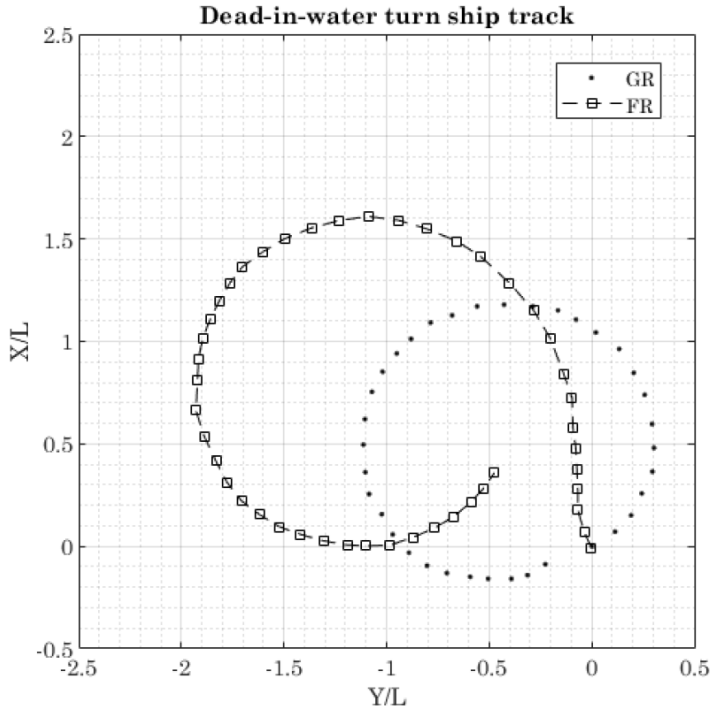

Figure 2.12: Comparison of full-scale measurements of the Gate Rudder and the flap rudder conducting the comparable maximum helm circle test from dead in the water

While the modelling of hydrodynamic forces and the resulting influence of the Gate Rudder on a vessel's motions was replicated relatively accurately, the study does not provide information on the applicability of the described model in powering predictions.

2.2.3. Potential challenges

There was no publicly available literature found that focuses on the disadvantages of the gate rudder concept. However, some potential drawbacks and challenges were identified over the course of this investigation into the state of research on the subject. In a manner similar in principle to ducted propellers, the added surface area might result in the increased frictional resistance overcoming any positive effects the system might have on the propulsive efficiency above certain ship design speeds, making it less suitable than a conventional rudder. Another potential disadvantage of GRS is the fact that the increased steering forces stemming from the deflection of the propeller slipstream only occur at high helm angles, limiting the dynamic responsiveness of a vessel in tight low speed manoeuvres due to the time it takes for the rudder blades to rotate from side to side. Additionally, because of the complexity of the Gate Rudder operation and the fact that the two blades can move independently, the most optimal control of the system might be too complicated for a human to manually operate. Instead, a smart steer-by-wire system would likely need to be implemented to get the most out of the concept, which might require a higher investment. What also raises the cost of installation is the need for two separate steering gear systems.

2.2.4. Conclusion on Gate Rudder research

It is clear that the Gate Rudder is a hydrodynamically complex device that requires further research to determine the mechanism behind reported efficiency gains and find its area of applicability. Due to conflicting data between full scale and model experiments, as well as numerical studies, especially due to the scale effect that introduces uncertainty in model scale tests, its viability as an energy saving device in freesailing conditions is not fully confirmed. Additionally, the majority of publicly available research was conducted by the same community. The amount of fully independent research published is limited. It would create more confidence in the concept if other industry experts published about the novelties related to this rudder system.

Both low speed as well as cruise speed manoeuvres were identified as areas through the elaboration of which the overall understanding of the gate rudder could be expanded. Judging from full scale test results, the increased low speed manoeuvrability could provide potential fuel and time savings when docking and undocking in ports, in addition to the enhanced control over the vessel and decreased need for tug assistance. At the same time, improved cruise speed manoeuvring characteristics could enable potential for fuel savings in real life operational conditions due to decreased steering resist-

ance and enhanced ship responsiveness to steering inputs, as seen in the reports from the sea trials and operational data of Shigenobu.

2.3. Ship motion modelling

In order to determine a ship's performance in specific situations without opting for expensive and time consuming full-scale trials, theoretical investigations can be conducted instead. To achieve this, a ship's model is needed, which mimics the real-life counterpart in desired qualities sufficiently accurately. This model can be a physical, scaled down version of the hull intended for use within a towing tank or a model basin, a digital mesh of points used in numerical studies, or a purely virtual input-output system of mathematical equations. In ship manoeuvring analyses, mathematical models usually serve as the tools used to predict the ship's motion.

2.3.1. Ship motion equations

Mathematical modelling of a ship's motion can be done in different ways. Some methods include integrated models based on the Taylor expansion to simulate the hydrodynamic loads on the hull, models based on the Manoeuvring Modelling Group which separate the hull, propeller and rudder and take account for their interactions, as well as various sorts of grey- and black-box models based on system identification algorithms [33]. Some physics-based methods typically involve an equation of motion, which describes the vessel's response to the forces acting on the hull. In manoeuvring simulations, usually only three degrees of freedom are taken into account, those being the surge, sway and yaw movements (planar motion). Therefore, the fundamental forces that influence a ship modelled in this way are the longitudinal force (X), the transverse force (Y) and the yaw moment (N). Apart from the hull form, the characteristics of the propulsion system and the rudder, and the environmental conditions, which are treated as inputs to the simulation, these forces depend primarily on the ship's velocities and accelerations in the same directions (surge, sway and yaw), the thrust from the ship's propellers and side thrusters, if installed, and the rudder angle, which are treated as simulation parameters. Additionally, large heel angles (typically above 10°) can influence these relations, but such conditions usually occur only in fast ships. In the most basic form, the motion equations take the form of a system of equations describing the effect of forces on the ship's acceleration:

$$\begin{cases} m(\dot{u} - vr) = X \\ m(\dot{v} + ur) = Y \\ I_{zG}\dot{r} = N \end{cases} \tag{2.1}$$

where u, v and r are the ship's velocities in surge, sway and yaw direction, m is the vessel's mass and I_{zG} is the moment of inertia of the ship around its center of gravity.

Different approaches to computations of body forces in the equations of motions have been developed. The most basic method is to use regression formulae based on the slender body theory, accompanied by empirical coefficients derived from model experiments. More direct and robust methods involve numerical studies. They can be grouped into the following categories, ordered by increasing degree of complexity:

- Lifting surface methods - these methods model the inviscid flow about a plate basing on the principles of potential flow, and taking into account various fundamental conservation laws and a superposition of boundary-simulating horseshoe vortices, according to the Kutta-Joukowski theorem.
- Lifting body methods - expansion of the previous methods through the introduction of finite body thickness.
- Field methods - RANS simulations of the viscous flow field about the hull, some taking into account the free surface effects. Very demanding in terms of computational resources, require complex turbulence models for full scale flow simulation.

Full manoeuvring simulations do not use numerical force evaluation methods, because they would be impractical due to computational demands. Therefore, the simplified, but much quicker methods based on the slender body theory are used. As mentioned, they require various coefficients to account for the effects of the above mentioned factors as well as coupling between degrees of freedom. These coefficients are numerous, and the accuracy of the simulation results depends on how well they reflect the ship's actual characteristics. While some of them can be calculated from formulae based on known relationship with other ship parameters, most of them need to be obtained from model tests and/or CFD simulations. Typically, they are determined using specific manoeuvres, such as those specified by the IMO and described in section 2.1.3 [13].

2.3.2. Rudder mathematical modelling

The goal of aero- and hydrodynamic control surfaces is to efficiently generate lift forces, that is, at minimum added drag. This lift force can then be used to control the motion of a vehicle. Rudders in sea-going vessels are a type of control

surfaces and any analysis of them will therefore have these forces as the main point of interest. The classic mathematical expressions describing the forces generated by a control surface are the following:

$$\begin{cases} L = 0.5 C_L \rho A U_0^2 \\ D = 0.5 C_D \rho A U_0^2 \end{cases} \tag{2.2}$$

where A denotes the planform (projected) area of the foil, U_0 is the inflow velocity of the fluid, ρ the density of the fluid and C_L and C_D the coefficients of lift and drag, respectively. While the rest of the parameters are easily obtained using design data and sensors (in case of real-life calculations) or motion data (in case of simulations), these lift and drag coefficients pose the biggest challenge for accurate force predictions - they depend on a lot of variables, not only related to the design of the foil, but also on the angle of attack and flow characteristics, like the Reynolds number (Re). Lift and drag coefficient curves may be created for an individual foil as functions of the angle of attack using numerical or experimental measurements, assuming operation within normal conditions. Naturally, though, this approach does not take into account the variation of velocity along the leading edge of the wing, which is often the case in marine rudders due to propeller slipstream and hull wake [8]. Nonetheless, such regression-based, semi-empirical models are a popular modelling method for ship rudders mainly due to the computational efficiency they feature.

Another approach to the modelling of foils in fluids is the lifting line method, first introduced by Ludwig Prandtl in 1918. It models the wing as a span-wise line, along which the wing's cross-sections are modelled as circulation-inducing vortices, with potential flow principles as basis for the system of equations. Typically, the method requires numerical solutions and produces accurate results up to the stall angle of attack [52]. Similarly, lifting surface and lifting body theories, described in the previous section, may also be used to calculate the lift and drag forces on a wing, with increasing computational demands. When high fidelity results are necessary, RANS-based CFD studies can also be performed, at high computational cost. They are typically employed in industrial applications.

A group of methods that utilize a completely different approach to the treatment of the rudder as a system of inputs and outputs and their dependencies are data-driven methods (DDM). These methods, which rely mostly on artificial neural networks or machine learning algorithms, have received attention in the recent years in numerous fields of science and technology and use historical observations to build models of underlying phenomena without any knowledge of physics behind them. While they can be computationally expensive during the model creation phase, the resulting prediction models are very efficient. Their accuracy depends heavily on the quality of the input data and while the general trends can be represented with high precision, such algorithms are known to provide physically inconsistent results in some cases [54]. Such models are sometimes referred to as black-box models, because they are, by nature, not transparent. In other words, the way they process the inputs to produce outputs is done so in a non-interpretable way, which prevents easy modifications or analyses of errors. One such algorithm was used to successfully create and validate a fuel consumption prediction model of a ship equipped with a Gate Rudder System [43]. Because this modelling approach was deemed prospective, a more detailed look into machine learning is presented in section 2.4.

A concept that combines the advantages of physics-based models and data-driven models is called a hybrid model. They use the physics-related knowledge to "guide" the data-dependent algorithm in order to deliver physically plausible data [54]. This approach reduces the necessary amount of data while potentially increasing the fidelity of the results when compared to pure black-box models [24].

2.3.3. Manoeuvring Modelling Group - MMG

A popular ship motion modelling approach has been developed in Japan in 1977 and expanded over the years. Named Manoeuvring Modelling Group after the research group it was introduced by, it has since been standardized and used in many practical applications. It is based on the slender body theory method mentioned in the previous section and operates on the following assumptions:

- The hull acts like a rigid body.
- Hydrodynamic forces acting on the ship are treated quasi-steadily.
- Lateral velocity component is small compared with longitudinal velocity component
- Ship speed is not fast that wave-making effect can be neglected
- Metacentric height GM is sufficiently large, and the roll coupling effect on manoeuvring is negligible.

These assumptions are therefore well suited towards simulating low-speed manoeuvres of displacement vessels. The base for the equations of motion is the same as in equation 2.1, albeit with slightly reorganized symbols. The equations are then expanded to form the following main motion equations:

$$\begin{cases} (m + m_x)\dot{u} - (m + m_y)v_m r - x_G m r^2 = X_H + X_R + X_P \\ (m + m_y)\dot{v}_m + (m + m_x)ur + x_G m\dot{r} = Y_H + Y_R \\ (I_{zG} + x_G^2 m + J_z)\dot{r} + x_G m(\dot{v}_m + ur) = N_H + N_R \end{cases} \tag{2.3}$$

where m_x and m_y denote the added mass in x and y directions, respectively, v_m is the lateral velocity at the midship point, x_G is the longitudinal coordinate of the ship's COG, the subscripts H, R and P next to the forces X, Y and moments N denote their source as hull, rudder and propeller, respectively, and J_z is the added moment of inertia. This formulation neglects the added mass coupling terms with respect to v_m and r. The main point of interest in the model is how the different forces are modelled. For instance, the hull forces are expressed as follows:

$$\begin{cases} X_H = 0.5\rho L_{pp} d U^2 X'_H(v'_m, r') \\ Y_H = 0.5\rho L_{pp} d U^2 Y'_H(v'_m, r') \\ N_H = 0.5\rho L_{pp} d U^2 N'_H(v'_m, r') \end{cases} \tag{2.4}$$

where U is the velocity magnitude, v'_m denotes non-dimensionalized lateral velocity defined by v_m/U, r' is the non-dimensionalized yaw rate by rL_{pp}/U, X'_H is expressed as the sum of resistance coefficient R'_0 and the 2nd and 4th order order polynomial function of v'_m and Y'_H and N'_H are expressed as the 1st and 3rd order polynomial function of v'_m and r', as following:

$$\begin{cases} X'_H(v'_m, r') = -R'_0 + X'_{vv} v'^2_m + X'_{vr} v'_m r' + X'_{rr} r'^2 + X'_{vvvv} x'^4_m \\ Y'_H(v'_m, r') = Y'_v v'_m + Y'_R r' + Y'_{vvv} v'^3_m + Y'_{vvr} v'^2_m r' + Y'_{vrr} v'_m r'^2 + Y'_{rrr} r'^3 \\ N'_H(v'_m, r') = N'_v v'_m + N'_R r' + N'_{vvv} v'^3_m + N'_{vvr} v'^2_m r' + N'_{vrr} v'_m r'^2 + N'_{rrr} r'^3 \end{cases} \tag{2.5}$$

where X'_{vv}, X'_{vr}, X'_{rr}, X'_{vvvv}, Y'_v, Y'_R, Y'_{vvv}, Y'_{vvr}, Y'_{vrr}, Y'_{rrr}, N'_v, N'_R, N'_{vvv}, N'_{vvr}, N'_{vrr}, N'_{rrr} are called the hydrodynamic derivatives on manoeuvring. These derivatives consist of many non-linear terms which are hard to obtain at a decent level of confidence, while usually not contributing to overall results significantly. When possible, they are therefore neglected, leaving only the linear terms. One such case when the non-linear terms make a significant contribution to overall hull forces is in scenarios where large yaw rates are expected [3] - this, therefore, does not concern investigations into manoeuvres of cargo ships.

The forces on a conventional rudder in the MMG model are calculated using comprehensible formulas:

$$\begin{cases} X_R = -(1 - t_R) F_N \sin\delta \\ Y_R = -(1 + a_H) F_N \cos\delta \\ N_R = -(x_R + a_H x_H) F_N \cos\delta \end{cases} \tag{2.6}$$

where F_N is the rudder normal force, t_R is the steering resistance deduction factor, which accounts for rudder resistance deduction and propeller thrust increase induced by steering, a_H is the rudder force increase factor, which accounts for the flap effect on the hull and x_H is the position of the additional lateral force component where the force induced by the flap effect acts. The rudder tangential force is neglected. Yasukawa et al. provide further derivations for all the coefficients that make up the calculation of steering forces [18].

As previously mentioned in section 2.2, a manoeuvring model of the Gate Rudder System based on the MMG model was developed by Carchen et al., where the equation 2.6 was adapted for GRS force prediction:

$$\begin{cases} X_{RP} = -(1 - t_R) F_{NP} \sin\delta_P \\ X_{RS} = -(1 - t_R) F_{NS} \sin(-\delta_S) \\ Y_{RP} = -(1 + a_{HP}) F_{NP} \cos\delta_P \\ Y_{RS} = -(1 + a_{HS}) F_{NS} \cos(-\delta_S) \\ N_{RP} = -(x_R + a_{HP} x_H) F_{NP} \cos\delta_P \\ N_{RS} = -(x_R + a_{HS} x_H) F_{NS} \cos(-\delta_S) \end{cases} \tag{2.7}$$

where the P and S subscripts correspond to coefficients and parameters related to the portside and starboard side rudder blade, respectively. The equations derived in the paper served as the base for the physics-based model developed in the first part of the execution phase of this project. The relevant formulas and the implementation of the model in a time domain simulation software are described in detail in section 4.1.

2.3.4. Validation and test cases

In scientific research on marine engineering, a popular method of validating computer models of ships is the use of common hull geometry. Previously obtained research data, which was verified to be accurate and is publicly available, can be used by researchers to check their ship motion and flow models or compare results. There are several such benchmark ship hulls, with some of the most popular being the KCS, KVLCC and DTMB 5415 - a medium container carrier, a large tanker and a navy vessel, respectively, introduced by the Korea Research Institute of Ships and Ocean engineering during the 2008 Workshop on Verification and Validation of Ship Manoeuvring Simulation Models (SIMMAN 2008). KVLCC was designed with two versions of the stern shape, named KVLCC 1 and 2, which have slightly different hull lines [12]. Another popular benchmark ship is the S175, a medium-sized container carrier, introduced by the ITTC in 1978 [14]. The main characteristics of the benchmark cargo ship hulls introduced above are presented in the following table:

	Lwl [m]	Lpp [m]	B [m]	T [m]	V [kn]	D_P [m]	A_R [m2]
KCS	232.5	230	32.2	10.8	24	7.9	54.5
KVLCC 1&2	325.5	320	58	20.8	15.5	9.86	136.7
S175		175	25.4	9.5		6.51	32.46

where V is design speed of the vessel, D_P is the diameter of the propeller and A_R is the projected rudder area.

2.4. Machine learning in engineering problems

Machine learning is a field of computer science which focuses on building an algorithm that relies on examples of a phenomenon to find relationships between them. Within the scope of supervised machine learning, which is the type of machine learning relevant to this project, a collection of such examples is called a dataset. In the dataset, every example takes the form of a pair of elements: a vector serving as the description of the example, called a feature, and a label, which can be a number, a class element or, in some less common cases, a more complex structure. The goal of supervised machine learning is to construct a model of relations between the features and the labels in a process called training. Once a model is trained on a sufficiently general dataset, it can be used to make predictions of labels based on an input in the same form as the features it was trained on.

2.4.1. Main applications

Typical uses of machine learning can be divided into classification and regression. Classification is a type of problem where a label (or a 'class') needs to be assigned to an example from a known list of classes. An easy to understand classification example is spam detection, which is typically a model that parses over the content of an email and assigns a probability of the message being an unwanted one. Regression, on the other hand, is a problem where the goal is to predict a value when given an example. A model that predicts house prices based on their location, number of bedrooms or the neighborhood is an example of a regression model. Because regression is the type of machine learning relevant to the project, classification was not further investigated in this study [29].

2.4.2. Data preprocessing

In order to create a machine learning model, a machine learning algorithm has to be used, which is a method of interpreting the provided examples and their labels in order to find dependencies in the analyzed data. Various algorithms differ in terms of problem applicability as well as speed of model building and prediction processing. They may also have different requirements for the form of the dataset. The preparation of the dataset prior to it being used to train the model is called preprocessing and can cover a range of different tasks with many goals, with compliance with the particular algorithm's requirements being one of them. Some of the most important preprocessing steps include data cleanup, feature scaling and division into sets. Data cleanup is the process of removing irrelevant, inaccurate or corrupt data from a dataset, typically performed on larger sets with a high degree of noise and measurement errors. Feature scaling is the process of bringing all features to similar orders of magnitude and/or distributions - this might lead to the model performing better, but it is not a guarantee. The use of feature scaling is typically considered good practice, and can be divided into normalization and standardization, with the former being the act of mapping the feature values into artificial ranges of values, such as [0, 1] with predefined rules, while the latter being the process of scaling the features so that they have the properties of a standard normal distribution around the mean value of 0 [34]. Typical examples of normalization methods are the min-max scaling, where the feature values are linearly mapped to a range of [-1, 1] (with -1 and 1 corresponding to the minimum and maximum values of each feature, respectively), and max-abs scaling, where the values of each feature are divided by the maximum value of that feature. Finally, division into sets is a step during which the dataset is split into subsets called the training set, the test set and the holdout set. The training set, typically comprising of the majority of the dataset, is used to build the model. Afterwards, the test set serves as a way to check the performance of the model when met with data it has not seen before. The holdout set can be then used at the final stage as a "sanity check", to make sure that the model identified as the best performing out of the tested ones is not just a coincidence. The split into these sets can be performed in a specified, predetermined manner, or randomly. After the split is performed, the data in each set is typically randomly shuffled to prevent bias during training [11], [29].

2.4.3. Algorithm hyperparameters

A lot of algorithms have different sets of hyperparameters, which are parameters that control the learning process and determine the values of model parameters an algorithm may end up with during training. The values of hyperparameters can be assigned manually or tuned to find the best set of hyperparameters for a given situation. The simplest tuning method is a grid search, which takes in a list of hyperparameter values and loops over each combination of them to produce a list of models. From that list, the best performing model is found, along with its list of hyperparameters best suited for the

task. Examples of other tuning methods, better suited for larger ranges of hyperparameter values or/and larger datasets, are random search and Bayesian hyperparameter optimization [29].

2.4.4. Examples of regression algorithms

There exists a large number of regression algorithms, each with its own typical applications. In this subsection, some examples of such algorithms will be provided.

The simplest regression algorithm is an ordinary least squares linear regression, which fits a linear model with a coefficient for every element in the feature vector. In a single element feature vector scenario, it could be imagined as a model that fits a line through the available datapoints through a process of minimising the squared error loss function. This algorithm does not have any tunable hyperparameters [11].

A way to improve the simple linear regression is the introduction of regularization. It is a range of methods that prevent a model from becoming too complex, in order to avoid a phenomenon called overfitting, which occurs when a training process causes the model to try to predict the training samples too perfectly, causing it to make poor predictions on test samples. The most often used types of regularization are L1 and L2 regularizations, which modify the objective function (the loss function in case of the linear regression) through the addition of a penalizing term, that gets higher as the model's complexity increases. A linear regression algorithm that uses the L1 regularization, which can be boiled down to the determination of which feature elements are essential for predictions, is called a lasso. Algorithms that use the L2 regularization type are called ridge regressors. A typical hyperparameter of algorithms with regularization is α or alpha, which denotes the regularization strength [11], [29].

When dealing with non-linear problems, some regression algorithms can use what's called a kernel trick. It is a method of transforming the data into a space of an implicitly higher dimension in order to find dependencies of higher orders. For example, kernel ridge regression is an expansion of the ridge regression algorithm that utilizes this functionality. Its hyperparameters consist of α, because it also uses L2 regularization, but also other parameters that are native to the chosen kernel. Among the typically used kernels is a polynomial kernel, which causes the algorithm to try to assign a polynomial curve to the datapoints (the degree of the polynomial can be specified by an additional hyperparameter), a radial basis function (RBF) kernel, or a sigmoid kernel. All of the mentioned kernel types share a hyperparameter γ or gamma, which typically is used in different ways by each of them [29].

A different kind of an algorithm also used to model non-linear phenomena is support vector regressor (SVR), which is a regression variant of a support vector machine (SVM). It is a complex algorithm that builds a model only taking into account support vectors, which are samples from the training dataset that lie outside of a target margin (specified by the tolerance hyperparameter ε or epsilon), which were identified by the algorithm as the most critical in defining a hyperplane that lies within that margin as much as possible. Like the kernel ridge algorithm, it can also use the kernel trick, which means that its hyperparameters also consist of those bound to the chosen kernel type. Additionally, it also uses L2 regularization, and therefore uses a hyperparameter C, denoting the strength of regularization [11], [29].

A completely different type of a regression algorithm is a decision tree regressor. Models built using this algorithm predict labels through the use of a set of decision rules derived from the training data. The depth of the decision tree, or the amount of consecutive decisions made during the prediction process, can be specified using a hyperparameter. An expansion of the decision tree regression algorithm is a random forest regressor, which fits a number of decision tree regressors on various sub-samples of the dataset and averages their outputs to improve predictive accuracy [11].

Another example of a different algorithm is k-nearest neighbours, or kNN. Its regressor variant is an algorithm that does not discard the training data during the construction of a model, and later uses samples similar to the provided example to predict the label through averaging of the labels of those selected samples. The amount of similar samples, their weights and the method with which the model identifies similar samples can be determined through hyperparameters [29].

Majority of regression algorithms learn the model parameters directly from the features of the training dataset. Algorithms that do not follow this behaviour are deep artificial neural networks, which are algorithms that form a model consisting of a nested function relating the features to the labels. The depth of these nested function depends on the amount of layers in the network. Without going into too much detail, the algorithm finds the best parameters for the nested functions through the optimization of a selected cost function. Typically, artificial neural networks require a large number of samples in the training dataset to make accurate predictions [22].

2.4.5. Model evaluation

Proper choice of a regression algorithm and its hyperparameters can ensure that the resulting model will perform well when predicting labels for the training dataset features. However, it is its performance on samples from the test set that the model has not experienced yet that ultimately determines its ability to capture the problem, or whether it can be called a 'good' model or not. This performance of a model can be quantified using a number of methods and metrics. This subsection provides examples of metrics typically used to judge a regression model's quality [29].

One of the most widely used performance metrics of any statistical models is the coefficient of determination, or R^2. It is an intuitive measure of how well the regressor predictions approximate real data points. Its values are independent of the data and typically range from 0 to 1, where a value of 1 indicates a perfect fit.

A popular method of evaluation of regression models is by means of the root mean square error or RMSE. It is a measure of differences between the true values and those predicted by the model. Values of RMSE depend on the data used, but they are always non-negative and can range from 0 to infinity, where a value of 0 indicates a perfect fit. Compared to R^2, RMSE is more sensitive to outliers, because larger deviations from ground truth have a disproportionately large effect on its value.

Mean absolute error is another example of a popular evaluation metric for regression models. It is a measure of error between predicted and actual values from the dataset [11]. In regression analysis, it is a measure similar to RMSE, with the difference lying in the type of average across the tested samples.

2.5. Ship motion simulation in time domain

As mentioned at the conclusion to section 2.2, ship manoeuvres in either low speed or cruise speed were selected as one of the areas Gate Rudder advantages could be demonstrated. This is why a time-domain ship motion simulator was selected as the type of software that could serve as an ideal tool to test the Gate Rudder system in such conditions.

2.5.1. The concept of time domain simulation

To obtain detailed information about the flow field around a vessel in a specific scenario, typically RANS-based CFD calculations are employed. However, when the efficiency of the calculations in more complex scenarios is the priority, while the required level of fidelity is less important as long as sufficient reproduction of ship behaviour is achieved, time domain simulations can be employed. Typically, time domain simulators can be characterised by their approach to time-stepping, which is usually dictated by their purpose:

- Real-time simulators are predominantly oriented towards seafarer training, where the motions of a vessel, together with its graphical representation need to be calculated several times per second in order to maintain a sufficiently realistic depiction of the simulated conditions. Similarly, the program needs to react in a timely manner to steering inputs of the trainee. These requirements mandate a comparably small time step of the calculations. Fidelity of the motion is usually sacrificed for the speed of the motion updates so that the program can keep up with real time.
- Fast-time simulators are typically suited for scientific studies of vessel motions at early development stages, such as when compliance with regulations needs to be checked. Scenarios are pre-programmed, and the main focus is put on the vessel's trajectory as well as other voyage parameters, for example the characteristics of a turning circle manoeuvre. As such, the simulation does not need to keep up with real time. This means that the time step can be much larger, which usually results in the simulations being completed much faster than the flow of time within them, hence the name, but contrary to one's intuition, it does not have to always be the case. The level of fidelity is typically higher than in real-time simulations.

One of the most computationally demanding tasks of calculating a ship's motion is the determination of the hydrodynamic forces acting on its hull. Time domain simulators typically go around this procedure by employing pre-calculated tables of resistance forces for different flow velocities and drift angles. This method sacrifices the accuracy of the results in exchange for a significant boost in the efficiency of calculations. Other forces, such as those generated by the propulsion or steering systems, are calculated "on the fly" during each time step, using simplified empirical formulas.

For the purpose of the project, two pieces of time-domain ship motion simulation software will be investigated. The first of them is ManWav, a fast-time ship motion simulator developed by the CRS group, designed for product development and assessment in the context of manoeuvrability. The other is Navi-Trainer Professional developed by Transas, a Wärtsilä subsidiary. By design, NTPro is a real-time simulaiton platform destined for training of ship officers, but it offers the possibility to switch to fast-time calculations for vessel manoeuvring evaluation. While there are other options available on the market, they were not considered, because they would either require an investment from the company, or they would require too much time and effort to be deemed viable for the project at hand. The following subsections will explore the two simulators in more detail.

2.5.2. ManWav - manoeuvring assessment program

Wärtsilä is a part the Cooperative Research Ships (CRS) group, which is a research organisation made up of companies and institutions from the maritime engineering sector, established in 1969. It conducts research projects from the field of ship resistance, seakeeping, marine propulsion, ship safety and more. One of the projects conducted by CRS was ManWav, which involved the development of a software used to evaluate manoeuvrability of ships. The result of the project is a

Matlab script that uses structured ship resistance and propulsion data in order to determine its performance in a predefined set of manoeuvres in chosen weather conditions. Due to the script-based nature of the software, it can be easily expanded through the addition of custom models and other functionalities in the form of Matlab functions/scripts.

The structure of ManWav is comprised of several scripts and functions that enable the simulation of ship motions in manoeuvres. After some corrections to enable the software's functioning on an example ship, the detailed order of actions executed by the program was studied. First, after a setup of the working directory, input files and the data structures, the ship data is loaded. It comprises of a collection of files, each containing different characteristics of the vessel:

- an MPP .ini file that contains general information about the ship, such as hull geometry parameters, speed/resistance curve to be used by ManWav, rudder and propeller positions as well as related parameters and open water characteristics,
- a .raodb.ini database containing the pre-calculated hull motion data and variable frequency wave loading characteristics at different velocities of the vessel under a given load condition, obtained with PRECAL_R or FATIMA numerical seakeeping assessment programs (of which the former is also available to CRS members),
- an MPP hull forces .txt file and an MPP linear coefficients .ini file, which contain hull forces and moments data at different drift angles and yaw rates, obtained from MPP (Manoeuvring Prediction Program, developed by MARIN, available to CRS members),
- an .mw2.ini configuration file, which specifies which of the available, above mentioned files are to be used, as well as provides ship air resistance and rudder control settings,
- an Excel sheet containing the list of desired manoeuvres and their parameters to be executed by the program [31].

These input files are then used to calculate the vessel's motion and other characteristics of the ship when performing the desired set of manoeuvres. To do this, ManWav solves the ship's equations of motion on each time step, while calculating all the forces acting on the hull, such as the propeller thrust, rudder forces or wave and wind loading. For the purpose of this project, a closer look was taken at the way the script calculates the forces generated by the rudders and how they interact with the hull and the propellers.

The rudder forces are calculated for every time step of the simulation. There are two rudder models available, both based on the MPP theory manual - basic, which employs a more simplistic approach to the calculation, following the procedure described in chapter 6 of said manual and taking into account less parameters, and a more advanced MPP model, which follows the same rudder force evaluation procedure used in chapter 7 of MPP theory manual. Both are using a regression-based semi empirical model, which employs a single lift and drag coefficient pair for the entire rudder, averaging out the flow parameters.

In the basic model, the inflow velocity vector is calculated in a simplified way, taking into account the propeller slipstream as a linear function of propeller outflow velocity with a single coefficient, which is then added to the local flow velocity due to ship motion, reduced by the local wave velocity. The rudder force vector is then calculated using a simple lift equation, using the previously established inflow velocity and angle, the rudder angle as well as the rudder's lift coefficient (calculated as a linear function of the angle of attack), lift to drag ratio and surface area, given as parameters.

In the MPP model, more effects are taken into account. If the rudder is not located within the propeller slipstream, the hull's wake fraction is taken into account to calculate the inflow velocity vector. When inside the propeller slipstream, a flow straightening coefficient is employed. For transverse velocity, the relative flow velocity due to ship motion is corrected by rotational and drift coefficients (C_{dr} and C_{db}, respectively) through the use of a rudder-specific coefficient and constant factors, depending on the rudder's position in relation to the ship's centerline. Hull's roll motion is also accounted for. The lift and drag forces are then calculated for constant rudder-specific lift and drag coefficients and adjusted to the hull's coordinate system through a non-linear function of lift, drag and the angle of attack. The MPP rudder model also enables the use of different rudder types, such as a Schilling rudder or a flap rudder [40].

The structure of ManWav necessitates the use of a predetermined set of manoeuvres to be executed by the vessel under investigation, in the form of an excel sheet, where the data such as the type of the manoeuvre, vessel speed, rudder control parameters and accompanying environmental conditions are to be determined by the user. The program then iterates over each of the manoeuvres from the list. The available manoeuvre types for ManWav 2.6.2 (current version at the time of writing) are listed below. Since no available documentation describes these options in any detail, their rough meaning was determined through the study of source code of the program.

- Turning circle - standard turning circle manoeuvre, as described in section 2.1.3. The target rudder angle is set by the input excel sheet.
- Zig-zag manoeuvre - standard zig-zag manoeuvre, as described in section 2.1.3. The target rudder angle and heading are set by the input excel sheet.
- Seakeeping - ship seakeeping tests, in which the program evaluates the vessel motion under a desired PID-based autopilot setting. The available autopilot seakeeping options are the following:

  - Heading keeping
  - Course keeping
  - Heading and track keeping
  - Course and track keeping
- Heading recovery manoeuvre - seemingly not implemented. Instead, a turning circle is executed.
- Rudder sweep - test of forces on a static ship hull for a range of rudder angles, oscillating according the a sine function from zero to the target rudder angle set by the input excel sheet.

Included with the software is a database containing a few example vessel types, for which input files compatible ManWav files are available. Examples consist of a small bulk carrier (Lpp = 85 m), a cruise ship (Lpp = 270 m), a large container carrier (Lpp = 355 m), a medium container carrier (Lpp = 203.8 m), DTMB 5415 Korea Research Insitute of Ships and Ocean Engineering (KRISO) navy surface combatant ship (Lpp = 142 m) and a benchmark S-175 container ship (Lpp = 175 m). The program was successfully tested on all of those example models, after slight adjustments to certain parameters in the default .ini files.

2.5.3. Transas software

Transas is a subsidiary of Wärtsilä specializing in marine navigation solutions, as well as training and simulation services [27]. In the company's portfolio are several pieces of software, most notable of which in the context of this project is Navi-Trainer Professional (NTPro) suite, a navigational simulator developed for training officers and captains serving on ships. By design, it is a real-time simulation software that has an option of switching to fast-time calculations. The software consists of several modules which enable the functioning of its multitude of features, one of which is Model Wizard, a package meant for the development of ship motion models, ship visual models, environment scenes and other related models used in NTPro. The component of Model Wizard responsible for management of the ship motion model is called Virtual Ship Yard (VSY). It enables the user to develop and modify the ship model as well as scenario characteristics. Due to the closed-source, executable nature of the program, the detailed structure of the program's functions could not be fully studied. However, source code related to the way forces on rudders and propellers are modelled was provided for the purpose of the project, therefore a sufficient comparison between the available ship motion simulators evaluated in this phase of the project could be made.

VSY relies on sophisticated pre-built motion models of ships to function. They consist of collections of ship parameters, correction factors and lookup tables for variables, such as the propeller thrust coefficient KT in relation to the advance ratio J. These parameters are divided into modules corresponding to the ship's systems, like the propeller, rudder, the engine or their control systems. These modules can be set to interact with each other, so as to reflect the interaction effect e.g. between the rudder and the propeller. Such a model is built for every ship on an individual basis and tuned by the developers to reflect the real-life counterpart. If the existing collection of modules and their tunable parameters does not reflect the needs of the user, custom modules can be created in the form of scripts written in the Python 2 programming language.

The program allows the user to define the investigated scenario in detail. A vast array of predefined manoeuvres are available, including the standard ones such as the turning circle, the zig-zag manoeuvre etc. Their parameters can be configured. It is also possible to define custom scenarios, with various settings for waves and wind loads as well as the depth.

The software employs a relatively simple rudder model, based on a regression-based semi empirical model, except notably less complex than the one encountered in ManWav. The calculation of forces is based on the standard lift and drag equations (2.2), with the lift and drag coefficients values extracted from the lookup tables in the input ship model, based on the inflow parameters. To better reflect the performance of different rudder types available in the program by default, such as a standard balanced rudder, a Schilling rudder (fish tail) or a Becker rudder (flap rudder), slight deviations to the calculation procedures are implemented in their respective functions [49].

A very large database of ship models created specifically for VSY exists. Available models range from small high-speed military craft to large cruise ships and tankers. The database access was provided for the project, with 24 individual cargo ship models made available at request after a brief selection process to single out prospective ship types. The list of ship models requested consists of 6 bulk carriers, 1 cement carrier, 3 chemical tankers, 2 coastal tankers, 4 container ships, 3 feeder container ships, 3 LNG carriers and 2 very large crude carriers (VLCCs).

2.5.4. Advantages and disadvantages of the options

The two pieces of software described in the sections above differ significantly due to the fact that they reside in the two distinct categories of time domain simulators. Consequently, their purpose is different, and so are the methods with which they handle the modelling of ship motions. To aid in further evaluation of the available time domain simulators, the key advantages and disadvantages have been collected and are presented below. What is important to establish, though, is the

fact that in the project at hand, the main focus will be the behaviour of the simulated ship's steering system and the forces it generates over time in predefined scenarios. The vessel will not have to respond to steering inputs in real time, nor will the position of the ship have to be updated many times per second, as is the case in real-time simulators.

ManWav is a fast-time software by design, which by default makes it more naturally suited for this project. The more sophisticated calculation methods employed by this piece of software cause a higher level of fidelity of the results when compared to VSY, which trades it off for higher frequency of position updates, a quality irrelevant to the project. Another advantage of ManWav is the fact that all the tools necessary to implement a custom model of a ship are available to Wärtsilä - this includes MPP, a software for the calculation of hull force coefficients, and PRECAL-R, a program for the calculation of the seakeeping characteristics.

What could be considered a downside of ManWav is the simplicity of the test scenarios the user can define. The program is limited to simple sequences of manoeuvres or track keeping, in static environmental conditions. However, it is likely that given sufficiently detailed assumptions, the project might not require more complexity than what is offered by this software.

The software developed by Transas, on the other hand, is a real-time simulator. It can be switched to operate in a fast-time mode, but the underlying simplifications that are necessary for the increased frequency of vessel position updates do not change. This results in a reduced accuracy of the calculated motion of the ship, when compared to ManWav. Because of its purpose, though, VSY can support much more complicated scenarios, with a capacity to plan routes. Water depth effects and bank effects in narrow waterways are also integrated in the calculations, among others. The level of complexity of the program is far higher than ManWav, and the user interface of VSY reflects that.

Possibly the largest downside of VSY is the fact that the implementation of custom models is not feasible from the project's standpoint, due to the complexity of the ship models used in the program. This is somewhat counteracted by the very large database of previously built models.

3. Project setup

The project's aim was to tackle the general problem identified with the gate rudder concept: gate rudder's reported performance in real-life applications is very attractive, but model scale and analytical studies have so far been unable to capture that performance. In terms of providing power savings, it is currently unknown where exactly the main operating principle of GRS lies. However, these theoretical studies did not include real-life conditions to which vessels are subjected while at sea, which force their steering system to fight constant drift angles and deviations from intended course - a factor that could be the missing link behind the mystery. Additionally, superior manoeuvring performance of the gate rudder system is claimed, but without strong scientific backup.

Computational fluid dynamics are not the tool with which either of these problems could be studied efficiently. Recreating weather conditions in CFD would be too numerically expensive to run a spectrum of waves loading the ship over a meaningful amount of time, while ship manoeuvres are typically too complex in their nature to be recreated in a CFD study. A tool that could be used to tackle either of these problems efficiently is time domain simulation. With this tool, the project's goal is to pave the way towards the understanding of the benefits of the gate rudder system through the creation of a gate rudder model in a time domain simulator.

3.1. Time domain simulation in Manwav

Presented with the choice between Manwav and NTPro described in section 2.5, it was the intention to first test both pieces of software through objective tests of ease of use, ease of modifications to the modules and ease of postprocessing of the results. From the start, Manwav seemed like the better choice for the nature of the project, being natively a fast-time simulator dedicated for research purposes, with all of its code being readily available for review and modifications by the author, but further investigation was deemed in good scientific practice. However, lack of support from the NTPro developers with regards to providing access to the S175 vessel described in the next section, which was necessary for the investigation to be carried out, meant that the Transas software could not be evaluated together with Manwav. This fact, coupled with prior preference for Manwav, resulted in the Matlab - based software to be selected as the only simulator to be considered in the project.

In order to achieve the goal of the project, Manwav's modular structure was utilized to implement different gate rudder models by modifying the default MPP rudder model. Below, in figure 3.1, is a simplified diagram of Manwav's simulation structure. The intended modifications were carried out in the components marked with color blue. The details of the modifications were described in detail in section 4.1.

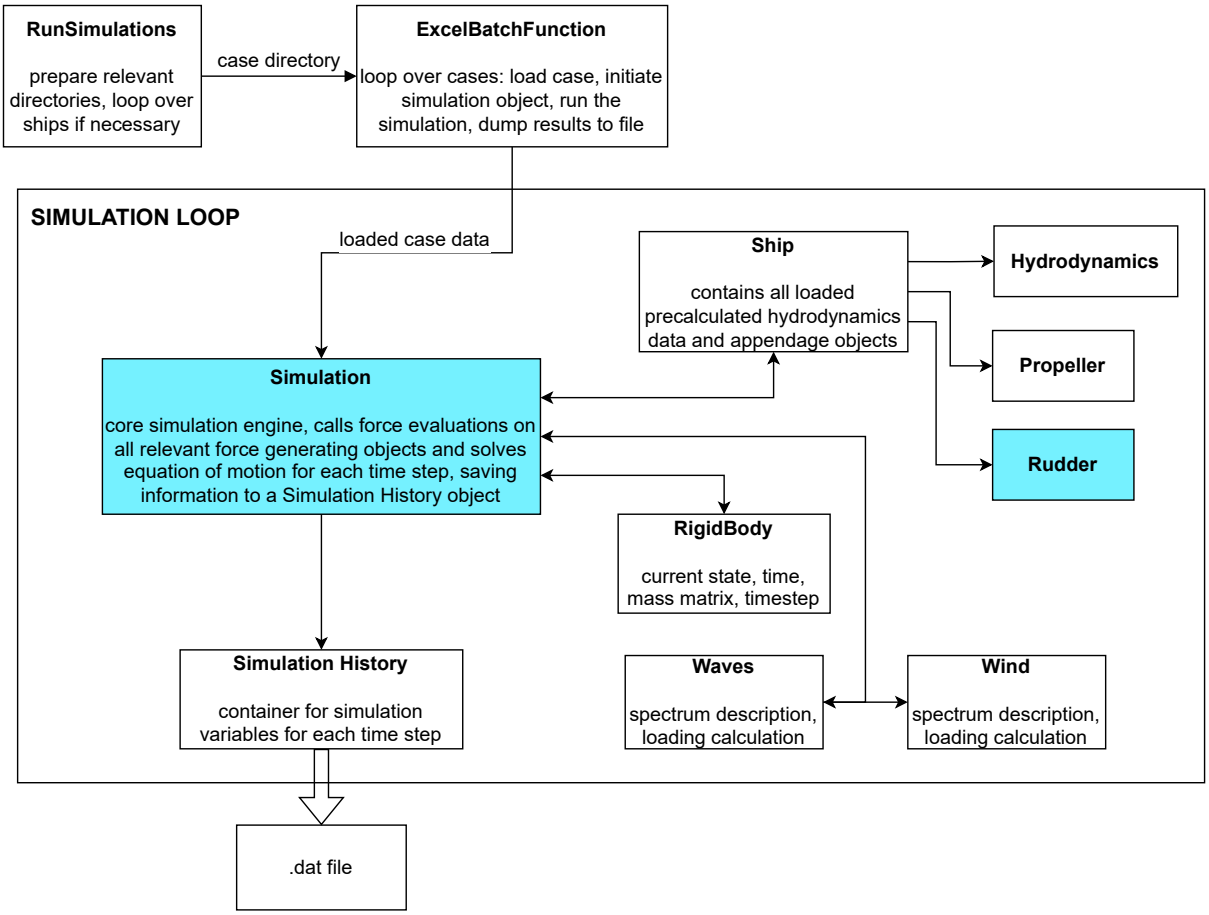

Figure 3.1: A simplified diagram of Manwav's code structure in Matlab.

3.2. The benchmark S175 container ship

In order to present tangible results of the gate rudder modelling efforts performed later in the project, a ship needed to be selected to run the test simulations on. Manoeuvring benchmark ships, such as KVLCC, KCS or S175 were considered, because of the availability of public test results that could serve as reference. A preferable feature was a roughly similar size and design Froude number to the vessel for which the CFD gate rudder dataset was created. Even though the closest fit in terms of size and Fr was the KCS, obtaining a model of it in Manwav would require a considerable amount time and effort to implement and validate before it could be considered a proper test case. Therefore, S175 was chosen, mainly due to a model of it already being implemented in Manwav as an example vessel, but also due to its dimensions and design parameters being not too different from the source vessel of the CFD dataset. Some of the main particulars of the S175 container ship are presented in the table below.

Hull length between perpendiculars	175 m
Breadth	25.4 m
Mean draught	8.5 m
Block coefficient	0.559
Prismatic coefficient	0.580
Rudder height	7.75 m
Rudder aspect ratio	1.823
Rudder surface area	33.04 m^2
Propeller diameter	6.5 m
Propeller pitch ratio	1.009

Table 3.1: Main particulars of the SR108/S175 container ship [4].

Referred to in older sources as the SR108 vessel, the S175 is a benchmark container ship developed and studied in Japan. A number of publicly available papers describe model-scale towing tank tests as well as simulated experiments, where

the vessel's manoeuvring performance can be analyzed through several standard tests, such as turning circles or zig-zag manoeuvres at various parameters. The publications picked as a reference for S175's manoeuvring performance in those tests were the 1982 article by Kyoung-Ho Son and Kensaku Nomoto titled "On the coupled Motion of Steering and Rolling of a High-speed Container Ship, as well as a series of two papers from 2006 and 2008 by Hironori Yasukawa, both titled "Simulations of Ship Manoeuvring in Waves". The model tests performed for the purposes of the papers used a 3 m model at Froude number equal to 0.3 (corresponding to a ship speed of 24.15 kn at full scale) in the Son & Nomoto paper and a 3.5 m model at a Froude number of 0.15 (corresponding to 12.08 kn in full scale) in the Yasukawa papers. To reduce the number of variables that would interfere with a proper comparison between the vessel performance in literature and that in the simulator, only calm water tests were considered. The plots related to the selected manoeuvres were digitized into separate .csv files using the WebPlotDigitizer tool. An example of the plots presented in the 2008 paper is presented in the figure 3.2. The full list of selected tests, their parameters and the data available to compare to were presented in table 3.2 The plots in the 1982 paper have been provided in full scale, while the ones in the 2006 and 2008 papers use the model scale results [7], [9].

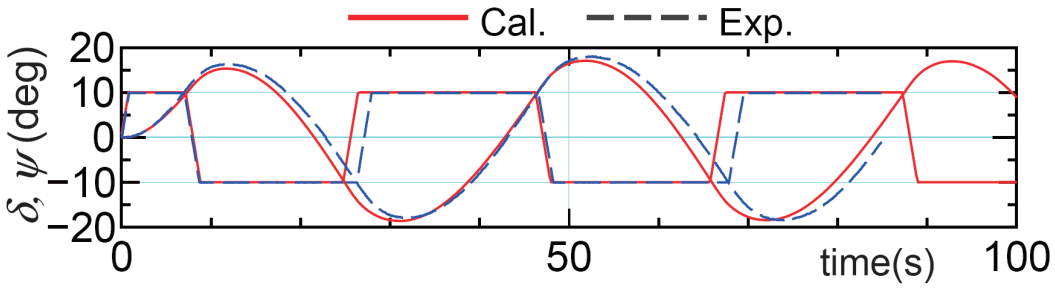

Figure 3.2: An example plot of one of the selected manoeuvres from the 2008 paper by Yasukawa [9].

	Manoeuvre type	Rudder (and heading target) setting [°]	Starting ship speed [kn]	Available plots in literature
1	Turning circle	15 SB	24.15	Ship track
2	Zig-zag	20 PS	24.15	Heading and rudder angle
3	Turning circle	35 SB	12.08	Ship track
4	Turning circle	35 PS	12.08	Ship track
5	Zig-zag	10 SB	12.08	Heading and rudder angle, drift angle, yaw rate, ship speed
6	Zig-zag	10 PS	12.08	Heading and rudder angle
7	Zig-zag	20 SB	12.08	Heading and rudder angle
8	Zig-zag	20 PS	12.08	Heading and rudder angle

Table 3.2: List of selected manoeuvres for comparison between literature and Manwav.

The S175 model in Manwav has been created by the developers together with other example ship models. By default, it was set to use the "simple" rudder model, with a maximum slew rate of 1.4 °/s, a lift coefficient slope of 0.04 rad^{-1} and a lift to drag ratio of 5. In addition, the GM of the vessel model was equal to 1.529. The selected manoeuvres were recreated in Manwav with the S175 model using constant torque setting for power control at a time step of 0.2 s and the results were subsequently compared, the results of which can be seen in figures 3.3 and 3.4. The results from the Yasukawa papers were scaled to full scale using Froude scaling principles. More comparison plots can be found in appendix A of this report.

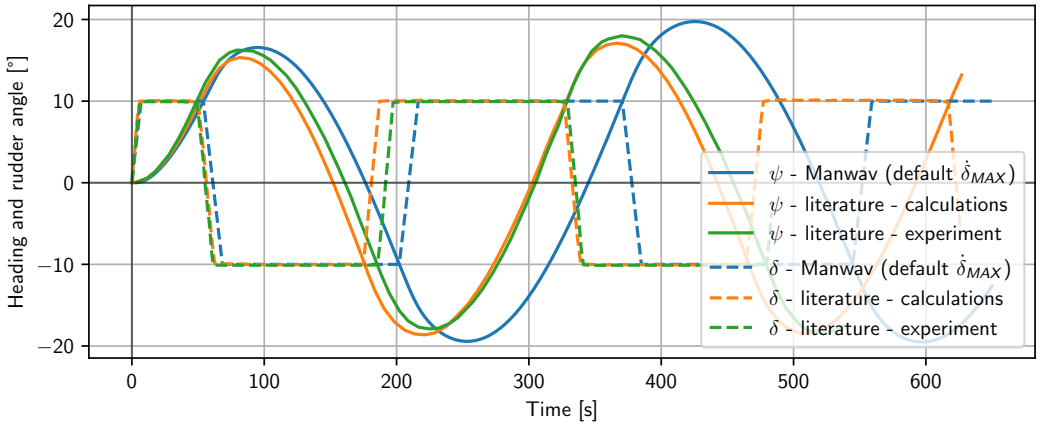

Figure 3.3: Ship heading and rudder angle comparison plot in the port 10/10 zig-zag manoeuvre at 12.08 kn. Default Manwav rudder slew rate.

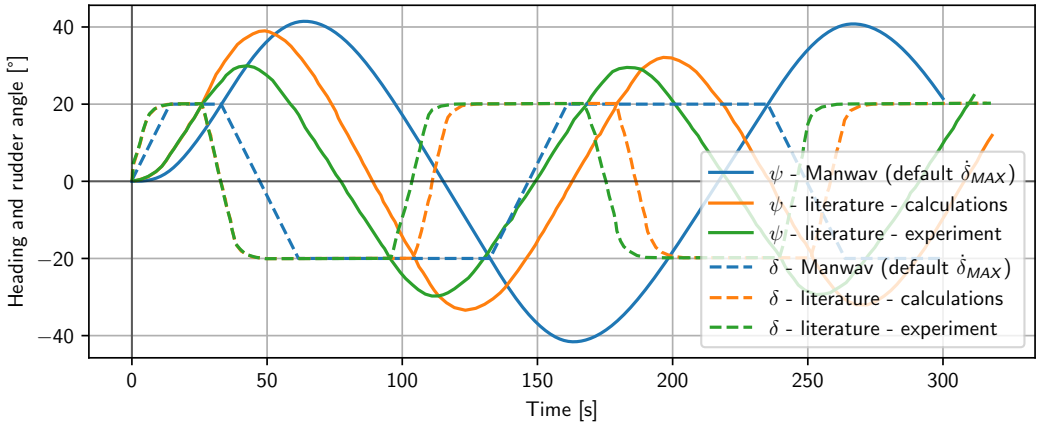

Figure 3.4: Ship heading and rudder angle comparison plot in the starboard 20/20 zig-zag manoeuvre at 24.15 kn. Default Manwav rudder slew rate. Note the difference between the rudder slew rates.

While the Manwav model was observed to underperform when compared to the reference, it was also determined that the rudder slew rate differed between the simulations. They were subsequently calculated for both literature sources using data extracted from the zig-zag plots and the resulting rudder slew rates are presented in table 3.3.

Son & Nomoto	Yasukawa model scale	Yasukawa full scale	Manwav (default for S175)
2.67 deg/s	9.18 deg/s	1.30 deg/s	1.4 deg/s

Table 3.3: Rudder slew rates of the S175 container ship from different sources.

Because of the underestimation of the manoeuvring performance by Manwav, as well as the original 1982 publication being considered a more direct source of knowledge related to the SR108/S175, it has been decided to modify the default rudder slew rate in the Manwav model to match the one from the paper by Son and Nomoto. The recalculated results are presented in figures 3.5. The main takeaway from the analysis of the results was that the agreement between the ship trajectories was improved.

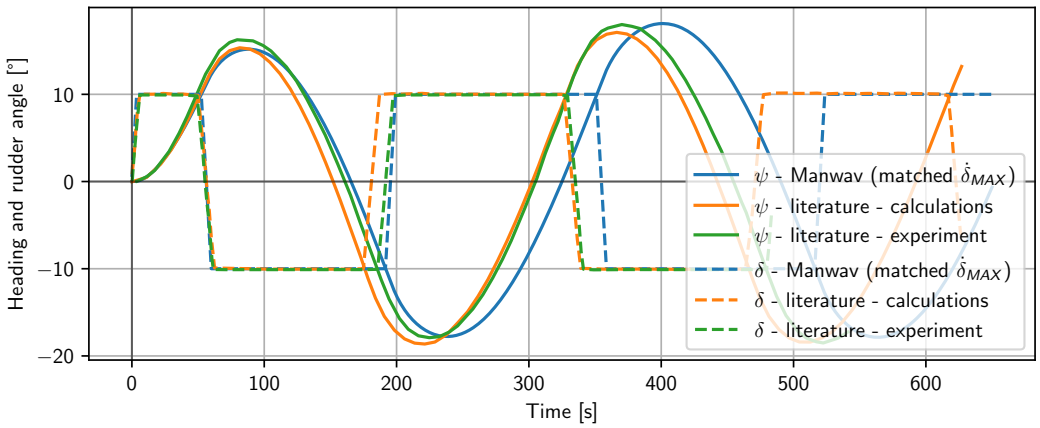

Figure 3.5: Ship heading and rudder angle comparison plot in the port 10/10 zig-zag manoeuvre at 12.08 kn. Manwav rudder slew rate matching the one from Son & Nomoto paper.

Afterwards, to test the available rudder models in Manwav, the rudder model for S175 was modified to employ the MPP model, which used the rudder dimensions as input. The matched rudder slew rate from the Son & Nomoto paper was retained for this rudder model as well. The simulations were again rerun, and the results were depicted in the figures figure 3.6.

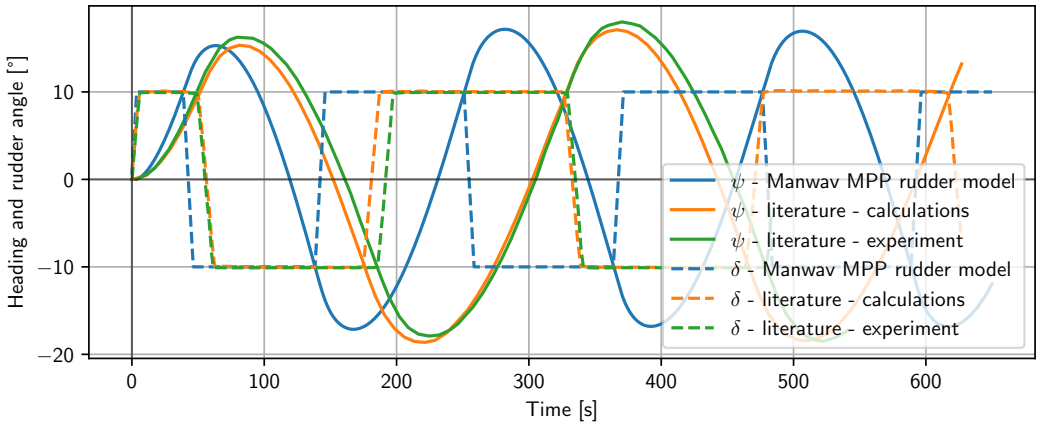

Figure 3.6: Ship heading and rudder angle comparison plot in the port 10/10 zig-zag manoeuvre at 12.08 kn. Manwav rudder model switched to MPP model.

This time, it was clear that the MPP model significantly overestimates the steering forces generated by the rudder compared to the previous configurations. Modifications of the MPP rudder model would require changes to the rudder geometry with regards to its dimensions from the original S175 design. It was therefore decided to revert the configuration back to the simple model, but modify the lift coefficient slope and the lift to drag ratio in order to obtain an even better match between the Manwav simulations and the reference plots. After a series of simulation reruns with modified values of the parameter, the final value of the CL slope was set to 0.046 °/s and the lift to drag ratio was increased to 5.5. The resulting performance of the vessel in the simulations can be seen in the figures 3.7 to 3.10. The remaining plots are included in appendix A.

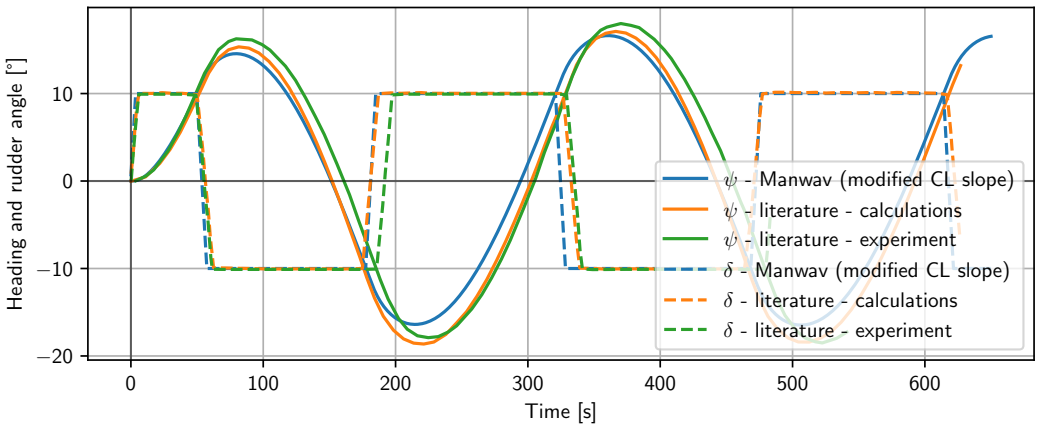

Figure 3.7: Ship heading and rudder angle comparison plot in the port 10/10 zig-zag manoeuvre at 12.08 kn. Adjusted CL slope and L/D ratio.

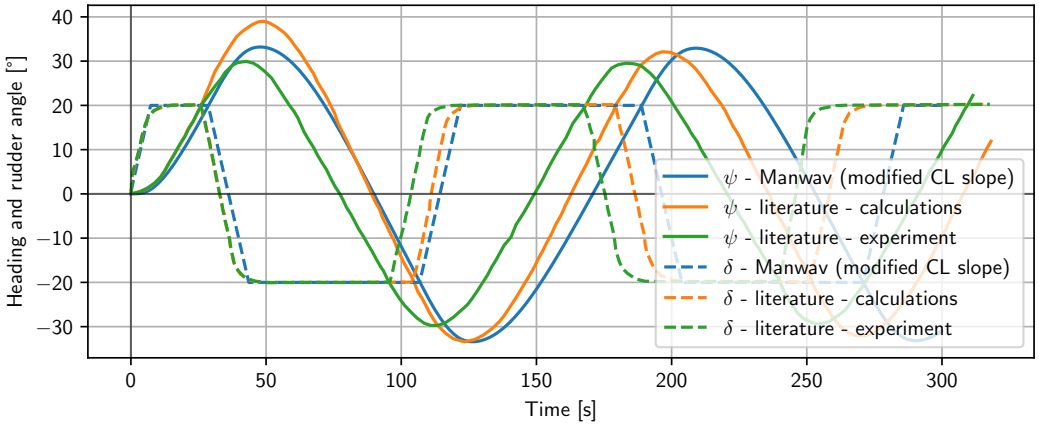

Figure 3.8: Ship heading and rudder angle comparison plot in the port 20/20 zig-zag manoeuvre at 24.15 kn. Adjusted CL slope and L/D ratio.

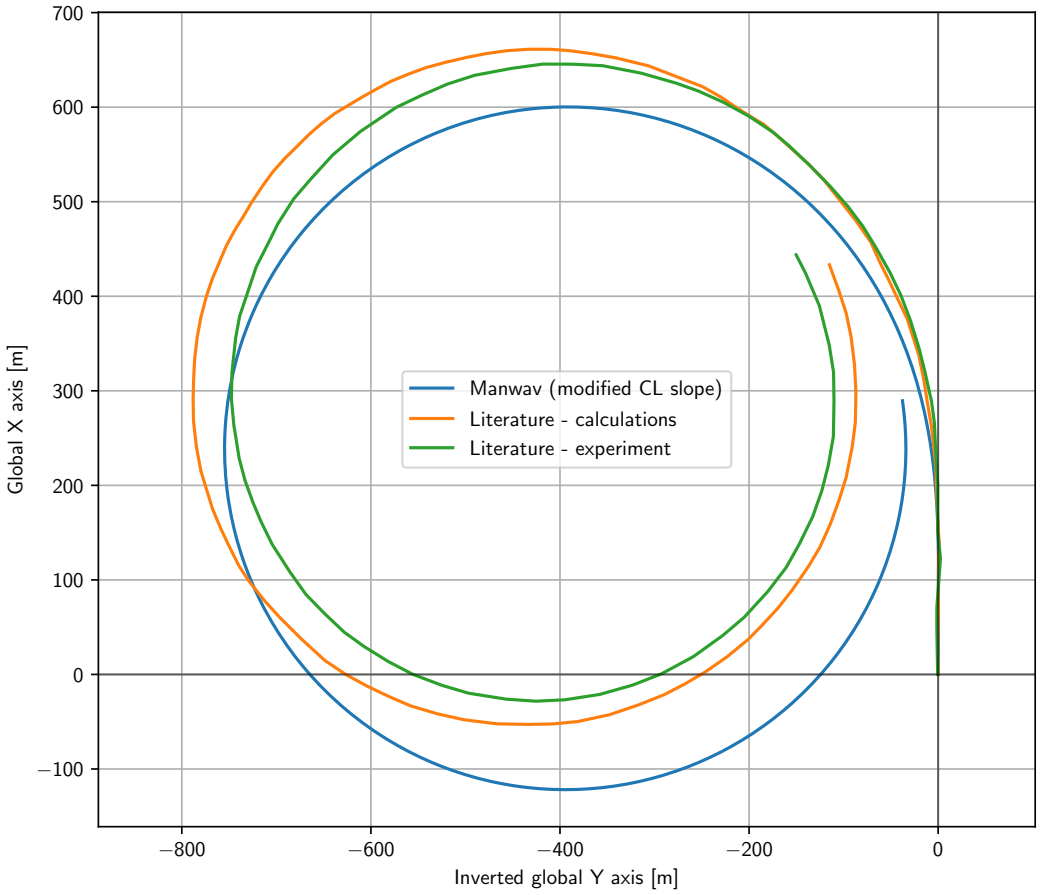

Figure 3.9: Ship track comparison plot in the 35° to port turning circle manoeuvre at 12.08 kn. Adjusted CL slope and L/D ratio.

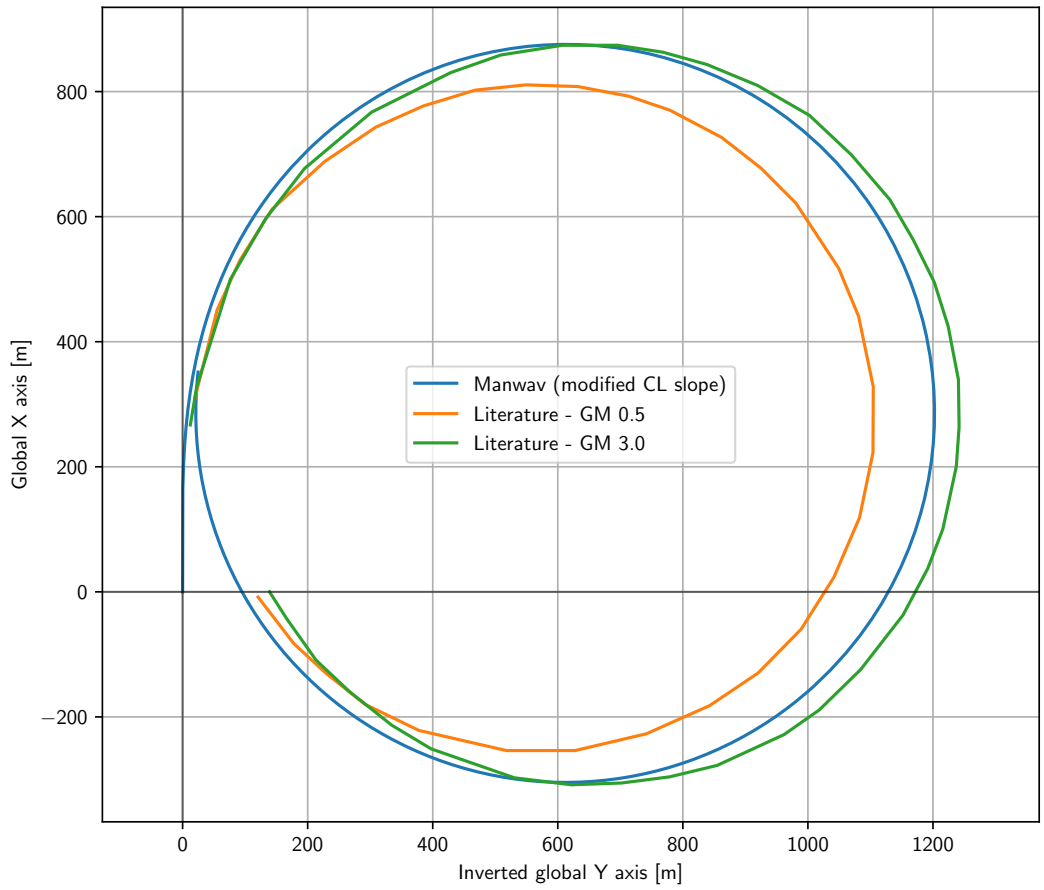

Figure 3.10: Ship track comparison plot in the 15° to starboard turning circle manoeuvre at 12.08 kn. Adjusted CL slope and L/D ratio.

The goal of the described modifications was to adjust the ship performance in selected manoeuvres to match the reference from selected literature sources through modifications to the default rudder model. After the modifications to the simple rudder model were implemented, the agreement between the ship tracks and other parameters has improved. A limiting factor in the efforts to match the literature results as closely as possible was the fact that a compromise was necessary to balance the model's overexagerrated performance in low-speed manoeuvres, and its underperformance in the high-speed manoeuvres when compared to the reference. The underyling principles of the rudder model would need to be modified in order to improve the similarity to reference, which is not the focus of this project. Therefore, in further considerations, the models of the gate rudder system tested within this thesis will treat the modified conventional rudder S175 model as a reference to how a ship's performance changes when switching from a conventional rudder to a different one.

4. Modelling

4.1. Physics-based rudder model recreation

The first gate rudder model created as part of the project at hand was a recreation of the mathematical model described in a 2020 paper titled ”Investigation of the manoeuvrability characteristics of a Gate Rudder system using numerical, experimental and full-scale techniques” by Alessandro Carchen et al. In this paper, the authors explain in detail the way to analytically calculate the forces generated by a gate rudder based on input parameters such as the steering angle, ship speed, its drift angle, the vessel’s yaw rate and propeller loading, together with a collection of static ship-specific coefficients that influence the flow field around the vessel’s stern. The model used the MMG rudder model as a basis for the structure of equations, CFD analyses of Shigenobu to perform a regression of flow velocity component’s with relation to the rudder and drift angle, as well as prior investigations into factors governing the performance characteristics of propellers and rudders.

4.1.1. Covered area ratio

The model operates on the assumption that the streams of water around the rudder corresponding to the propeller slipstream and the flow outside of it are independent and ”approach” the rudder blades at different velocities angles of attack, thereby generating on them separate lift and drag forces. In order to define the influence of each of those flow parts on the total forces generated on a rudder blade, a blade coverage ratio μ based on the rudder deflection angle is introduced, which specifies the fraction of the rudder blade area within the propeller slipstream. It is an especially important parameter of the gate rudder system, because unlike in a conventional rudder, the blades of a GRS constantly enter and leave the propeller slipstream as the steering command changes. The formula with which μ is calculated is derived in the paper as following:

$$\mu = \frac{A_{CV}}{A_R * \eta} \tag{4.1}$$

where A_R is the rudder blade area, η is the ratio of propeller diameter to rudder span and A_{CV} is the rudder area inside the propeller slipstream (referred to here as the covered blade area). This method does not take into account the propeller slipstream contraction for simplification, but in case of the gate rudder system, it would be very challenging to do so accurately, mostly because of variable distance of the rudder blades from the propeller. The covered blade area can be calculated using basic geometrical principles, which are best illustrated using a diagram, as seen in figure 4.1a.

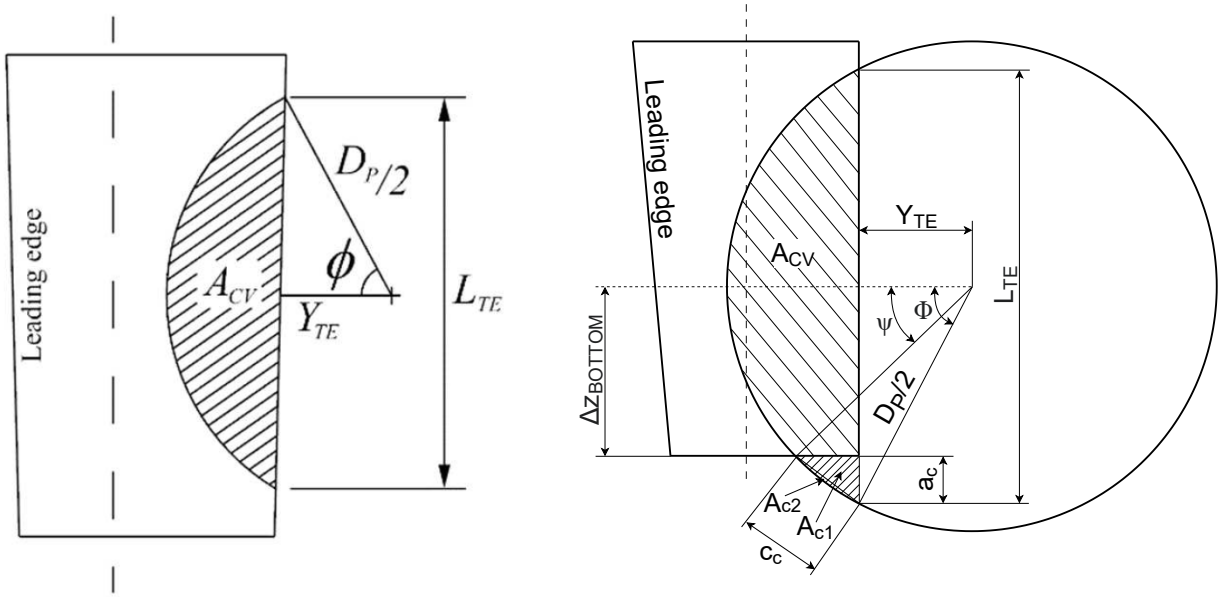

(a) The original diagram depicting the derivation of A_{CV} [35]. **(b)** The diagram depicting an improved method of calculating A_{CV}.

Figure 4.1: Diagrams used to calculate the covered blade area.

The dimensions used to calculate the covered blade area are calculated by the authors of the 2020 paper through the

following formulas:

$$L_{TE} = \begin{cases} 0, & \text{if } \delta < 0 \vee Y_{TE} > \frac{D_P}{2} \\ 2\sqrt{\frac{D_P^2}{4} - Y_{TE}^2}, & \text{elsewhere} \end{cases} \tag{4.2}$$

$$\Phi = \arctan\left(\frac{L_{TE}}{2Y_{TE}}\right) \tag{4.3}$$

where D_P is the diameter of the propeller, Y_{TE} is the horizontal distance from the center of propeller slipstream cylinder to the trailing edge of the rudder blade, L_{TE} is the chord of the segment of the circle that is projected onto the rudder blade by the propeller slipstream and Φ is the angle between Y_{TE} and the projected circle's radius connected to one of the segment's edges. A_C can therefore be calculated as a difference between the area of the circle's sector and that of the triangular portion:

$$A_{CV} = \frac{\Phi D^2}{4} - \frac{L_{TE}Y_{TE}}{2} \tag{4.4}$$

While mathematically correct, this method of calculation of A_{CV} assumes that the trailing edge's ends are always outside of the propeller slipstream. In certain GRS designs, it is not impossible that this might not be the case at high rudder deflection angles. Although it would not affect the calculated covered blade area significantly, the A_{CV} calculation method was modified to take this case into account. Using a modified diagram seen in figure 4.1b, the area of the bottom section that needs to be "cut" from the total covered area can be split into the triangular A_{C1} and the segment A_{C2}. Their areas can be calculated as follows:

$$a_c = \frac{L_{TE}}{2} - \Delta z_{bottom} \tag{4.5}$$

$$\psi = \arcsin\left(\frac{\Delta z_{bottom}}{R}\right) \tag{4.6}$$

$$c_c = (\Phi - \psi)R \tag{4.7}$$

$$A_{c1} = \frac{a_c\sqrt{c_c^2 - a_c^2}}{2} \tag{4.8}$$

$$A_{c2} = (\Phi - \psi)R^2 - \frac{c_c\sqrt{R^2 - \left(\frac{c_c}{2}\right)^2}}{2} \tag{4.9}$$

This approach requires the possibility to determine the relative position of the rudder blade edges (top and bottom) with respect to the propeller axis in order to calculate Δz_{bottom}. This set of equations was presented for the case where the area needed to be removed from A_{CV} is at the bottom, and naturally, a similar process can be performed in case the top rudder blade edge enters the propeller slipstream. Finally, an improved formula for A_{CV} was derived:

$$A_{CV} = \frac{\Phi D^2}{4} - \frac{L_{TE}Y_{TE}}{2} - (A_{c1} + A_{c2})_{bottom} - (A_{c1} + A_{c2})_{top} \tag{4.10}$$

where the additional areas A_{c1} and A_{c2} could be zero for either top or bottom side, or both. In the last case, the formula would be unchanged with respect to the original.

Another issue in the formula for the covered area ratio from the 2020 paper is the inclusion of the parameter η, which stands for the ratio of propeller diameter to rudder span. A clear indication of this being wrong is the fact that at 90° rudder blade deflection angle, μ should be equal to exactly A_{CV}/A_R, regardless of the difference in size between the rudder and the propeller. On the other hand, in any other angle of deflection, the covered area is different from the segment of the propeller slipstream circle because of non-perpendicular projection angle. Therefore, in place of the η parameter in the formula, it should include a mechanism to account for the changing projection angle caused by rudder deflection.

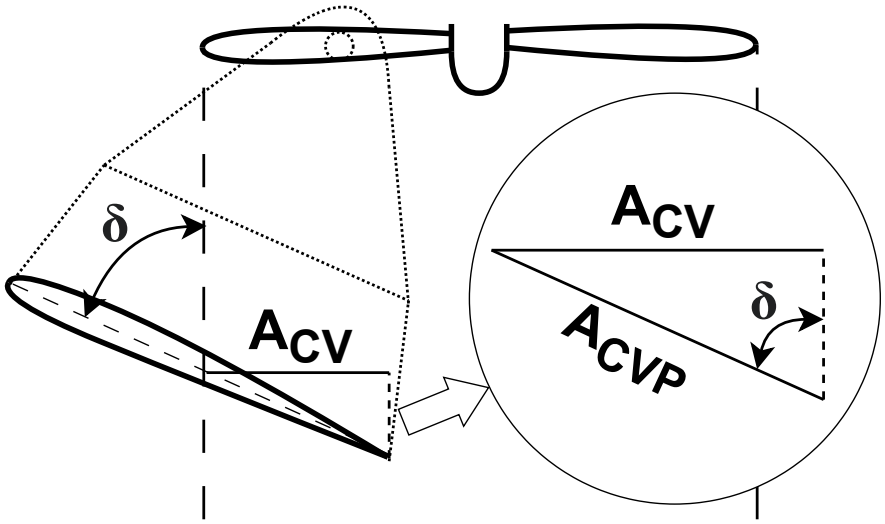

Figure 4.2: Simplified top view of the propeller and one of the gate rudder blades, showcasing the projection angle correction for covered blade area. A_{CVP} stands for the projected covered blade area, equal to $A_{CV}/\sin(\delta)$

For simplification purposes, it will be assumed that the blade onto which the projection is investigated is a vertical plane passing through the average chord line of the actual rudder blade. At 90° deflection angle, the projected area is equal to the covered area calculated above, because the projection plane and the propeller plane are parallel. As the blade retracts from the 90° deflection angle, the angle between the two planes changes, "stretching" the projected area in the direction of the blade's chord. Therefore, to account for the projection angle, the corrected formula for covered area ratio would become:

$$\mu = \frac{A_{CV}}{A_R * \sin(\delta)} \tag{4.11}$$

However, because the goal of the project was to implement the gate rudder from the paper in an unchanged form, these issues were also kept in the equations it is based on. These elaborations on the possible ways to fix them only serve as a critique of the potential limitations of the model and the likely inaccuracy of the results it produces.

4.1.2. Other governing equations

The rest of the model functions predominantly on the standard principles of lift and drag on hydrodynamic profiles. As mentioned before, those forces are calculated separately for the streams outside and inside of the propeller slipstream and summed per each blade. To calculate those forces, a basic formula for normal force on a hydrofoil is used:

$$\begin{cases} F_{No} = 0.5\rho A_R U_{Ro}^2 f_\alpha \sin(\alpha_{Ro}) \cos(\alpha_{Ro}) \\ F_{Ni} = 0.5\rho A_R U_{Ri}^2 f_\alpha \sin(\alpha_{Ri}) \cos(\alpha_{Ri}) \end{cases} \tag{4.12}$$

where A_R is the surface area of the rudder blade, U_R is the flow velocity magnitude, f_α is the lift gradient coefficient based on the rudder blade aspect ratio and α_R is the angle of attack between the rudder blade and the direction of the analyzed part of the flow. Additionally, the o and i subscripts denote whether the variable refers to the outside or the inside of the propeller's slipstream. The f_α parameter used by the authors is calculated using formula $f_\alpha = 6.13AR/(2.25 + AR)$, where AR is the aspect ratio of the blade. A very similar formula is used in the MPP rudder model, with effective aspect ratio based also on the relation between the ship's draft and the rudder's span instead of the base aspect ratio. Because there is no mention of a different formula for AR or the use of an effective aspect ratio in the paper on the gate rudder MMG-based model, it was not used in this project. Despite the formula for f_α also being used by the sophisticated MPP model, its use in the gate rudder model has been identified as a potential flaw of the model, because in MPP theory manual, it is described as a formula meant specifically for a conventional rudder [40]. Without a dedicated investigation, it is unknown whether this formula also accurately approximates the lift coefficient of a gate rudder blade.

The addition of the cosine function at the end of the normal force formula is meant to account for stall on the rudder blade beyond a certain attack angle. The focus of the authors of the paper was a sufficient study of the flow field around the gate rudder that would allow to derive U_R and α_R for each blade.

The flow velocity components in- and outside of the propeller slipstream were analyzed through CFD studies of the flow field in Shigenobu's aft section, which resulted in regressed formulas used to calculate the parameters necessary to

determine the hydrodynamic forces:

$$\begin{cases} u_{Ri} = U_R \varepsilon (1 - w_P) \left[1 + \mu \sqrt{1 + \frac{8K_T}{\pi J_P^2}}\right] \\ u_{RoSB} = U_R * (0.85 - 0.0859 * \delta_{PS}) \\ u_{RoPS} = U_R * (0.85 + 0.0859 * \delta_{SB}) \\ v_{RSB} = U_R * (0.15 - 0.0573 * \delta_{PS} + 0.573 * \beta - x_R r) \\ v_{RPS} = U_R * (-0.15 + 0.2865 * \delta_{SB} + 0.2865 * \beta - x_R r) \end{cases} \tag{4.13}$$

where ε is the ratio of wake fraction at rudder and propeller positions, w_P is the propeller wake fraction, K_T/J^2 is the propeller loading coefficient defined as the ratio between thrust coefficient K_T and square of the advance coefficient J, β is the drift angle of the ship, x_R is the longitudinal position of the rudder with relation to the ship's center of gravity (assumed by the authors of the paper to be in midship, for simplification) and r is the ship's yaw rate. The SB and PS subscripts denote the blade for which the selected velocity component is calculated. Transverse velocity component is assumed to be the same outside and inside of propeller slipstream. A potential issue was identified in the formula for u_{Ri}, where seemingly, the slipstream velocity is only affected by the propeller loading parameters if the covered area ratio is non-zero. The author suspects that this is an error and the intended form of the equation joined the adjacent 1 with μ in a parenthesis, so that propeller loading always influences the slipstream velocity. As covered area ratio increases, the flow is constricted, which further increases its velocity. Unfortunately, there is no explanation as to how the original formula was derived in the paper, so this suspicion would need to be confronted with its authors. Due to lack of conviction that the suspected intended form of the equation is correct, this change was not implemented in the model.

For each blade and each stream (in- and outside of propeller slipstream), the velocity magnitude can be calculated as the square root of sum of squares of longitudinal and transverse components of that velocity, while the angle of attack is equal to the difference between the arctangent of those velocity components and the rudder blade deflection angle.

When the relevant flow velocities and the resulting partial normal forces for each stream are known, they are summed according to their contributing factor based on the covered area ratio. This calculation is performed for each rudder blade.

$$F_N = F_{No}(1 - \mu) + \mu F_{Ni} \tag{4.14}$$

Once the total normal force on each blade is calculated, it is split into lift and drag forces in the ship's coordinate system. The former are also used to calculate the components of yaw moment induced by the rudder blades. The only parameter needed for the conversion between the coordinate systems is each rudder blade's relative position in relation to that coordinate system, which is dictated by their deflection angles, as seen in figure 2.7. In this version of the model, the authors did not include the influence of drag forces on the rudder blades on the yaw moment, likely due to the moment arms being too small for these forces to make an impact on the total steering moment of the ship.

4.1.3. Manwav implementation

The mathematical model described in previous sections was analyzed and implemented in Manwav. The class structure of the MPP rudder model was copied in order to minimise compatiblity issues and necessary modifications in the rest of the code. First, the data structure of the simulation needed to be changed to accommodate two separate signals of rudder angle, one for each gate rudder blade. Similarly, the signals of separate drag and lift forces per blade were added, together with an execute counter, which indicates where the steering command has changed during the simulation (for example during zig-zag manoeuvres). In the rudder class, the fields were modified to accommodate for additional gate rudder input parameters, such as the offset between the posts or the length of the pivot arms. Other static parameters, t_R or x_H mentioned in the previous subsection were also included and calculated during object construction. Control scheme had to be modified to manage the steering of two rudder blades separately, with different maximum deflection angles depending on the direction of rotation. A separate method was added that calculated the covered area ratio for each rudder blade, as described in subsection 4.1.1. Finally, the method responsible for the evaluation of forces on the rudder system was almost completely rewritten to follow the system described in subsection 4.1.2.

In the revised form of the force evaluation method, wake fractions w_P and w_R are first determined, together with their ratio ε. Covered area ratio μ is also established for each rudder blade, according to equation 4.1. Flow velocities on rudder blades are then calculated, followed by the velocity magnitudes and inflow angles. Afterwards, the method calculates the normal force for each rudder blade according to equations 4.12 and 4.14. Then, after the rudder force increase factor a_H is determined based on whether the selected blade is upstream or downstream with regard to the ship under drift angle, the normal forces are converted drag, lift and steering moment according to equation 2.7, with the last two also accounting for the change in the coordinate system from blade-based to the ship based. An illustration of the force calculation process in the model is presented in figure 4.3

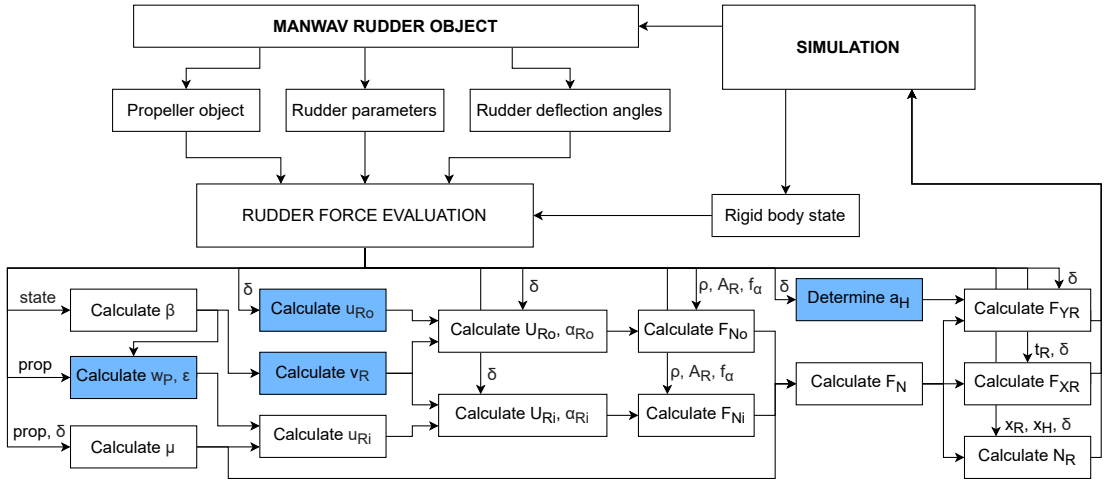

Figure 4.3: Diagram of the force evaluation in the physics based GR model in Manwav. Blue color of some of the calculation steps indicates that they are formulas directly regressed from CFD data without known setup parameters.

4.1.4. Physics-based model performance

In the 2020 paper by Carchen et al., the gate rudder model is subjected to an evaluation based on comparisons between ship tracks and plots of other parameters of manoeuvres with a simulated Shigenobu model and model tests, as well as some full-scale trials. Unfortunately, a similar test case was not available for the purposes of this project. Because in a manner similar to KCS, obtaining a comparable model of Shigenobu in Manwav would require considerable amounts of time and effort to implement and validate, it was decided that this physics-based gate rudder model will only be tested as part of the case study that follows in chapter 5. Because the model lacks the necessary validation and verification, it will be used under the assumption that it was implemented correctly.

4.2. Machine learning model

The physics-based model described in the previous section was a reproduction of an existing MMG-based mathematical model of the gate rudder system. The main effort related to that model within this project lied in its implementation in Manwav, which required structural modifications to the program's code to properly accommodate the specific nature of the gate rudder's twin rudder blades, most notably because of the rudder forces being calculated separately per blade. These modifications paved the way for the implementation of the data-driven model described in this section, which was the main focus of the work performed within the project.

4.2.1. Gate Rudder CFD dataset

Wärtsilä has been investigating the concept of the gate rudder since the company acquired the license for the use of the japanese patent in 2020. As part of a study on manoeuvrability of the rudder system for one of Wärtsilä's clients, a series of CFD analyses was performed, which focused on the performance parameters of the rudder at different drift angles and rudder deflection angles. It resulted in a dataset of 60 datapoints, one for each combination of a steering angle and a drift angle, collecting various parameters, such as forces on rudder blades and propulsive performance characteristics. The details of the vessel's geometry on which the study was performed, as well as the setup parameters for the analyses, have been described in a confidential appendix to the report.

The dataset was made available for the purposes of the project by Wärtsilä, and although small, it was deemed sufficient for a proof-of-concept rudder model that could function in a basic form without additional CFD studies required, but that could also be later improved through the expansion of the base dataset. First, to prepare the data for use in the model development, it was inspected and non-dimensionalized. The non-dimensionalization of the rudder forces was performed according to the following formula:

$$C_F = \frac{F}{0.5\rho\frac{A_R}{2}V_s^2} \tag{4.15}$$

where C_F is the force coefficient, F is the force being non-dimensionalized, ρ is the water density, A_R is the total area of rudder blades and V_s is the ship's velocity magnitude. The same transformation was performed for both lift and drag forces, creating coefficients of lift (C_L) and drag (C_D), respectively. The total rudder area is halved in the formula, because the forces and the coefficient correspond to individual blades of the rudder system. To illustrate the dataset and the influence of individual variables, it has been visualized in figures 4.4 and 4.5.

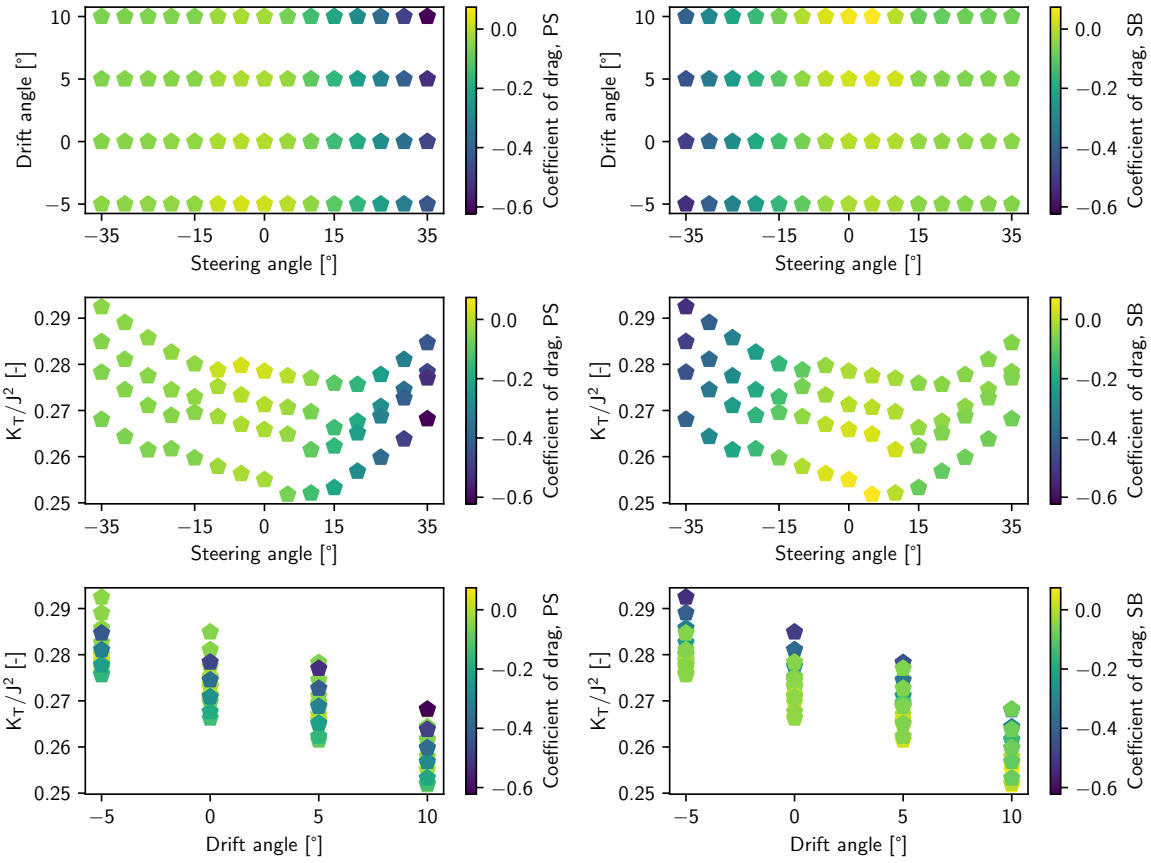

Figure 4.4: Drag coefficient scatter plots of the datapoints from the gate rudder CFD dataset.

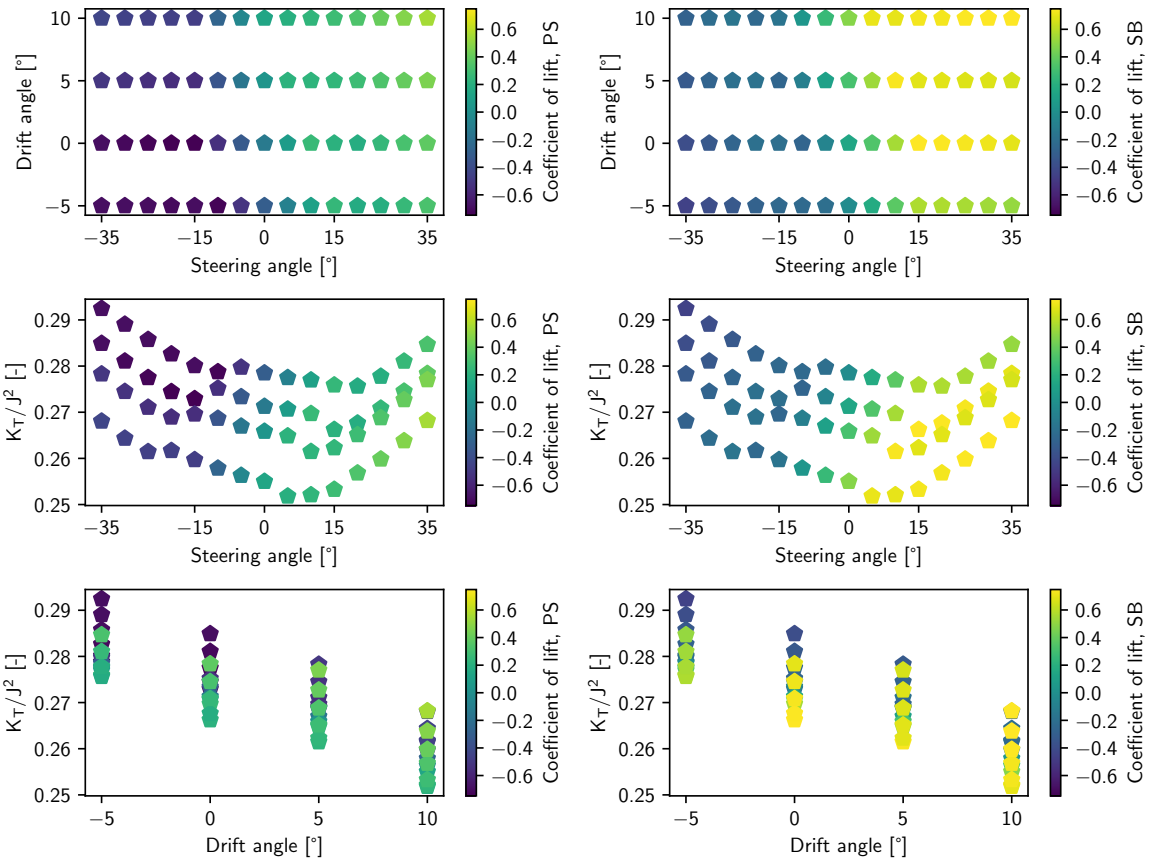

Figure 4.5: Lift coefficient scatter plots of the datapoints from the gate rudder CFD dataset.

4.2.2. Modelling method selection

To start the process of modelling method selection, some basic facts about the problem were identified. The model needed to estimate drag and lift forces on the rudder blades, therefore it had to belong to a quantity prediction category or, in other words, a regression algorithm was needed. Additionally, the small number of samples in the dataset had to be noted, which influenced the number of algorithm types suitable for the problem, as well as ensured that training time would not play a role in the selection process. Prediction speed would not be an issue either, because the project focuses on fast-time simulation, which does not have strict computational speed requirements. Lastly, the data is non-linear, so kernel-based methods will likely yield more accurate predictions.

Next, relevant features of the dataset needed to be determined. The CFD study performed a sweep of analyses for steering angle ranging from -35° to +35° with 5° steps as well as drift angles ranging from -5° to +10°, also with 5° increments. Drift angle was an obvious pick for a feature. The steering angles were split into individual rudder deflection angles for each blade, giving additional two features. Finally, from the parameters gathered in each of the CFD analyses, the propeller loading coefficient, defined as a ratio of K_T/J^2, mentioned before in equation 4.13, was calculated for each combination of the primary features, serving as an auxilliary feature. This made the selected features amount to a total of four: drift angle, starboard side rudder angle, port side rudder angle and propeller loading coefficient. Propeller loading is a useful metric describing the relation between the thrust generated by the propeller and the inflow velocity, which is a parameter unaffected by the rotational speed of the propeller and can be also used to quantify the propeller-rudder interaction due to rudder's deflection affecting the flow upstream of the propeller.

The machine learning method selection was started by ruling out the use of an artificial neural network, because the dataset did not consist of a large enough number of samples - typically, neural networks require a larger dataset to make accurate predictions [22]. Next, scikit-learn's model selection sheet was used as reference, where the recommended regression algorithms were a linear ridge regression and, if unsuccessful, support vector regression (a regression variant of the support vector machine, or SVM) with a radial basis function (RBF) [51]. It was decided to investigate the performance of additional algorithms, increasing in level of complexity, in order to determine the best one suited to capture the problem at hand. Ultimately, the list of selected algorithms consisted of an ordinary least squares linear regression, ridge regression, kernel ridge regression with a polynomial kernel, kernel ridge regression with a radial basis function (RBF) kernel and support vector regression with RBF kernel. A separate model for the prediction of each of the forces in question individually, as a single output, would be the result of each training run.

Eventually, the trained estimators would be deployed within Manwav, which would suggest that a more efficient approach would be to stay within the Matlab environment, where the statistics and machine learning toolbox would likely fulfill the needs of each of the above listed algorithms. However, for a number of reasons, the scikit-learn library in Python was selected as the environment the estimators would be developed in. This is because of the open-source nature of the language, as well as Wärtsilä's familiarity with the library. Additionally, as previously mentioned, prediction speed was not a priority, so it was acceptable to sacrifice some computational efficiency due to Matlab executing an external Python script. The 2023b version of Matlab used in this project offers the capability to launch Python scripts up to Python version 3.11, so that was the version chosen. The version of the scikit-learn library used was 1.5.2 [11].

4.2.3. Data-driven model development

The machine learning model development was done using a Python script which loads in the CFD dataset and loops over the different regression algorithms, collecting statistics on their performance. To gather them, it performs 400 iterations of data fitting for each algorithm. In each iteration, the dataset is randomly split into 50 training samples and 10 test samples. No holdout set was created due to the small size of the dataset. The features were ultimately not normalized due to reasons explained later in section 4.3. After each random test-train split, the script enters another loop, which is a manually written grid search algorithm. A set of hyperparameter values is assigned for each investigated regression algorithm, and the grid search loops over each of the combinations of the values to test the algorithm's performance. The hyperparameter values used for the grid search are presented in table 4.2.

Algorithm	Hyperparameter	Values
Linear regression	-	-
Ridge regression	Alpha	$1, 1e^{-1}, 1e^{-2}, 1e^{-3}, 1e^{-4}, 1e^{-5}, 1e^{-6}, 1e^{-7}, 1e^{-8}, 0$
Kernel ridge - polynomial kernel	Alpha	$1e^{-2}, 1e^{-3}, 1e^{-4}, 1e^{-5}, 1e^{-6}, 1e^{-7}, 1e^{-8}$
	Gamma	$1, 1e^{-1}, 1e^{-2}, 1e^{-3}, 1e^{-4}, 1e^{-5}$
	Polynomial degree	2, 3, 4, 5, 6
Kernel ridge - RBF kernel	Alpha	$1e^{-3}, 1e^{-4}, 1e^{-5}, 1e^{-6}, 1e^{-7}, 1e^{-8}$
	Gamma	$1e^{-2}, 1e^{-3}, 1e^{-4}, 1e^{-5}, 1e^{-6}, 1e^{-7}$
Support vector regression	Epsilon	$1e^{-1}, 1e^{-2}, 1e^{-3}, 1e^{-4}, 1e^{-5}, 1e^{-6}, 1e^{-7}$
	C	1, 10, 100, 1000, 10000, 100000
	Gamma	$1e^{-1}, 1e^{-2}, 1e^{-3}, 1e^{-4}$

Table 4.2: Hyperparameter values used in the grid search for each of the regression algorithms.

An estimator is then trained for every combination of hyperparameters, and the best estimator is selected based on the highest obtained coefficient of determination (R^2) for that specific split of training and testing samples. When the best combination of the hyperparameters is found, root mean squared error metric is also calculated for the corresponding estimator. If the estimator's R^2 is negative, it is set to zero instead. After all the iterations of random test-train data splits for the given regression algorithm are finished, the collected performance metrics are analyzed. Their mean and standard deviation values are calculated, and their probability density functions are approximated with kernel density estimation using Scipy's default Scott's bandwidth estimation [5]. The combined performance metrics for each regression algorithm are presented in figure 4.6.

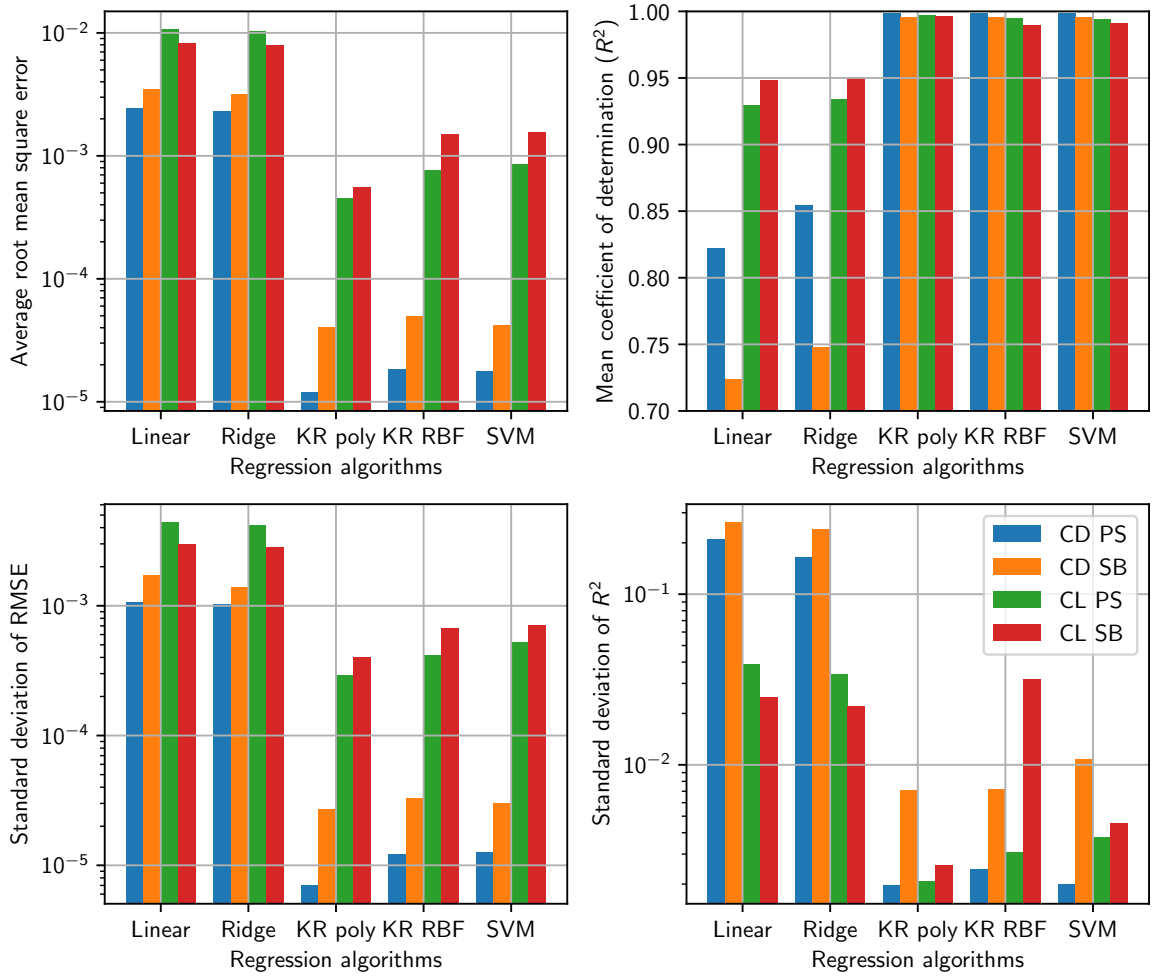

Figure 4.6: Bar plots of different performance metrics for every evaluated regression algorithm.

As can be seen in the bar plots above, statistically, the investigated estimators can generally be grouped into two categories under the performance criterion. The first are the linear regressors (linear regression and ridge regression), which performed relatively poorly when predicting drag and decently when predicting lift coefficient. The second group consists of the remaining regression algorithms (kernel ridge with a polynomial kernel, kernel ridge with RBF kernel and support vector machine), all of which achieved similarly high accuracy levels, with some variation in performance in specific rudder forces.

The best all-around regression algorithm initially appeared to be the kernel ridge regressor with a polynomial kernel, which beat the other algorithms in every way taken into account at this stage. Not only was it the most accurate for every rudder force, reaching highest values of R^2 and lowest values of root mean square error, it was also the most consistent to hit such high scores, as characterised by the lowest values of standard deviations for both of those metrics. The other two non-linear regressors seemed to perform similarly to each other, with the only notable difference being a much larger standard deviation of coefficient of determination on starboard lift coefficient reached by the kernel ridge regressor with RBF kernel. The distributions of the performance metrics achieved by the kernel ridge regressor with a polynomial kernel can be seen in figure 4.7. For reference, the same plots of performance metrics of linear regression and support vector machine are presented in figures 4.8 and 4.9. The same distribution plots for the remaining regression algorithms can be found in appendix B.

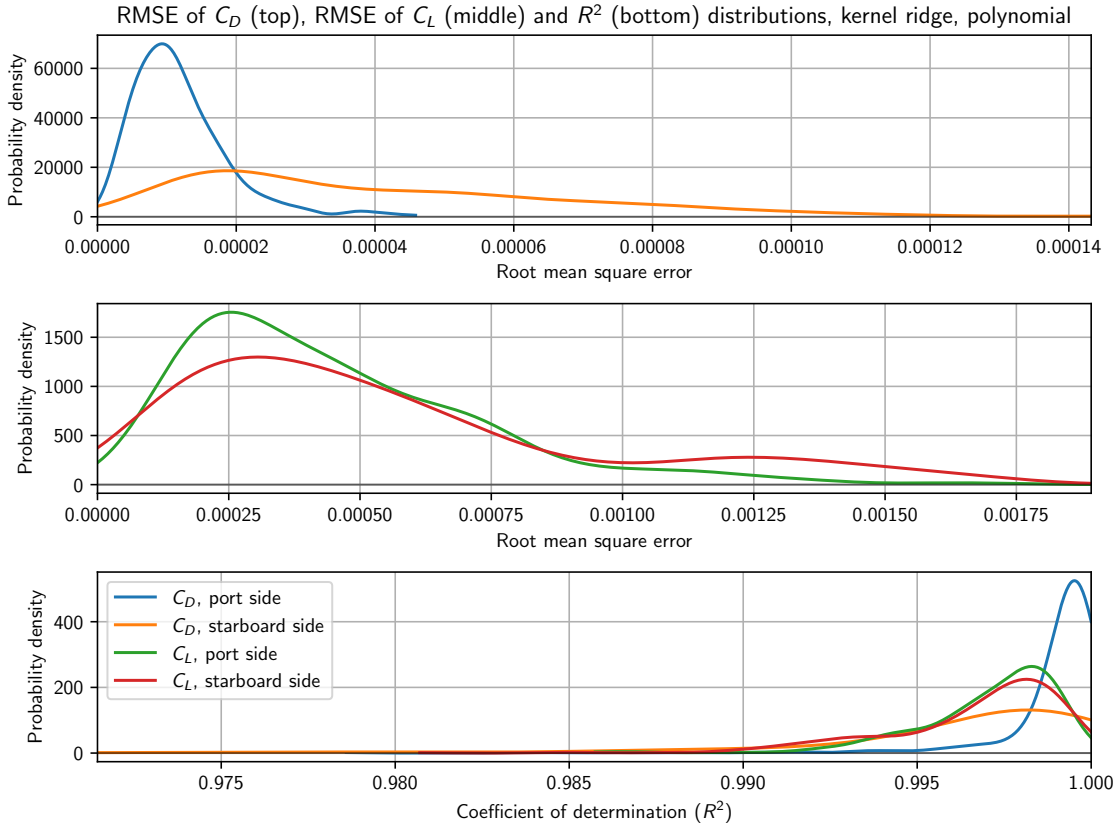

Figure 4.7: Distributions of root mean square error and coefficient of determination for the kernel ridge algorithm with a polynomial kernel.

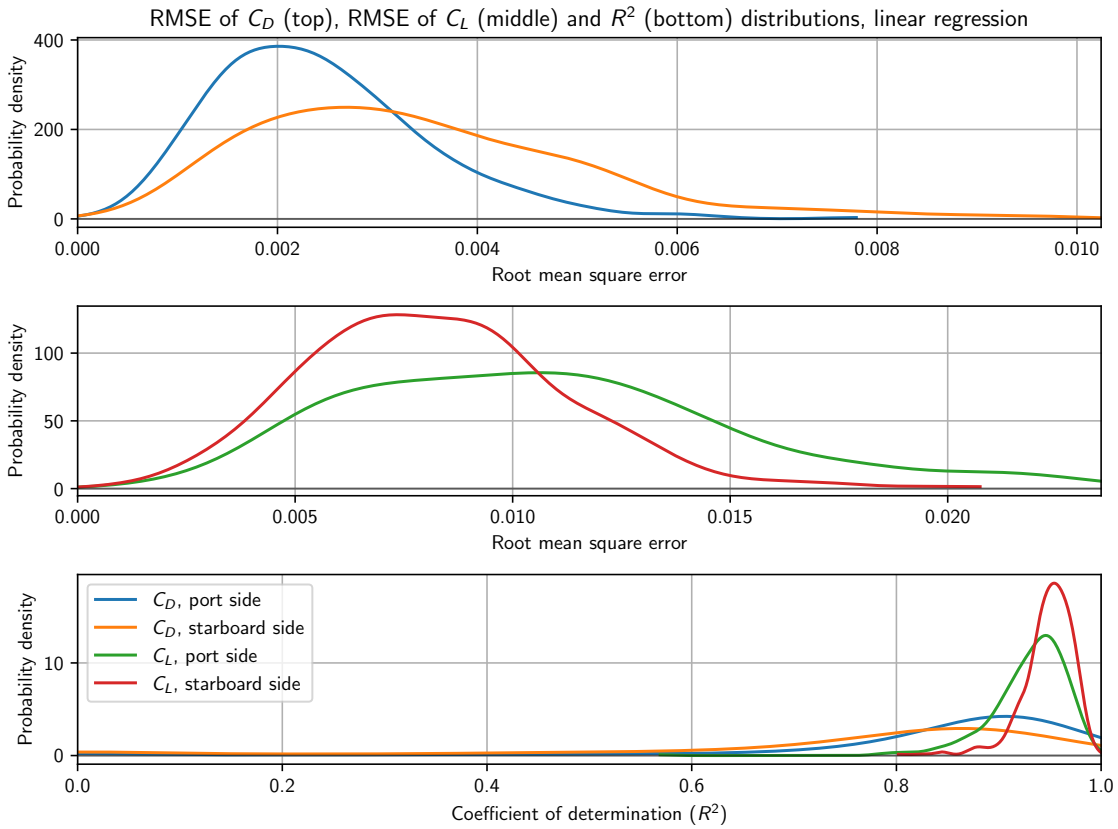

Figure 4.8: Distributions of root mean square error and coefficient of determination for the linear regression algorithm. Note that in a number of instances, R^2 was negative, hence the slight rise in the plot around zero.

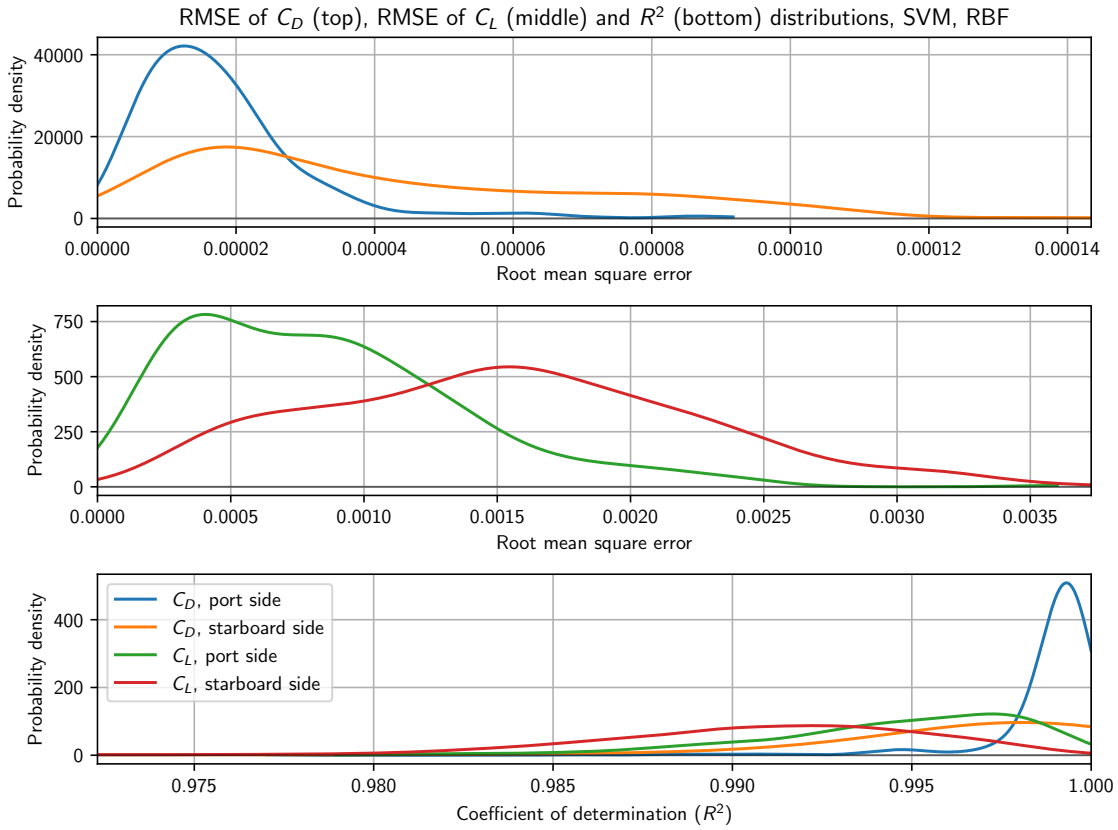

Figure 4.9: Distributions of root mean square error and coefficient of determination for the SVM algorithm.

Despite promising statistics regarding the polynomial kernel ridge algorithm's performance in the feature space from the dataset, problems were encountered when the estimators trained using this method were tested in Manwav through a recreation of the CFD conditions, following the procedure described in section 4.2.5. These problems related to the estimator's sensitivity to the features were described in section 4.3. They are the reason why ultimately, the SVM-based estimators were selected due to their preferred behaviour, even though the performance statistics of this algorithm were slightly weaker.

After every iteration of the SVM algorithm, the coefficient of determination for the random test/train split of the dataset was compared to the previous best estimator for each of the rudder forces, and if the old estimator performed worse, it was replaced. Ultimately, the best performing estimator objects were collected and serialized into a pickle file, which would be later opened by the interface script called by Manwav during rudder force evaluation. For reference, pickle files are a method of object serialization native to Python, with which all Python objects and variables can be streamed into a binary file and later unpacked. The performance evaluation of the selected estimators is described in section 4.2.5.

4.2.4. Model deployment in Manwav

This section describes the step by step process of how the trained estimators are used in a Manwav simulation. To illustrate the data-driven model's layout and the modifications made to the original model, a diagram was created, which can be seen in figure 4.10. After the models for each rudder force were packed into a pickle file, the next step was to modify the Manwav gate rudder model from the previous section to incorporate them into the rudder force evaluating method. The entire section between the calculation of drift angle and total rudder forces and moment (X_R, Y_R and N_R) was cleared. The drift and rudder angle inputs are converted to degrees. Because of the differences between coordinate systems of Manwav and the CFD analyses, drift angle is also inverted before being passed to the estimators. Afterwards, the collected inputs are used to call the Python interface script, which unpacks the estimator objects from the pickle file and passes the inputs to them. Resulting force coefficients are then returned, and are redimensionalized according to formula 4.16 before being used to calculate the total rudder forces and yaw moment.

$$F = C_F * 0.5\rho\frac{A_R}{2}V_s^2 \tag{4.16}$$

The model has been implemented such that during any given simulation drag forces are set to zero and steering forces are made equal while rudder deflection angles and drift angles are within 0.01 rad of zero - this is to ensure that the initial run-up before the manoeuvre starts produces no discrepancies between the starting parameters of a ship equipped with different rudder models. The total steering force uses the same method of calculation of additional steering force on the hull due to flap effect. The method of calculation of steering moment was improved, taking into account the influence of drag forces as well as the variable moment arms of the rudder forces. The resulting rudder forces and steering moment are then passed back to the simulation the same way they are in the original gate rudder model.

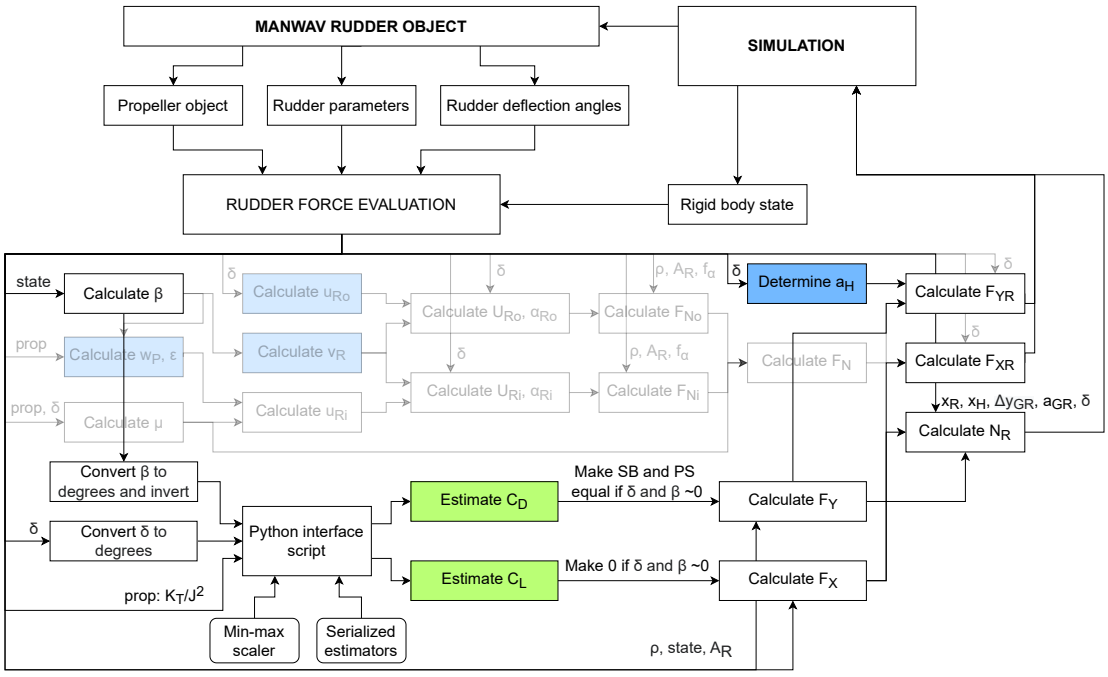

Figure 4.10: Diagram of the force evaluation in the physics-based GR model in Manwav. Steps marked by green color indicate that they are directly based on CFD data with known setup parameters.

4.2.5. Data-driven model performance

Before testing of the model implemented in Manwav was carried out, the accuracy of the estimators from the pickle file was tested on the entire dataset in order to rule out possible sources of discrepancies in later investigations. The metrics of estimator accuracy together with hyperparameters selected by the grid search algorithm can be seen in table 4.3. A scatter plot of predicted vs. actual values was also created for this evaluation and is presented in figure 4.11.

	R^2	RMSE	Hyperparameters used
C_D, port	0.999825	0.002058	Epsilon = $1e^{-5}$, C = 10000, Gamma = 0.001
C_D, starboard	0.999032	0.004433	Epsilon = $1e^{-6}$, C = 100, Gamma = 0.001
C_L, port	0.999123	0.012403	Epsilon = $1e^{-5}$, C = 10000, Gamma = 0.001
C_L, starboard	0.996989	0.032550	Epsilon = $1e^{-2}$, C = 1000, Gamma = 0.001

Table 4.3: Metrics of selected SVR estimators' accuracy on the entire dataset feature space and their hyperparameters.

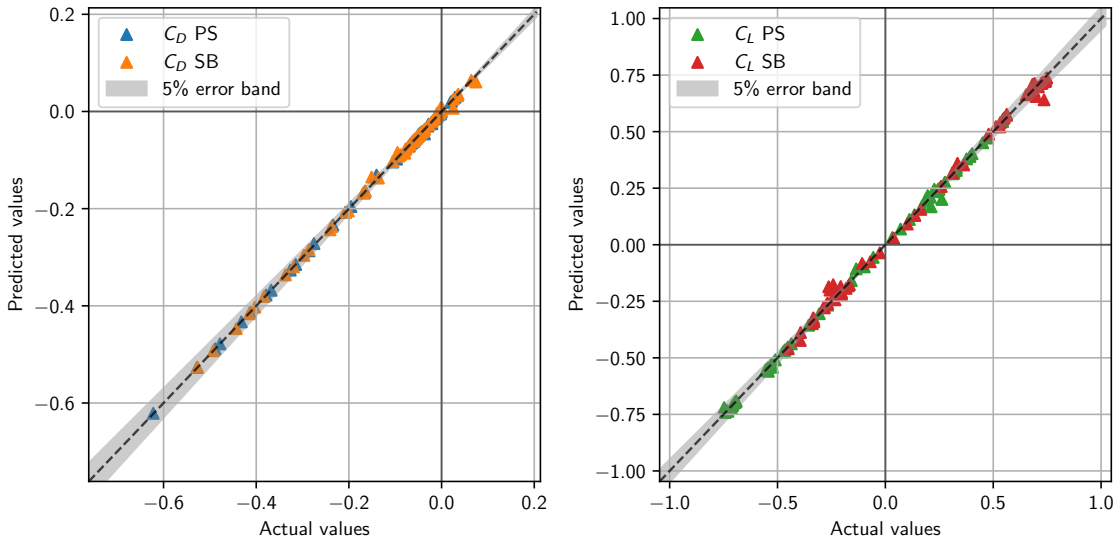

Figure 4.11: Scatter plot of predicted vs. actual values for the estimators of each of the rudder forces tested on the entire CFD dataset.

After the model deployment was complete, it was verified with respect to the source CFD data it was based on. To do this, the force coefficients obtained in Manwav using the captive rudder sweep manoeuvre were compared to the original data. These manoeuvres were simulated on the S175 vessel with the rudder model swapped to the data-based gate rudder model, set to the same ship speed as in the CFD analyses. The simulation runs matched the constant power setting as well as the drift angles set in the CFD analyses (-5°, 0°, 5° and 10°, corresponding to 5°, 0°, -5° and -10° in the Manwav coordinate system), and the steering angle was swept through a sine function between the bounds of the steering angles (-35° to 35°). Unfortunately, because the simulations needed to be run on a specific ship model, and the CFD source vessel was not implemented in Manwav (which would be a very time-consuming task considered outside of the scope of the project), they were performed on the S175 model. This meant that the propeller loading coefficient values could not be reconstructed in Manwav, for two reasons. The main reason for this is the difference between the ships used for the CFD analysis and for this test in Manwav, which have different propulsive characteristics - this causes a baseline difference between propeller loading at all times. However, it is also due to the fact that in the CFD analyses, rudder deflection influence on the flow field upstream of the propeller is properly represented in the propeller performance characteristics. The Manwav model does not have the functionality to imitate this behaviour, therefore the propeller loading coefficient is influenced only by the drift angle of the ship. This difference is the only possible explanation for the mismatch seen in the plot in figure 4.13. The scatter plots of the propeller loading coefficient values and their counterparts in Manwav obtained during the rudder sweeps manoeuvres for the same values of rudder deflection and drift angles can be seen in figure 4.12.

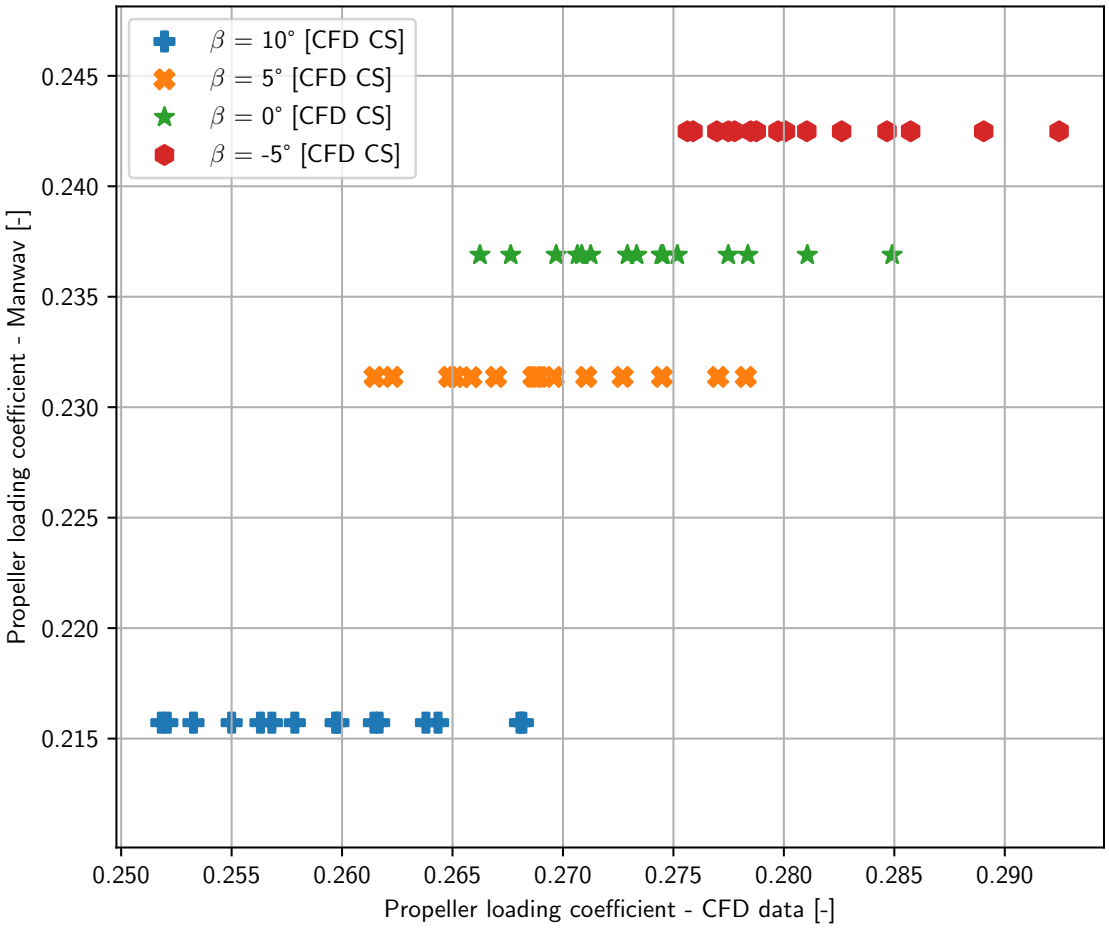

Figure 4.12: Comparisons of propeller loading coefficient values in the CFD dataset and their counterparts in Manwav during the rudder sweep manoeuvres.

The key takeaway from the observation of the scatter plot above is that there are two major differences between the propeller loading coefficient extracted from the CFD analyses and those from Manwav. The first is the simple fact that Manwav does not model the influence of propeller characteristics due to rudder deflection, as explained above, which causes the values from the simulator to form ”flat lines” along singular propeller loading coefficient values, one for each drift angle setting. The other major difference is the fact that while the order of magnitude of the variable is the same, there is a mismatch between the exact ranges of values, indicated by the ”lines” of constant propeller loading coefficient values in Manwav not lying within the ranges of their equivalents from CFD data - this shows the discrepancy between the vessels the tests were conducted on, as the propeller loading coefficient calculated for the S175 in these test manoeuvres is smaller than that of the CFD source vessel’s.

In order to obtain more accurate matches to the steering angles from the dataset at discrete time stamps, the time step was lowered to 0.1 s. Drag and lift coefficient generated in the rudder system were sampled at an interval of one degree of rudder deflection and passed to a Python script that produced the relevant plots. They can be seen in figure 4.13.

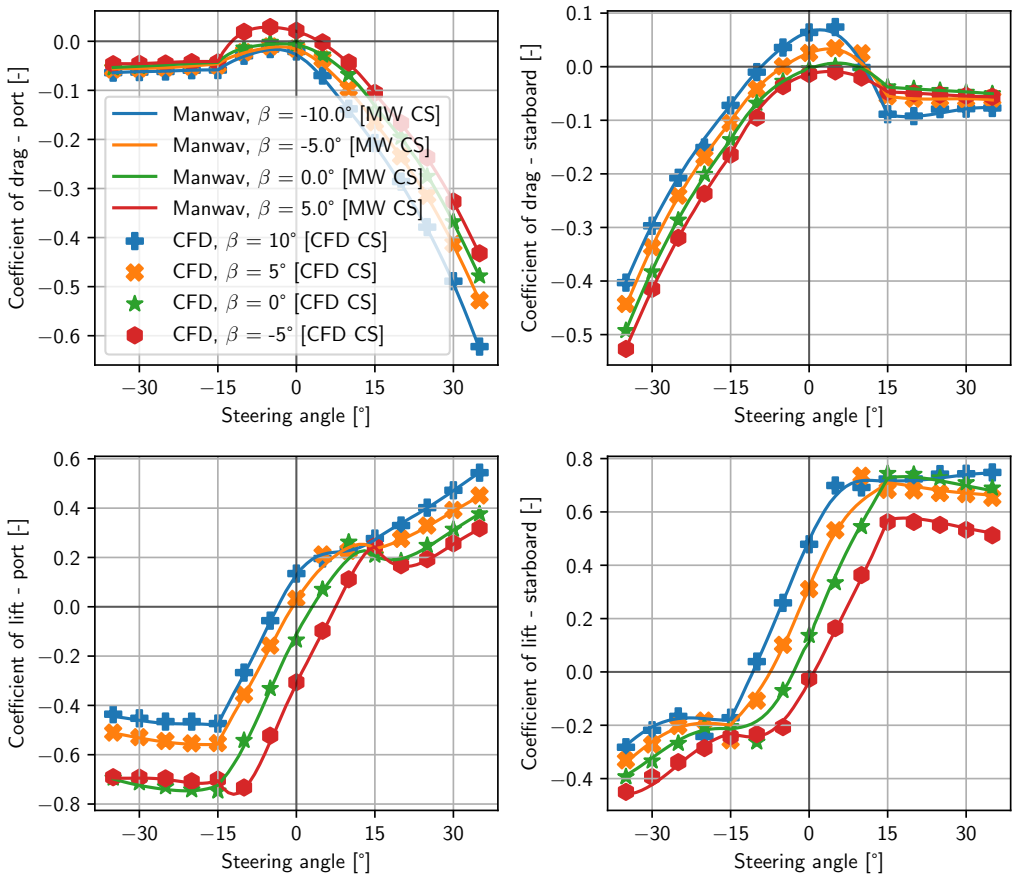

Figure 4.13: Comparisons between the force coefficient values from the CFD analyses and those obtained in Manwav during the rudder sweep manoeuvres from the SVM estimators trained on non-normalized data.

The match between the estimated force coefficient values obtained in Manwav and the source data was found to be good. The plots closely followed the datapoints for the entire range of the CFD dataset, with the exception of two points for the starboard lift coefficient at +10° and -15° of rudder deflection, where the flow regime around the blade transitions into stall. Despite this mismatch, which causes a smoother transition into stall, the accuracy of the model was deemed acceptable.

4.3. Problems encountered during estimator fitting

As previously mentioned, while performing the regression algorithm selection, some problems were encountered that changed the decisions made regarding the selection of the algorithm and normalization. These problems caused unwanted behaviour in the estimators when presented with inputs outside of the original feature space of the CFD dataset.

During the development of the methodology for the regression algorithm selection and estimator fitting, it was initially decided to use normalization in the pre-processing of the CFD dataset, simply due to the fact that it is considered good practice. Additionally, during initial testing, it was found that for certain combinations of hyperparameters, the polynomial kernel ridge algorithm reported warnings related to the ill-conditioning of the matrices when normalization was not used, which further supported the use of feature scaling. The algorithm performance statistics showed both kernel ridge algorithms and the support vector machine to be performing at a similar level of accuracy, with slight advantage of SVM in terms of standard deviation of the metrics. However, upon reaching the second phase of testing, where the outputs of the estimators implemented in a Manwav scenario recreating the conditions from the CFD simulations (the source of the CFD dataset) were compared to the original values from the dataset, a significant problem revealed. The discrepancy in the values of propeller loading coefficient was causing the predicted force coefficient plots to be heavily deviated from the original distribution of datapoints, as showcased in one of the examples in figure 4.14.

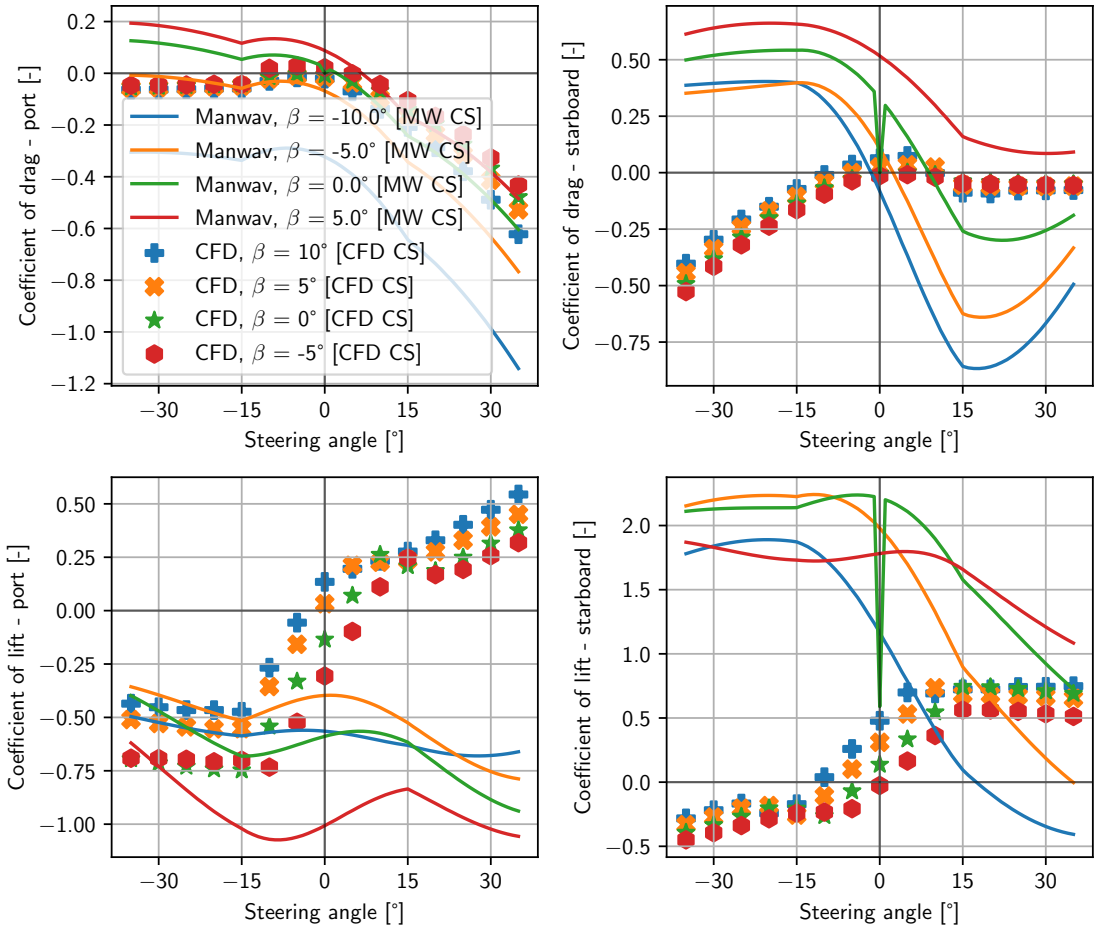

Figure 4.14: Comparisons between the force coefficient values from the CFD analyses and those obtained in Manwav during the rudder sweep manoeuvres from the SVM estimators trained on normalized data.

Since there is no full-scale measurement data of gate rudder forces publicly available, there was no possibility to perform validation of the model. Therefore, the CFD analyses which are the source of the data used in the model's creation will be treated as ground truth.

It was expected that the inability to replicate the exact values of propeller loading coefficient in Manwav due to the tests being performed on a different vessel would cause some mismatch between the force coefficient values predicted in the simulator and those from the CFD dataset. However, the difference between the plots was large, which pointed to the fact that the propeller loading coefficient, being the only parameter that differed between the compared scenarios, was given too much bias. The suspected reason for this exaggerated bias was the normalization. This was not an acceptable behaviour, so the fitting had to be adjusted. Estimator behaviour without normalization was therefore investigated.

When the algorithm evaluation calculations were run without normalization of features, the performance metrics statistics favoured kernel ridge estimators over SVM. However, a similar kind of discrepancy between force coefficient values obtained in testing performed in the Manwav CFD recreation manoeuvres was encountered for kernel ridge estimators with both polynomial and rbf kernel. This behaviour is presented in figure 4.15. In the figure, only one of the rudder forces shows the mismatch between the estimated and the source values. However, such behaviour was observed for at least one of the rudder forces in every training run, corrupting the performance of the estimators seemingly at random.

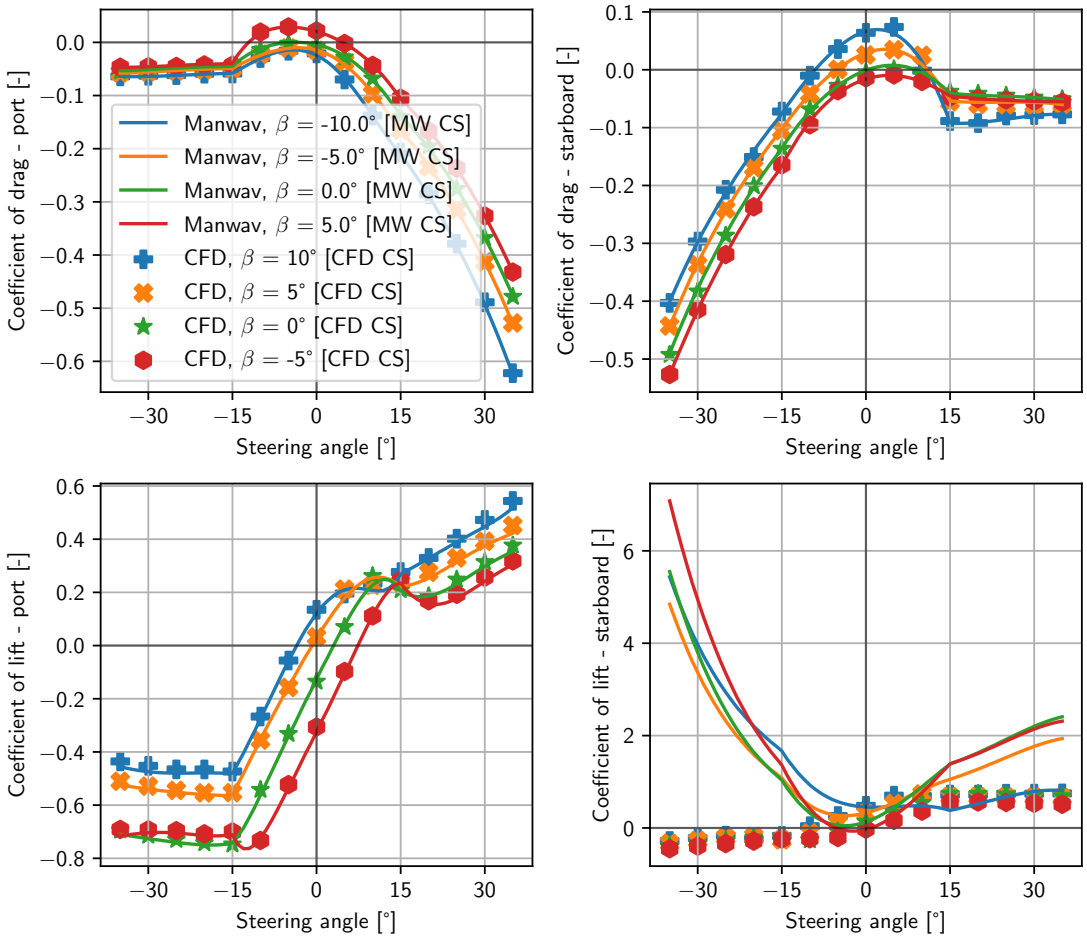

Figure 4.15: Comparisons between the force coefficient values from the CFD analyses and those obtained in Manwav during the rudder sweep manoeuvres from the polynomial kernel ridge estimators trained on non-normalized data.

This time, the bias assigned to the propeller loading coefficient was not caused by the normalization, because it was not used. Therefore, even though the statistics from the algorithm evaluation showed it to perform slightly worse on average, SVM was also tested in the same scenario in Manwav. It showed a near perfect match with the dataset values, as shown in figure 4.13. As mentioned before, slight shift between the values was expected and would have been deemed acceptable, but the perfect match with very small priority given to the propeller loading coefficient was considered a more desirable outcome than the discrepancies encountered before, so the SVM-based were selected for the final implementation.

Getting into the exact details of the unwanted behaviour of the estimators was deemed outside of the project's scope, since a sufficiently accurate algorithm that did perform as intended in all tests was identified, meaning that the work could continue. Among the future recommendations discussed in section 6.3, one of the most important upgrades to the work presented in this report is an expansion of the dataset through, among others, a wider range of values of the propeller loading coefficient. Once it is done, the influence of this parameter should be possible to estimate accurately and without bias, both with and without normalization.

5. Case study

After the model deployment and initial testing were completed, the gate rudder model was ready for use in simulated manoeuvres on a ship model in Manwav. The goal of this project was to showcase the influence of a gate rudder system on a ship's manoeuvrability, serving as a proof of concept for the method of investigating gate rudder capabilities through time domain simulation. This chapter focuses on the analysis of manoeuvring performance of the model of the S175 container ship equipped with three different rudder models discussed in previous chapters: the default Manwav simple rudder model for a conventional rudder, a physics based model derived from a mathematical MMG-based gate rudder model presented in literature, and a data-based model built using machine learning regression on CFD data. All three of these models have flaws and limitations, as does the ship manoeuvring model they are used on.

The default Manwav simple rudder model is based on a highly simplified mathematical model of a hydrofoil that calculates the rudder forces using the inflow velocity magnitude and angle as input variables and lift coefficient slope as well as lift to drag ratio as static parameters. It does not take into account the influence of drift on the flow field in ship's aft section or any advanced hydrodynamic effects like the flap effect or stall, making the result of its calculations inaccurate beyond small rudder deflection angles. Additionally, the input parameters of lift coefficient slope and lift to drag ratio have to be tuned arbitrarily for every ship in order to match the manoeuvring performance.

The physics-based gate rudder model described in section 4.1 is a much more sophisticated rudder model that takes into account a lot of effects associated generally with hydrofoils, but also those specific to the gate rudder system. However, the formulas that were regressed by the authors of the paper from CFD data were based on Shigenobu, a comparatively small ship, with a similarly low design speed of 16 knots. Clear errors were found in the methodology for covered area ratio calculation and were corrected to the author's best ability, but in addition to that, some of the formulas used by the authors of the source paper were not given sufficient explanation and doubts were raised whether they were derived correctly. Examples of this are the regression formula for axial velocity in the propeller slipstream and the formula for rudder blade's lift coefficient, but they were nonetheless kept in the Manwav model. Lastly, the ability of the model to predict rudder forces accurately was not tested by the authors, even on CFD analyses for verification.

The data-based gate rudder model described in section 4.2 is a model directly derived from rudder force values tied to specific variables in the system. It is based on a vessel larger than S175, but the size difference is not as significant as in the case of comparison to Shigenobu. Still, the size of the vessels might influence the accuracy of the force predictions. Additionally, while the model was verified with respect to source data and should perform accurate force predictions within the feature space from the dataset it was based on, deviations from the ranges of rudder and drift angles might compromise the estimators' accuracy.

Both gate rudder models showcased in this chapter also feature a specific set of dimensions, described in more detail in the next section. They were determined using relationships between Sakura, Shigenobu and S175. The author does not claim to be an expert in the design of gate rudder systems and the final values of these parameters need to be treated only as reference. It is quite possible that in the event that a similar ship to the S175 would be equipped with a gate rudder system, it would be designed with a different set of dimensions, resulting in a different tradeoff between manoeuvrability and added drag due to steering.

Finally, the hull hydrodynamics model of the S175 vessel on which all of the rudder models are ”mounted” as modules is also an imperfect representation of a real-life vessel that never existed, which in itself is a limitation due to lack of reference to the vessel's real hydrodynamics. Ship models in Manwav are created using outputs from two other programs, MPP and PRECAL, which also simplify the hull hydrodynamics.

5.1. Gate rudder design parameters used

Because no real-life gate rudder system designed specifically for the S175 container ship exists, the dimensions used in the model to calculate the forces needed to be established in a different way. Measurements of rudder systems of Sakura and Shigenobu, the sister vessels equipped with a conventional rudder and a gate rudder, respectively, can be accessed in GATERS report D1.1 titled ”Report of the Selected Vessels and Operational Data” [39]. The schematic used to determine most of Shigenobu's rudder measurements can be seen in figure 5.1.

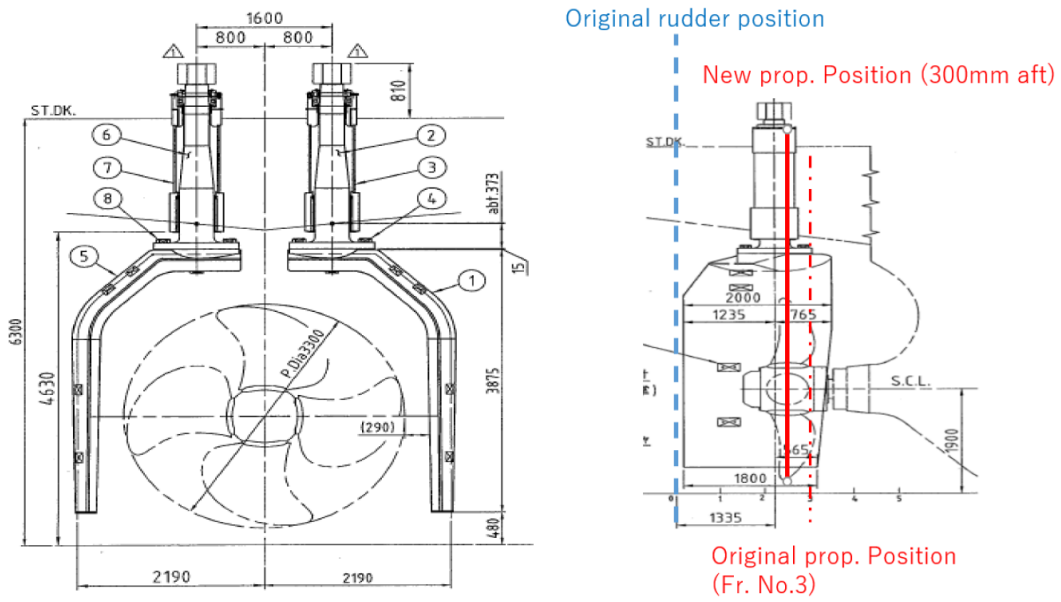

Figure 5.1: General arrangement of Shigenobu gate rudder system [39]

Key measurements were extracted from the report in order to serve as reference, together with the dimensions of the original S175 conventional rudder, for the dimensions of the gate rudder system for the S175 ship. First, the total rudder area was calculated as 150% of the conventional S175 rudder area. This is because typically, gate rudder area is larger than that of a comparative conventional rudder, with Shigenobu's total rudder area equalling ~121% of Sakura's serving as an example. Additionally, due to S175's higher design speed than Shigenobu's, a decision was made to use a larger rudder area multiplier of 1.5. Afterwards, the aspect ratio of S175 gate rudder blades was determined to be the same as Shigenobu's in order to achieve a similar behaviour with regard to blades entering the propeller slipstream. Chord length was then derived from the following equation:

$$A_R = 2CS = 2C\frac{S}{C}C = 2C^2AR \tag{5.1}$$

where A_R is total rudder area, C is the chord length, S is the span and AR is blade's aspect ratio. Span was then derived from its relationship with total rudder area and chord length. Rudder stock offset and arm were then calculated by multiplying their respective values in Shigenobu by the ratio of propeller diameters of S175 and Sakura. Vertical position of propeller shaft z_P was kept the same as in S175, and the vertical location of rudder's midspan z_R was set to slightly less than that, following the same convention as in Shigenobu. Finally, the part of the chord extending aft of the rudder stock was derived by multiplying Shigenobu's equivalent by the ratio of chord lengths of S175's gate rudder and Shigenobu. The relevant dimensions and their values are presented in table 5.1.

	Sakura	S175 - CR	Shigenobu	S175 - GR	Description of reasoning
Total area [m^2]	9.25	33.04	11.2	49.56	S175 rudder area multiplied by a static factor of 1.5
Chord [m]	2.5	4.26	1.9	4	Result from the equation $A_R = 2c\frac{h}{c}c$ because $h = c\frac{h}{c}$
Span [m]	3.7	7.76	2.95	6.2	Blade area divided by chord length
Aspect ratio [-]	1.48	1.82	1.55	1.55	Same as in Shigenobu
z_P [m]	1.9	4	1.9	4	Same as in S175
z_R [m]	2.2	4	1.8	3.8	Arbitrary, slightly lower than z_P
Propeller diameter	3.5	6.5	3.3	6.5	Same as in S175
Rudder stock offset [m]	0	0	0.8	1.49	Shigenobu offset multiplied by ratio of D_P in S175 and Sakura
Rudder stock arm [m]	0	0	1.3	2.41	Shigenobu arm multiplied by ratio of D_P in S175 and Sakura
Chord portion aft of stock [m]	-	-	1.235	2.6	Shigenobu aft chord portion multiplied by ratio of chord of S175 GR and Shigenobu

Table 5.1: Design parameters of the S175 gate rudder system.

5.2. Simulation setup

Because the plan for this case study was to showcase the influence of rudder models on the manoeuvrability of the chosen vessel, some representative manoeuvres needed to be selected. In order to stay within the parameters the base S175 model was tested for, they needed to be chosen from the list of manoeuvres in table 3.2, which were investigated in section 3.2. It was the intention that each of the manoeuvres selected for the case study would provide additional information about the relative performance of the ships with different rudder models. Ultimately, the manoeuvres for the case study were selected and are presented in table 5.2. They are turning circles and zig-zag manoeuvres performed at different ship speeds and target rudder angles, which allowed to get the most out of the comparisons.

	Type	Rudder (and heading) target setting [°]	Starting ship speed [kn]
1	Turning circle	15 SB	24.15
2	Turning circle	35 PS	12.08
3	Zig -zag	20 PS	24.15
4	Zig-zag	10 SB	12.08

Table 5.2: List of selected manoeuvres for comparison between S175 with different rudder models.

The manoeuvres listed above were all performed with a time step of 0.2 s. Additionally, each run had a constant torque power setting, which ensured that engine parameters would not exceed their limits. An interesting observation about the simulator performance during calculations is the fact that the calculation efficiency was lower on the data-based gate rudder model, as expected. For comparison, the time to calculate the second turning circle manoeuvre was around 7 seconds, compared to approximately 2 seconds needed to finish the calculations of the same maneouvre on the other rudder models. An obvious reason for this is the fact that on every iteration of the simulation, the python interface script is called and the estimators need to be unpacked from the pickle file.

5.3. Analysis of results

After the simulations were complete, comparison plots were created for three variants of the S175. Only selected plots were shown in the chapter, with the other plots generated for the manoeuvres being available in appendix C. First, the turning circle manoeuvres were analyzed.

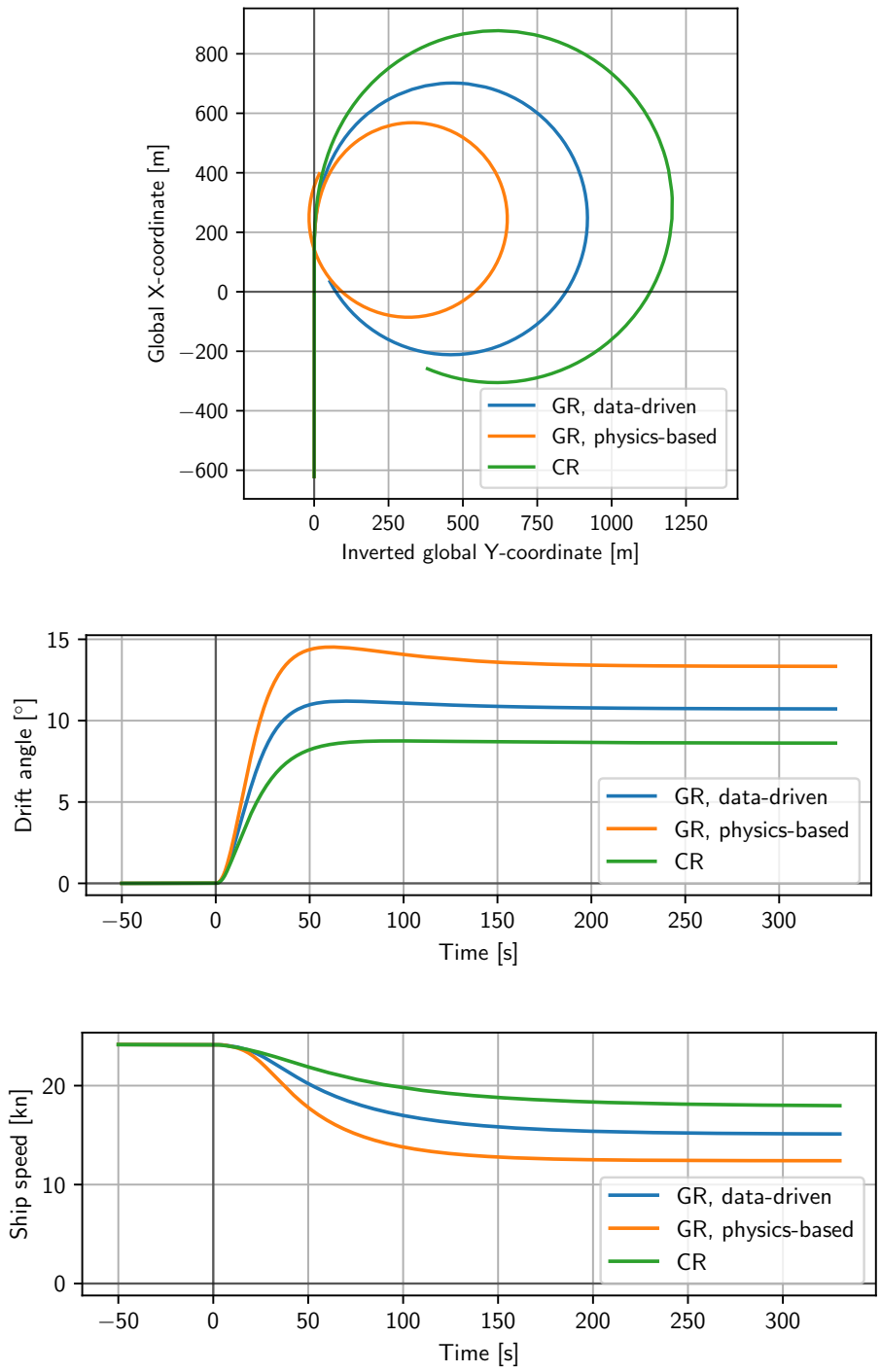

Figure 5.2: Ship track, drift angle and ship speed plots of the 15° to starboard turning circle manoeuvre at 24.15 kn.

In the high-speed turning circle manoeuvre, considerable differences can be observed between the performance of the three vessels. Both gate rudder models cause their vessel to make a tighter turn than the original conventional rudder, at the cost of a higher drop in ship speed for both. Drift angle was higher for both GR models, and while the conventional rudder vessel gradually reached a stable drift angle, the two other vessels experienced a slight overshoot of the drift angle, settling down on their respective stable drift angles later into the manoeuvre. Generally, the physics-based model performed more extremely than the data-driven one from all analyzed perspectives.

	CR	GR - physics-based	GR - data-driven
Advance	871 m	558 m	693 m
Tactical diameter	1197 m	640 m	910 m

Table 5.3: Performance metrics of the three test vessels in the 15° to starboard turning circle at 24.15 kn.

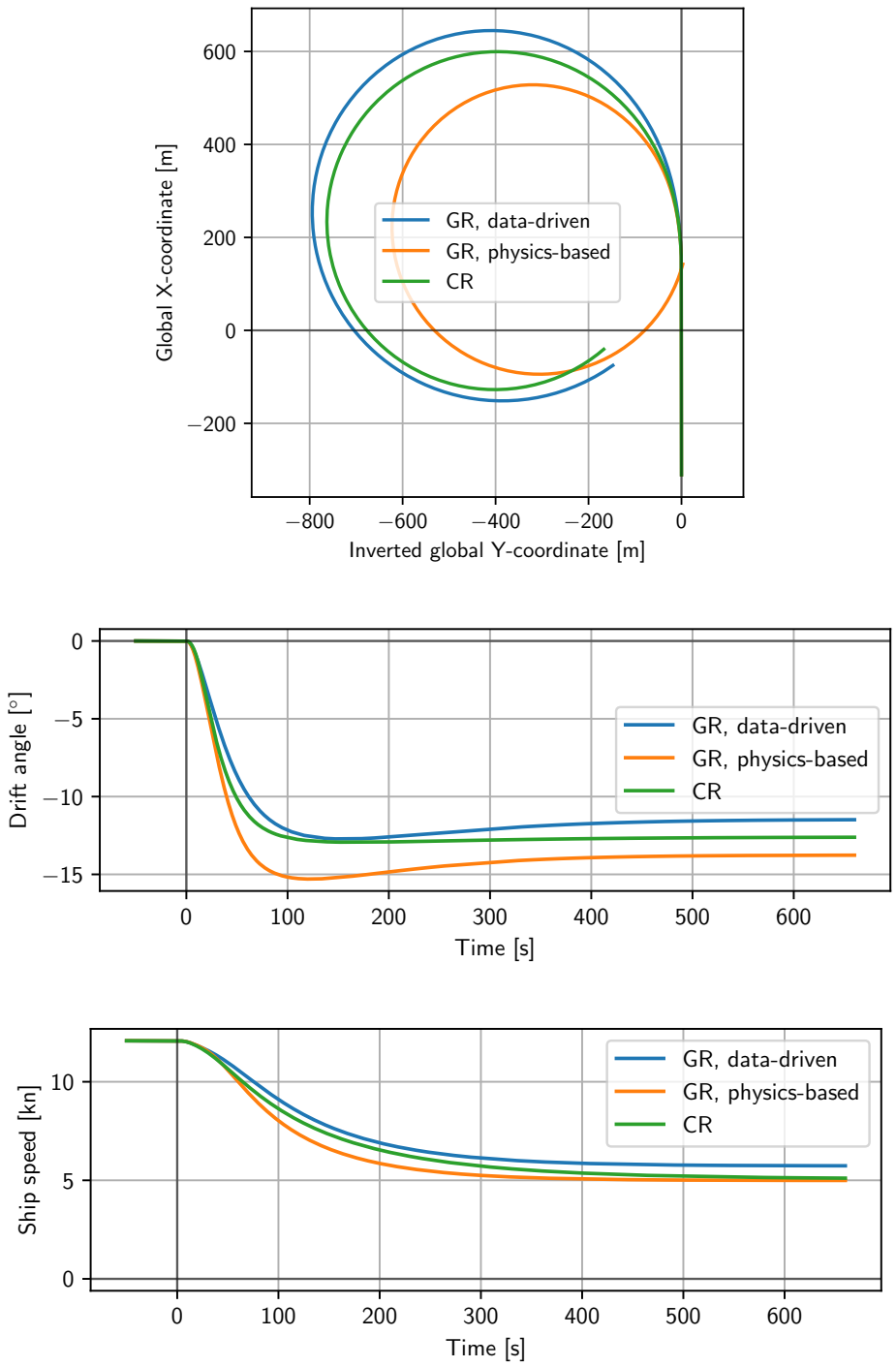

Figure 5.3: Ship track, drift angle and ship speed plots of the 35° to port turning circle manoeuvre at 12.08 kn.

The low-speed turning circle manoeuvre yielded different results. In this case, the vessel with the physics-based rudder model again made the tightest turn by a considerable margin (advance and tactical diameter were 12.3% and 18.7% lower, respectively, compared to the conventional rudder), which was the result of a higher drift angle sustained during the manoeuvre. At the end of the manoeuvre, the ship's velocity was still decreasing steadily, reaching the speed sustained by the conventional rudder vessel. On the other side, the vessel using the data-driven model made a slightly wider turn than the ship with the conventional rudder. The drop in ship speed and the sustained drift angle were also smaller than for the conventional rudder.

	CR	GR - physics-based	GR - data-driven
Advance	590 m	518 m	635 m
Tactical diameter	754 m	613 m	786 m

Table 5.4: Performance metrics of the three test vessels in the 35° to port turning circle at 12.08 kn.

Afterwards, a closer look was done at the zig-zag manoeuvres. Even though it is the convention to combine plots of heading and rudder angle in zig-zag manoeuvres, the rudder angle plots were excluded from the heading plots for the sake of clarity.

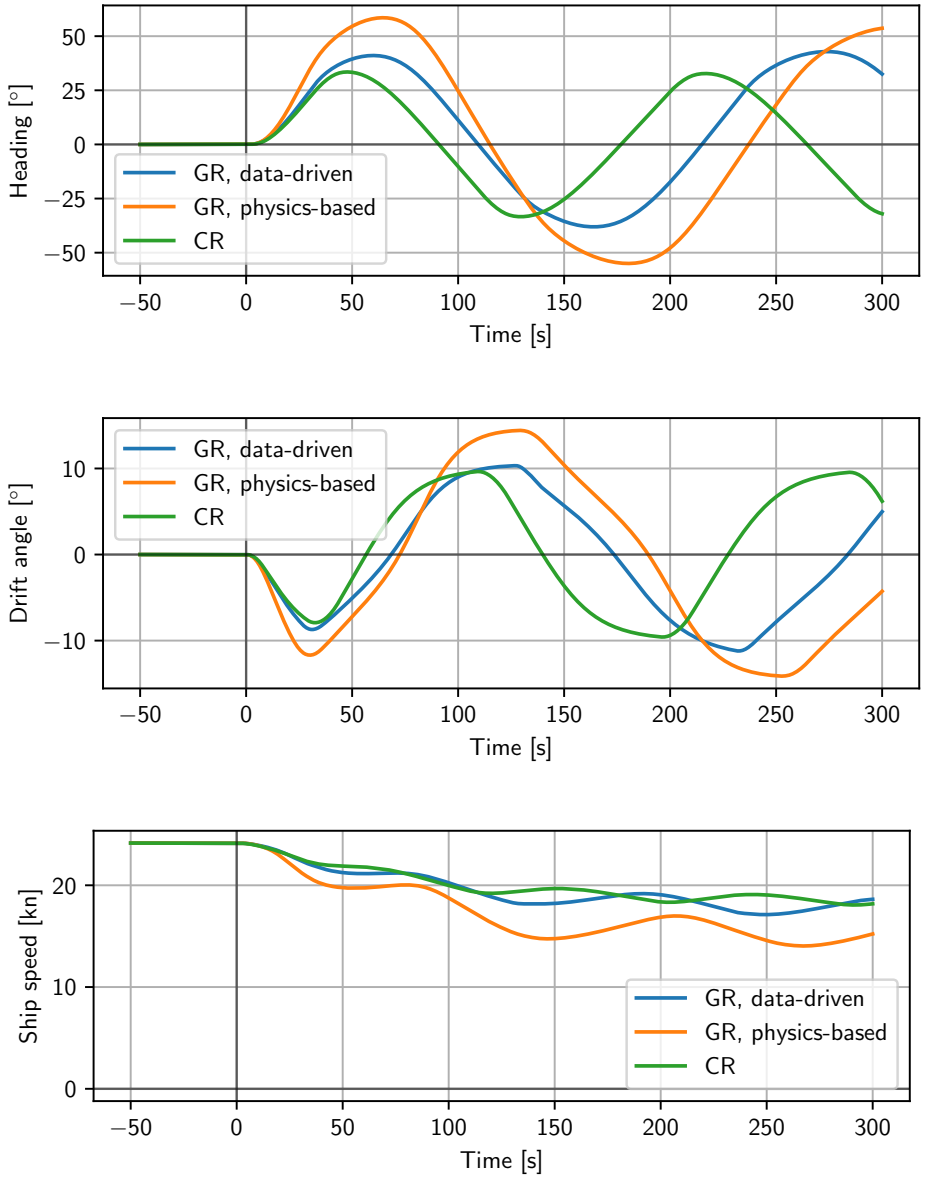

Figure 5.4: Plots of the port 20-20 zig-zag manoeuvre at 24.15 kn.

In the high-speed zig-zag manoeuvre, both gate rudder vessels displayed worse manoeuvrability than the conventional rudder vessel, even though their drift angles were larger. An unexpected fact is that although they reached higher overshoot angles, both lost more speed than the reference. At the start of the manoeuvre, one can observe higher initial response of the vessel with the physics-based rudder model, but immediately afterwards, it starts to struggle to reverse its angular momentum. The data-driven model, on the other hand, seems to perform largely in the same, but slightly slower manner as the conventional rudder.

	CR	GR - physics-based	GR - data-driven
1st overshoot	13.5°	38.5°	21.1°
2nd overshoot	13.4°	35.0°	18.1°

Table 5.5: Performance metrics of the three test vessels in the port 20-20 zig-zag manoeuvre at 24.15 kn.

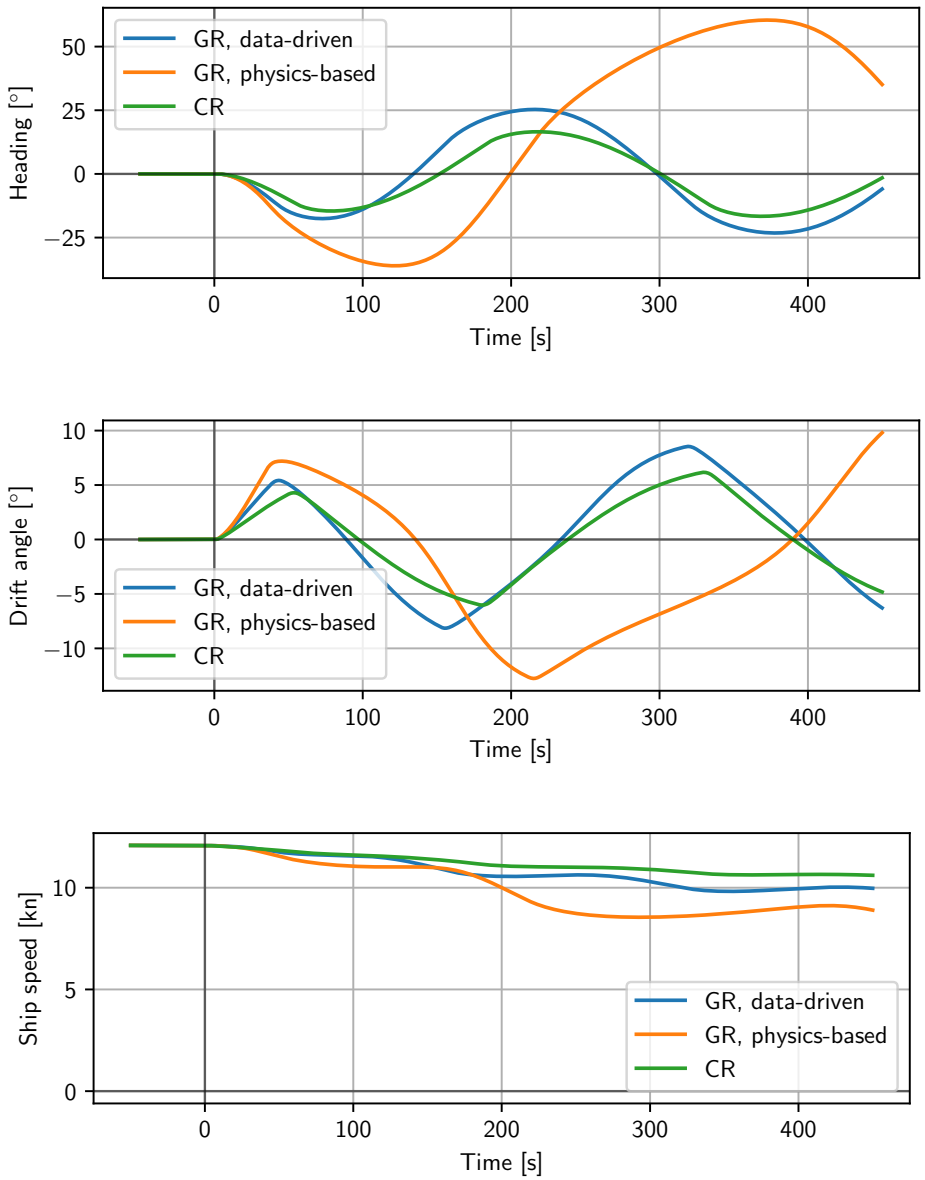

Figure 5.5: Plots of the port 10-10 zig-zag manoeuvre at 12.08 kn.

The final analyzed manoeuvre had the most surprising results. While the relationship between the vessel with the data-driven rudder model and the one with the conventional rudder model, with the former behaving similarly, albeit being slightly slower to react, with regard to the former, the physics-based model produced results vastly different from the other two vessels. The same observation about the fast initial reaction turning into a struggle to reverse the angular momentum can be made here, but at a more significant scale. Another observation is that again, both gate rudder vessel lost more speed than the conventional rudder vessel.

	CR	GR - physics-based	GR - data-driven
1st overshoot	4.6°	26.1°	7.6°
2nd overshoot	6.6°	50.4°	15.3°

Table 5.6: Performance metrics of the three test vessels in the starboard 10-10 zig-zag manoeuvre at 12.08 kn.

The main conclusion from the initial analysis was the fact that the two models supposed to represent the performance of the same rudder system produced vastly different results. Because of this behaviour, the physics-based model was excluded from further analysis, which focused on the power characteristics of the vessels during each manoeuvre.

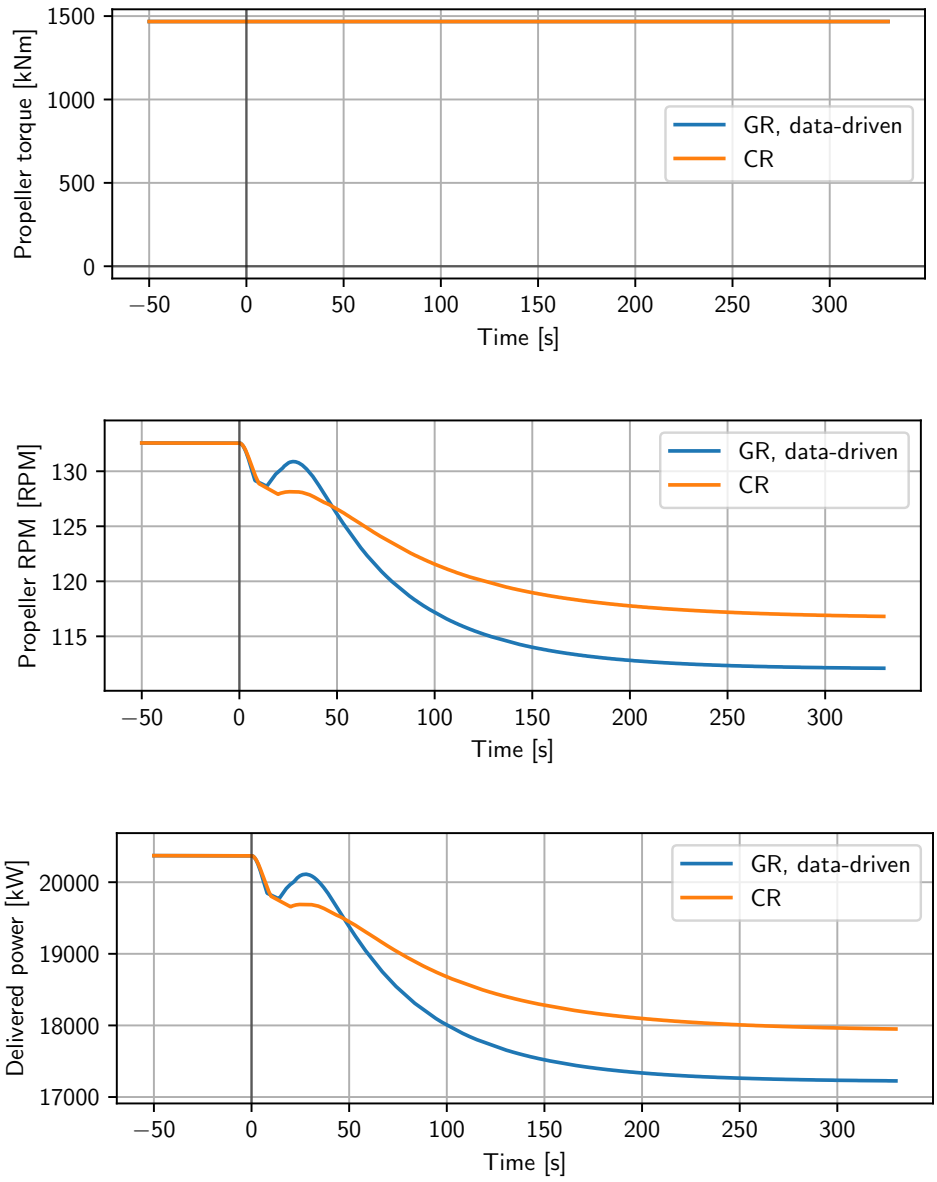

Figure 5.6: Power characteristics plots of the 15° to starboard turning circle manoeuvre at 24.15 kn.

Propeller torque was correctly set by the simulator to a constant value based on the required vessel speed. This meant that the only variable parameter in the power characteristics was propeller RPM. This is why the plots of RPM and delivered power have the same shape for each of the manoeuvres.

In the high-speed turning circle manoeuvre, one can observe the delivered power dip down at the start of the manoeuvre, before the plots for the two different rudder models sharply diverge due to the vessel equipped with the gate rudder encountering a sudden rise in power. Afterwards, both plots gradually descend to stable values, with a sharper descent observed for the gate rudder vessel, causing the final power value for that rudder model to be lower than that for the conventional rudder. The average power drawn by the gate rudder vessel over the entire manoeuvre was approximately 2.6% lower.

	CR	GR, data-driven
Mean delivered power [kW]	18762	18273

Table 5.7: Mean delivered power for each analyzed rudder type in the 15° to starboard turning circle manoeuvre at 24.15 kn.

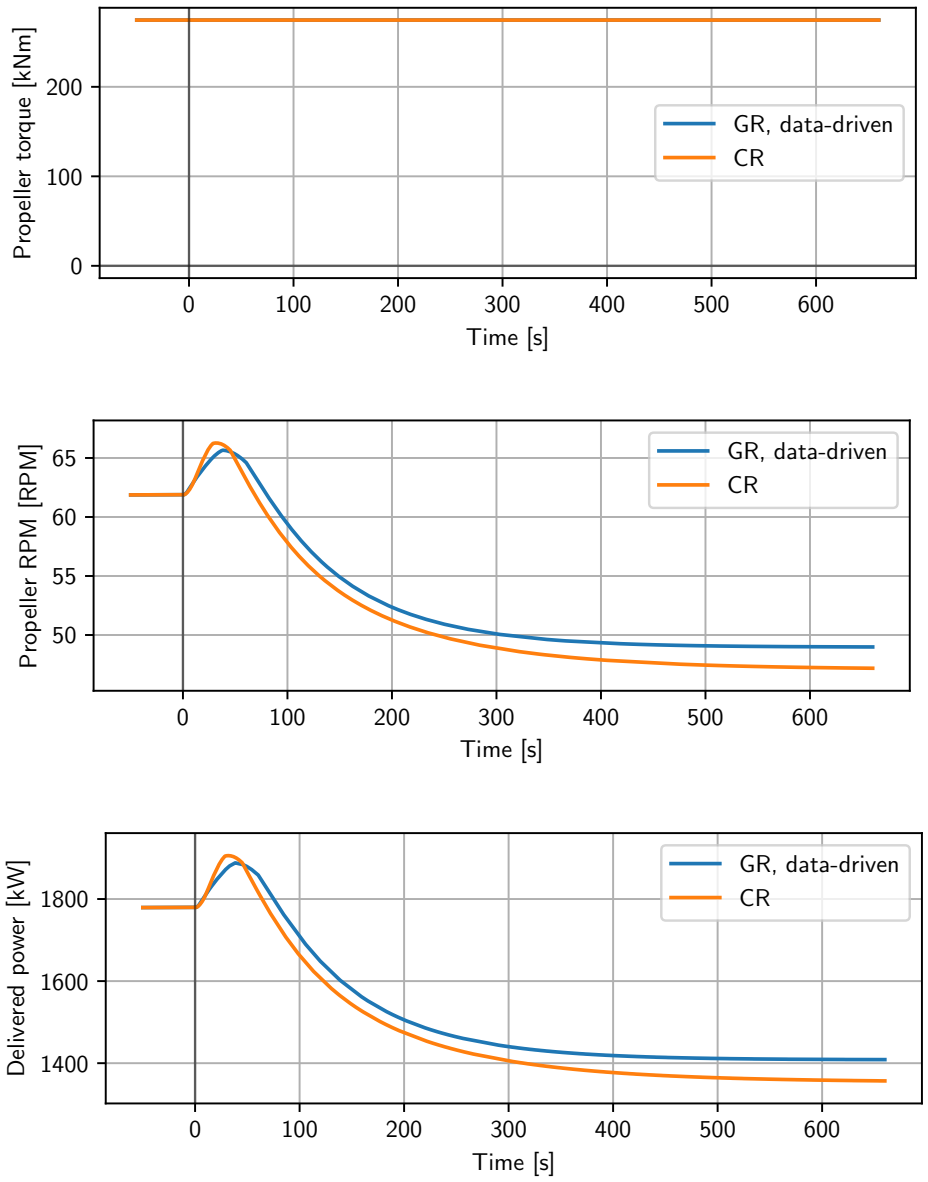

Figure 5.7: Power characteristics plots of the 35° to port turning circle manoeuvre at 12.08 kn.

In the low-speed turning circle manoeuvre, the delivered power plots have a different shape than in the previously analyzed manoeuvre. In this case, both vessel experienced a sudden rise in drawn power at the start of the manoeuvre, before gradually descending to stable values. The plots for both rudder types have roughly the same shape, with the conventional rudder vessel ending up drawing less power in the end, despite its initial peak being slighly higher than that of the vessel with the gate rudder. This time, the mean power draw over the entire manoeuvre was lower for the conventional rudder by ~2.2%.

	CR	GR, data-driven
Mean delivered power [kW]	1496	1530

Table 5.8: Mean delivered power for each analyzed rudder type in the 35° to port turning circle manoeuvre at 12.08 kn.

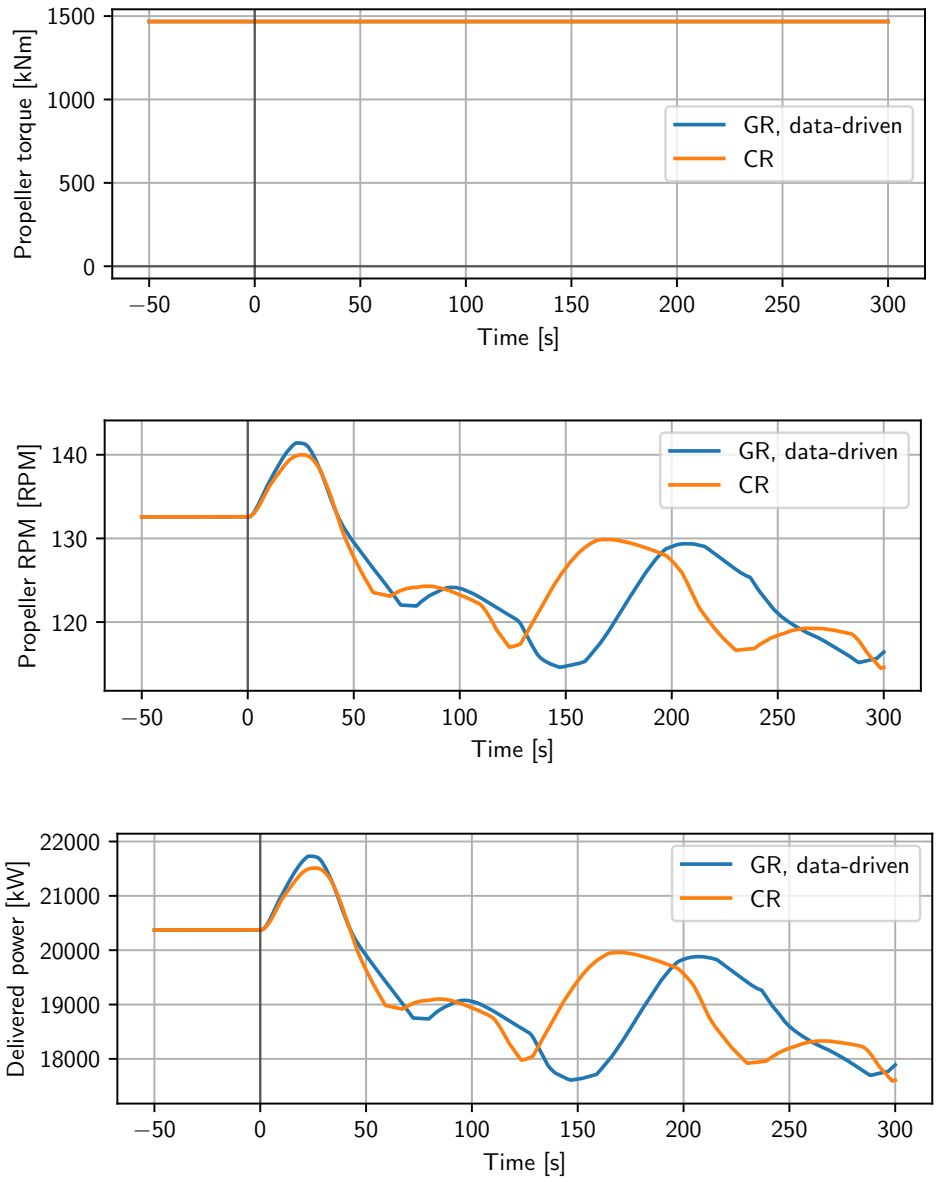

Figure 5.8: Power characteristics plots of the port 20-20 zig-zag manoeuvre at 24.15 kn.

In the high-speed zig-zag manoeuvre, the plots take on a more complicated form. Power plots for both rudder types are a collection of gradual peaks and troughs occuring between the moments of rudders changing direction of deflection. The shapes of both plots are similar, with peaks corresponding to the peaks of heading for each vessel, and the plot for the conventional rudder being more compacted in time, which is a result of the better responsiveness displayed by the vessel during the manoeuvre. While the gate rudder vessel performed worse in this manoeuvre, it drew less power on average, by 0.25%.

	CR	GR, data-driven
Mean delivered power [kW]	19333	19285

Table 5.9: Mean delivered power for each analyzed rudder type in the port 20-20 zig-zag manoeuvre at 24.15 kn.

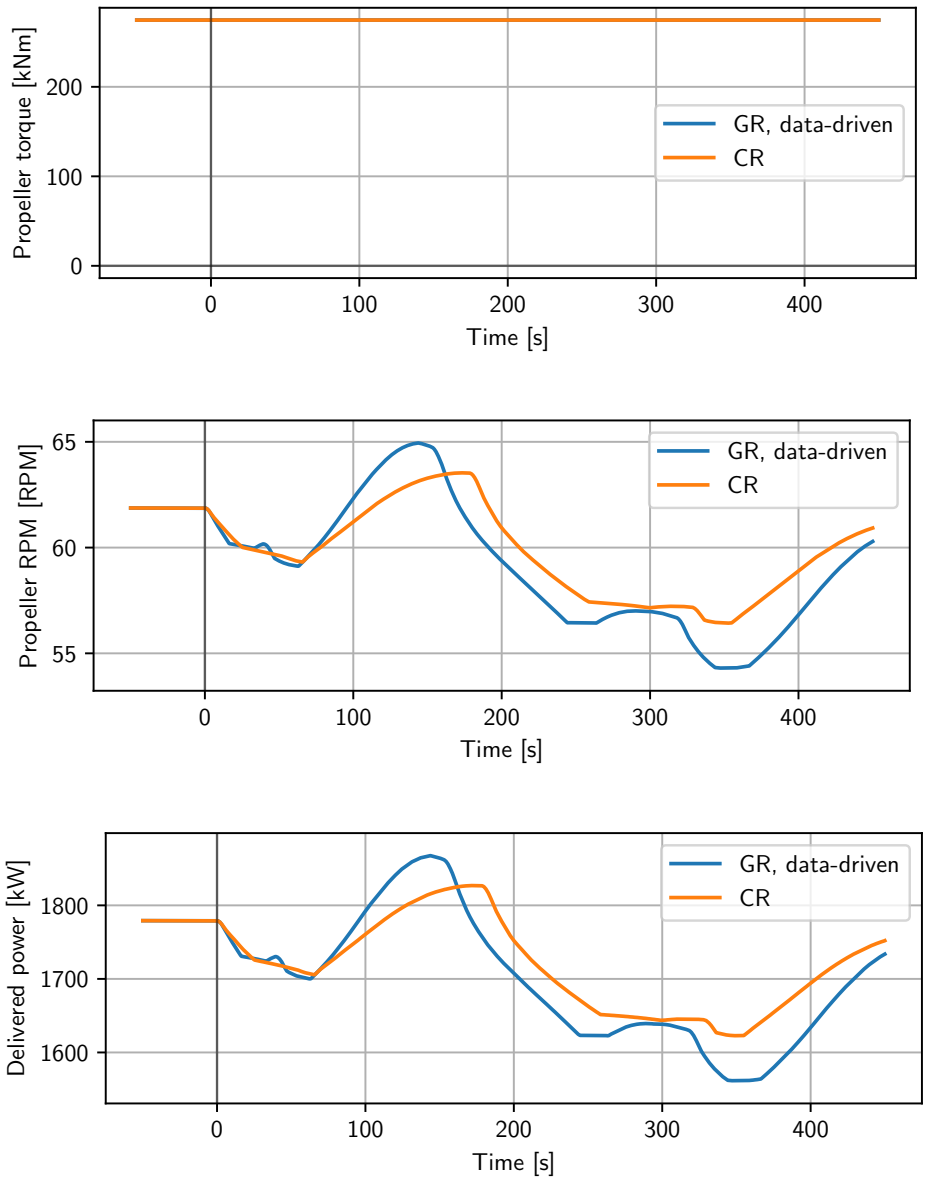

Figure 5.9: Power characteristics plots of the port 10-10 zig-zag manoeuvre at 12.08 kn.

In the low-speed zig-zag manoeuvre, the peaks on power plots for both rudder types were better lined up, corresponding to the similarity in the responsiveness of both vessels during this manoeuvre. Peaks and troughs on the gate rudder plot are more pronounced. The vessel with this rudder model also achieved a lower mean power draw than the conventional rudder ship, by approximately 1%.

	CR	GR, data-driven
Mean delivered power [kW]	1722	1704

Table 5.10: Mean delivered power for each analyzed rudder type in the starboard 10-10 zig-zag manoeuvre at 12.08 kn.

The general conclusion from the case study is that the gate rudder, as implemented in the data-driven model, changes the performance of a vessel it is mounted on. How a vessel's performance is affected is dependent on a lot of variables, including the vessel's parameters, manoeuvre settings and design parameters of the rudder system. In the analyzed scenarios, in three out of four manoeuvres, the gate rudder vessel performed worse than the reference vessel with a conventional rudder, measured through advance and tactical diameter metrics for turning circles and through overshoot angles for the zig-zags. In a different combination of three manoeuvres, though, it achieved a lower mean power draw. Such results were observed for a particular combination of rudder design parameters, though, so these facts should not be treated as a statement about the general effect a gate rudder system has on a ship's performance. When rudder deflection's influence on propeller loading is implemented in the model, the dataset it is based on is expanded to include a wider range of propeller

loading coefficient values and the model and the vessel it is mounted on are validated, the model could be used to estimate the manoeuvring performance and power savings stemming from the use of a gate rudder on a vessel.

5.4. Cancelled validation attempt

The initial plan of the project included an implementation of Shigenobu in the simulation software, but after a consideration of the added scientific value such investigation would have, a decision was made to not carry out this analysis. This is because at the current state of research into the gate rudder concept, a model of Shigenobu in Manwav could not be considered a proper validation case. Even if the vessel model was properly verified and validated, the data-driven gate rudder model would not be possible to validate using the design parameters of Shigenobu's rudder system, because no direct measurements of rudder forces on the vessel are available publicly. Such case study would therefore provide no more value than the study described in this report already does.

While it would nonetheless be interesting to perform such a case study that eliminates the doubts related to the design parameters of the rudder system, implementation of a ship model in Manwav would be a process that would take a lot of time and effort. Not only is it not an easy task to successfully create a full set of input files with the use of MPP and PRECAL, the following verification and validation would also require considerable work. Due to the strict time constraints of the project, this idea for a more interesting case study was not pursued. It is, however, one of the main recommendations for the future use of this work to do so with the data-driven model trained at least on a dataset based on a similar CFD study on the geometry of Shigenobu. Later, as the research on the concept progresses and validation data becomes available, the model could be completed in full for a specific set of parameters.

6. Conclusions and recommendations

This chapter provides a summary of the work done in the project, a description of the findings from its results and its potential applications. Then, the research questions from the introduction are addressed. Afterwards, the limitations of the rudder model developed over the course of the project are identified and described in detail. Finally, The chapter is concluded with a list of recommendations for future developments of the project.

6.1. General discussion

This study investigates the modelling of a gate rudder system in the form of two distinct rudder models for a time-domain simulator: a physics-based model, developed from a derivation of the MMG rudder model and a data-driven model, built using a small CFD dataset and machine learning regression methods. The models are implemented in Manwav and their impact on a ship's performance in a set of test manoeuvres is presented.

The physics-based model did not perform as expected. It greatly exaggerated the forces in the rudder system close to the start of the manoeuvre and underestimated them at sustained states, leading to much tighter turning circle manoeuvres at the cost of high drop in vessel speed, as well as a significantly impaired manoeuvrability in one of the zig-zag tests. The reason for this behaviour is possibly caused by a number of errors and uncertainties identified in the mathematical model over the course of its implementation in Manwav. They were not investigated further, because this model was only treated as a baseline for the data-driven model, the main focus of the project.

The data-driven model performed as expected, moderately changing the vessel's manoeuvrability with respect to the conventional rudder serving as reference. While the vessel's reactions to the steering inputs are slower than reference in most investigated manoeuvres, it needs to be noted that the showcased results were obtained for a specific combination of the gate rudder system design parameters serving as an example of the model's usage.

The models developed in this study were not validated with respect to real-life measurements. This is because no adequate validation case was found for them, neither through comparison of rudder forces to their measurements, nor through comparison of ship tracks in similar manoeuvres - such data of sufficient quality is not available at this stage of the concept's development.

The current applications of the model are limited mostly due to lack of validation and data, but the steps that need to be taken to improve it and expand its range of uses are clear. They are explained below, in section 6.3. When they are successfully addressed, the improved model will make it possible, among other future applications, to test the hypothesis linking the power savings observed in sea trials of ships equipped with a gate rudder system to sailing in realistic weather conditions.

6.1.1. Project applications

The result of the project described in this report is a model of the gate rudder system at an early stage of development. Currently, its applications are limited, but they will expand as the limitations of the model, as described in section 6.3 are dealt with. For now, the model can be used to estimate how a ship's freesailing manoeuvrability would be impacted with a gate rudder system of a certain size (expressed in the combined surface area of the rudder blades), which can be easily modified. This functionality can be used to determine the approximate size of the rudder system necessary for a ship to comply with IMO standards for manoeuvrability, or any other related requirements. The results of such an investigation may also be used to showcase the impact a gate rudder system would have on a vessel's manoeuvrability (within a limited range of conditions) in comparison to other options, for example to present to a client the potential effects of their decisions in early stages of ship design.

As more recommendations for the improvements of the work are carried out, the capabilities of the model will be expanded. Most notably, once the uncertainties related to the simulation of weather conditions are resolved, it will be possible to use the model to determine whether the hypothesis on the gate rudder power savings formed in section 1.3 is true or not. In order to carry out such a test reliably, a voyage would have to be simulated, with realistic wave and wind spectra in effect. In such conditions, two or more ship models equipped with different rudder systems would sail the same route at the same simulated weather conditions and the log of their power draw over the course of the journey could be used to estimate the differences in overall power consumption, as demonstrated in the case study in chapter 5. If the power savings presented in the results of sea trials of Sakura and Shigenobu could be reproduced in the time domain simulator the model would be used in, it would constitute a breakthrough in the research on the concept, due to the working principle of the gate rudder power savings finally being found. The accuracy of the results could be improved further through the implementation of a functionality that allows for rudder deflection to impact the propeller characteristics, as well as through an expansion of

the base dataset, most notably through the inclusion of yaw rate as one of the parameters.

When the dataset on which the model is built is expanded and the functionality to simulate the effect of rudder deflection on propulsive characteristics of the vessel is implemented, two additional applications of the model will become available. The first is the ability to accurately simulate a vessel's behaviour in all kinds of manoeuvres, both low-speed and freesailing. This means that a ship's full extent of manoeuvring ability provided by a gate rudder system would be possible to estimate and consequently, compared to the performance of other rudder systems, showcasing their strengths and weaknesses and allowing to determine which rudder system would be the best fit for a vessel in which manoeuvrability would play an important role. Additionally, once a suitable methodology is developed, a vessel's power consumption and emissions during port manoeuvres, as well as time spent performing them, could also be subject to such comparisons using this model. The second additional application of the model will allow for the development of a more sophisticated optimal control strategy, as described in more detail in section 6.3. The model could serve as both a foundation for the algorithm tasked with the determination of an optimal deflection of the rudder blades, as well as a testing platform, because the effects could be easily evaluated in the environment native to the model itself.

6.1.2. Conclusions on the research questions

The research questions accompanying the thesis described in this report were formed in section 1.4. The answers to them were found over the course of the project. In this section, first, the supporting questions are answered, followed by an answer to the main research question at the end.

SQ 1: What are the principles of ship manoeuvrability?

The principles of ship manoeuvrability are a combination of several fields of maritime technology. Movement of a ship's hull through the water is dictated mostly by the flow of water around it, which adheres to the laws of hull hydrodynamics. Most ships steer using rudders, which act like control surfaces. They are also governed by control surface hydrodynamics, at a smaller scale than the hull. However, the flow patterns generated by the propeller and the hull's aft section greatly complicate the analysis of rudder performance. Both the hull and the control surfaces of a ship can be treated as hydrofoils in the context of ship manoeuvres, where lift and drag forces are generated depending on the angle of attack. This perspective is especially important for the mathematical description of ship manoeuvres, as it is possible to create mathematical models that can approximate those forces based on a vessel's state and other parameters. Lastly, the International Maritime Organization mandates sea-going vessels to comply with a set of regulations for ship manoeuvrability, where minimum standards dictating how a ship has to perform in certain benchmark manoeuvres in relation to her size and design speed are described.

SQ 2: What methods can be used to model the forces on a gate rudder in a time domain simulation software?

One of the defining features of time domain simulators is the fact that they trade off the accuracy of the calculations for their lower computational cost and for a wider array of scenarios that they are able to simulate, including voyages, weather effects and sequences of rudder inputs. The high computational cost of conventional CFD makes it unsuitable for use in such simulators, where the flow field around the rudder blades would need to be recalculated in every time step. Instead, simpler modeling methods have to be used, where the forces are calculated using basic dependencies with respect to relevant inputs. These methods can be divided into three categories: physics-based models, data-driven models and hybrid models. Models from the first group typically involve equations derived from physical principles coupled with empirical approximations of relevant coefficients based on measurements from experiments (also known as semi-empirical models). Data-driven models typically involve the use of regression analysis in order to estimate the values of required variables based directly on historical data from measurements. The last group, hybrid models, share the features of both previous categories. In the project, two separate models were developed, each belonging to a different category. Due to available data, the focus of the project was put on the data-driven model.

SQ 3: How can the impact of a rudder model on a ship's manoeuvrability be evaluated?

The goal of creating rudder models for time domain simulators is, among others, to investigate the impact a specific rudder system would have on a ship's performance in scenarios too complicated to warrant a CFD analysis in practice. Once the relevant rudder models have been developed and tested, their effects on ship motion can be tested by comparing a ship's model's manoeuvrability across different rudder models and scenarios. The simplest example of such scenarios is a series of benchmark manoeuvres, such as turning circles or zig-zag tests, performed under different conditions or parameters, like initial vessel speed or rudder deflection. The International Maritime Organization uses the results of such manoeuvres to extract indicators signifying a vessel's manoeuvrability, on which the regulations are based. Similar indicators can be extracted from simulation data to make numerical comparisons between the performances of vessels using different rudder models. In the thesis, advance and tactical diameter are the parameters used for the comparisons of vessel performance

in turning circles. In zig-zag tests, overshoot angles are used instead. For all manoeuvres presented in the case study, average power consumption is also used to showcase the ability to compare data related to the vessel's energy efficiency as well. In addition to the numerical comparisons between the ships, comparisons of certain key variables, such as ship tracks, ship speed or drift angle were also presented in the form of plots showing the values of those variables over time for each ship.

MRQ: How to model a gate rudder system performance using a limited amount of data in order to investigate its impact on a ship's manoeuvrability and power consumption?

It is possible to create a model of the gate rudder based on a small CFD dataset through the use of machine learning regression techniques, as indicated by the findings of this thesis. This data-driven model is able to simulate the impact a gate rudder system might have on a ship's performance, as well as provide estimations of power consumption. However, due to the small size of the dataset it is based on, the range of scenarios and ship sizes where its estimations can be expected to be acceptably accurate is limited. Additionally, because validation of the model was not possible to be carried out, it cannot be said how accurate the predictions of the model are in specific applications. Other limitations were also identified and elaborated on in section 6.2. Because of these issues, it is not possible yet to reliably put the hypothesis about the gate rudder savings stemming from sailing in realistic weather conditions to test, but clear guidelines on how to improve the model for it to reach that capability and other possible applications were provided in section 6.3.
It is very likely that if the problems related to the physics-based gate rudder model are resolved, it will also accurately predict the forces generated by the rudder system. However, such effort was not carried out in this thesis, because this model was not the focus of the project. basically yes, it is possible, i am able to simulate the impact, BUT eg im unable to reliably investigate the power savings in realistic conditions hypothesis

6.2. Model limitations

While the goal of the project to develop a functioning model of a gate rudder in a time domain simulator software was reached successfully, the full potential of the work cannot yet be achieved. This is because of several limitations of the data-driven model identified over the course of the project. The physics-based model is considered out of scope for this section, but resolving the issues related to the covered area ratio, axial velocity in propeller slipstream and lift coefficient calculation would be necessary before serious investigation into its viability and accuracy could be carried out.

- **Manwav does not model the influence of rudder deflection on propeller loading characteristics.** When a manoeuvre starts, the ship's power characteristics are set based on the initial ship speed set for the manoeuvre and the propulsion control setting (constant power, constant torque or constant RPM). Afterwards, whichever characteristic is set to stay constant is maintained throughout the manoeuvre, while the others adapt to the changing ship speed. Rudder deflection is known to restrict the flow upstream of the propeller, decreasing its inflow velocity, which increases the loading. Consequently, the power characteristics are influenced by this effect, which is important to consider when trying to determine power savings stemming from an implementation of a different rudder system on a ship. The data-driven model developed in this project can roughly account for changes in propeller loading coefficient, but in a limited range of the variable's values.
- **The data-driven model described in this report was built using a small dataset based on CFD simulations of only one vessel.** The force coefficient estimators are accurate within the bounds of the features of the dataset and the setup parameters, it should be expected that this accuracy will diminish as the dimensions of the vessel or other key variables deviate from those native to the source dataset. This means that as long as manoeuvring tests simulated in Manwav using the data-driven gate rudder model are performed on a model of a vessel similar in size and design speed to the source vessel for the dataset, the rudder model should provide accurate force predictions. However, it is unconfirmed how much deviation from those base parameters will keep the rudder force predictions within acceptable accuracy levels.
- **The training data for the data-driven model only encompasses rudder behaviour in freesailing conditions**, where the vessel speed is stable and rudder deflections are moderate. It is therefore these conditions in which the rudder model should be expected to perform accurate force predictions, while other kinds of manoeuvres that significantly deviate from the ranges of variables are not yet suitable to be simulated using this model. This is because heavily drag-dominated flow regimes present in low-speed manoeuvres at high rudder deflection angles and variable propeller speeds can be characterised by high non-linearity. Simulating crabbing manoeuvres with the gate rudder additionally adds another layer of significant degree of interaction between the rudder blades, further complicating the flow around them. Because of these flow aspects not being properly represented in the base dataset, attempts to simulate such manoeuvres using the current data-driven gate rudder model would likely result in inaccurate force predictions.
- A potential problem with attempting to simulate the performance of the gate rudder system in realistic weather conditions is the **influence of waves on the flow pattern in the aft section of a ship.** While the effects of wave

loads on ship motion are modelled in Manwav through the use of precalculated quadratic transfer functions (QTFs) [31], there is no mechanism that would incorporate the effect of the presence of a wave system on rudder forces. In the default rudder models, the force evaluation methods include an input that defines the orbital wave velocity vector, which is summed with the rudder inflow velocities. However, that vector is always set to zero, with no sign of there being an alternative way of calculating the value of its components and no mention of it in Manwav manuals. It is unconfirmed how significant of a difference the inclusion of wave velocity impact on rudder forces would make on the accuracy of overall vessel performance evaluations and comparisons, but the lack of such functionality in the simulator may be a potential problem.

6.3. Future recommendations

In order for the work performed in this project to be improved, several key upgrades to the rudder model were identified. They will be elaborated in this section. Just like in the previous section, the scope of the proposed improvements is limited to the data-driven model.

- The most important upgrade to the project is the **expansion of the dataset on which the data-driven model is built**. The further the dataset is expanded through the inclusion of additional parameters and their values, the more robust will the rudder model be, leading to a wider range of scenarios and vessel types for which the time domain simulation results could be considered accurate. Such expansion would have to be done through the addition of new CFD simulations of vessels with a gate rudder system that would include more variables or more values of existing ones. Some new variables whose inclusion in the dataset would positively impact the applicability of the rudder model in a wider range of scenarios are ship's yaw rate, vessel speed and size, and a parameter that could describe the ship's stern shape (for example, bulk carriers differ in hull shape from container vessels, which changes the flow pattern in the aft section, influencing the performance of the gate rudder system). Existing steering angle values could be expanded to include more extreme deflection angles as well as operation in the crabbing mode, where both rudder blades are deflected away from the ship, deflecting the propeller slipstream almost entirely. Propeller loading coefficient values should be expanded as well in order to better reflect the conditions in which the vessel is not operating at its design speed, which is necessary for the simulation of low-speed manoeuvres in tight waterways or in harbours. Drift angle values could also be expanded to match those typically reached during turning circle manoeuvres (~15-20°). When the dataset is expanded, the model will need to be retrained on the new data.
- The lack of means for the **validation of the gate rudder model developed in the project** is mostly related to the fact that the gate rudder concept is still in a relatively early stage of development. As already described in section 5.4, as soon as data that would allow to carry out a validation study becomes available, it should be performed to make sure that the model enables an accurate representation of a vessel's manoeuvring performance in real life. First, a model of the validation vessel will have to be implemented in Manwav and validated on its own. Then, with attention paid to the correction for environmental conditions in which the validation manoeuvres were performed, the comparison between measured and simulated ship tracks will make it possible to determine whether the rudder model can be treated as accurate. Alternatively, if force measurements were possible to be taken on a real gate rudder system tested in similar conditions to those simulated in the CFD dataset, the comparison would be even more direct, cutting out the uncertainties related to the model of the ship in Manwav. Such a measurement setup would, however, be challenging to create, therefore this scenario is unlikely.
- As described in the previous section, one of the limitations of the model is the fact that it doesn't take into account the effect of orbital wave velocity on rudder performance. It is unknown how significant of a difference this functionality would make. A **study investigating the impact of water motion in waves on rudder system performance** would therefore be necessary. If it was found to be not negligible, its findings could be used to make adjustments to the flow velocities used to calculate rudder forces in Manwav. Without such a study, an investigation into power savings of the gate rudder system in realistic weather conditions could yield inaccurate results.
- Another previously mentioned limitation of the model that should be addressed before it can be used to accurately assess the gate rudder system's potential to provide power savings in realistic weather conditions in Manwav is the lack of a **mechanism that adjusts the propeller loading based on the deflection of the rudder behind it**. A dedicated study focused on determining the dependency between these two parameters in a gate rudder system could use the existing CFD dataset the data-driven gate rudder model is based on, treating the propeller loading coefficient or other propulsion characteristics as a target. Afterwards, the study's findings could be used to make a correction in propulsion characteristics in the propeller object in Manwav.
- An improvement that should make a significant difference in the gate rudder system's efficiency, both in the time domain simulations as well as in real life applications, would be the **development of a more sophisticated steering control strategy.** The current strategy used in the model and, to the author's knowledge, in real ships equipped with a gate rudder, is very simple - rudder blades linearly follow the helm command in degrees of deflection and each is limited by rudder rate and maximum deflection angles (+35 and -15 degrees). A better, more advanced solution would take advantage of the fact that a gate rudder is a system with two degrees of freedom by treating the two blades

as separate, in order to optimise for minimal total rudder drag while achieving the necessary lift. Ship state data, such as vessel speed, drift angle or yaw rate could be used by such algorithm to determine the most advantageous deflection angle of rudder blades at every moment. The model created in this project could, after an expansion of the base dataset, be used to develop such a control strategy.

- The final beneficial modification (from this list of recommendations) to the project would be the **inclusion of more gate rudder design parameters on the system's performance.** As of now, the rudder blade area is the only parameter that reflects both the vessel's size as well as the rudder system's geometry, at the same time. A study on how different GRS design parameters influence its performance would allow for a more accurate simulation of the rudder system forces and, for example, the ability to predict how changes to those parameters would impact vessel's manoeuvrability and compliance with IMO regulations.

6.4. Authorship statement

The work presented in this thesis was performed by its author, Piotr Pietrzak. The idea for the topic of the project was proposed by Teus van Beek of Wärtsilä. The direction of the project during its different stages of development were defined by the author together with his daily supervisor from Wärtsilä, Ian Hubbard. Access to NTPro software for evaluation purposes was provided by Wärtsilä, and access to Manwav was provided by the CRS group (of which Wärtsilä is a member). Access to MATLAB was provided by TU Delft. The tuning of the S175 vessel was done by the author. The mathematical model behind the physics-based gate rudder model was created by Alessandro Carchen and other authors of the 2020 paper titled "Investigation of the manoeuvrability characteristics of a Gate Rudder system using numerical, experimental and full-scale techniques". That model was adapted into Manwav by the author. The results of the CFD analyses forming the dataset which served as the basis of the data-driven gate rudder model was provided by Marc Beerens of Wärtsilä. The methodology for the creation of the data-driven model was developed by the author and Ian Hubbard. The scripts related to the training of the gate rudder force estimators, as well as the modifications and scripts related to the deployment of the model in Manwav were done by the author. The selection of gate rudder design parameters and the reasoning behind their relation to reference vessels was done by the author. Lastly, the entirety of the code related to post-processing of results, data visualization and creation of plots was done by the author, with minor assistance from Ian Hubbard.

References

[1] C. J. Wenzinger, "Pressure distribution over an airfoil section witha flap and tab", National Advisory Comitee for Aeronautics, Report no. 574, 1936. [Online]. Available: https://apps.dtic.mil/sti/citations/ADA298176 (visited on 06/04/2024).

[2] International Maritime Organisation, *International convention for the safety of life at sea*, 1974. [Online]. Available: https://treaties.un.org/doc/Publication/UNTS/Volume%201184/volume-1184-I-18961-English.pdf (visited on 18/03/2024).

[3] S. Inoue, M. Hirano and K. Kijima, "Hydrodynamic derivatives on ship manoeuvring", *International Shipbuilding Progress*, vol. 28, no. 321, 1981. [Online]. Available: https://repository.tudelft.nl/islandora/object/uuid%3A44033e73-4118-40b2-b07d-8192957cbc51 (visited on 11/04/2024).

[4] K.-H. Son and K. Nomoto, "On the coupled motion of steering and rolling of a ship in following seas", *Journal of the Society of Naval Architects of Japan*, vol. 1982, no. 152, pp. 180–191, 1982. DOI: 10.2534/jjasnaoe1968.1982.152_180.

[5] D. W. Scott, "Multivariate Density Estimation: Theory, Practice, and Visualization" (Wiley Series in Probability and Statistics). John Wiley & Sons, Inc., 17th Aug. 1992, 358 pp., ISBN: 978-0-471-54770-9.

[6] International Maritime Organisation, *Standards for ship manoeuvrability*, 4th Dec. 2002. [Online]. Available: https://wwwcdn.imo.org/localresources/en/KnowledgeCentre/IndexofIMOResolutions/MSCResolutions/MSC.137(76).pdf (visited on 01/03/2024).

[7] H. Yasukawa, "Simulations of ship maneuvering in waves", *Journal of the Japan Society of Naval Architects and Ocean Engineers*, vol. 4, pp. 127–136, 2006. DOI: 10.2534/jjasnaoe.4.127.

[8] A. F. Molland and S. R. Turnock, "Marine Rudders and Control Surfaces". Butterworth-Heinemann, 2007, ISBN: 978-0-7506-6944-3. [Online]. Available: https://www.sciencedirect.com/book/9780750669443/marine-rudders-and-control-surfaces.

[9] H. Yasukawa, "Simulations of ship maneuvering in waves", *Journal of the Japan Society of Naval Architects and Ocean Engineers*, vol. 7, pp. 163–170, 2008. DOI: 10.2534/jjasnaoe.7.163.

[10] International Maritime Organisation, "Second IMO GHG study 2009", 2009. [Online]. Available: https://wwwcdn.imo.org/localresources/en/OurWork/Environment/Documents/SecondIMOGHGStudy2009.pdf.

[11] F. Pedregosa, G. Varoquaux, A. Gramfort *et al.*, "Scikit-learn: Machine learning in python", *Journal of Machine Learning Research*, vol. 12, no. 85, pp. 2825–2830, 2011, ISSN: 1533-7928. [Online]. Available: http://jmlr.org/papers/v12/pedregosa11a.html (visited on 08/10/2024).

[12] F. Stern, K. Agdrup, S. Kim *et al.*, "Experience from SIMMAN 2008-the first workshop on verification and validation of ship maneuvering simulation methods", *Journal of Ship Research*, vol. 55, no. 2, pp. 135–147, Jun. 2011. [Online]. Available: https://www.marin.nl/publications/experience-from-simman-2008-the-first-workshop-on-verification-and-validation-of-ship-maneuvering-simulation-methods (visited on 12/04/2024).

[13] V. Bertram, "Practical Ship Hydrodynamics". Oxford: Butterworth-Heinemann, 2012, ISBN: 978-0-08-097150-6. DOI: 10.1016/B978-0-08-097150-6.10007-7. [Online]. Available: https://www.sciencedirect.com/science/article/pii/B9780080971506100077 (visited on 28/02/2024).

[14] S. Liu and A. Papanikolaou, "ADDED RESISTANCE OF SHIPS IN QUARTERING SEAS", presented at the V International Conference on Computational Methods for Coupled Problems in Science and Engineering, Ibiza, Spain, 18th Jun. 2013. DOI: 10.13140/2.1.3003.7446. [Online]. Available: https://www.researchgate.net/publication/267763613_ADDED_RESISTANCE_OF_SHIPS_IN_QUARTERING_SEAS (visited on 03/04/2024).

[15] N. Sasaki, "ZEUS and NOAH projects of NMRI", in *Proceedings of the Third International Symposium on Marine Propulsors - SMP'13*, Launceston, Australia: Australian Maritime College, University of Tasmania, May 2013, ISBN: 978-0-646-90334-7. [Online]. Available: http://ns-evolution.com/wp/wp-content/uploads/2018/05/ZEUSNOAH2013-Tasmania.pdf.

[16] N. Sasaki, M. Atlar and S. Kuribayashi, "Advantages of twin rudder system with asymmetric wing section aside a propeller", *Journal of Marine Science and Technology*, vol. 21, no. 2, pp. 297–308, 29th Dec. 2015, ISSN: 1437-8213. DOI: 10.1007/s00773-015-0352-z. [Online]. Available: https://doi.org/10.1007/s00773-015-0352-z (visited on 28/02/2024).

[17] S. Turkmen, A. Carchen, N. Sasaki and M. Atlar, "A new energy saving twin rudder system - gate rudder", presented at the International Conference on Shipping in Changing Climates (SCC 2015), Glasgow, Scotland, 24th Nov. 2015. [Online]. Available: https://www.researchgate.net/publication/289961248_A_New_Energy_Saving_Twin_Rudder_System_-_Gate_Rudder.

[18] H. Yasukawa and Y. Yoshimura, "Introduction of MMG standard method for ship maneuvering predictions", *Journal of Marine Science and Technology*, vol. 20, no. 1, pp. 37–52, 1st Mar. 2015, ISSN: 1437-8213. DOI: 10.1007/s00773-014-0293-y. [Online]. Available: https://doi.org/10.1007/s00773-014-0293-y (visited on 01/03/2024).

[19] A. Carchen, W. Shi, N. Sasaki and M. Atlar, "A prediction program of manoeuvrability for a ship with a gate rudder system", in *Proceedings of AYOCOL - the 2nd International Meeting on Recent Advances in Prediction Techniques for Safe Manoeuvring of Ships and Submarines*, Istanbul, Türkiye, 17th Nov. 2016. [Online]. Available: https://pureportal.strath.ac.uk/files-asset/81267804/Carchen_etal_2016_A_prediction_program_of_manoeuvrability_for_a_ship.pdf.

[20] N. Sasaki, "The new hull form with twin rudders utilizing duct effects (3rd report)", JASNAOE 2016 Annual Spring Meeting, Fukuoka, Japan, 26th May 2016. [Online]. Available: https://www.gatersproject.com/publications/new-2023/presentations/the-new-hull-form-with-twin-rudders-utilizing-duct-effects-jasnaoe-2016.pdf.

[21] American Bureau of Shipping, *Guide for vessel maneuverability*, Feb. 2017. [Online]. Available: https://ww2.eagle.org/content/dam/eagle/rules-and-guides/current/conventional_ocean_service/145_vesselmaneuverability/Vessel_Maneuverability_Guide_e-Feb17.pdf (visited on 05/02/2024).

[22] I. Hubbard and G. D. Weymouth, "Physics-based and learning-based roll-damping predictions", presented at the 20th Numerical Towing Tank Symposium, Wageningen, the Netherlands: Curran Associates, Inc., 22nd Sep. 2017, pp. 92–97.

[23] J. S. Carlton, "Marine Propellers and Propulsion", 4th ed. London: Butterworth-Heinemann, 2018, ISBN: 978-0-08-100366-4. [Online]. Available: https://www.sciencedirect.com/book/9780081003664/marine-propellers-and-propulsion (visited on 11/03/2024).

[24] A. Coraddu, M. Kalikatzarakis, L. Oneto, G. J. Meijn, M. Godjevac and R. D. Geertsma, "Ship diesel engine performance modelling with combined physical and machine learning approach", in *Proceedings of the International Ship Control Systems Symposium*, vol. 1, Glasgow, Scotland, 2018. DOI: 10.24868/issn.2631-8741.2018.011. [Online]. Available: https://repository.tudelft.nl/islandora/object/uuid%3Ac990afcc-20ff-448a-9d40-f8850fb3c7c8 (visited on 11/04/2024).

[25] M. Fukazawa, S. Turkmen, A. Marino and N. Sasaki, "Full-scale gate rudder performance obtained from voyage data", in *Proceedings of AYOCOL - the 3rd International Meeting*, Istanbul, Türkiye, 15th Nov. 2018, pp. 71–76. [Online]. Available: http://www.ayocol.itu.edu.tr/files/AYOCOL2018_Proceedings.pdf (visited on 28/02/2024).

[26] N. Sasaki, S. Kuribayashi and M. Atlar, "GATE RUDDER", in *INT-NAM 2018: 3rd International Symposium on Naval Architecture and Maritime, proceedings*, Istanbul, Türkiye, 19th Jul. 2018, ISBN: 978-975-461-548-7. [Online]. Available: https://www.researchgate.net/publication/326478152_GATE_RUDDER.

[27] Wärtsilä Corporation. "Wärtsilä acquires transas to accelerate its smart marine ecosystem vision", Wartsila.com. (19th Mar. 2018), [Online]. Available: https://www.wartsila.com/media/news/19-03-2018-wartsila-acquires-transas-to-accelerate-its-smart-marine-ecosystem-vision-3212107 (visited on 13/03/2024).

[28] N. Yilmaz, S. Turkmen, B. Aktas, P. Fitzsimmons, N. Sasaki and M. Atlar, "Tip vortex cavitation simulation of a propeller in a gate rudder® system", in *Proceedings of AYOCOL - the 3rd International Meeting on Progress in Propeller Cavitation And its Consequences: Experimental and Computational Methods for Predictions*, ISSN: 2018-1116 Num Pages: 1265149, Istanbul, Türkiye, 15th Nov. 2018. [Online]. Available: https://pureportal.strath.ac.uk/files/84809186/Yilmaz_etal_IMPPC_2018_Tip_vortex_cavitation_simulation_of_a_propeller.pdf (visited on 28/02/2024).

[29] A. Burkov, "The Hundred-Page Machine Learning Book". Andriy Burkov, 2019, ISBN: 978-1-77700-547-4.

[30] Det Norske Veritas, *Rules for classification of ships - part 6 - additional class notations, chapter 3 - navigation, manoeuvring and position keeping*, Jul. 2019. [Online]. Available: https://standards.dnv.com/explorer/document/81901DB58CB64362BB72DAB6DD553B9E/26 (visited on 19/03/2024).

[31] MARIN, "ManWav 2.5.0 user manual", Internal document 28504, Sep. 2019.

[32] N. Sasaki and M. Atlar, "Scale effect of gate rudder", in *Proceedings of the Sixth International Symposium on Marine Propulsors - SMP'19*, Rome, Italy, 30th May 2019. [Online]. Available: https://pureportal.strath.ac.uk/en/publications/scale-effect-of-gate-rudder.

[33] X. Zhang, W. Xiong, X. Xiang and Z. Wang, "Real-time simulation of a rescue ship maneuvering in short-crested irregular waves", *IEEE Access*, vol. 7, pp. 133 936–133 950, 2019, Conference Name: IEEE Access, ISSN: 2169-3536. DOI: 10.1109/ACCESS.2019.2941591. [Online]. Available: https://ieeexplore.ieee.org/abstract/document/8839055 (visited on 22/02/2024).

[34] A. Burkov, “Machine Learning Engineering”. True Positive Incorporated, 2020, ISBN: 978-1-77700-546-7.

[35] A. Carchen, S. Turkmen, B. Piaggio, W. Shi, N. Sasaki and M. Atlar, “Investigation of the manoeuvrability characteristics of a gate rudder system using numerical, experimental, and full-scale techniques”, *Applied Ocean Research*, vol. 106, p. 102 419, 7th Dec. 2020, ISSN: 0141-1187. DOI: 10.1016/j.apor.2020.102419. [Online]. Available: https://www.sciencedirect.com/science/article/pii/S0141118720309780 (visited on 29/02/2024).

[36] N. Sasaki, S. Kuribayashi, M. Fukazawa and M. Atlar, “Towards a realistic estimation of the powering performance of a ship with a gate rudder system”, *Journal of Marine Science and Engineering*, vol. 8, no. 1, p. 43, Jan. 2020, Number: 1 Publisher: Multidisciplinary Digital Publishing Institute, ISSN: 2077-1312. DOI: 10.3390/jmse8010043. [Online]. Available: https://www.mdpi.com/2077-1312/8/1/43 (visited on 29/02/2024).

[37] Z. Tacar, N. Sasaki, M. Atlar and E. Korkut, “An investigation into effects of gate rudder® system on ship performance as a novel energy-saving and manoeuvring device”, *Ocean Engineering*, vol. 218, p. 108 250, 15th Dec. 2020, ISSN: 0029-8018. DOI: 10.1016/j.oceaneng.2020.108250. [Online]. Available: https://www.sciencedirect.com/science/article/pii/S0029801820311720 (visited on 29/02/2024).

[38] Wärtsilä Corporation. “Wärtsilä signs agreement with kuribayashi steamship in japan for deployment of innovative gate rudder technology”, Wartsila.com. (30th Mar. 2020), [Online]. Available: https://www.wartsila.com/media/news/30-03-2020-wartsila-signs-agreement-with-kuribayashi-steamship-in-japan-for-deployment-of-innovative-gate-rudder-technology-2672893 (visited on 28/02/2024).

[39] B. Aktas, A. Gurkan and M. Atlar, “Report of the selected vessels and operational data”, University of Strathclyde, D1.1, 31st Jul. 2021. [Online]. Available: https://www.gatersproject.com/microsites/gaters/publications/new-2023/public-deliverables/d1.1-report-of-the-selected-vessels-and-operational-data.pdf (visited on 26/09/2024).

[40] MARIN, “MPP theory manual”, Internal document 30009-9-MAN, Jun. 2021.

[41] N. Sasaki, S. Kuribayashi, N. Bulten and M. Yazawa, “JOINT SEA TRIAL OF SHIPS WITH GATE RUDDER® AND CONVENTIONAL RUDDER”, presented at the Full Scale Ship Performance online conference, 10th Feb. 2021. [Online]. Available: https://scholar.archive.org/work/lcddunfs4bfalfow2glplfyroi/access/wayback/https://s3-eu-west-1.amazonaws.com/pfigshare-u-files/38258529/RINA_Paper_JOINTSEATRIAL.pdf?X-Amz-Algorithm=AWS4-HMAC-SHA256&X-Amz-Credential=AKIAIYCQYOYV5JSSROOA/20221130/eu-west-1/s3/aws4_request&X-Amz-Date=20221130T003423Z&X-Amz-Expires=10&X-Amz-SignedHeaders=host&X-Amz-Signature=96a2c31dbeee9dbbe4b79aab8b697be79ce9483e45347739348ec54fca6e40a1.

[42] C. Çelik, S. Özsayan, C. Koksal, D. Danışman, E. Korkut and O. Goren, “On the full-scale powering extrapolation of ships with gate rudder system (GRS)”, in *Proceedings of AYOCOL - the 4th International Meeting*, Istanbul, Türkiye, 15th Dec. 2022. [Online]. Available: https://www.researchgate.net/publication/366548399_On_the_Full-Scale_Powering_Extrapolation_of_Ships_with_Gate_Rudder_System_GRS.

[43] S. Gökçay, Z. Saydam, G. N. Küçüksu and M. İnsel, “Data-driven fuel consumption rate estimation by using deep learning”, in *Proceedings of AYOCOL - the 4th International Meeting*, Istanbul, Türkiye, 15th Dec. 2022. [Online]. Available: https://www.ayocol.itu.edu.tr/files/AYOCOL2018_Proceedings.pdf.

[44] A. Gurkan, B. Aktas, U. O. Ünal and M. Atlar, “Investigation of gate rudder blade design for ship powering using the design of experiment (DoE) method”, in *Proceedings of AYOCOL - the 4th International Meeting*, Istanbul, Türkiye, 15th Dec. 2022. [Online]. Available: https://www.ayocol.itu.edu.tr/files/AYOCOL2018_Proceedings.pdf.

[45] M. D. Hussain, M. M. Karim and N. Sasaki, “Numerical assessment of the scale effects on the propulsive performance of a ship with gate rudder system”, *Ocean Engineering*, vol. 249, p. 110 889, 1st Apr. 2022, ISSN: 0029-8018. DOI: 10.1016/j.oceaneng.2022.110889. [Online]. Available: https://www.sciencedirect.com/science/article/pii/S0029801822003274 (visited on 29/02/2024).

[46] International Maritime Organisation. “EEXI and CII - ship carbon intensity and rating system”. (2022), [Online]. Available: https://www.imo.org/en/MediaCentre/HotTopics/Pages/EEXI-CII-FAQ.aspx (visited on 11/03/2024).

[47] C. Koksal, B. Aktas, A. Gurkan, E. Korkut, N. Sasaki and M. Atlar, “Experimental powering performance analysis of m/v ERGE in calm water and waves”, in *Proceedings of AYOCOL - the 4th International Meeting*, Istanbul, Türkiye, 15th Dec. 2022. [Online]. Available: https://www.researchgate.net/publication/369439571_Experimental_Powering_Performance_Analysis_of_MV_ERGE_in_Calm_Water_and_Waves.

[48] United Nations, “Review of maritime transport 2022”, presented at the United Nations Conference on Trade and Development, United Nations Publications, 2022, ISBN: 978-92-1-113073-7. [Online]. Available: https://unctad.org/publication/review-maritime-transport-2022.

[49] Wärtsilä Voyage Ltd., “Navi-trainer professional 5000: Ship motion mathematical model description”, Internal document, Feb. 2022.

[50] M. Atlar, "A review of gate rudder system retrofitting of the GATERS target ship "MV ERGE"", Unpublished confidential document, Unpublished confidential document, 11th Jul. 2023.

[51] "Choosing the right estimator", scikit-learn. (Sep. 2023), [Online]. Available: https://scikit-learn.org/1.3/tutorial/machine_learning_map/ (visited on 08/10/2024).

[52] J. M. K. Godø and S. Steen, "An efficient method for unsteady hydrofoil simulations, based on non-linear dynamic lifting line theory", *Ocean Engineering*, vol. 288, p. 116 001, 15th Nov. 2023, ISSN: 0029-8018. DOI: 10.1016/j.oceaneng.2023.116001. [Online]. Available: https://www.sciencedirect.com/science/article/pii/S0029801823023855 (visited on 11/04/2024).

[53] International Maritime Organisation. "Improving the energy efficiency of ships". (2023), [Online]. Available: https://www.imo.org/en/OurWork/Environment/Pages/Improving%20the%20energy%20efficiency%20of%20ships.aspx (visited on 08/03/2024).

[54] M. Kalikatzarakis, "Data-driven and hybrid models for the underwater radiated noise of cavitating marine propellers", Ph.D. dissertation, University of Strathclyde, 20th Mar. 2023. [Online]. Available: https://pureportal.strath.ac.uk/en/studentTheses/data-driven-and-hybrid-models-for-the-underwater-radiated-noise-o (visited on 20/02/2024).

[55] Lloyd's Register, *Rules and regulations for the classification of ships - section 1 general requirements*, Jul. 2023. [Online]. Available: https://r4s.oneocean.com/regulation/page/266253 (visited on 05/02/2024).

[56] Bureau Veritas, *Rules for the classification of steel ships - part f - additional class notations*, Jan. 2024. [Online]. Available: https://marine-offshore.bureauveritas.com/nr467-rules-classification-steel-ships (visited on 05/02/2024).

A. Appendix A: S175 model tuning comparison plots

A.1. Default rudder slew rate comparisons

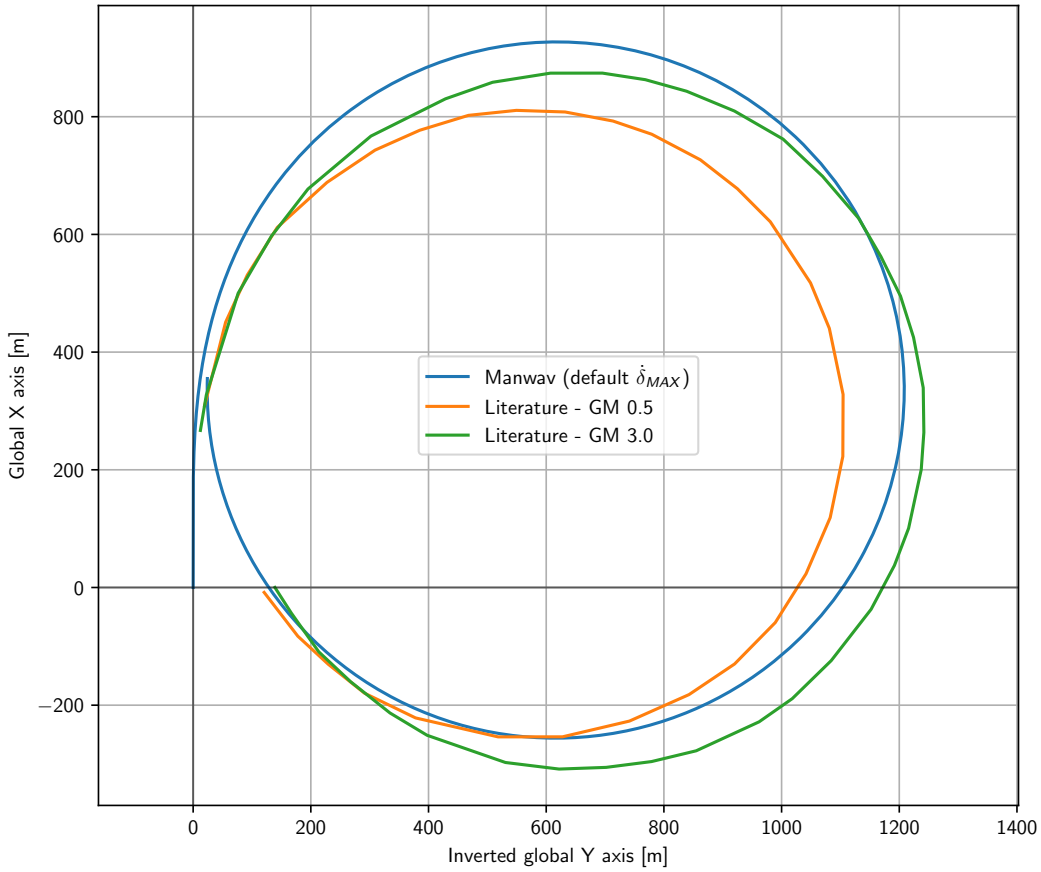

Figure A.1: Ship track comparison plot in the 15° to starboard turning circle manoeuvre at 24.15 kn. Default Manwav rudder slew rate.

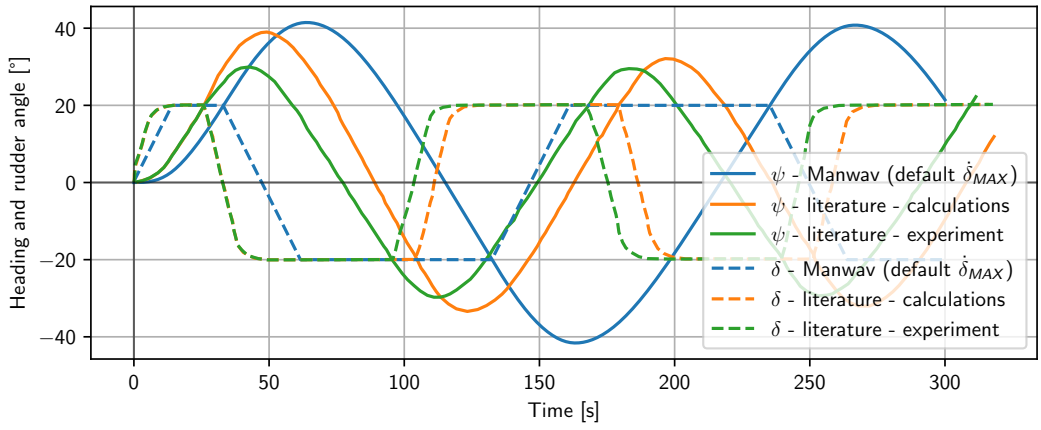

Figure A.2: Ship heading and rudder angle comparison plot in the starboard 20/20 zig-zag manoeuvre at 24.15 kn. Default Manwav rudder slew rate.

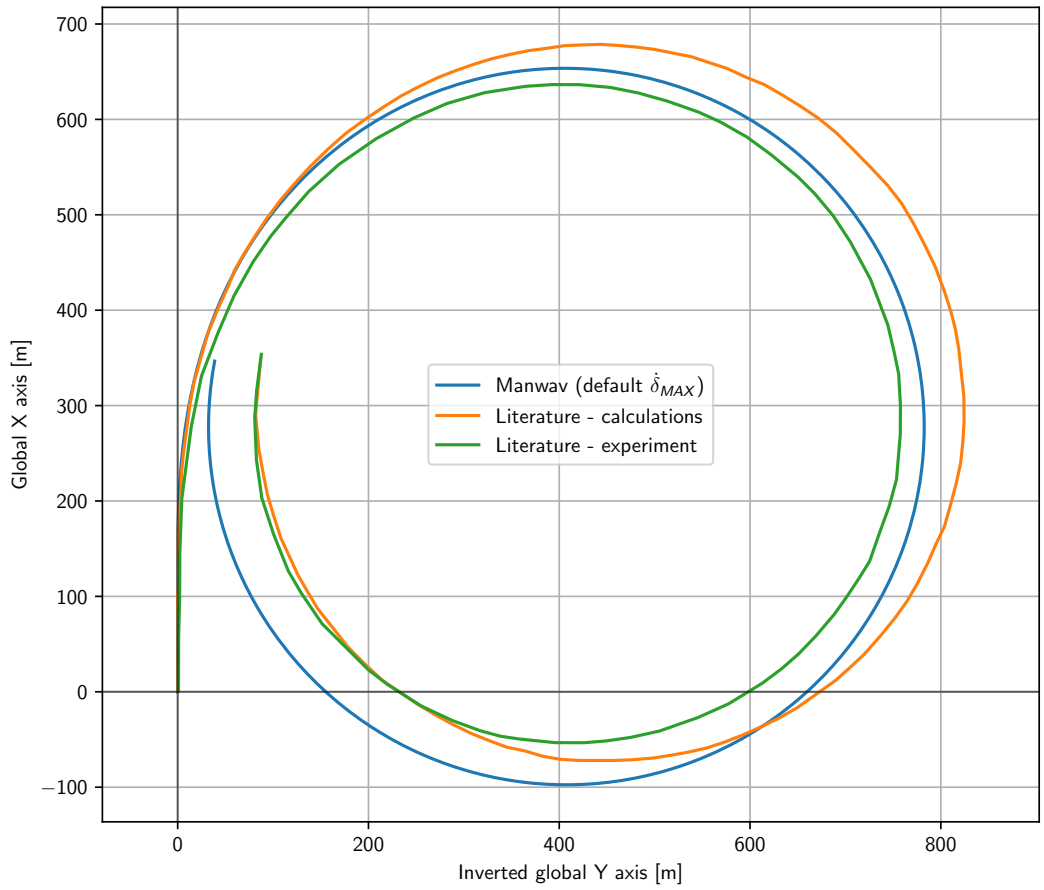

Figure A.3: Ship track comparison plot in the 35° to starboard turning circle manoeuvre at 12.08 kn. Default Manwav rudder slew rate.

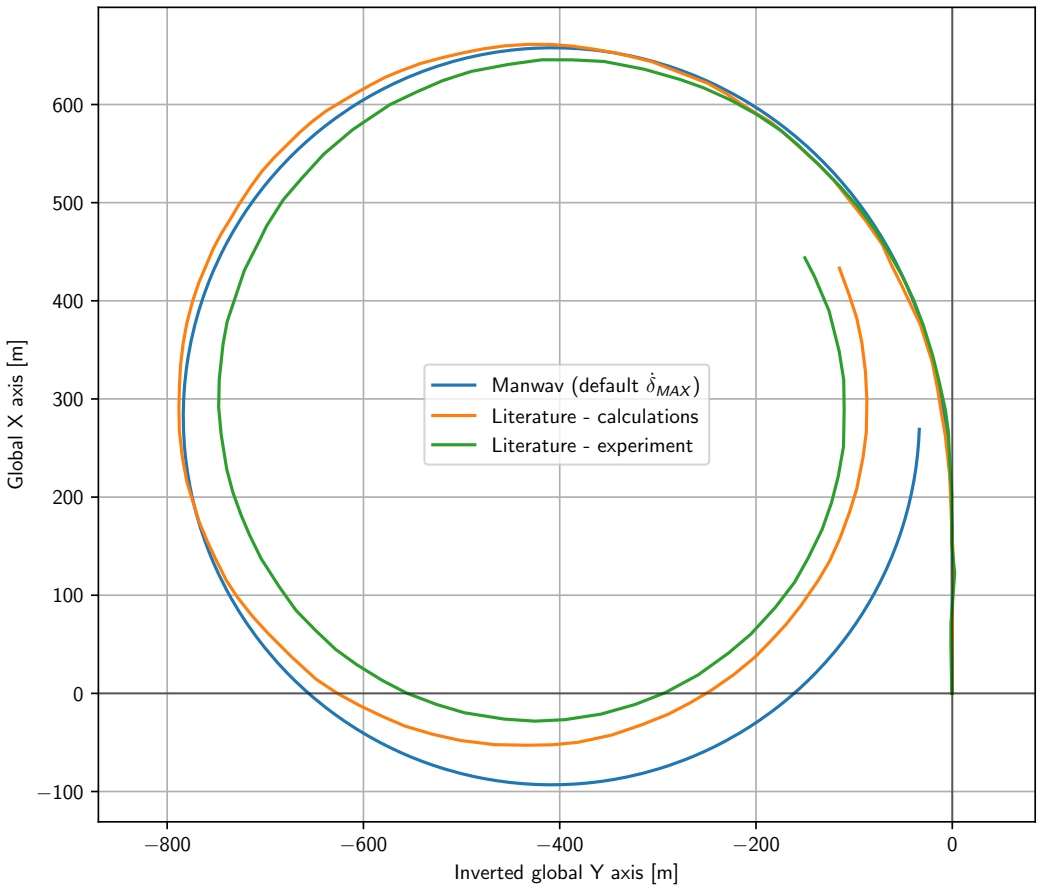

Figure A.4: Ship track comparison plot in the 35° to port turning circle manoeuvre at 12.08 kn. Default Manwav rudder slew rate.

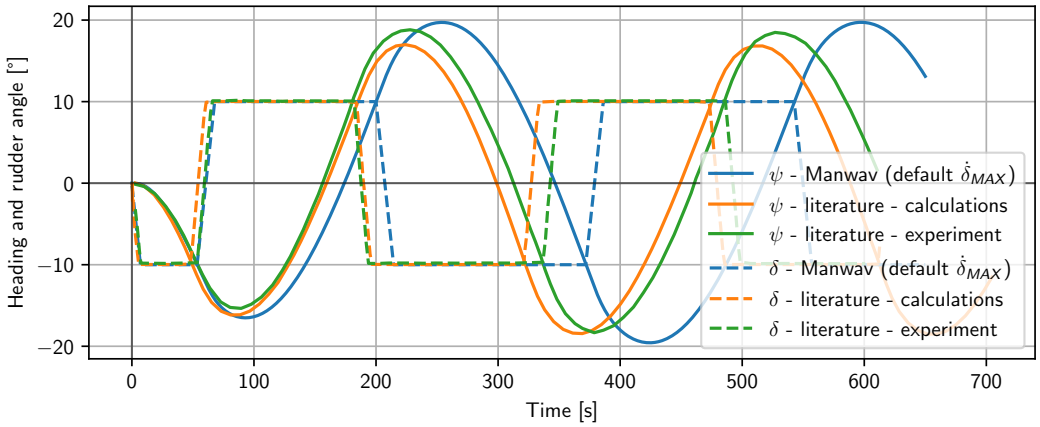

Figure A.5: Ship heading and rudder angle comparison plot in the port 10/10 zig-zag manoeuvre at 12.08 kn. Default Manwav rudder slew rate.

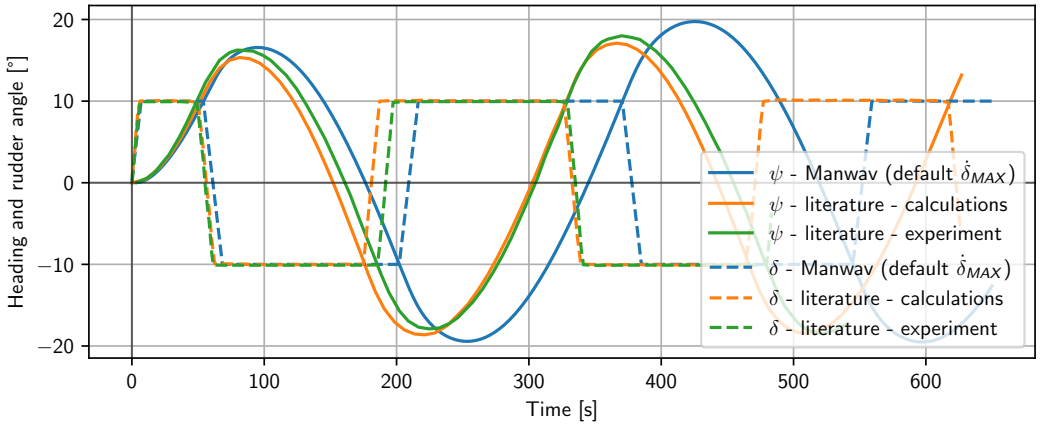

Figure A.6: Ship heading and rudder angle comparison plot in the port 10/10 zig-zag manoeuvre at 12.08 kn. Default Manwav rudder slew rate.

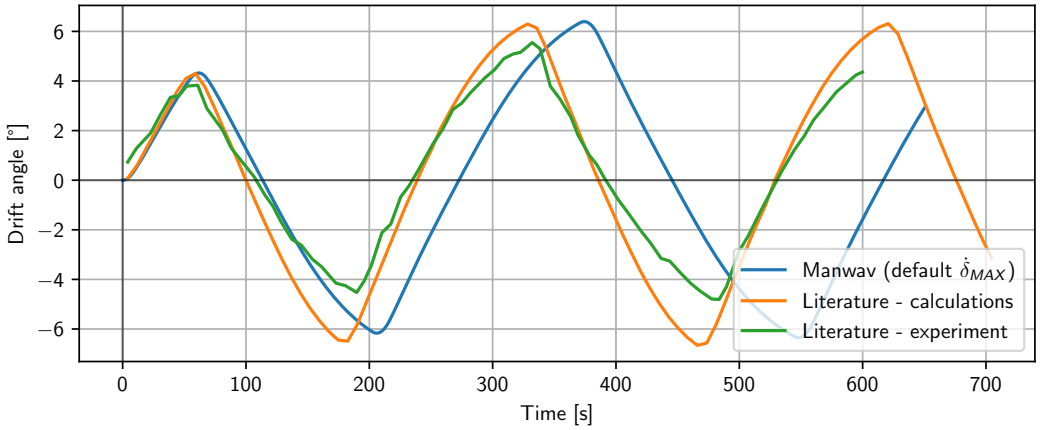

Figure A.7: Drift angle comparison plot in the port 10/10 zig-zag manoeuvre at 12.08 kn. Default Manwav rudder slew rate.

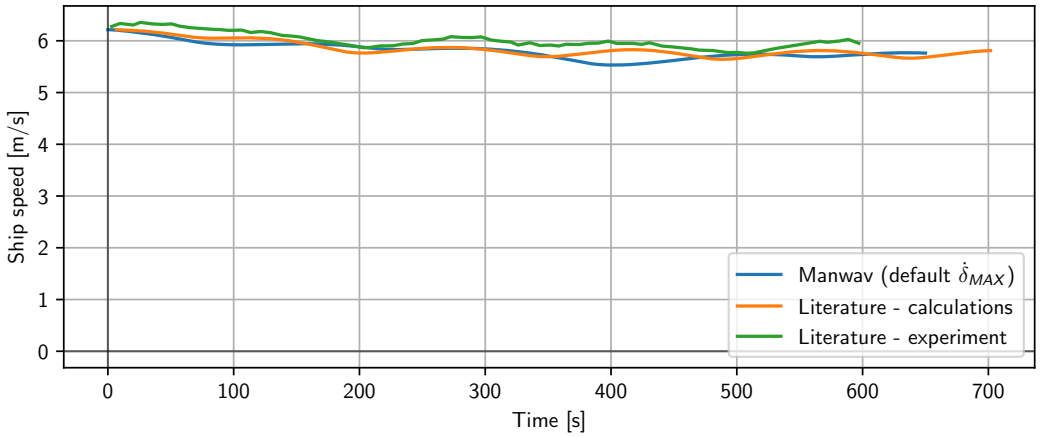

Figure A.8: Ship speed comparison plot in the port 10/10 zig-zag manoeuvre at 12.08 kn. Default Manwav rudder slew rate.

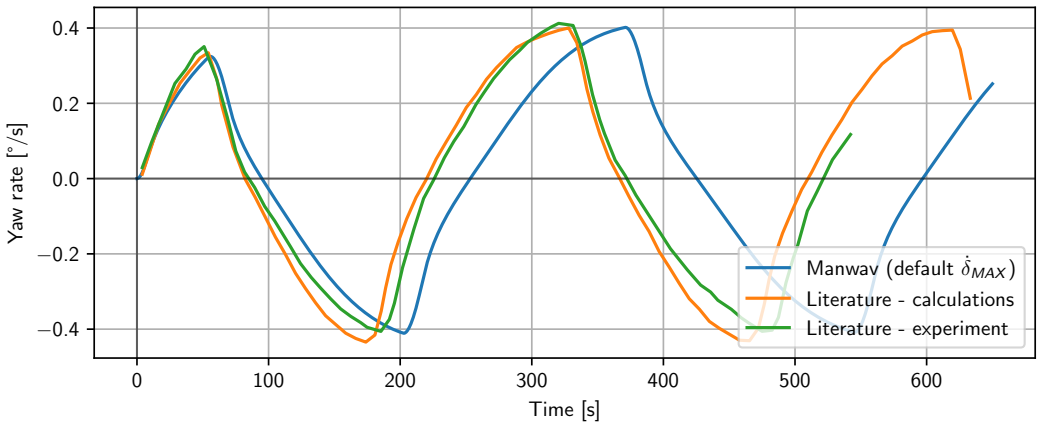

Figure A.9: Yaw rate comparison plot in the port 10/10 zig-zag manoeuvre at 12.08 kn.
Default Manwav rudder slew rate.

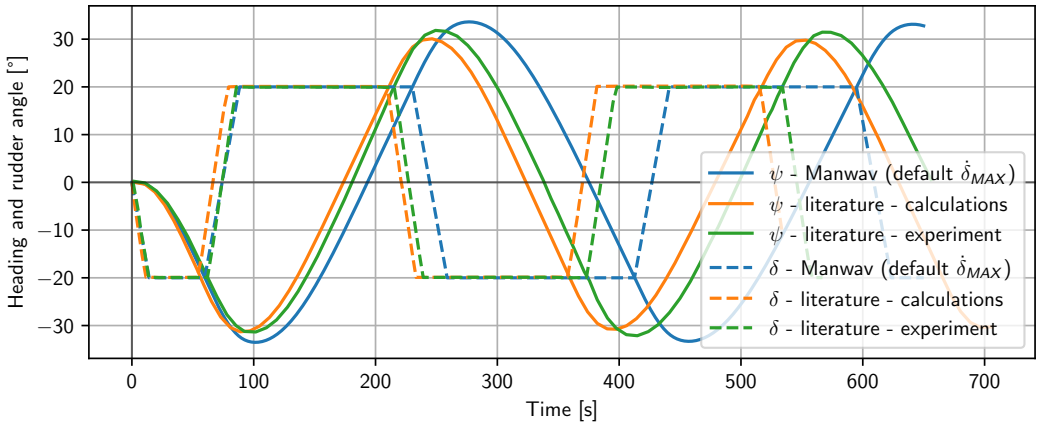

Figure A.10: Ship heading and rudder angle comparison plot in the starboard 20/20 zig-zag manoeuvre at 12.08 kn.
Default Manwav rudder slew rate.

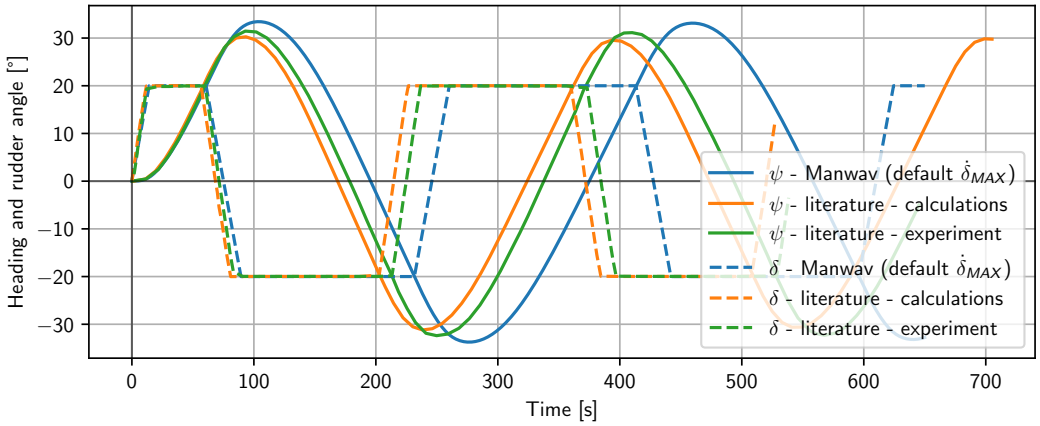

Figure A.11: Ship heading and rudder angle comparison plot in the port 20/20 zig-zag manoeuvre at 12.08 kn.
Default Manwav rudder slew rate.

A.2. Modified rudder slew rate comparisons

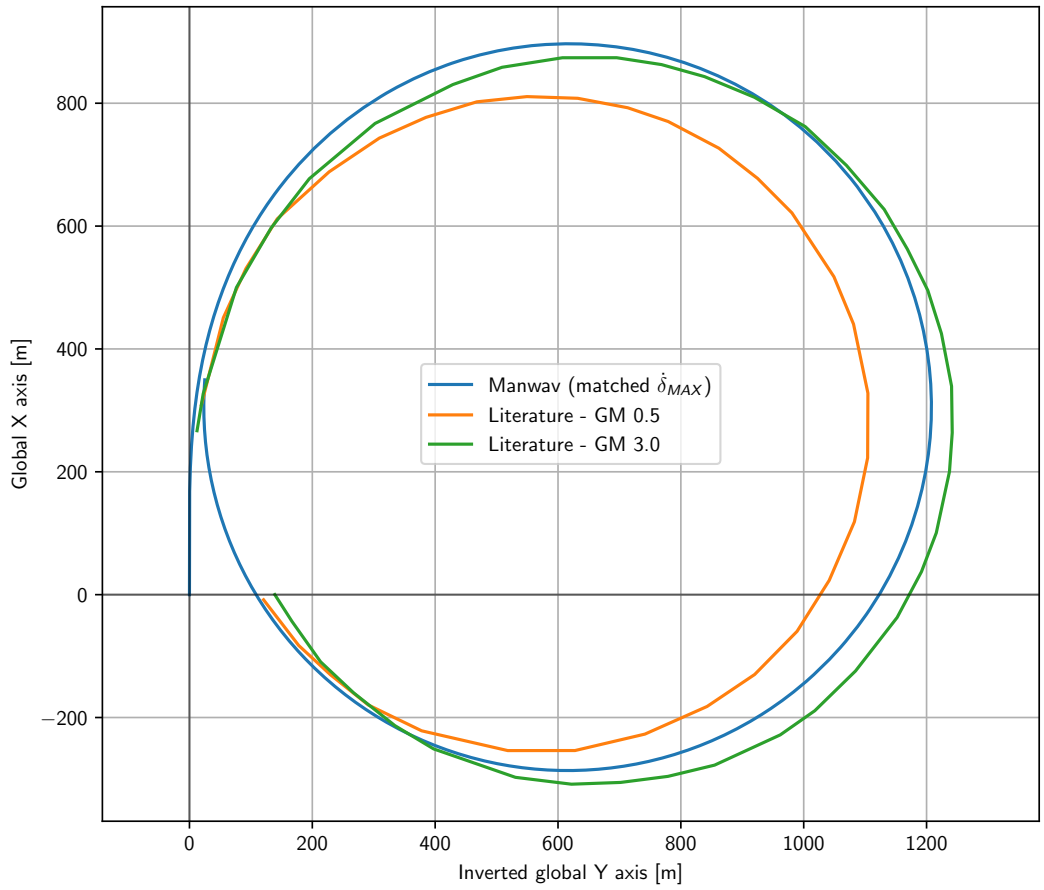

Figure A.12: Ship track comparison plot in the 15° to starboard turning circle manoeuvre at 24.15 kn. Manwav rudder slew rate matching the one from Son & Nomoto paper.

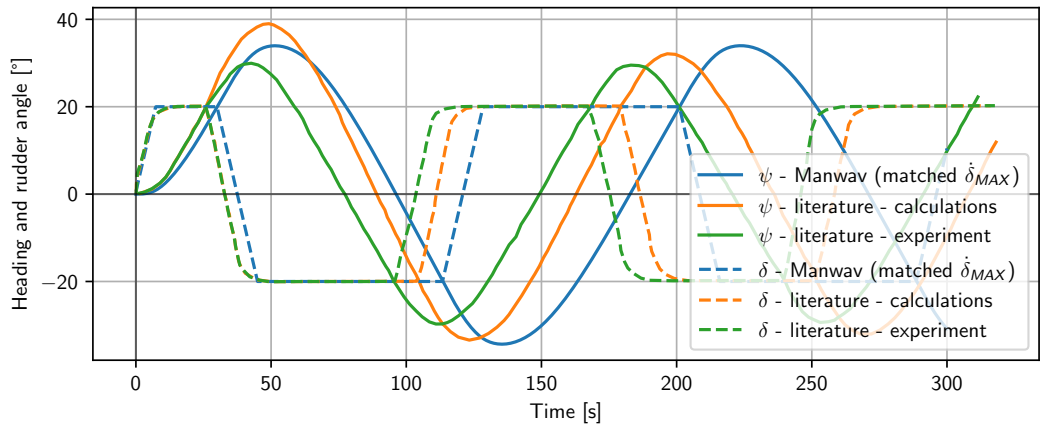

Figure A.13: Ship heading and rudder angle comparison plot in the starboard 20/20 zig-zag manoeuvre at 24.15 kn. Manwav rudder slew rate matching the one from Son & Nomoto paper.

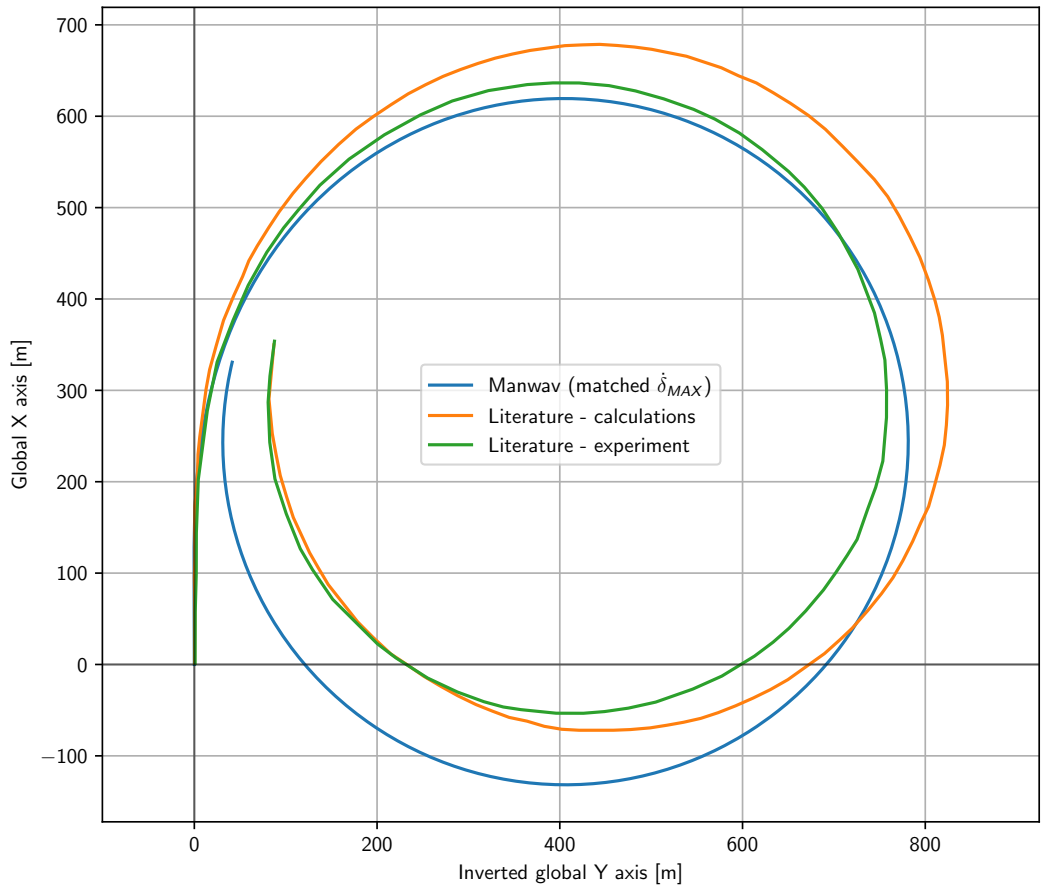

Figure A.14: Ship track comparison plot in the 35° to starboard turning circle manoeuvre at 12.08 kn. Manwav rudder slew rate matching the one from Son & Nomoto paper.

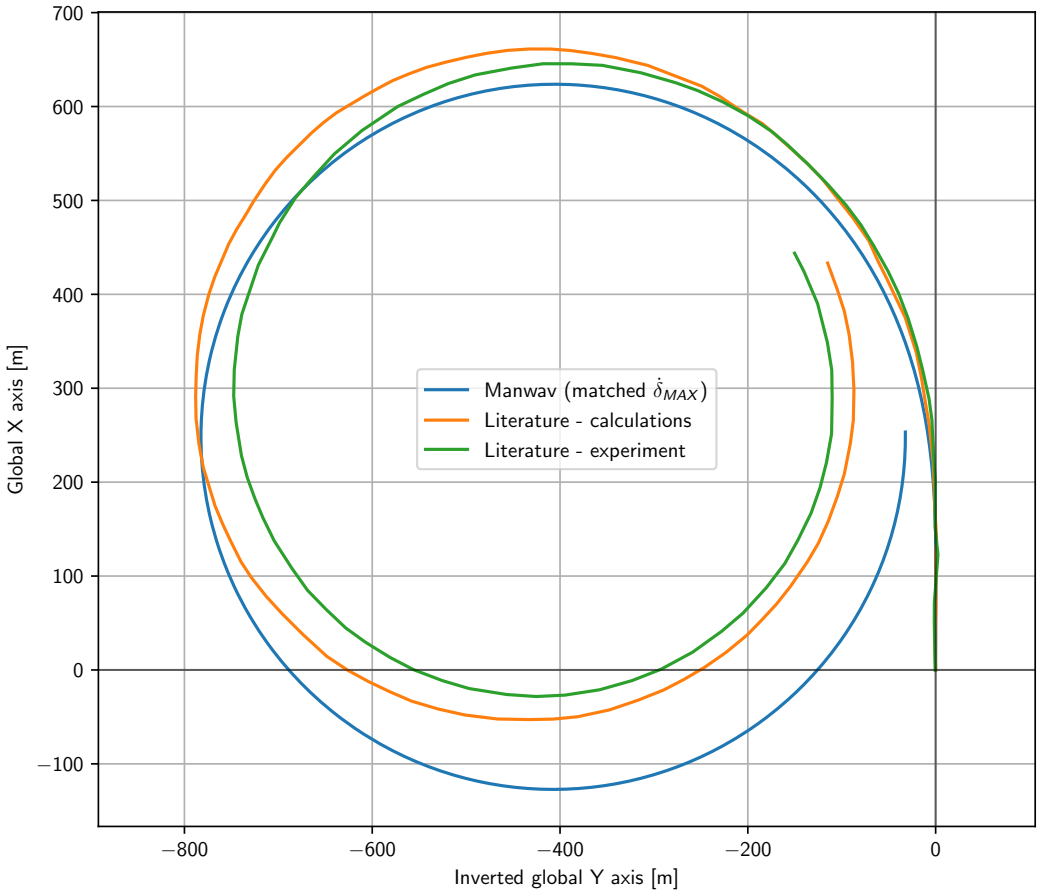

Figure A.15: Ship track comparison plot in the 35° to port turning circle manoeuvre at 12.08 kn. Manwav rudder slew rate matching the one from Son & Nomoto paper.

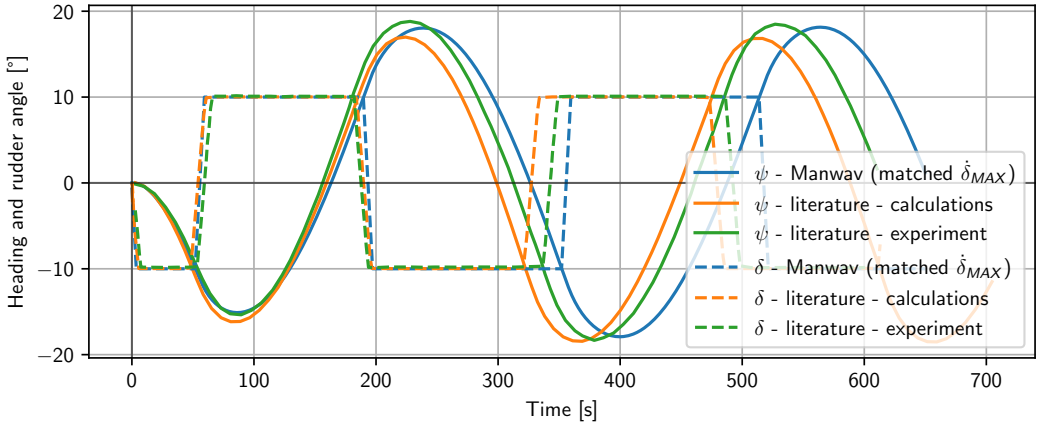

Figure A.16: Ship heading and rudder angle comparison plot in the starboard 10/10 zig-zag manoeuvre at 12.08 kn. Manwav rudder slew rate matching the one from Son & Nomoto paper.

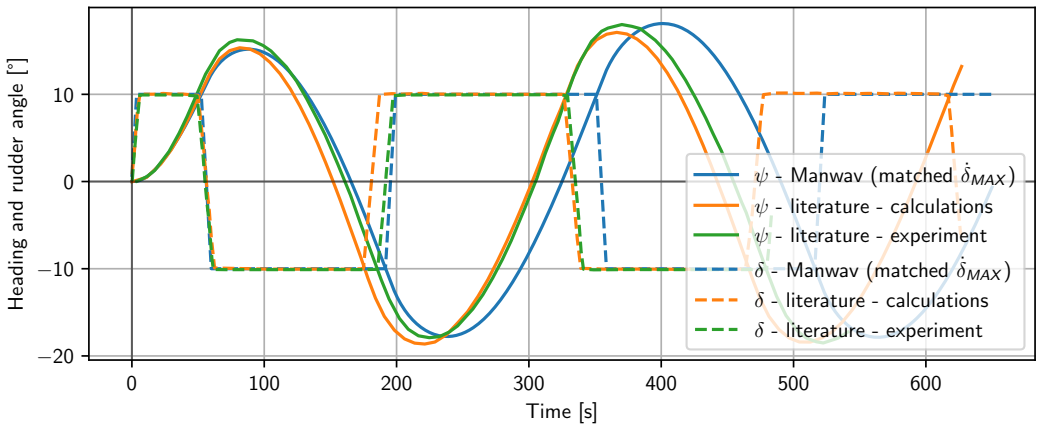

Figure A.17: Ship heading and rudder angle comparison plot in the port 10/10 zig-zag manoeuvre at 12.08 kn. Manwav rudder slew rate matching the one from Son & Nomoto paper.

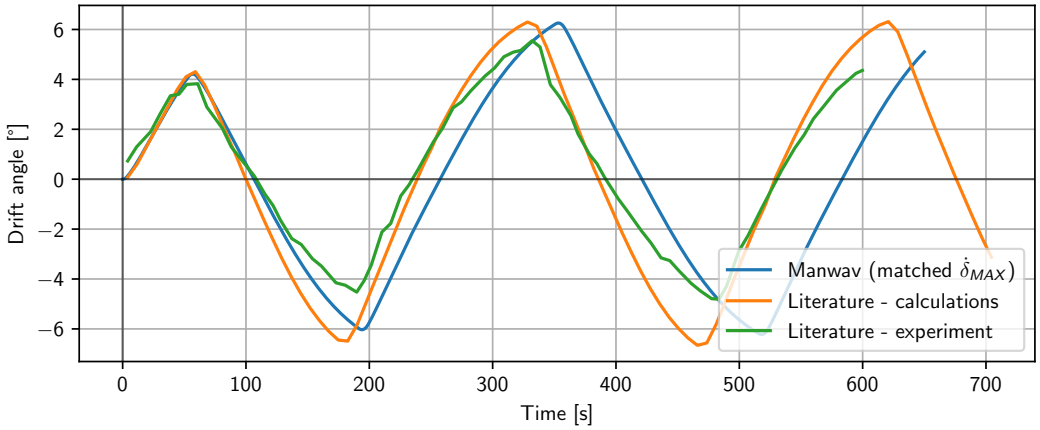

Figure A.18: Drift angle comparison plot in the port 10/10 zig-zag manoeuvre at 12.08 kn. Manwav rudder slew rate matching the one from Son & Nomoto paper.

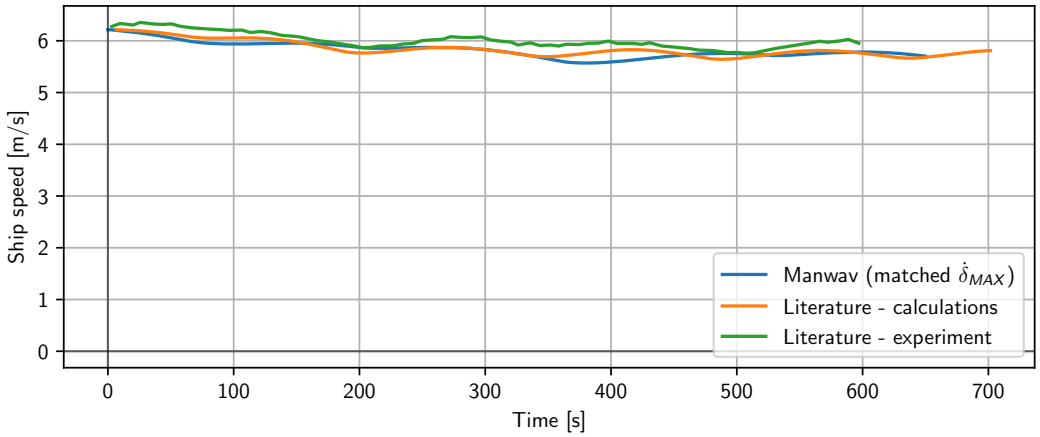

Figure A.19: Ship speed comparison plot in the port 10/10 zig-zag manoeuvre at 12.08 kn. Manwav rudder slew rate matching the one from Son & Nomoto paper.

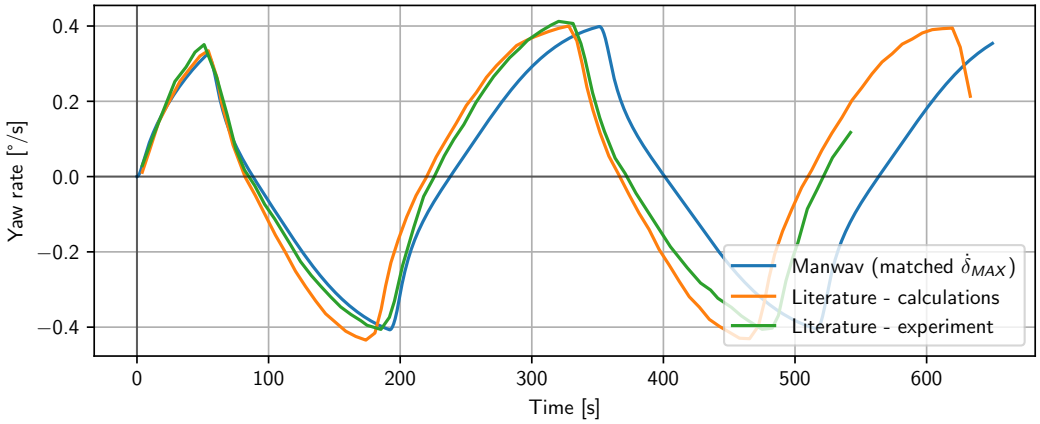

Figure A.20: Yaw rate comparison plot in the port 10/10 zig-zag manoeuvre at 12.08 kn. Manwav rudder slew rate matching the one from Son & Nomoto paper.

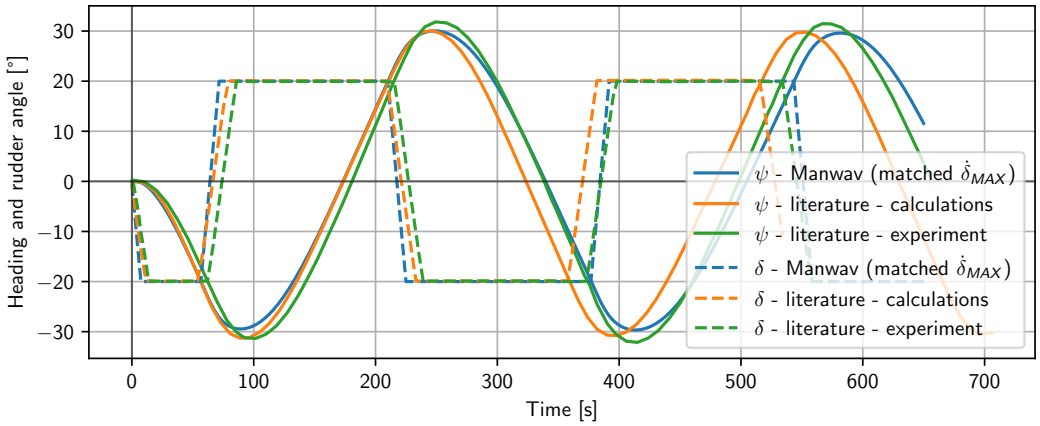

Figure A.21: Ship heading and rudder angle comparison plot in the starboard 20/20 zig-zag manoeuvre at 12.08 kn. Manwav rudder slew rate matching the one from Son & Nomoto paper.

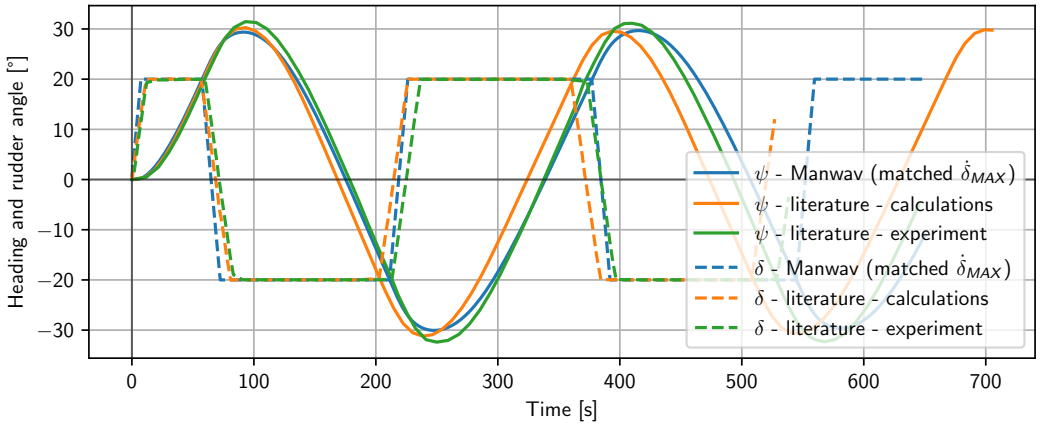

Figure A.22: Ship heading and rudder angle comparison plot in the port 20/20 zig-zag manoeuvre at 12.08 kn. Manwav rudder slew rate matching the one from Son & Nomoto paper.

A.3. Manwav MPP rudder model comparisons

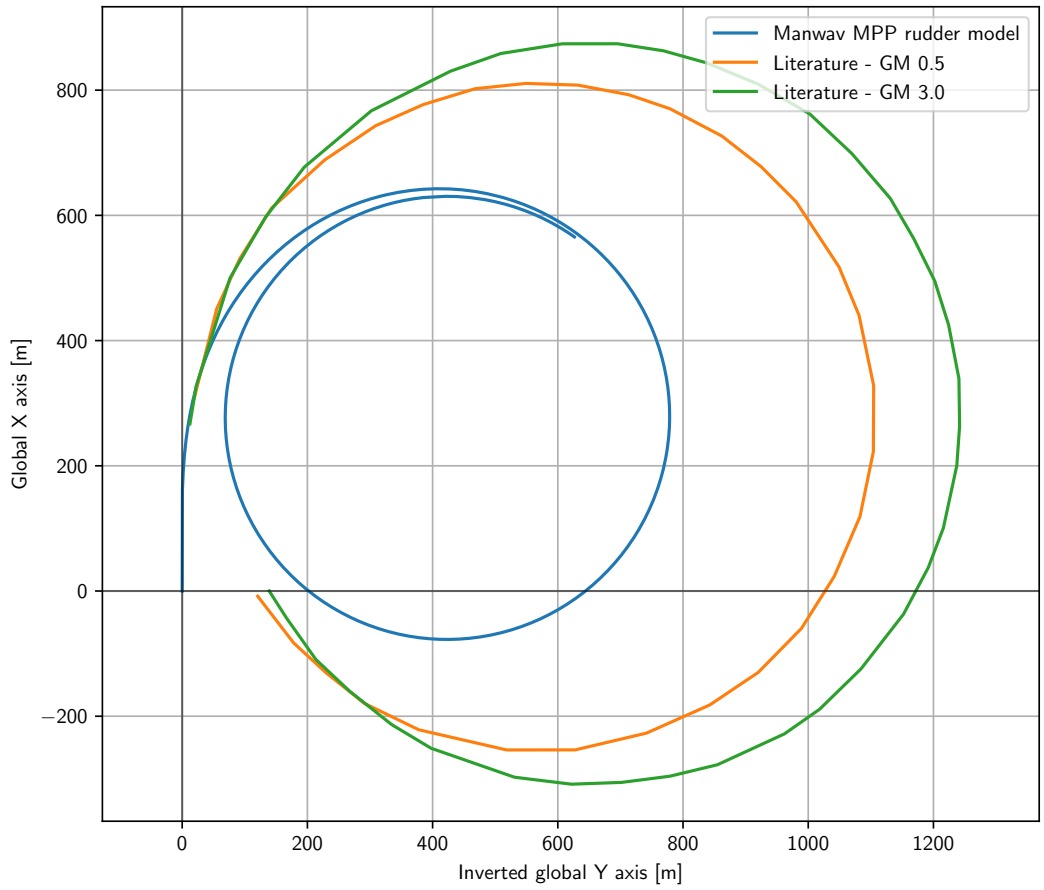

Figure A.23: Ship track comparison plot in the 15° to starboard turning circle manoeuvre at 24.15 kn. Manwav rudder model switched to MPP model.

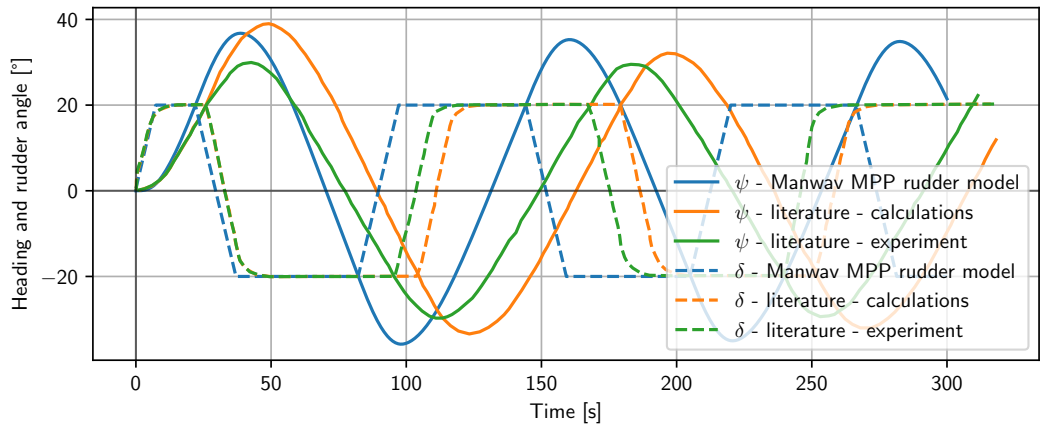

Figure A.24: Ship heading and rudder angle comparison plot in the starboard 20/20 zig-zag manoeuvre at 24.15 kn. Manwav rudder model switched to MPP model.

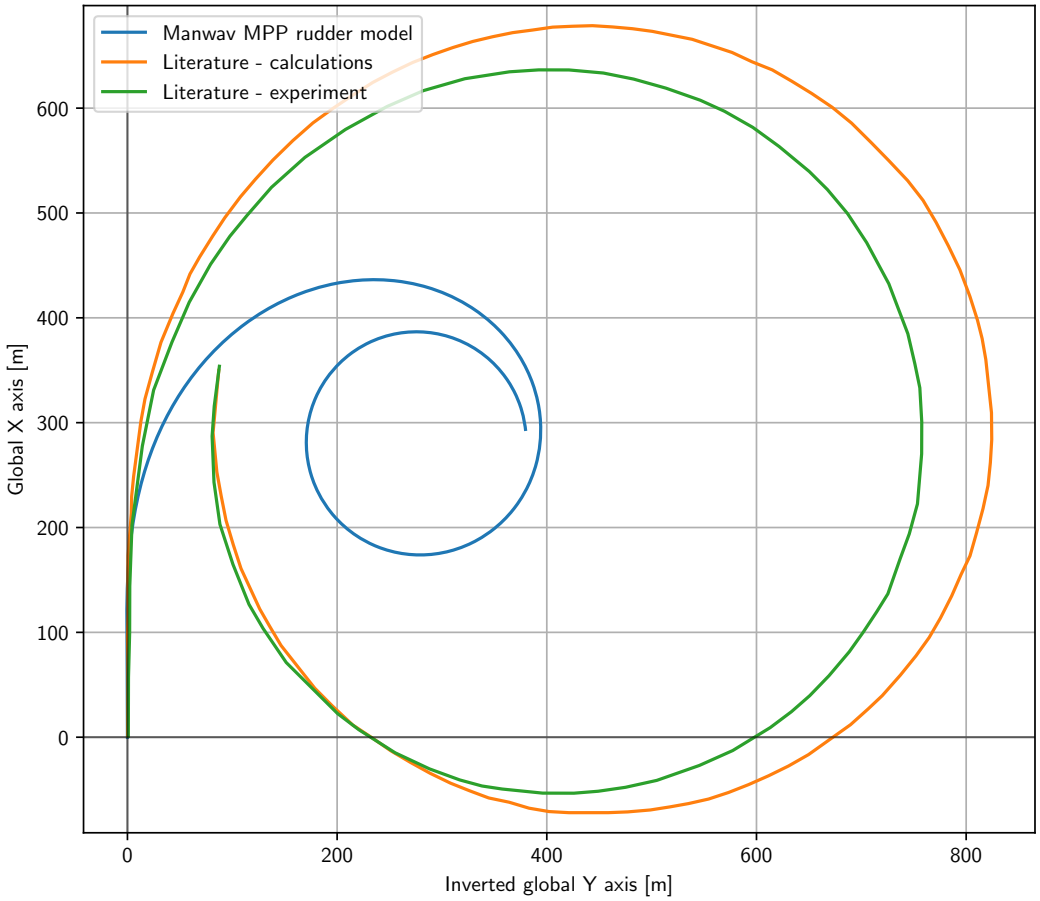

Figure A.25: Ship track comparison plot in the 35° to starboard turning circle manoeuvre at 12.08 kn. Manwav rudder model switched to MPP model.

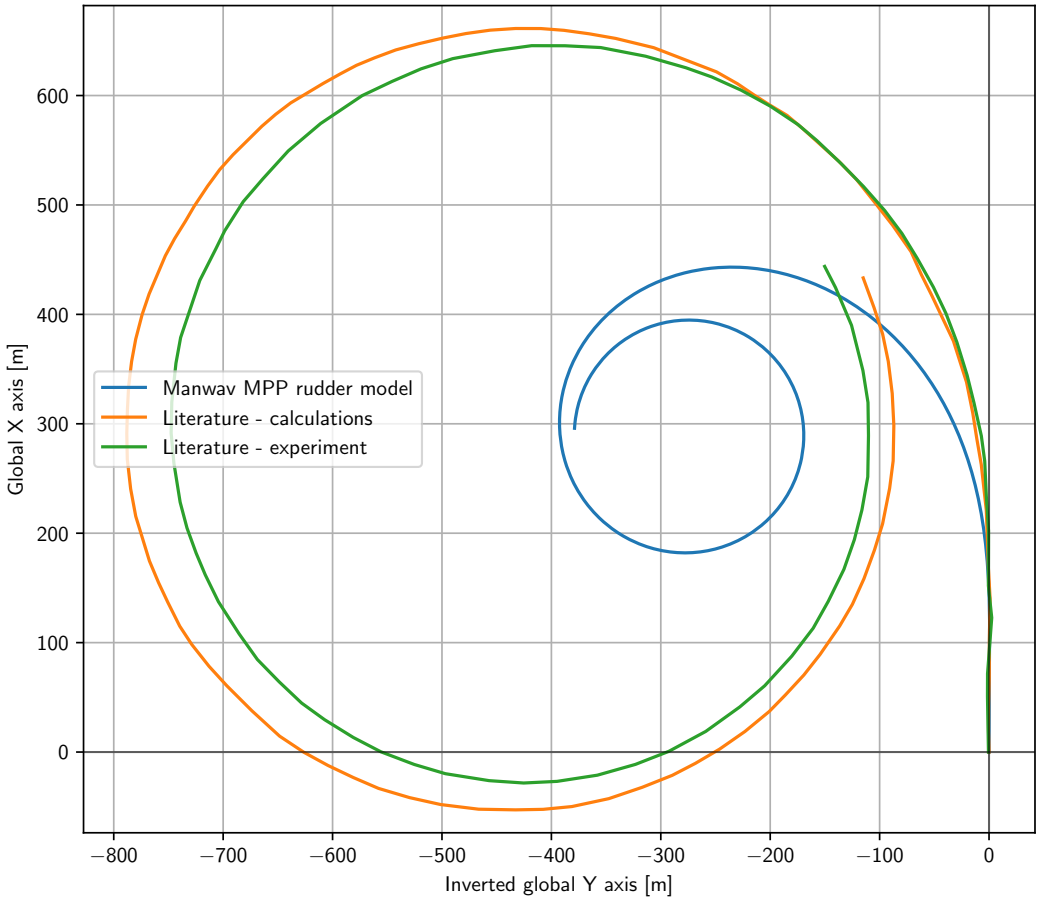

Figure A.26: Ship track comparison plot in the 35° to port turning circle manoeuvre at 12.08 kn. Manwav rudder model switched to MPP model.

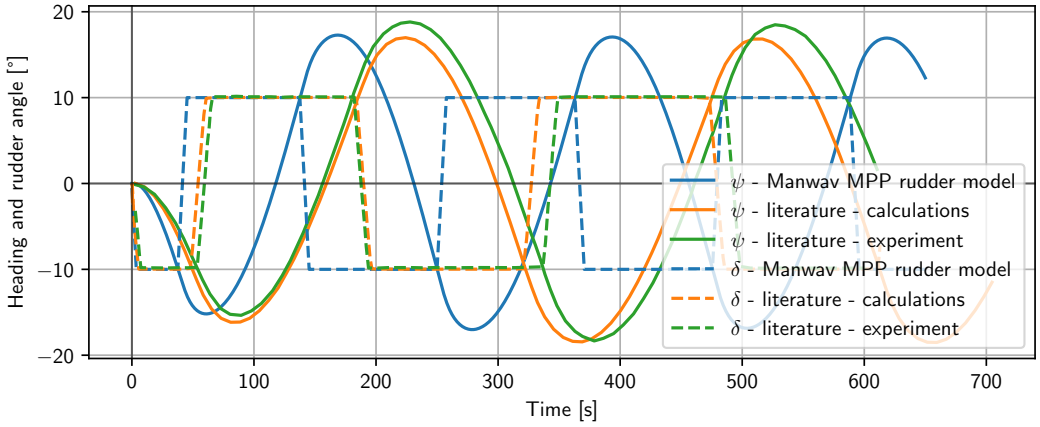

Figure A.27: Ship heading and rudder angle comparison plot in the starboard 10/10 zig-zag manoeuvre at 12.08 kn. Manwav rudder model switched to MPP model.

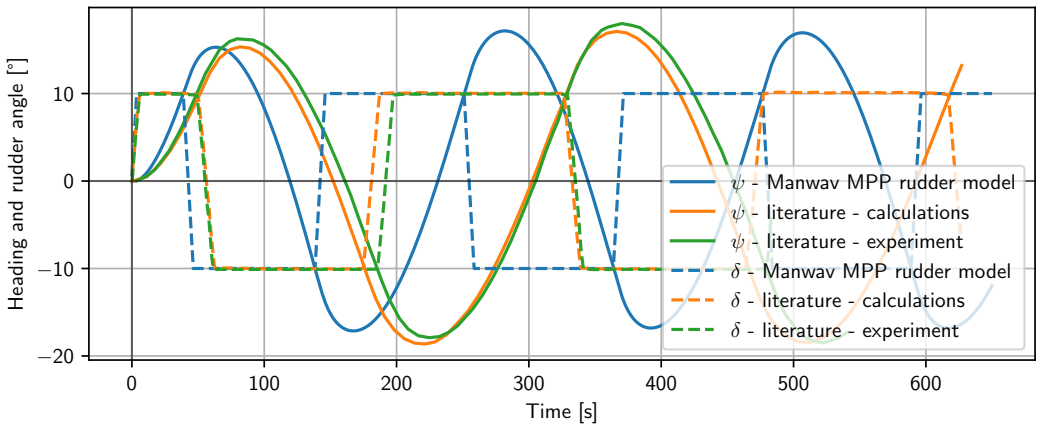

Figure A.28: Ship heading and rudder angle comparison plot in the port 10/10 zig-zag manoeuvre at 12.08 kn. Manwav rudder model switched to MPP model.

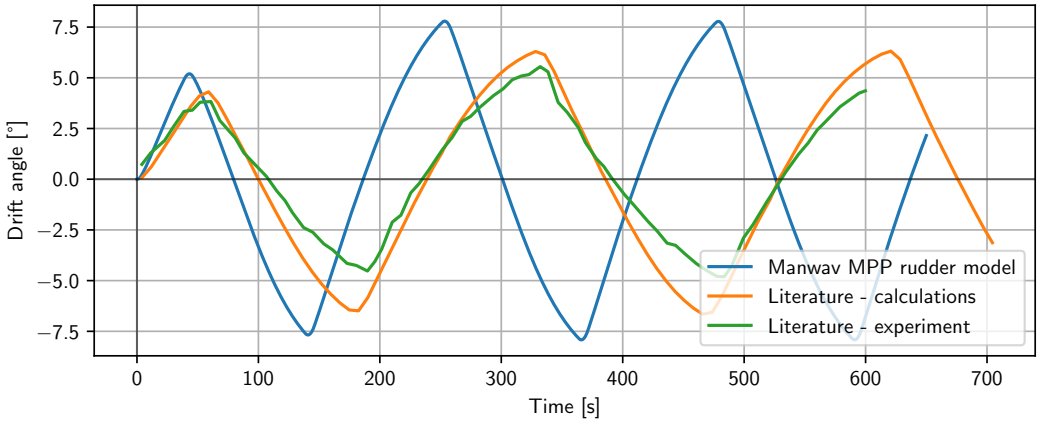

Figure A.29: Drift angle comparison plot in the port 10/10 zig-zag manoeuvre at 12.08 kn. Manwav rudder model switched to MPP model.

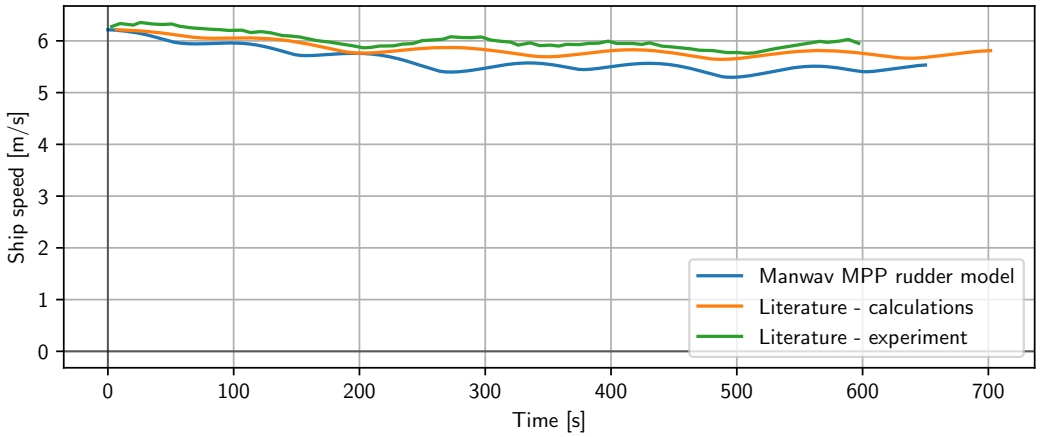

Figure A.30: Ship speed comparison plot in the port 10/10 zig-zag manoeuvre at 12.08 kn. Manwav rudder model switched to MPP model.

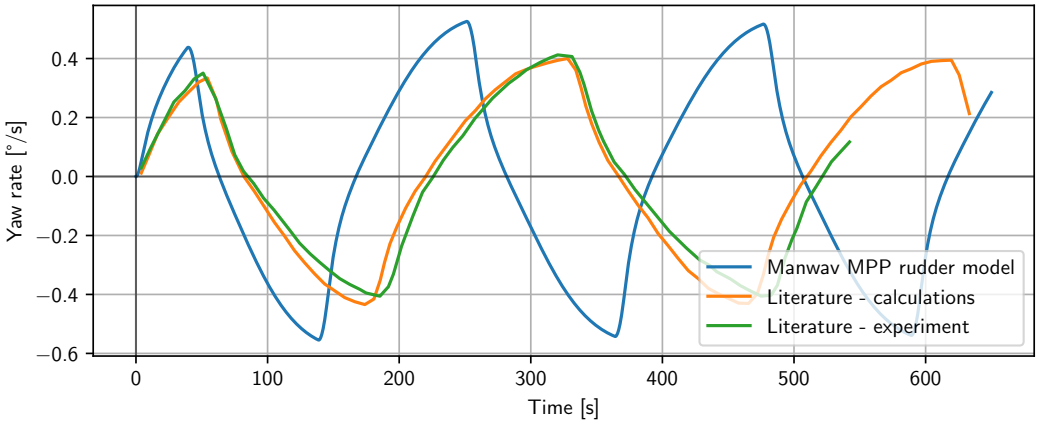

Figure A.31: Yaw rate comparison plot in the port 10/10 zig-zag manoeuvre at 12.08 kn.
Manwav rudder model switched to MPP model.

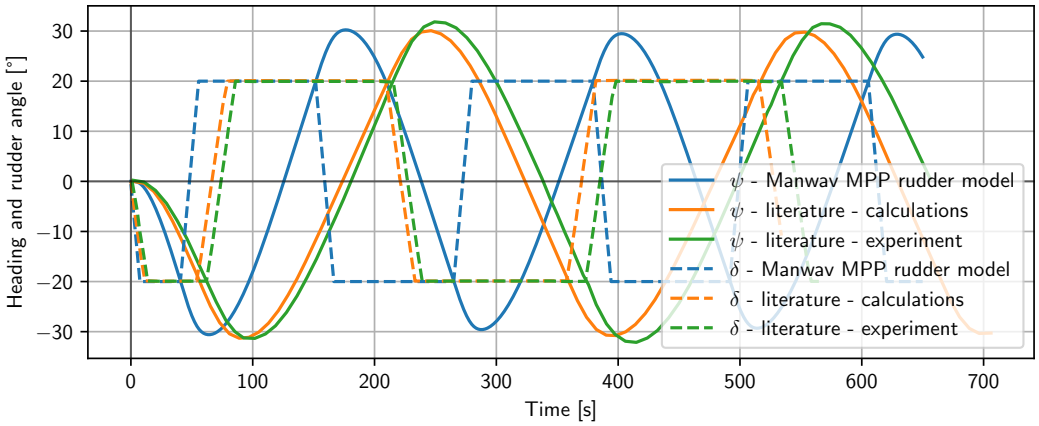

Figure A.32: Ship heading and rudder angle comparison plot in the starboard 20/20 zig-zag manoeuvre at 12.08 kn.
Manwav rudder model switched to MPP model.

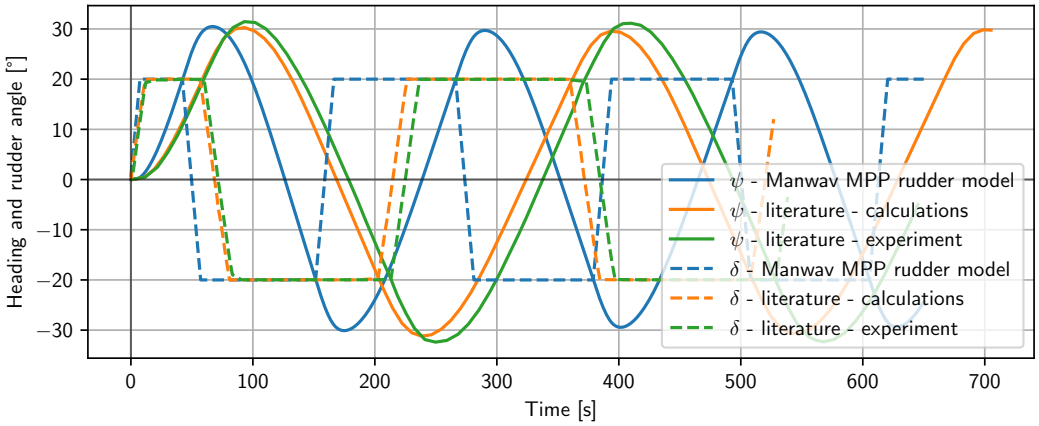

Figure A.33: Ship heading and rudder angle comparison plot in the port 20/20 zig-zag manoeuvre at 12.08 kn.
Manwav rudder model switched to MPP model.

A.4. Modified rudder CL slope and L/D ratio comparisons

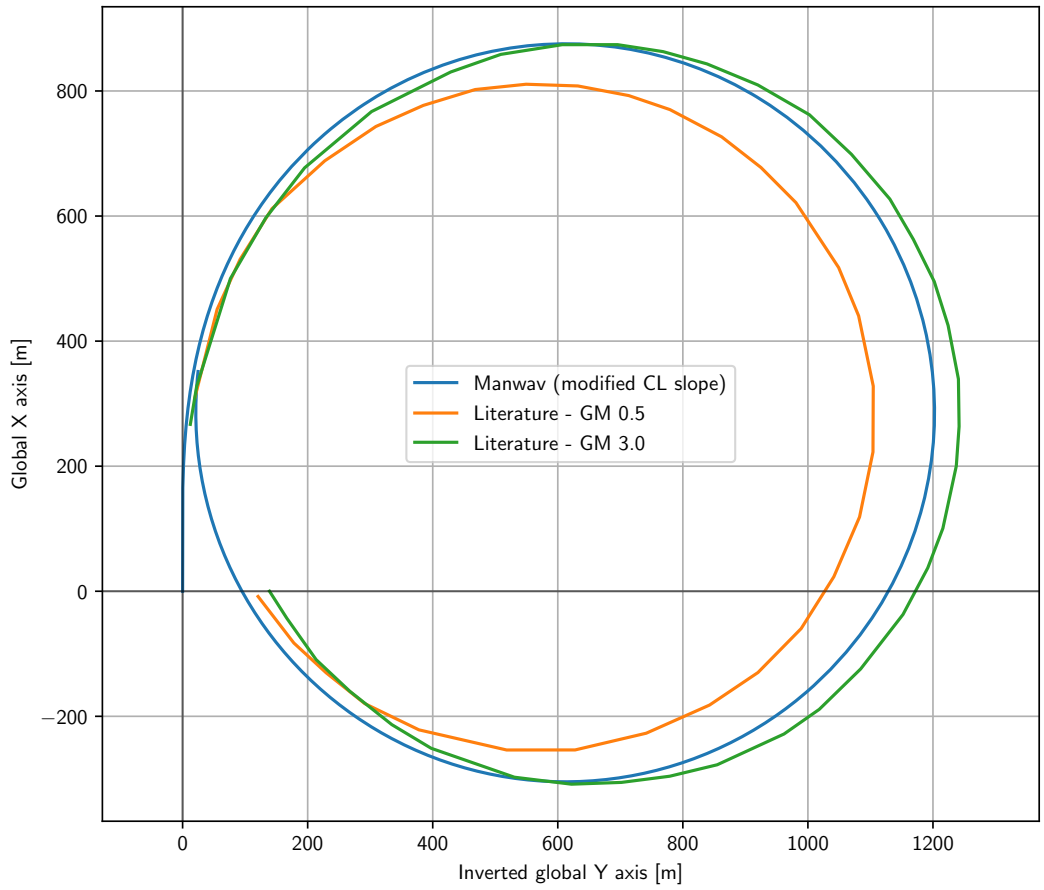

Figure A.34: Ship track comparison plot in the 15° to starboard turning circle manoeuvre at 24.15 kn. Adjusted CL slope and L/D ratio.

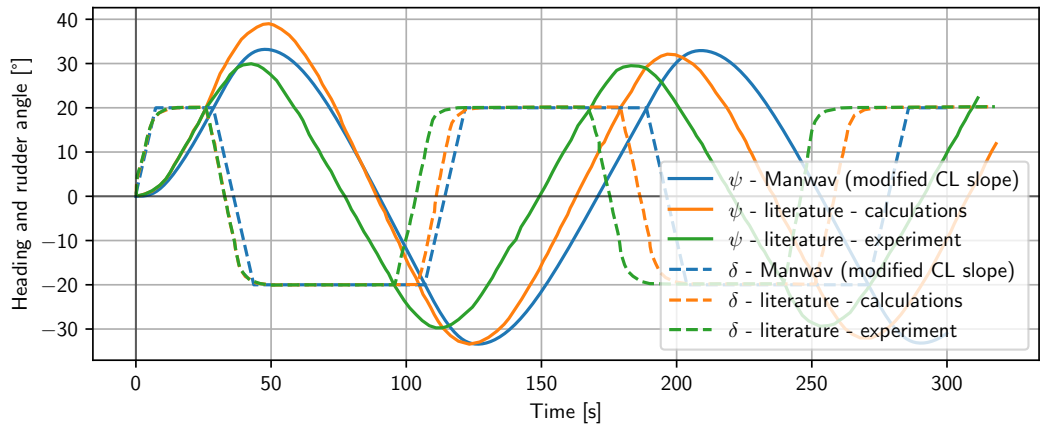

Figure A.35: Ship heading and rudder angle comparison plot in the starboard 20/20 zig-zag manoeuvre at 24.15 kn. Adjusted CL slope and L/D ratio.

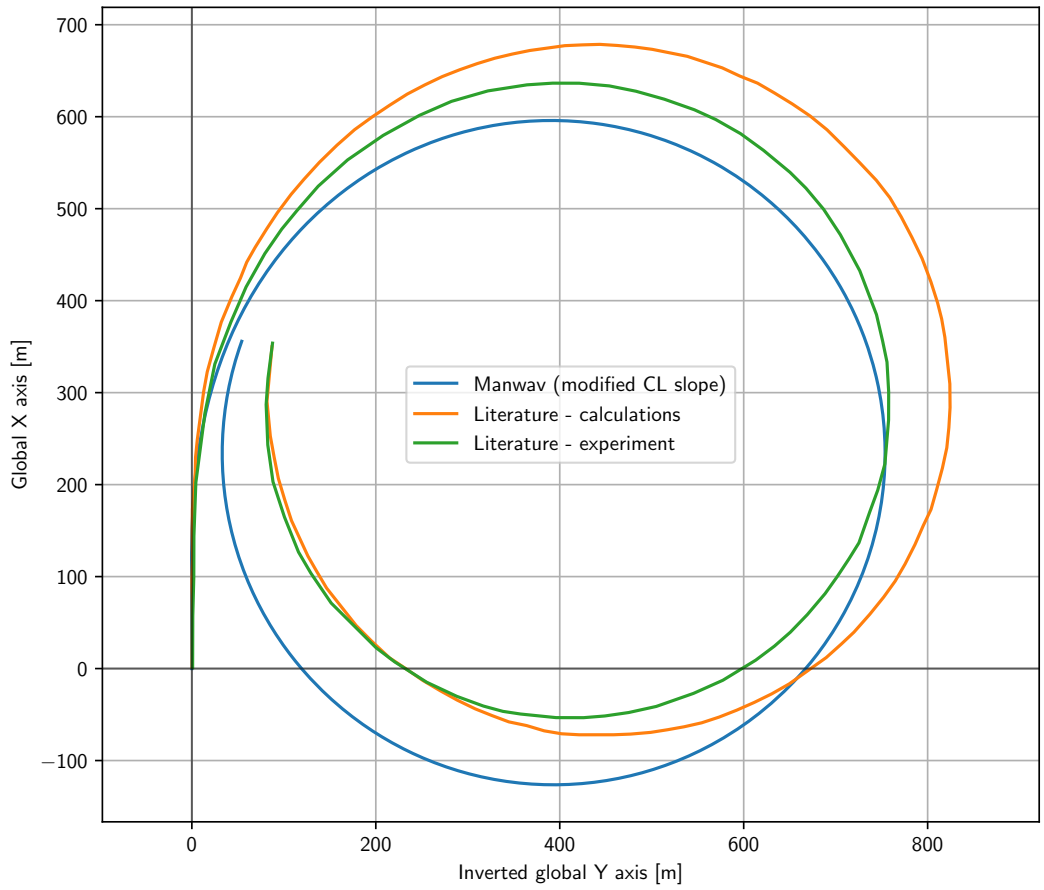

Figure A.36: Ship track comparison plot in the 35° to starboard turning circle manoeuvre at 12.08 kn. Adjusted CL slope and L/D ratio.

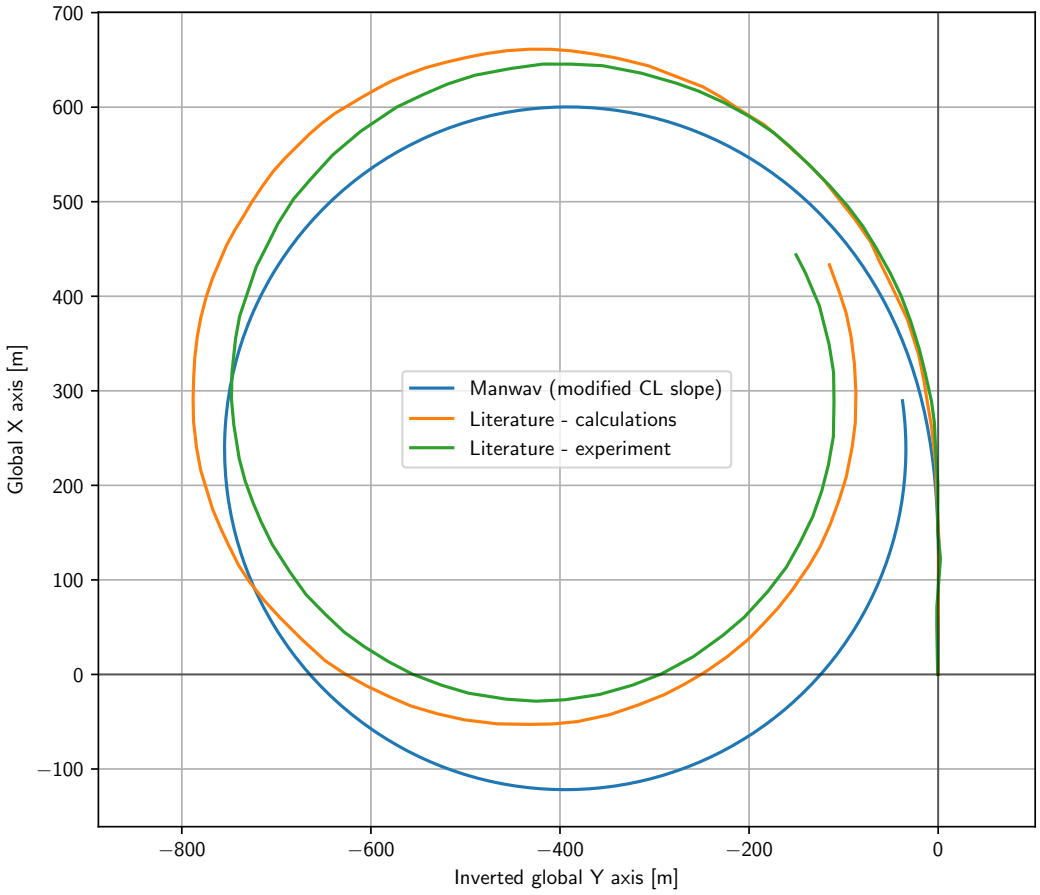

Figure A.37: Ship track comparison plot in the 35° to port turning circle manoeuvre at 12.08 kn. Adjusted CL slope and L/D ratio.

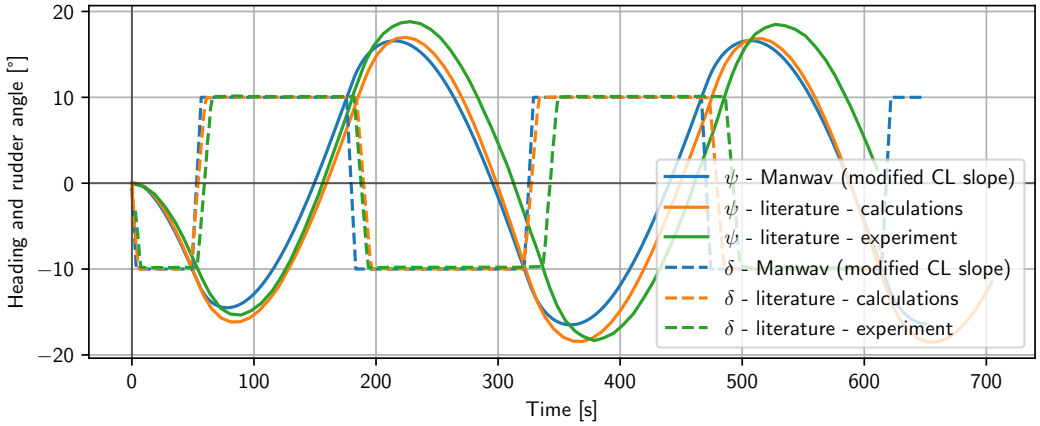

Figure A.38: Ship heading and rudder angle comparison plot in the starboard 10/10 zig-zag manoeuvre at 12.08 kn. Adjusted CL slope and L/D ratio.

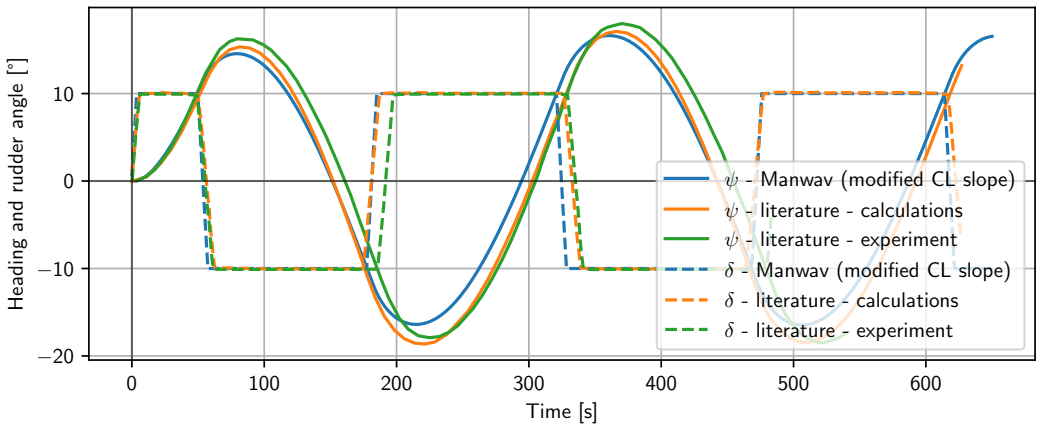

Figure A.39: Ship heading and rudder angle comparison plot in the port 10/10 zig-zag manoeuvre at 12.08 kn. Adjusted CL slope and L/D ratio.

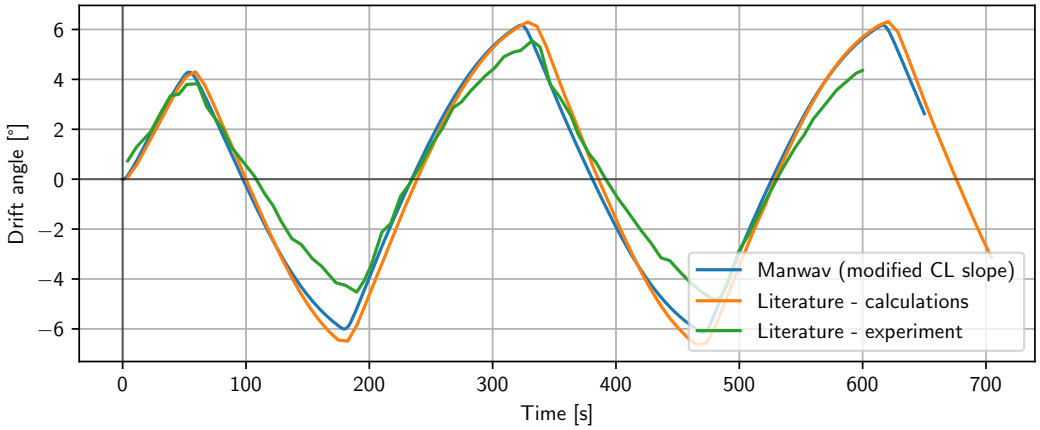

Figure A.40: Drift angle comparison plot in the port 10/10 zig-zag manoeuvre at 12.08 kn. Adjusted CL slope and L/D ratio.

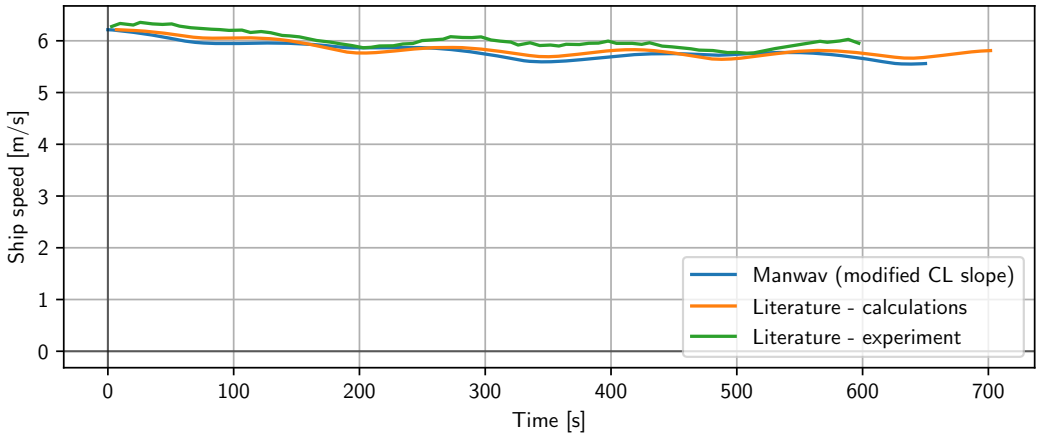

Figure A.41: Ship speed comparison plot in the port 10/10 zig-zag manoeuvre at 12.08 kn. Adjusted CL slope and L/D ratio.

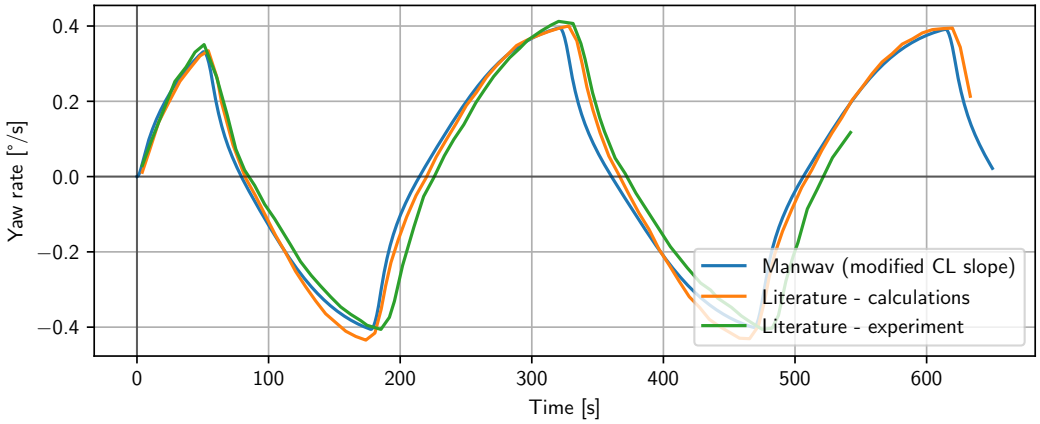

Figure A.42: Yaw rate comparison plot in the port 10/10 zig-zag manoeuvre at 12.08 kn.
Adjusted CL slope and L/D ratio.

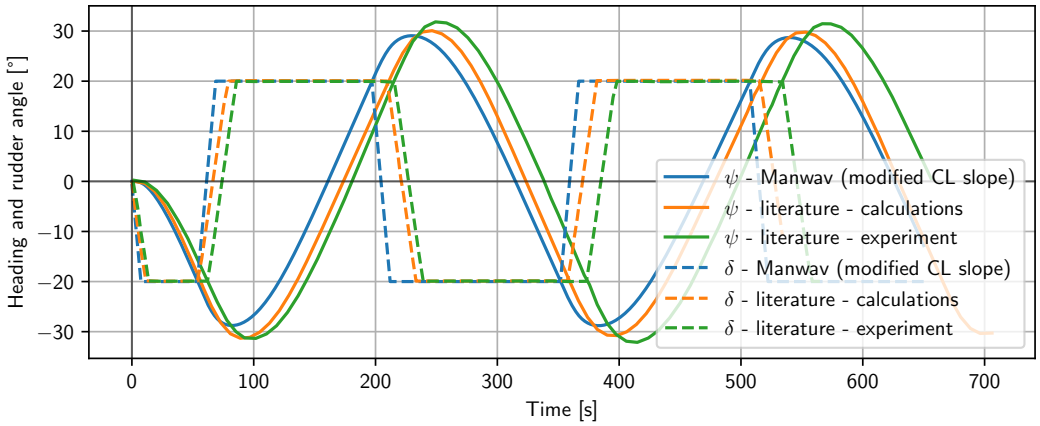

Figure A.43: Ship heading and rudder angle comparison plot in the starboard 20/20 zig-zag manoeuvre at 12.08 kn.
Adjusted CL slope and L/D ratio.

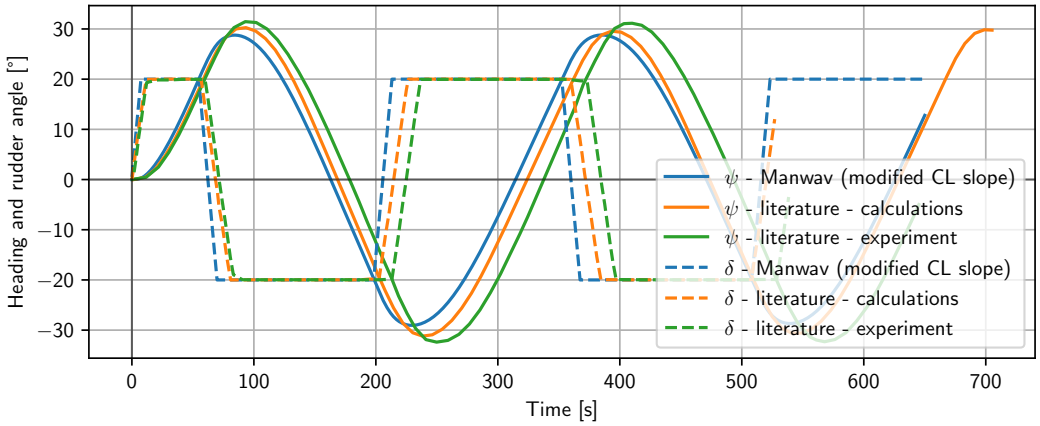

Figure A.44: Ship heading and rudder angle comparison plot in the port 20/20 zig-zag manoeuvre at 12.08 kn.
Adjusted CL slope and L/D ratio.

B. Appendix B: Data-based model algorithm performance plots

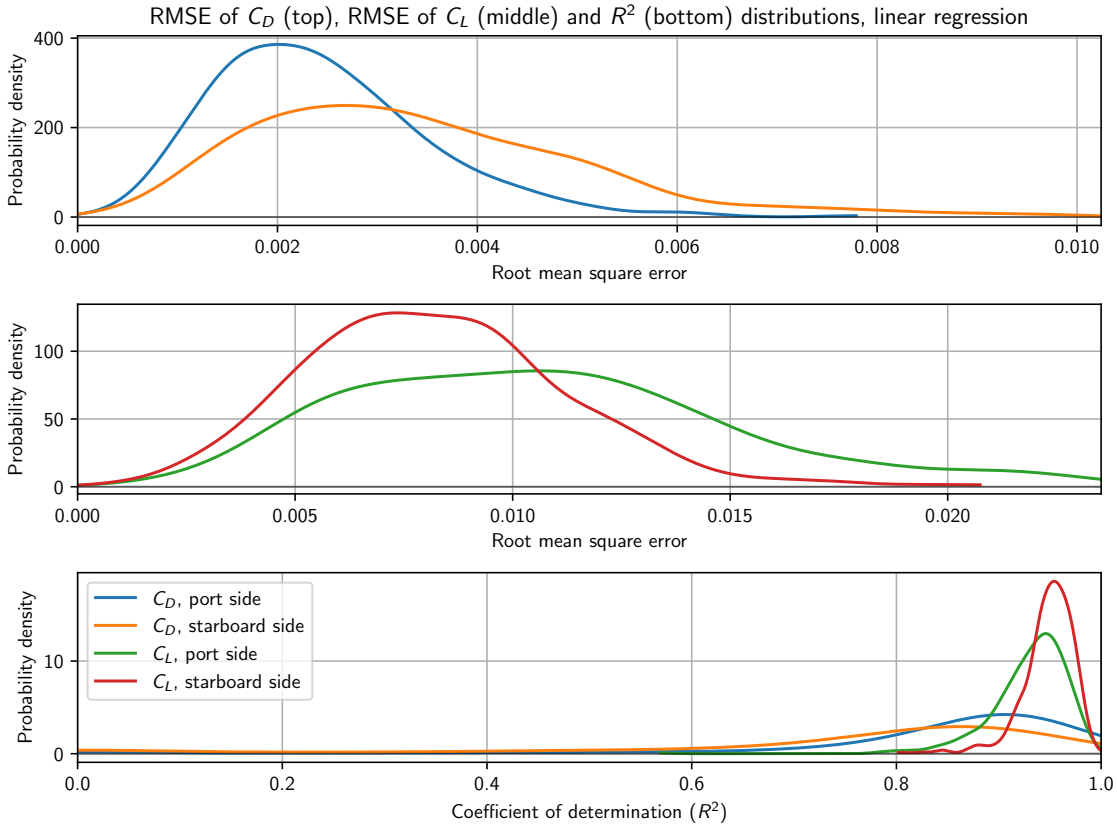

Figure B.1: Distributions of root mean square error and coefficient of determination for the linear regression algorithm.

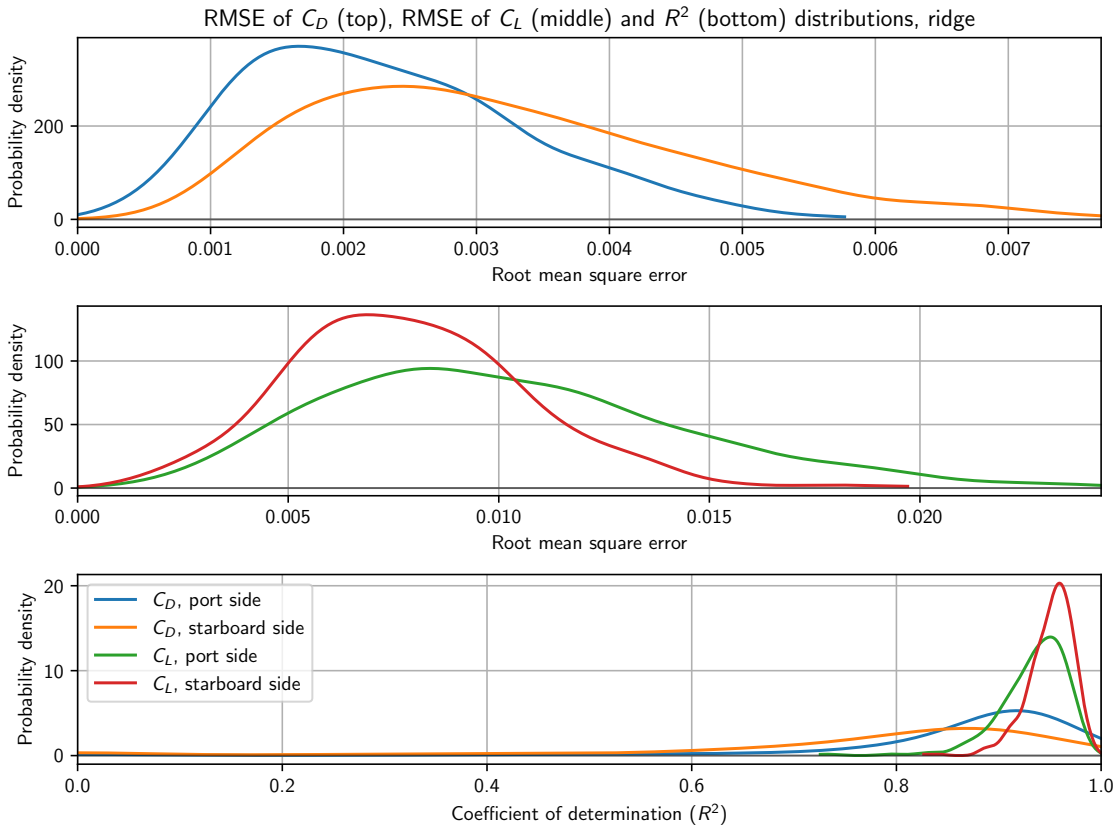

Figure B.2: Distributions of root mean square error and coefficient of determination for the ridge regression algorithm.

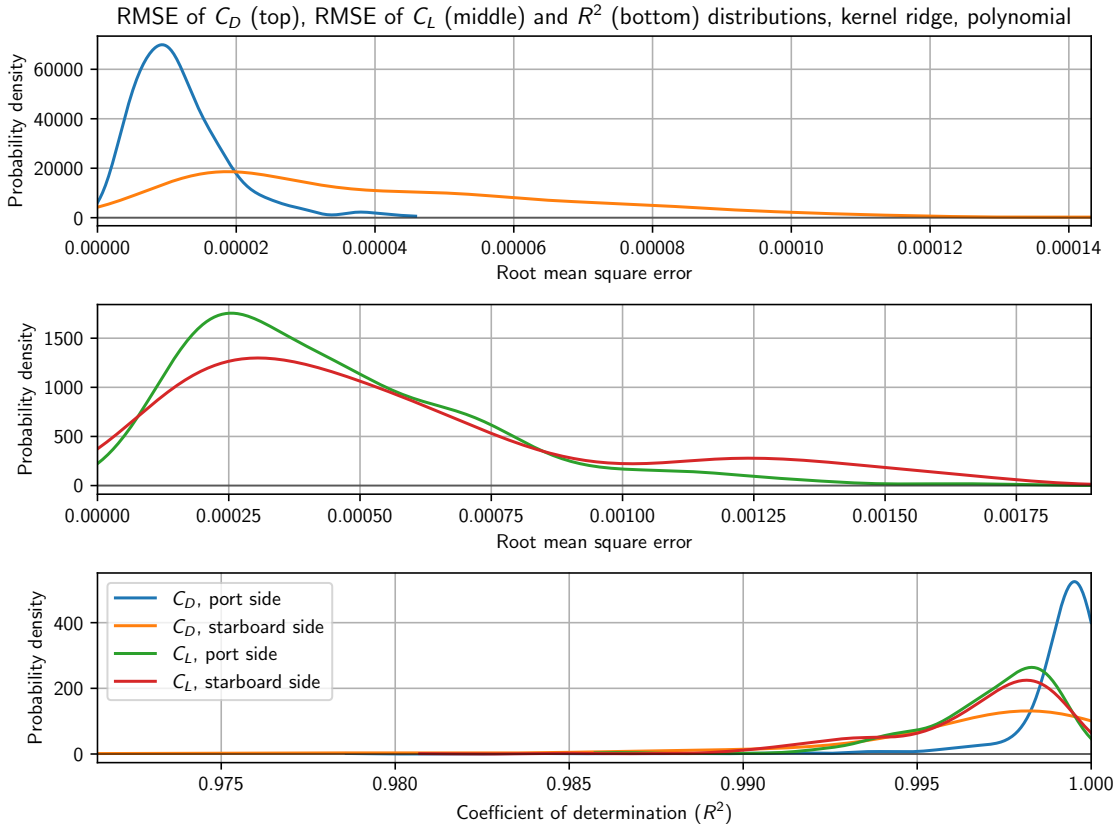

Figure B.3: Distributions of root mean square error and coefficient of determination for the kernel ridge regression algorithm with a polynomial kernel.

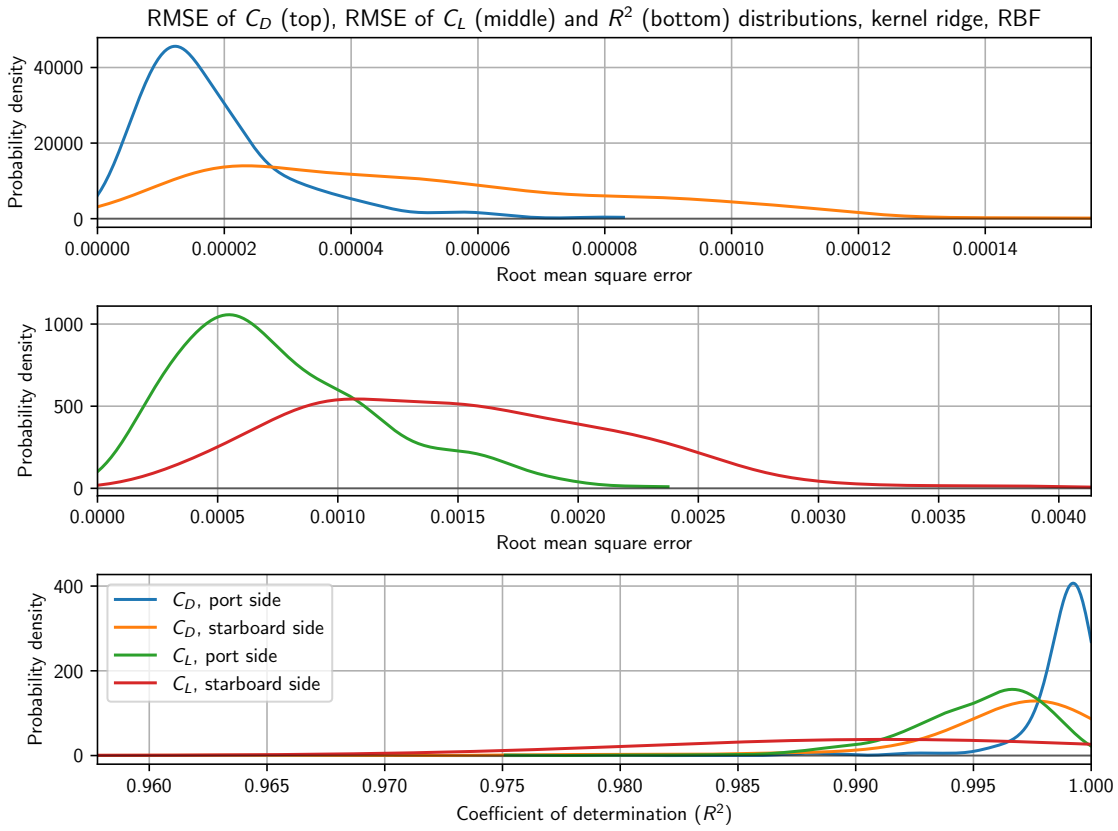

Figure B.4: Distributions of root mean square error and coefficient of determination for the kernel ridge regression algorithm with a RBF kernel.

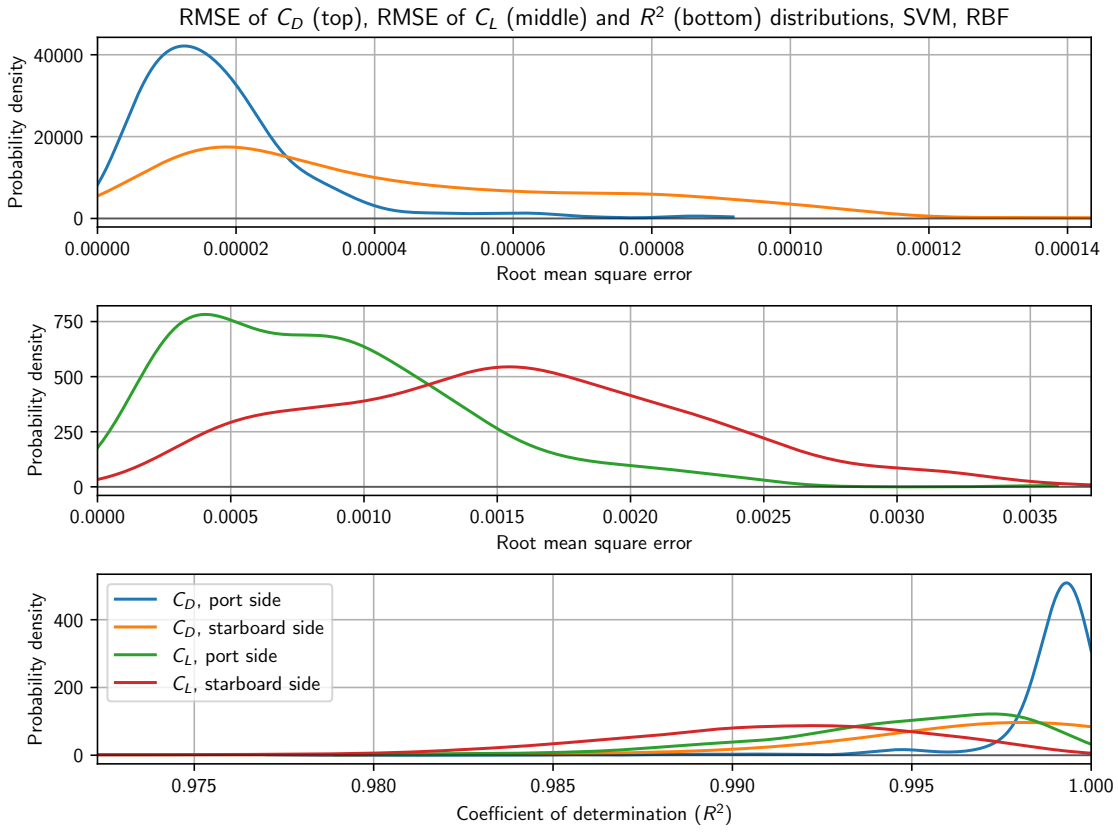

Figure B.5: Distributions of root mean square error and coefficient of determination for the support vector regression algorithm with a RBF kernel.

C. Appendix C: Case study manoeuvres comparison plots

C.1. Turning circle 15° to starboard @ 24.15 kn

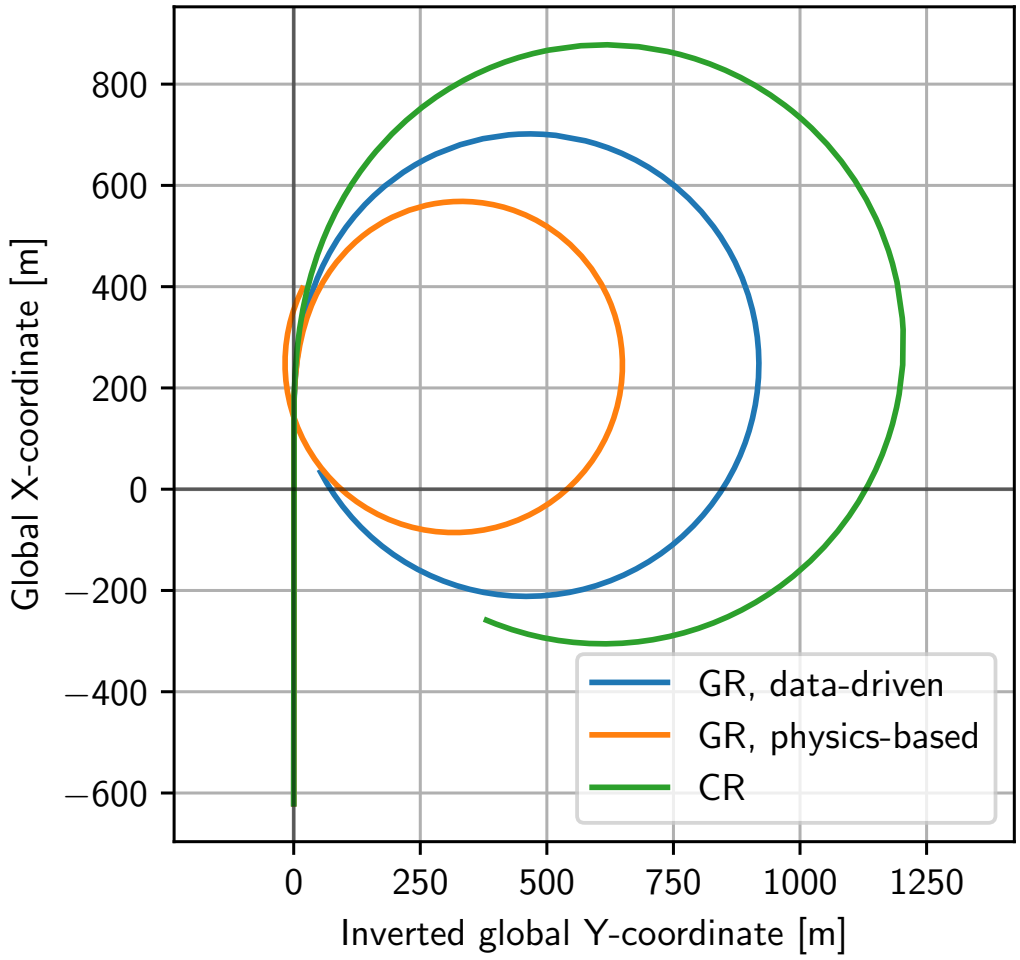

Figure C.1: Ship track comparison plot in the 15° to starboard turning circle manoeuvre at 24.15 kn.

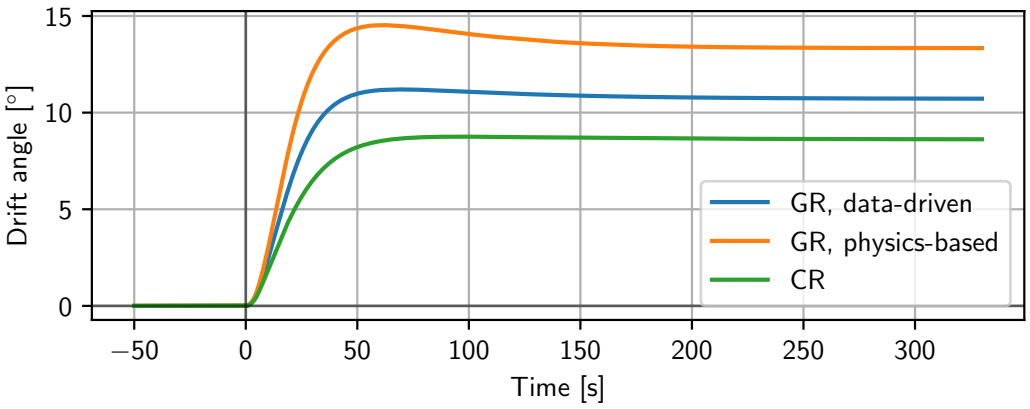

Figure C.2: Drift angle comparison plot in the 15° to starboard turning circle manoeuvre at 24.15 kn.

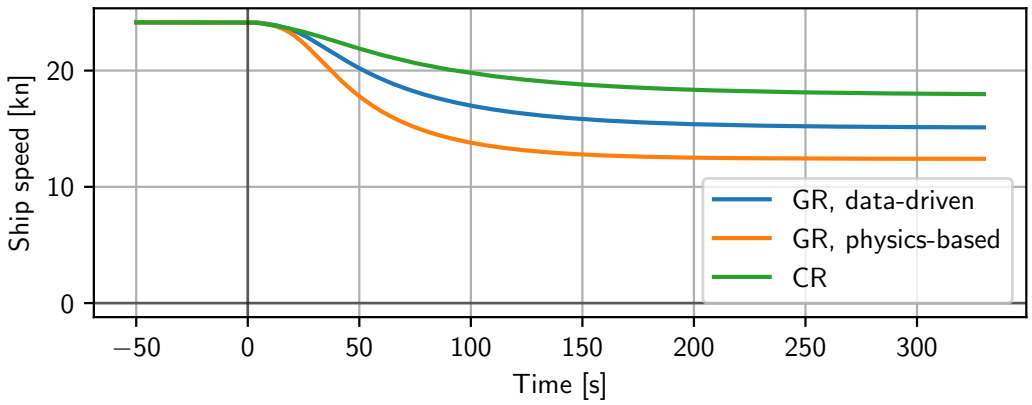

Figure C.3: Ship speed comparison plot in the 15° to starboard turning circle manoeuvre at 24.15 kn.

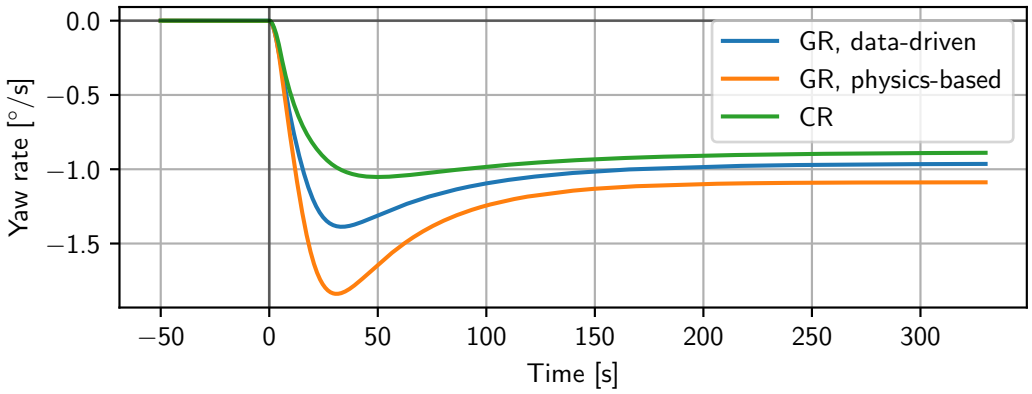

Figure C.4: Yaw rate comparison plot in the 15° to starboard turning circle manoeuvre at 24.15 kn.

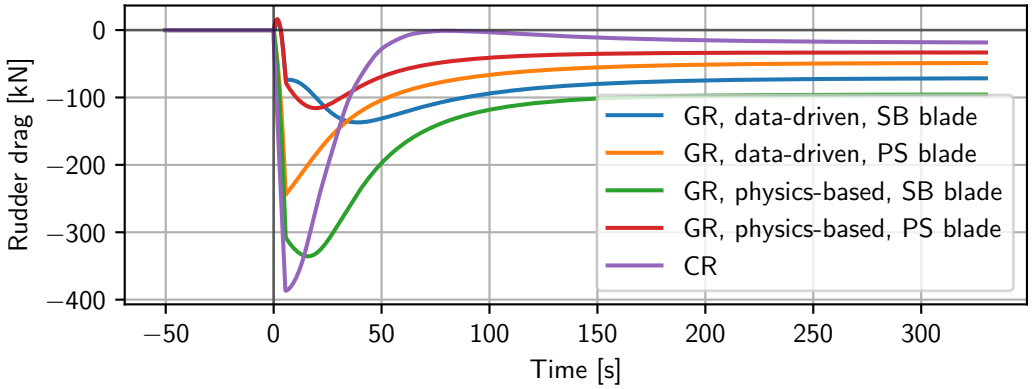

Figure C.5: Rudder drag force comparison plot in the 15° to starboard turning circle manoeuvre at 24.15 kn.

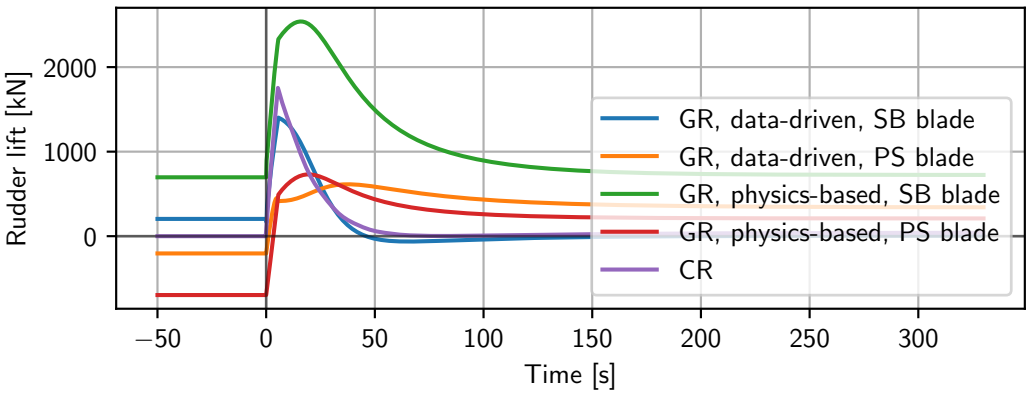

Figure C.6: Rudder lift force comparison plot in the 15° to starboard turning circle manoeuvre at 24.15 kn.

C.2. Turning circle 35° to port @ 12.08 kn

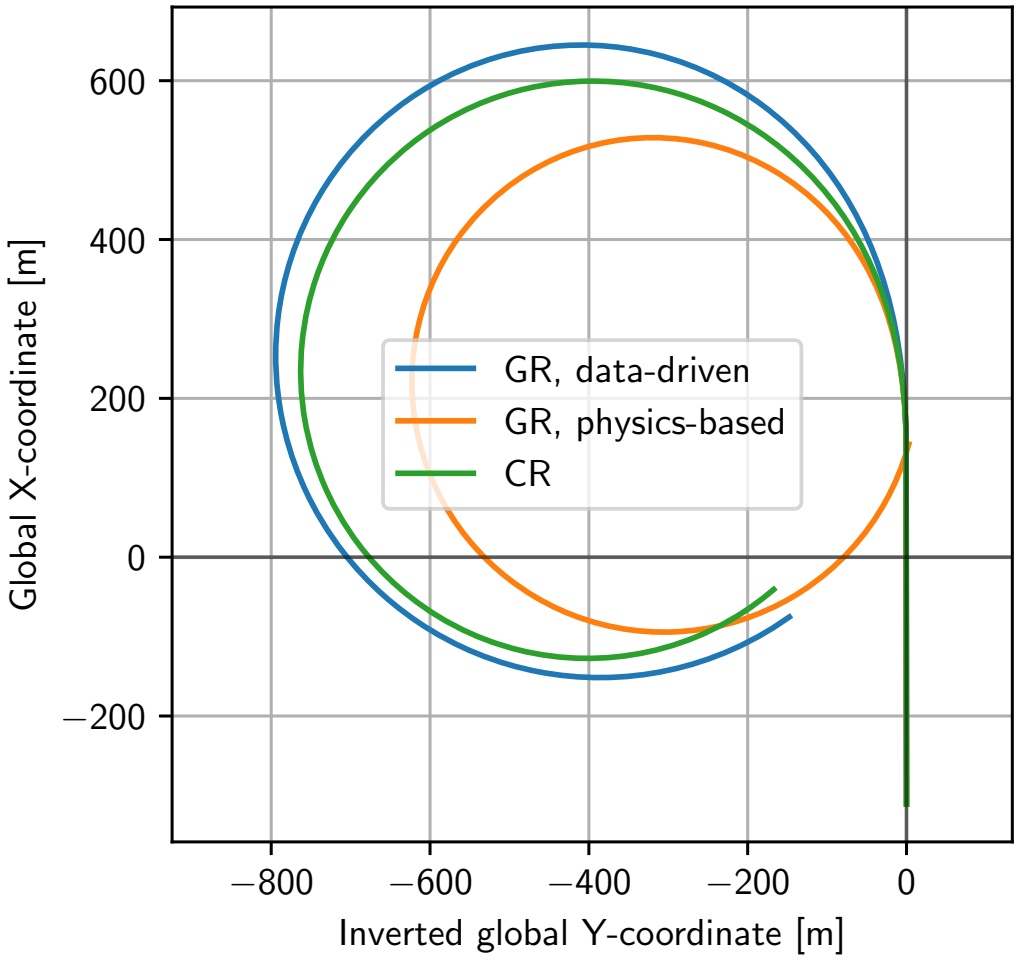

Figure C.7: Ship track comparison plot in the 35° to port turning circle manoeuvre at 12.08 kn.

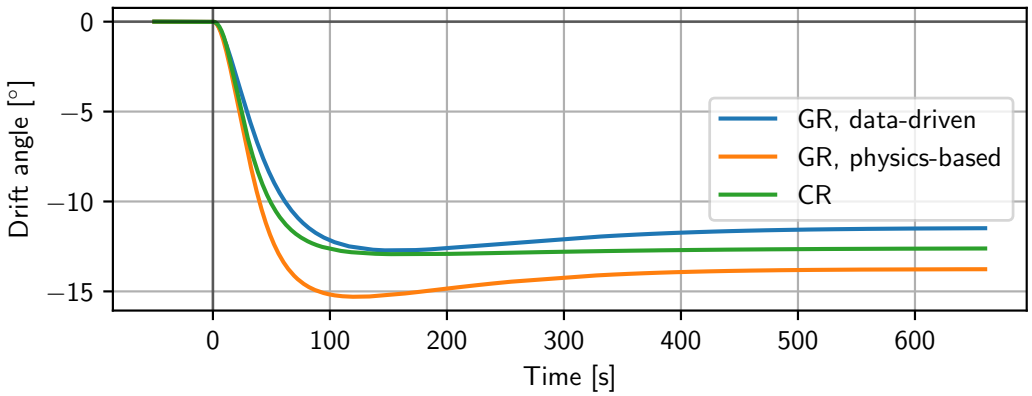

Figure C.8: Drift angle comparison plot in the 35° to port turning circle manoeuvre at 12.08 kn.

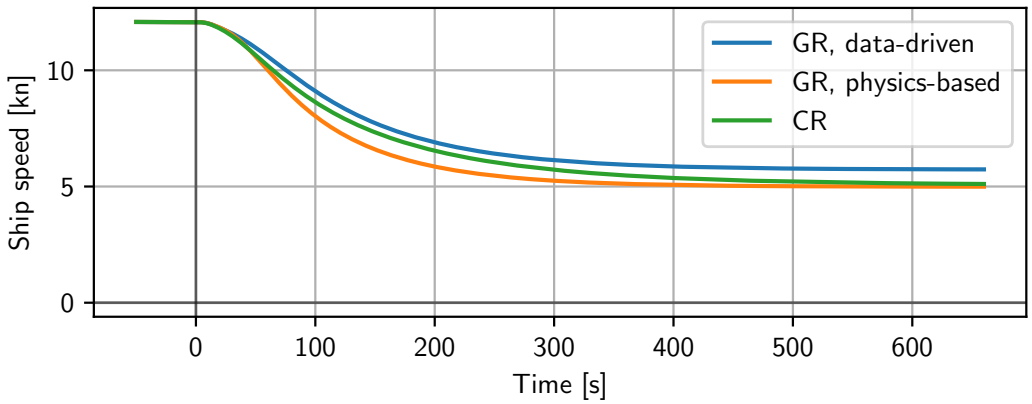

Figure C.9: Ship speed comparison plot in the 35° to port turning circle manoeuvre at 12.08 kn.

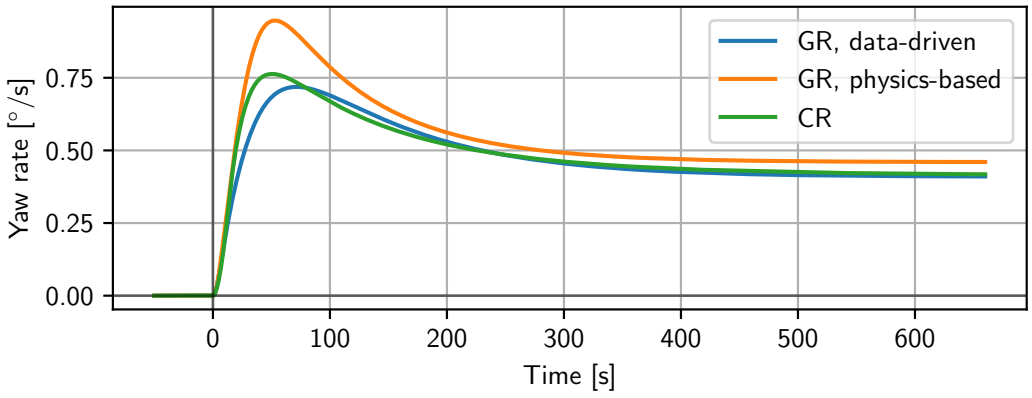

Figure C.10: Yaw rate comparison plot in the 35° to port turning circle manoeuvre at 12.08 kn.

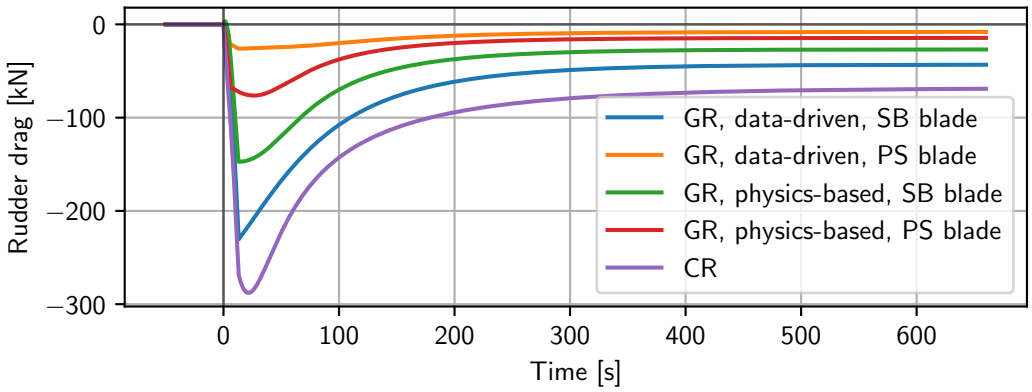

Figure C.11: Rudder drag force comparison plot in the 35° to port turning circle manoeuvre at 12.08 kn.

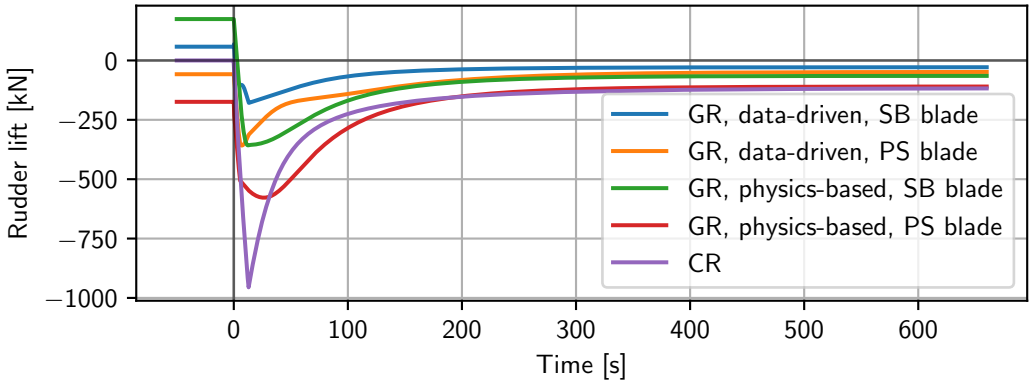

Figure C.12: Rudder lift force comparison plot in the 35° to port turning circle manoeuvre at 12.08 kn.

C.3. Zig-zag 20° to port @ 24.15 kn

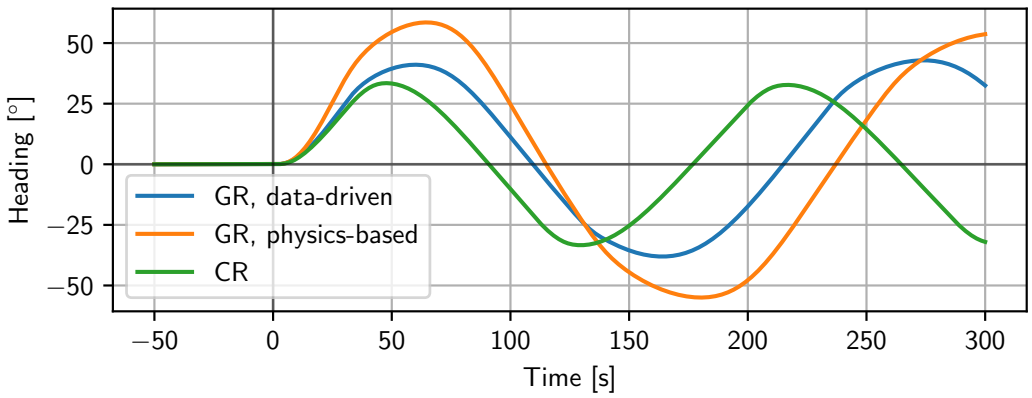

Figure C.13: Heading angle comparison plot in the port 20/20 zig-zag manoeuvre at 24.15 kn.

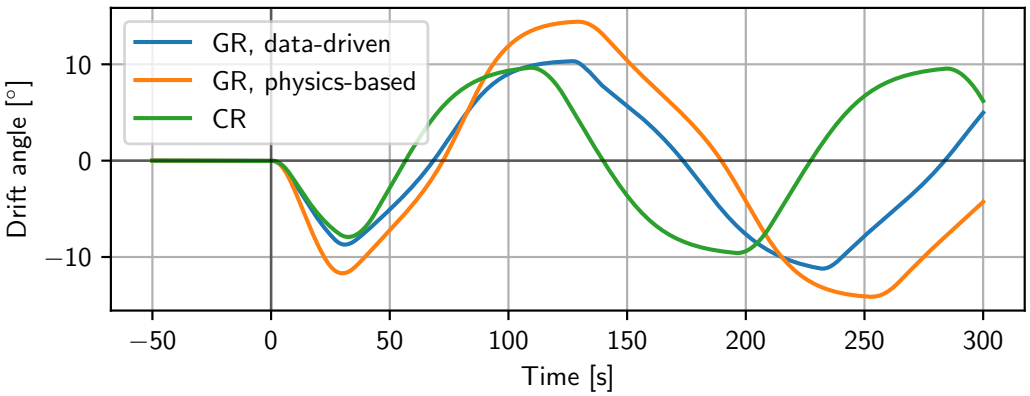

Figure C.14: Drift angle comparison plot in the port 20/20 zig-zag manoeuvre at 24.15 kn.

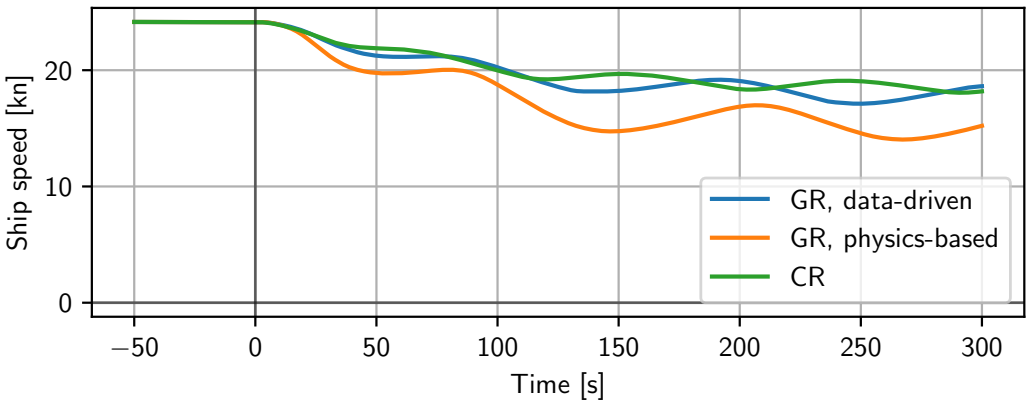

Figure C.15: Ship speed comparison plot in the port 20/20 zig-zag manoeuvre at 24.15 kn.

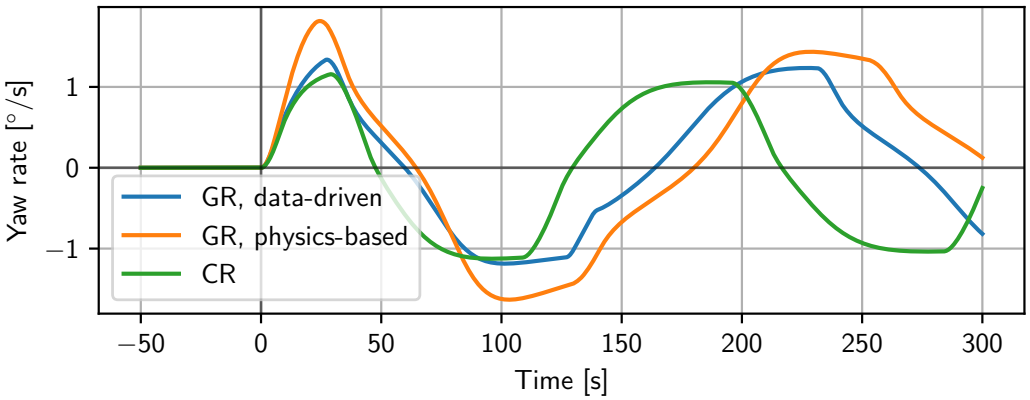

Figure C.16: Yaw rate comparison plot in the port 20/20 zig-zag manoeuvre at 24.15 kn.

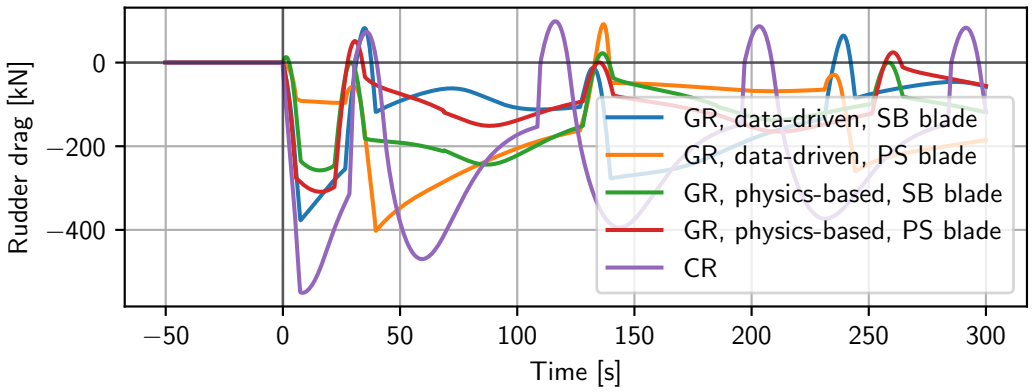

Figure C.17: Rudder drag force comparison plot in the port 20/20 zig-zag manoeuvre at 24.15 kn.

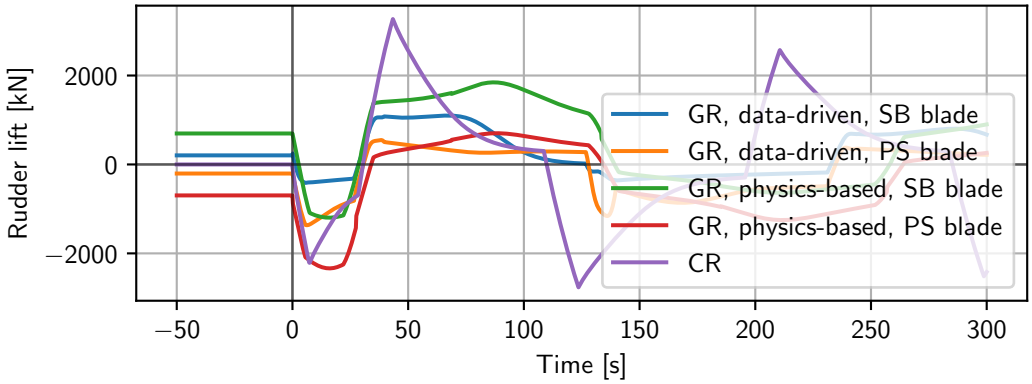

Figure C.18: Rudder lift force comparison plot in the port 20/20 zig-zag manoeuvre at 24.15 kn.

C.4. Zig-zag 10° to starboard @ 12.08 kn

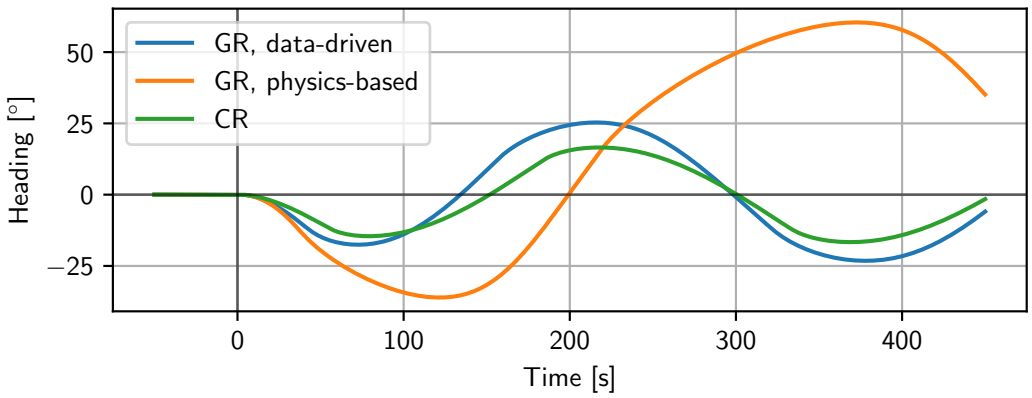

Figure C.19: Heading angle comparison plot in the starboard 10/10 zig-zag manoeuvre at 12.08 kn.

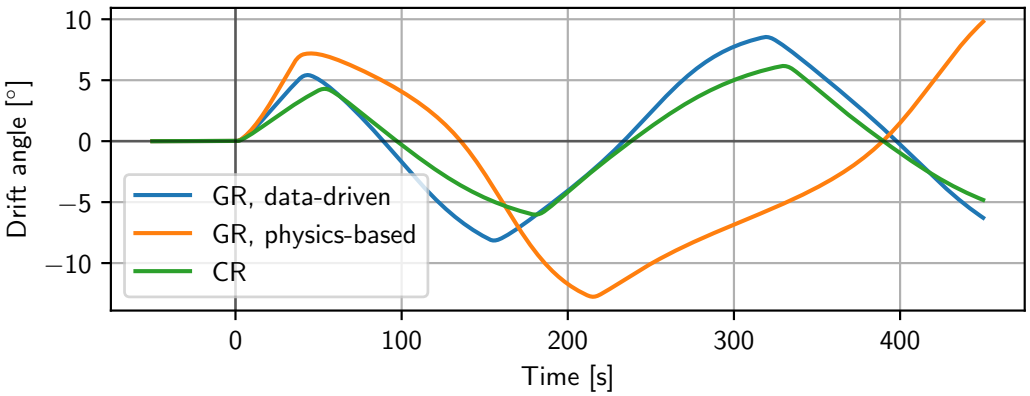

Figure C.20: Drift angle comparison plot in the starboard 10/10 zig-zag manoeuvre at 12.08 kn.

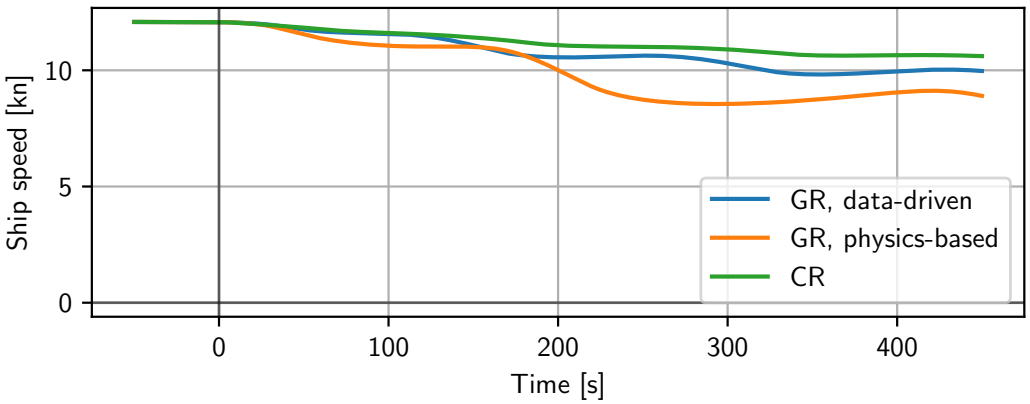

Figure C.21: Ship speed comparison plot in the starboard 10/10 zig-zag manoeuvre at 12.08 kn.

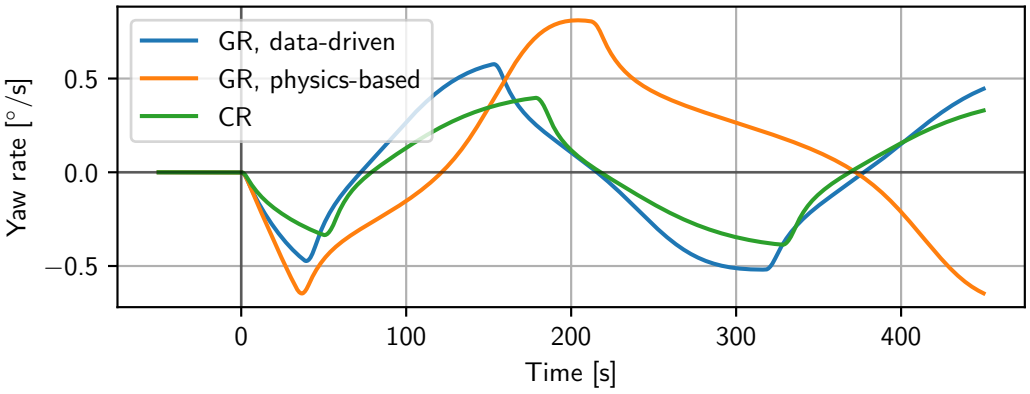

Figure C.22: Yaw rate comparison plot in the starboard 10/10 zig-zag manoeuvre at 12.08 kn.

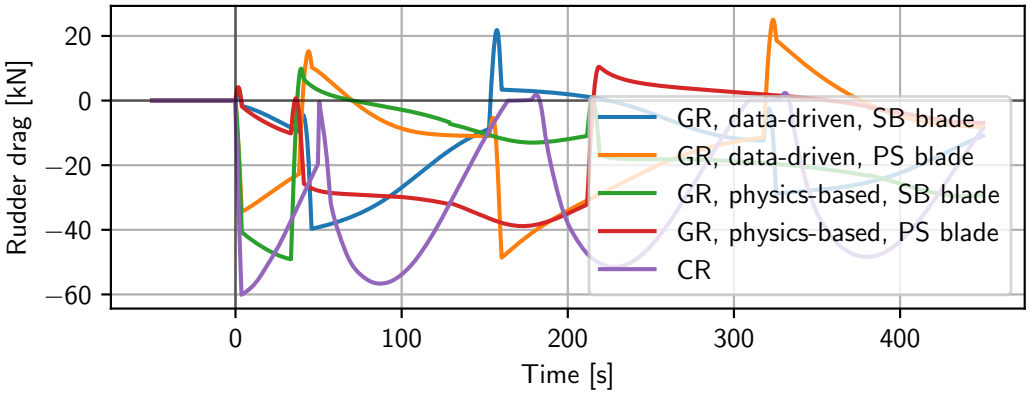

Figure C.23: Rudder drag force comparison plot in the starboard 10/10 zig-zag manoeuvre at 12.08 kn.

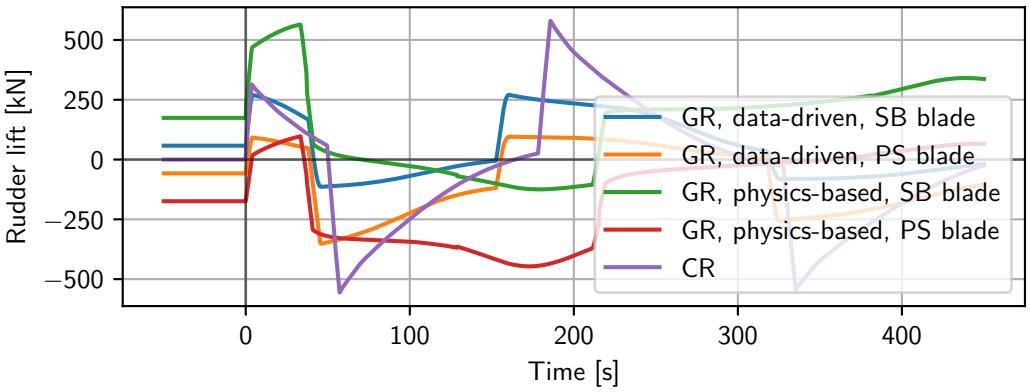

Figure C.24: Rudder lift force comparison plot in the starboard 10/10 zig-zag manoeuvre at 12.08 kn.